THE UNIVERSITY OF CHICAGO

TO CRAWL, AND FEEL THAT ONE IS CRAWLING:

LOCOMOTOR COORDINATION AND PROPRIOCEPTION IN LARVAL DROSOPHILA

A DISSERTATION SUBMITTED TO

THE FACULTY OF THE DIVISION OF THE BIOLOGICAL SCIENCES

AND THE PRITZKER SCHOOL OF MEDICINE

IN CANDIDACY FOR THE DEGREE OF

DOCTOR OF PHILOSOPHY

COMMITTEE ON NEUROBIOLOGY

BY

MARIE ROSE GREANEY

CHICAGO, ILLINOIS

JUNE 2025

TABLE OF CONTENTS

LIST OF FIGURES

LIST OF TABLES

ACKNOWLEDGMENTS

This dissertation would not exist without the contributions of many individuals, to whom I owe my sincerest, warmest gratitude:

My advisors, Ellie Heckscher and Matt Kaufman, whose enthusiasm for science and generous, thoughtful mentorship truly made this research possible. Ellie, thank you for the opportunity to do research that really excited me and for the trust you placed in me to get it done. Matt, thank you for taking the chance on working on weird little invertebrate tubes who have very little to do with motor cortex. Thanks to both of you for the wonderful scientific discussons and creative problem-solving sessions, for your constant support, and for investing in me as a scientist, as a lab member, and as a person. You met me where I was and challenged me to grow throughout this whole process. I have benefited in countless ways from working with you, and I am deeply grateful.

Thanks to the other members of my thesis committee, Ruth Anne Eatock and Dan Margoliash, for your helpful feedback on my scientific results and ideas throughout this process, as well as for your kindness and for encouraging me over the finish line.

I have been fortunate to belong to not just one, but two fantastic labs, whose members have been great colleagues in every sense of the term. To the members, past and current, of the Heckscher and Kaufman labs: thank you for caring both about each other's science and about each other's well-being. I have loved every minute of chatting, troubleshooting, workshopping, dreaming, complaining, and celebrating with you all.

I have had many other wonderful comrades in the neuroscience programs over the years, who made it a joy to do science here and who made me feel like I belong to a larger scientific

effort. I would especially like to thank Jen Ding and Ross Mansouri-Rad for their companionship and willingness to talk through any problem, scientific or otherwise, no matter how small.

I would never have embarked on this journey in the first place without the incredible mentorship of my advisor at NYU, David Schoppik. I am so fortunate to have landed in your lab and learned the ups and downs of science there. Thank you for your support both then and since, and thanks to you and Kathy Nagel for broadening my vision of what science should be like.

I am incredibly grateful to my family, especially my parents and my sister, Amy. I could not imagine a better or more loving family; I am so, so lucky to have you. Your unflagging support, encouragement and love sustained me through many periods of doubt. I also owe my gratitude to the wonderful aunts, uncles, and cousins who have been there for me throughout.

Finally, I cannot thank enough my dear friends, Nell Durfee and Mary Buchanan, whose friendship has anchored me through many stormy patches, and been the wind in my sails the rest of the time. Your collective generosity, warmth, humor, talent, and character have been an inspiration to me, and I am unendingly grateful to have shared this journey with you both.

ABSTRACT

Larvae of the fruit fly *Drosophila melanogaster* are a promising genetic model system in which to investigate how limbless animals coordinate locomotor movements across body segments. Proprioceptive sensory feedback is critical for coordinating segmental movements during locomotion, but how it is routed into central neural circuits that use it to inform movements remains unclear. On the behavioral level, it is unknown how flexible or consistent the coordination of segmental movements is across the larval body. Moreover, it remains unclear how locomotor movements relate to underlying neuromuscular drive. Both anatomical and behavioral advances are therefore needed to understand what features of larval movement are coordinated during locomotion, and how.

In this dissertation, I investigate both the anatomy of larval proprioceptive neurons and the coordination of body segments during locomotor behavior. First, I use a published larval nerve cord electron microscopy dataset and connectome to characterize features of larval proprioceptive neurons that likely affect how proprioceptive feedback is routed to central neural circuits, and how it can be used to coordinate movement. I find both segregation and overlap of proprioceptive neuron outputs in multiple central spatial domains, consistent with specific local convergence of proprioceptive subtypes that either reflects or shapes downstream connectivity. I also report features of larval proprioceptive neurons in this dataset that defy expectations for the routing and processing of proprioceptive feedback: I find almost no direct sensory-to-motor reflex connections, as well as no anatomical evidence of presynaptic gain control onto proprioceptive neurons. These results both inform our understanding of larval proprioceptive

processing and highlight the potential diversity of proprioceptive processing strategies in nature, making larval Drosophila an intriguing comparator model for study of proprioception.

Next, I describe a method to simultaneously record larval locomotor behavior and its underlying muscle activity inside linear agarose channels. Leveraging this method, I analyze relationships between body segments' contractions across many cycles of locomotion, investigate the flexibility of segmental coordination, and relate contraction to muscular recruitment. I find unexpected axial differences both among segments' contractions and among their muscle recruitments that suggest diversity in the neural coordination of locomotion across the body. I also find more regular timing relationships among segments' contractions than among their recruitments, indicating axial diversity in neural coordination may be partially counteracted by the biomechanics of locomotion inside channels. Finally, I find greater flexibility in the relationships between anterior as compared to posterior segments' contraction durations, consistent with distinct behavioral roles for these groups of segments during locomotion. Altogether, in comparison with other locomotor models, these results suggest both conserved and unanticipated principles for the coordination of locomotion in larval Drosophila.

This Dissertation includes the following Supplementary Files:

Supplementary Video 1: Example single-channel fluorescence microscopy video of crawling jGC7f larva (ID: "larva 1"); green channel gamma-adjusted for visualization purposes and displayed in inverted greyscale. Video display rate: 20 fps (~real time).

Supplementary Video 2: Example dual-channel fluorescence microscopy video of crawling Gerry larva (ID: "larva 22"); green channel shown in green, red channel shown in

magenta. Both channels gamma-adjusted for visualization purposes. Video display rate: 13 fps (~real time). N.B.: The larva emerges from under the coverslip near the end of the video; however, only cycles during which the larva was fully contained underneath the coverslip were included in analysis.

Supplementary Video 3: DeepLabCut network tracking of Supplementary Video 1.

Supplementary Video 4: DeepLabCut network tracking of the red channel from Supplementary Video 2, displayed as greyscale.

CHAPTER 1

GENERAL INTRODUCTION

1.1 Introduction

The work contained in this thesis aims at explaining how the segmented nervous system of a limbless, soft-bodied animal generates and coordinates the muscle activity that moves this small animal through its world. The central question of the work is how body segments are coordinated to produce limbless locomotion. To date, this question has been tackled in countless animal species, but most extensively in two model systems: the lamprey (genera including *Ichthyomyzon*, *Petromyzon*) and the leech (genus *Hirudo*). This General Introduction will, first, provide an abbreviated overview of the principles that have been uncovered in these two models, primarily for the coordination of undulatory swimming locomotion. Second, it will highlight a few of the more crucial outstanding questions that cannot yet be addressed in these, or in most, animal models of locomotion. Finally, it will introduce the animal model featured in the remainder of the thesis: the larval stage of the fruit fly *Drosophila melanogaster* (herein, "Drosophila"). To place the research in Chapters 2-4 in context, it will provide an overview of what is known about locomotor coordination in larval Drosophila, highlighting areas where the work in this thesis can fill important gaps by addressing the identified outstanding questions.

1.2 Aquatic limbless locomotion: anguilliform swimming in lampreys

The undulatory swimming of the lamprey, so-called "anguilliform" swimming, is a particularly well-studied locomotor behavior (Sigvardt, 1989; Mullins et al., 2011; Grillner and El Manira, 2019; Grillner and Kozlov, 2021). Many decades of research in this system have established a number of principles for control of undulatory swimming locomotion that we will

briefly review here, as examples of the various means by which limbless animals may coordinate body segments. Later, we will go on to compare limbless locomotion in the leech and in larval Drosophila, and introduce outstanding questions for understanding the coordination of limbless locomotor behaviors. (N.B.: Because most research into lamprey locomotion focuses on the axial propagation of undulatory waves of neural activity and body contractions, it has effectively been studied as a limbless behavior; therefore, I take the liberty of classing lamprey swimming as "limbless locomotion" despite their use of fins (Mentel et al., 2006).)

Anguilliform swimming in the lamprey manifests as a wave of left-right undulatory movements that pass down the body from head to tail end. These undulations are generated by alternating left-right contractions of the lamprey's body segments that occur with highly regular phase delays between segments (Wallén & Williams, 1984; Williams et al., 1989). The "wavelength" of the undulatory wave varies with speed, but is typically close to one full body length, meaning that at any given time during locomotion, the lamprey's body is in the shape of one cycle of a sine wave (Lighthill, 1969; Cohen et al., 1992). To speed up, lampreys increase the frequency of the wave and increase the amplitude of undulations mainly at the head end of the body (Ellerby et al., 2001; Tytell, 2004).

Most often, the form of swimming that is studied is "fictive swimming": rhythmic activity of spinal cord neurons or nerve roots that resemble the patterns seen in the swimming animal. To study fictive swimming, the brain and spinal cord are dissected away from the rest of the lamprey, also called an "isolated" preparation (Mullins et al., 2011). The spinal cord of the lamprey is small and experimentally tractable compared to those of most vertebrates: it comprises about 100 segments of roughly 1000 neurons each, and the isolated brain-spinal-cord

preparation can be kept relatively healthy for multiple days in the laboratory (Grillner & Wallén, 2002). Fictive swimming can be induced by bath application of D-glutamate, or by electrical stimulation either of the brainstem mesencephalic locomotor region or of reticulospinal fibers in the spinal cord (Buchanan and Cohen, 1982; Grillner, 2003). Alternatively, in "semi-intact" preparations, the brain and spinal cord are exposed by partial dissection of the body but are left connected to peripheral tissues, so that muscle activity and sensory feedback remain. In "intact" or "nearly-intact" preparations, the animal is partially restrained, but only minimal surgical interventions are performed to enable muscle or limited neuronal recording. In semi-intact and intact preparations, swimming is often induced by mechanically stimulating one end of the body (Mullins et al., 2011).

Research into lamprey swimming has long focused on how segments of the spinal cord produce highly regular, rhythmic motor activity, and how segments are coordinated to propagate a wave of activity along the body axis with consistent phase relationships among segments (e.g., Rovainen, 1985; Cohen, 1987; Hagevik and McClellan, 1999). From this research has emerged a set of principles for locomotor coordination in this system, which appear to be shared with many other locomotor systems (Hill et al., 2003; Grillner, 2003; Ryczko et al., 2010; Grillner and El Manira, 2019). We will briefly summarize some of the main conclusions in sections below: 1) the central pattern generator model for left-right alternating movement; 2) mechanisms of intersegmental coupling to establish appropriate phase delays, including interneuronal connectivity, as well as 3) roles for proprioceptive feedback and 4) neuromodulatory inputs; and 5) principles (from a largely distinct body of research) as to the importance of biomechanics for locomotor behavior, including how forward movement is effected in the water.

The central pattern generator model for undulatory locomotion

Distributed in each segment of the lamprey spinal cord are neural circuits capable of generating highly rhythmic activity in response to certain stimuli, such as the aforementioned exposure to D-glutamate (Grillner, 1985). These circuits are generally called central pattern generators (CPGs; Marder and Bucher, 2001; Kiehn, 2006). In the lamprey, a small number of CPG constituent interneuron classes have been identified, whose membrane properties, connectivity, and synaptic transmission have been extensively investigated and modeled (Grillner, 2003). To produce alternating left and right side contractions, a combination of excitatory and inhibitory input produces oscillatory bursting in motor neurons; the motor neurons on either side of the body burst in opposite phases. Ipsilateral glutamatergic interneurons provide most of the excitation, supplemented by ipsilateral stretch receptors, while inhibition comes from contralateral glycinergic interneurons and stretch receptors (Di Prisco et al., 1990; Buchanan, 1999; Grillner, 2003). The left-right alternating pattern relies on contralateral inhibition, although isolated hemisegments or halves of the spinal cord can still produce rhythmic activity (Cangiano and Grillner, 2003). There are ongoing debates as to the importance of reciprocal inhibition for both rhythm generation and axial wave propagation in the intact animal (Messina et al., 2017; Cangiano and Grillner, 2018; McClellan, 2018).

Intersegmental coupling and wave propagation

Swimming locomotion relies on the maintenance of consistent phase relationships among segments along the body axis (Lighthill, 1969; Skinner and Mulloney, 1998; Hill et al., 2003). In the lamprey, two primary mechanisms appear to be responsible: asymmetric coupling between segments, with stronger synaptic connectivity in the direction of wave propagation (Hagevik and

McClellan, 1999); and a gradient of CPG oscillation frequencies (Cohen, 1987; Matsushima and Grillner, 1992). Local connectivity, up to a range of a few segments, is thought to provide the majority of intersegmental phase coordination (Williams et al., 1990; Miller and Sigvardt, 2000; Ayali et al., 2007; Mullins et al., 2011). However, connections over longer distances do provide some amount of intersegmental coupling, as demonstrated by the partial maintenance of undulatory phase relationships in semi-intact preparations after the spinal cord has been locally transected, or when only a small number of segments are prevented from firing using low-calcium saline in a split-bath experiment (Cohen and Wallén, 1980; Hagevik and McClellan, 1999; Miller and Sigvardt, 2000). Long-distance coupling of segments' phases is thought to arise mainly from propriospinal projection interneurons, although a number of candidate interneuron classes have been identified (Buchanan, 1982; Rovainen, 1985; Mullins et al., 2011). To my knowledge, the involvement of any of these classes has yet to be directly demonstrated.

Proprioceptive feedback in lamprey swimming

Another potential determinant of segmental coordination is proprioceptive feedback. Stretch receptor neurons called edge cells provide proprioceptive feedback to segmental circuits (Grillner et al., 1984). During fictive swimming, stretch receptor feedback is capable of entraining rhythmic segmental activity, and the phase relationships between segments differ between isolated and semi-intact preparations, which together suggests that propriceptive feedback is used in vivo to coordinate the timing of segments' movements (Grillner et al., 1982; Guan et al., 2001). Intriguingly, anterior and posterior segments differ in their capacity to be entrained by stretch receptor feedback: posterior segments can entrain to a wider range of frequencies than anterior segments, and can be entrained more reliably to a single plateau

frequency, whereas anterior segments end up with more variance in frequency relative to the entraining stimulus (McClellan and Sigvardt, 1988; Hill et al., 2003; Tytell and Cohen, 2008). Additionally, as mentioned above, proprioceptive feedback likely plays a role in coupling CPGs' activities at longer distance, via propriospinal projection neurons (Rovainen 1985, Sigvardt, 1989). However (in contrast to leech swimming, below), this long-distance feedback is thought to be of relatively little importance for coordinating segments' phases in unperturbed swimming conditions (Ekeberg and Grillner, 1999; Hill et al., 2003).

Neuromodulation in lamprey swimming

Several neuromodulators have been implicated in control of swimming, including serotonin, dopamine, substance P, endocannabinoids, and tachykinins (El Manira, 2014; Grillner and El Manira, 2019). Serotonin is particularly important, as it is likely required for the initiation of swimming (Brodin et al., 1985; Zhang and Grillner, 2000). Additionally, as in other vertebrate locomotor models, serotonin is thought to not only modify locomotor rhythms, but also aspects of segmental coordination (Schmidt and Jordan, 2000; Grillner and El Manira, 2019; Flaive et al., 2020). For instance, in fictive swimming preparations, bath application of serotonin both slows the oscillatory bursting rhythm of individual segments and prolongs the lags between segments, among other effects (Harris-Warrick and Cohen, 1985; Wallén et al., 1989; Biró et al., 2006). Serotonin is released from local sources within the spinal cord as well as descending raphe projections. Meanwhile, other neuromodulators listed above may have less of a short-term effect on segmental coordination, but have been shown to contribute to local motor neuron bursting properties or to long-term circuit plasticity (Kettunen et al., 2005; Parker and Bevan, 2007; Thörn Perez et al., 2009; El Manira, 2014). The effects of neuromodulators also interact at

the cellular level, which makes their contributions to behavior an especially knotty challenge to unravel (Kyriakatos et al., 2007; Thörn Perez et al., 2009; Marder, 2012).

Biomechanics and fluid dynamics of anguilliform swimming

Lastly, the biomechanics of locomotion, including how the body interacts with the environment to move, are generally well-characterized for swimming behaviors, including anguilliform swimming (Lighthill 1969; Tytell et al., 2010; Di Santo et al., 2021). In anguilliform swimming, because of the unusually large-amplitude head undulations, thrust can be generated along the entire body (Lucas et al., 2020); this strategy is unusual for swimming behaviors, which more typically keep thrust generation localized to the tail end (Lighthill 1969; Di Santo et al., 2021; Liao 2022). Both mathematical and physical modeling have suggested that various combinations of undulatory wavelengths and head-end versus tail-end undulatory amplitudes lead to distinct speed-efficiency tradeoffs (Tytell et al., 2010; Anastasiadis et al., 2023). Additionally, body stiffness is an important parameter for determining how muscle contractions translate into useful forces; it differs constitutively among fish species and along the body axis (Summers and Long Jr, 2006; Jimenez et al., 2024) and is also actively managed by the recruitment of muscles (Tytell et al., 2018, Jimenez et al., 2024). The importance of this form of biomechanical control for lamprey swimming remains to be determined.

I will end this section by noting an interesting property of the relationship between the body and the environment that highlights the critical need for mechanical understanding in the study of locomotor behaviors. This property, also shared by most fish, is a "neuromechanical phase lag": a mismatch in the propagation speeds/wavelengths between the wave of neural circuit activity and the wave of undulatory movements, which holds true across swimming

speeds (Grillner and Kashin, 1976; Williams et al., 1989; Wardle et al., 1995). Because of this lag/mismatch, different segments along the body have different relationships between neuromuscular activation and movement. At the head end, intuitively, muscle contraction on the left or right side coincides with shortening that side of the body. In contrast, at the tail end, muscle contraction happens mostly while that side of the body is elongated. What this contraction at the tail end achieves, rather than shortening segments, is stiffening them and providing resistance against the water as the tail moves laterally, which generates the power needed to move forward (Rome et al., 1993; Wardle et al., 1995; McMillen et al., 2008). Thus, without a model for how the environment and the body interact to shape locomotion, the apparent discrepancy between neuromuscular activity and movement along the body axis would make very little sense.

In all, the lamprey model of anguilliform swimming is one of the best-studied and understood vertebrate behaviors. Nonetheless, debates and knowledge gaps remain about the importance of mechanisms that couple CPGs together across sides and along the body axis, debates that are unlikely to be resolved without the ability to precisely target interneuron classes for perturbation during swimming (McClellan, 2018; Grillner and El Manira, 2019). For this reason, most of the near-term follow-up work on coordination of swimming behaviors is expected to occur in the more genetically-tractable larval zebrafish (Dallmann et al., 2023).

1.3. Leech: one body, two modes of locomotion

Among segmented limbless invertebrates, the leech (*Hirudo*) long swam uncontested as the pre-eminent model for study of locomotion. By isolating the leech's ventral nerve cord, which comprises a head brain, tail brain, and 21 midbody ganglia whose neurons can be

identified repeatably across segments and preparations, it has been possible to characterize the neurons and synaptic connections that drive fictive locomotor behaviors in great detail (Kristan Jr. et al., 2005). Therefore, in contrast to the lamprey, where the neurons that comprise and couple CPGs are understood as classes of neurons (e.g., the contralaterally and caudally projecting interneurons class, "CCINs"), the leech swimming CPG is described at the level of individual neurons, whose anatomical and physiological properties and synaptic/electrical connections have been unusually well-characterized (Hill et al., 2003; Mullins et al., 2011).

Leech swimming

Swimming in the leech is similar to that in the lamprey in many respects. Although the undulatory movements are created by alternating dorso-ventral contractions, as opposed to left-right alternation, they feature similarly regular phase relationships between segments (Mullins et al., 2011). CPG circuits have been identified (Pearce and Friesen, 1985; Kristan Jr. et al., 2005). These circuits contain 13 candidate swim oscillator interneurons, so defined because they are active in phase with swimming rhythms in isolated preparations, injecting current into any of them can shift the phase of the swimming rhythm, and they have synaptic interactions with the other candidate interneurons (Kristan Jr. et al., 2005). All of these interneurons also project either anteriorly or posteriorly in lateral nerve cord connectives; their projections can span up to 10 segments (Poon et al., 1978; Weeks, 1982; Friesen and Hocker, 2001). However, these connectives may not be required for intersegmental coordination (see below; Yu et al., 1999).

Further similarities include the importance of serotonin for swimming: like in lamprey, local serotonergic cells are present throughout the nerve cord, and serotonin appears to be necessary for expression of a normal CPG rhythm, although its importance for intersegmental

coordination is unclear (Nusbaum 1986; Nusbaum and Kristan Jr, 1986; Crisp and Mesce, 2003). Also as in anguilliform swimming, proprioceptive feedback from stretch receptors affects the intersegmental phase relationships observed in fictive swimming, and is able to entrain rhythmic activity (Yu et al., 1999; Cang and Friesen, 2000; Yu and Friesen, 2004); in leech, this feedback occurs via gap junctions with locomotion-generating central neurons (Cang et al., 2001). In contrast to lampreys or eels, however, leeches can continue to produce coordinated swimming with stable (but increased) intersegmental phase relationships even after the nerve cord has been fully severed (Yu et al., 1999), suggesting that sensory feedback alone is capable of coordinating segments' activities. Further, leech swimming is believed to operate using the same fluid dynamic interactions with the environment as lamprey swimming (Friesen & Kristan Jr, 2008; Chen et al., 2011). On the other hand, no neuromechanical phase lag has been observed in swimming leeches (Chen et al., 2012). Moreover, leeches are soft-bodied, having no spinal cord or notochord, and they actively flatten their bodies as part of the swimming behavior, which modifies body stiffness, presumably in a very different way from lampreys (Chen et al., 2012; Tytell et al., 2018); the biomechanics of leech swimming have not, to my knowledge, been compared to those of lamprey or fish swimming.

In 2014, a detailed neuromechanical model of leech swimming was developed by Iwasaki, Chen, and Friesen, bringing together modeling work done on many separate aspects of swimming. These researchers modeled the leech's body as a chain of rigid links subject to hydrodynamic forces, controlled by muscles with passive and active spring properties that respond to motor neuron bursting, and modeled nervous system control of the body using 17 coupled CPGs that each received tonic excitatory drive and stretch feedback. Units in the CPGs

had connectivity and membrane properties modeled after those of small numbers of interneurons, grouped by phase of activity. All parameters in the combined CPG and body model were fixed from experimental data, with the exception of sensory feedback gain, which they fit to kinematic data from swimming leeches. Their model predicted that, while thrust production is maximal at the tail end, most of the mechanical power for leech swimming comes from midbody segments (Chen et al., 2011). Additionally, once fit to kinematic data collected in normal water conditions, their model was able to predict environment-specific alterations to the swimming leech's oscillation patterns: they recapitulated the shorter wavelengths produced when leeches swam in highly viscous fluid, as well as the standing wave produced when a leech with brain removed "swims" in air (Iwasaki et al., 2014). To match these altered swimming patterns, they had to reduce overall excitatory drive to their network model, which would seem to predict that changes to descending inputs must supplement sensory feedback to adapt leech behavior to unusual environmental conditions. Confusingly, the group concluded that sensory feedback alone was able to drive the adaptation of model behavior in different fluid environments.

Their results are a convincing demonstration of the ability to combine cellular, circuit, biomehcanical, and sensory feedback into a biologically realistic model that can be used to predict features of neural control that are otherwise difficult to measure in vivo. However, it is not clear (to me) at this point how to use it to make additional testable predictions for control of leech swimming, because the ability to tweak model parameters such as membrane properties, connection strengths between components, or muscle activation dynamics does not correspond to an ability to manipulate these properties in the leech itself. Moreover, recent work characterizing a CPG interneuron when the head brain was left attached revealed that the cellular properties that

form the basis of the model may be fundamentally altered in the presence of descending inputs, and again altered in a semi-intact preparation with feedback from the body wall (Mullins and Friesen, 2012). Perhaps the next useful direction to take the detailed model of Iwasaki and colleagues would be to attempt to account for changes to the network's activity in the presence/ absence of neuromodulators (Calviño and Szczupak, 2008), or with connections to the head brain preserved (Mullins et al., 2012).

Regardless of any technical limitations, the detailed cellular and circuit-level models now available make it clear that neural control of locomotion is exceptionally well characterized in the leech swimming model. Next, we turn to a far less understood locomotor behavior in the same organism.

Leech crawling

The leech is particularly fascinating for its use of two extraordinarily different locomotor strategies: undulatory swimming when immersed in water, or crawling when partially or fully exposed to air (Gray et al., 1938). Two variants of crawling locomotion have been described, "vermiform" and "inchworm" crawling, which differ in how low to the substrate the body segments remain when moving and in how closely head and tail suckers are placed when attached to the substrate (Stern-Tomlinson et al., 1986). Far more work has been done on vermiform crawling, which will be described hereafter. A leech that is only partially immersed in water will typically choose crawling rather than swimming locomotion; in fact, stimulation of the same "command neuron" in a semi-intact leech can lead to either swimming or crawling, depending on the depth of saline around the body (Esch et al., 2002; Friesen and Kristan Jr., 2008). To crawl, the leech engages descending brain neurons that suppress swimming, likely by

release of dopamine, which inhibits fictive swimming activity but activates fictive crawling activity in isolated leech nerve cords (Brodfuehrer and Friesen, 1986; Crisp and Mesce, 2004; Puhl and Mesce, 2008).

Crawling and swimming behaviors overlap extensively in which segmental neurons they engage (Briggman et al., 2005). However, they exhibit major differences in how segments are used and coordinated. First, the muscle contractions and movements that produce crawling scarcely resemble those that produce swimming (Gray et al., 1938; Stern-Tomlinson et al., 1986; Cacciatore et al., 2000). At the beginning of a crawling cycle, the leech is attached via suckers on the tail to the substrate. It elongates the body, beginning with the head-most segments; a wave of segmental elongations propagates from head end to tail end. To elongate, a body segment's circularly-oriented muscles contract. At some (variable) point after the head end of the body has extended in this way, the head attaches to the substrate via suckers and elongation stops; elongation does not need to have reached the tail-most segment before this point. Once the head has attached, the tail detaches, and the animal transitions from lengthening to shortening: a wave of contractions begins, also starting with the head-most segments and propagating toward the tail. To shorten, a body segment's longitudinally-oriented muscles contract. Notably, the wave of segmental contractions passes more quickly through the body than does the wave of elongations. At the end of the contraction wave, the tail re-attaches to the substrate, and the locomotor cycle may repeat. As crawling speeds up, the durations of each segment's elongation and contraction phases tend to scale linearly with (decreasing) cycle periods, as do the intersegmental delays (Stern-Tomlinson et al., 1986).

To summarize central differences in the movements of crawling as compared to swimming: extension and contraction movements are dorso-ventrally symmetrical, rather than dorso-ventrally alternating, and involve different muscle contraction patterns; elongation and contraction phases each pass as a wave through all or most of the body before switching, rather than alternating rhythmically within-segment; further, these two phases of movement have no fixed durations and thus no fixed timing relationship to each other, in contrast to the tightly phase-locked relationships between dorsal and ventral contractions during swimming; lastly, the means of moving the body forward involves attaching anchor points (suckers) at head and tail ends and thereby pushing off of a substrate, rather than producing thrust against the water (Gray et al., 1938; Stern-Tomlinson et al., 1986; Cacciatore et al., 2000).

Next, the phase relationships among segments, and how these are maintained, differ from those of swimming. In contrast to the uniformly linear contraction phase relationships among segments for swimming, phase relationships among segments during crawling can be linear or nonlinear from cycle to cycle (Stern-Tomlinson et al., 1986). In the crawling animal, phase relationships manifest at least one additional point of flexibility that is not present in swimming: leeches are sometimes observed to pause in the middle of crawling cycles, make searching movements and occasionally re-orient, and then resume from the segment in which the wave paused (Stern-Tomlinson et al., 1986; Cacciatore et al., 2000; Harley et al., 2013). To do this requires a degree of flexibility in producing "rhythmic" activity in each segment that would be impractical for swimming (Skinner and Mulloney, 1998; Cacciatore et al., 2000; McMillen et al., 2008; Puhl and Mesce, 2010) Additionally, during fictive crawling, midbody ganglia do not express appropriate phase relationships without descending inputs from the head brain,

suggesting that coordination of crawling behavior, unlike swimming, may require descending control (Puhl & Mesce, 2010; Puhl et al., 2012). Both descending input and local intersegmental connectivity are required to maintain coordination across the body axis, as blocking synaptic transmission in a region of just three ganglia is sufficient to interrupt coordination on either side of the blockade, despite relatively intact bursting in descending connectives (Puhl et al., 2012).

In concordance with differences in movements and intersegmental phase relationships, CPG control of crawling also differs from that of swimming. In 1997, Baader characterized the involvement of several motor neurons and interneurons using intra- or extracellular recording in partially-restrained, semi-intact crawling leeches. He discovered engagement of interneurons that were inhibited during swimming, as well as other interneurons that fired with different patterns during crawling than during swimming. In 2005, voltage dye imaging of almost a full leech midbody ganglion was combined with nerve root recordings and stimulation to (randomly) elicit either fictive swimming or crawling (Briggman et al., 2005). This study showed that both fictive swimming and fictive crawling engaged a highly overlapping set of interneurons, but that many of these neurons were active with very different phases relative to the overall locomotor cycle. To date, however, little else is known about the identities of neurons forming the crawling CPG (Rotstein et al., 2017; Alonso et al., 2020). Thus, intersegmental connectivity underlying the coordination of crawling also remains unknown.

Finally, the role of proprioceptive feedback in coordination of crawling is quite different from its role in swimming. Two experiments were performed to manipulate segment stretch by attaching weights to pull on the posterior end of the animal during the contraction phase. Attaching heavier weights slowed the propagation of contraction and increased the contractile

forces produced by segments, but did not lead to changes in phase relationships among segments (Gray et al., 1938); attaching lighter weights did not change either contraction wave propagation speed or phase relationships among segments (Cacciatore et al., 2000). In both experiments, attachment of the tail sucker was delayed, suggesting a major function of proprioceptive feedback is to time the transition between the contraction and elongation phases of crawling. Further, surgical denervation of six midbody segments, which severed both sensory and motor neuron axons, led to no change in intersegmental phase delays between segments on either side of the lesion, suggesting local sensory feedback is not used to time segments' elongations or contractions (Cacciatore et al., 2000). These results contrast strongly with leech swimming, where proprioceptive feedback is required to observe the normal intersegmental phase delays.

1.4. Limitations and outstanding questions

In all, lamprey and leech represent two evolutionarily distant species that, between them, express the three best-understood modes of limbless locomotion. In particular, the study and comparison of swimming in both systems, alongside other models such as tadpole, salamander, and zebrafish, has led to substantial progress in determining conserved, apparently fundamental features of undulatory locomotion and its coordination along the body axis (Ryczko et al., 2010; Grillner and El Manira, 2019).

However, a major limitation of both the lamprey and leech, as well as most other models of limbless locomotion, is that studying the neural contribution to locomotor coordination relies heavily on access to an exposed nerve cord or spinal cord (Mullins et al., 2011; Tomina and Wagenaar, 2017). This greatly restricts the type of experimental manipulations that can be performed while animals behave: researchers can deliver specific sensory stimuli, drug

injections, or focal electrical stimulation; they can transect nerves or connectives, have animals recover, and observe changes to behavior. Clearly, much progress has been made using these methods. However, to achieve more targeted perturbations, genetic access to particular neural (or other) cell types is required (Kiehn, 2016; Ausborn et al., 2021).

One result of this limitation is that, in the limbless locomotor models above, it has not been possible to test how factors that modify segmental coordination, such as proprioceptive feedback, operate in the context of the moving body. As discussed above, proprioceptive feedback plays an important role in coordinating, at minimum, segments' phase relationships in vivo. However, abundant evidence suggests that proprioceptive feedback to central locomotor circuits differs when studied in semi-intact preparation as compared to in the intact body (Pearce and Friesen, 1984; Guan et al., 2001; Tuthill and Azim, 2018). Integration of proprioceptive feedback in the behaving body has been extensively modeled for swimming, particularly in the leech, but it has not been modeled similarly for leech crawling, nor for any terrestrial limbless models -- with the notable exception of the nematode, whose body and nervous system are not segmented and are expected to use a very distinct locomotor coordination strategy (Fouad et al., 2018; Wen et al., 2018). Therefore, it is essential to develop systems in which the role of sensory feedback (as well as neuromodulators, etc.) can be compared between semi-intact and intact animals.

A further limitation, alluded to above, is the difference in the extent of characterization of terrestrial versus aquatic limbless locomotor behaviors. Terrestrial limbless locomotion has been studied in a range of species from a kinematic and biomechanical standpoint, including earthworms, snakes, and caecilians (Gray et al., 1938; Gaymer, 1971; Gans, 1973; Quillin, 1999;

Hu et al., 2009; Dorgan et al., 2010; Tanaka et al., 2011). However, even in the well-studied leech, far less is known about the neuronal underpinnings of crawling compared to swimming (Kristan Jr. et al., 2005).

As a result, important questions remain as to the differences between forms of limbless locomotion that prevail in different environments. For one, it has been repeatedly observed that phase relationships among segments are more flexible in terrestrial forms of locomotion, likely the result of needing to adapt locomotor movements to the comparatively unpredictable environment (Bässler, 1993; Lavoie et al., 1995; Cacciatore et al., 2000). In the leech, this flexibility includes the ability to pause mid-elongation, re-orient the body, and then resume the locomotor cycle from where it paused. However, how this additional flexibility is achieved remains unclear. In general, it has been proposed to require descending control (Georgopoulos and Grillner, 1989; Puhl & Mesce, 2010, Puhl et al., 2012). While a candidate descending pathway has been identified in the leech, it has not yet been possible to manipulate this pathway to test its ability to adjust intersegmental phase relationships or pause crawling, nor has it been possible to identify sites of action in a crawling CPG (Puhl & Mesce, 2010; Puhl et al., 2012). Therefore, in the leech, mechanisms for establishing flexible phase relationships will be challenging to establish (Friesen and Kristan Jr., 2008; Kearney et al., 2022). More broadly, the field lacks a satisfying model for neural control of crawling.

1.5. Larval Drosophila: an emerging model of limbless locomotion

We will first provide an overview of larval locomotor behaviors, focusing on the production of the basic "wave" pattern for forward movement, and on how the larval locomotor system manifests the principles of limbless locomotor coordination discussed in the previous

sections for lamprey and leech. A brief description of what has been discovered thus far in each topic, and how, will also serve to illustrate a few of the more salient advantages and limitations of the larval Drosophila model system.

1.5.1. An overview of larval Drosophila locomotor behavior

The larval locomotor pattern is referred to as "crawling," and the basic repeating unit of larval locomotion is interchangeably termed a "stride" or "wave." During each cycle of locomotion, a larva contracts its body segments sequentially in a peristaltic wave that begins at the tail and propagates anteriorly along the body (hence "wave"). The initial contraction and subsequent wave move the larva forward by a fixed distance (hence "stride"; Green et al., 1983; Heckscher et al., 2012). The initial contraction of the tail also pushes forward the internal organs in what is called a "visceral piston" (Simon and Trimmer, 2010; Heckscher et al., 2012). Throughout, I will use locomotor waves to refer to the series of segmental contractions that larvae produce to crawl.

Larvae may crawl for a number of reasons. The first is to find food. Adult flies lay eggs inside potential food sources. When larvae hatch from eggs, their priorities are growth and survival. If they find themselves on a suitable food source, they burrow into it to eat, typically in the company of many other larvae. Larvae cooperatively extrude saliva to break down the food in a layer beneath the surface (Gregg et al., 1990). If they do not find themselves on or in a suitable food source (e.g., food contains too high a concentration of alcohol), they will at some point move in search of better food (Green et al., 1983; Ruiz-Dubreuil et al., 1996; Wosniack et al., 2022). Navigating to better food depends primarily on olfactory sensing and has been extensively studied in larvae crawling over flat surfaces, described further below. As an aside,

the likelihood that a larva will abandon a food source to go in search of a new one turns out to be largely genetically determined: larvae can be "rovers" or "sitters," which are respectively prone to more frequent locomotion and greater travel distance through the environment, or the converse (Sokolowski, 1980; Sokolowski, 1985; Wosniack et al., 2022).

Another cause of crawling occurs at the end of the larval life stage. In order to pupate, larvae leave the food source they have been exploiting and crawl in search of more optimal environmental conditions; preferred sites are those that are away from other larvae, are low-moisture and low-illumination (Markow, 1979; Pandey and Singh, 1993; Sokolowski, 1985). Thus, even larvae that luckily hatch into an abundance of food will, at some point, use crawling locomotion to move themselves through their environment.

A larva crawling on a flat surface typically performs locomotor runs, comprising multiple forward waves, alternating with re-orienting turns (Green et al., 1983; Lahiri et al., 2011). The frequency of runs and turns depends partly on the animal's sensory experience. Animals that are navigating towards an attractive olfactory stimulus, or away from an aversive thermal or light stimulus, use a characteristic strategy that has been described as an improvement over a biased random walk (Holmes, 1905; Gomez-Marin and Louis, 2012). In a biased random walk, an organism (such as a bacterium) traveling in a favorable direction along a sensory gradient tends to perform long runs of locomotion, whereas when traveling in an unfavorable direction, it performs shorter runs interrupted by more frequent random re-orientation events (Marken and Powers, 1989). Larval Drosophila not only increase the length of runs when traveling in a favorable direction, but also improve over the biased random walk by actively sampling the environment. They use sensory organs on the head end to sample to either side, either by making

small lateral head movements during locomotor runs or by pausing to make larger movements of the head end, in either case comparing sensory information collected on each side of the body and biasing turns to the favorable direction (Holmes, 1905; Luo et al., 2010; Gomez-Marin et al., 2011; Lahiri et al., 2011). The neural substrates of this decision-making have been investigated and modeled by the Gershow, Louis, Samuel, and Webb labs, among others, and will not be described further here.

As part of the navigation process, larvae execute both small- and large-amplitude head movements (or "head casts"). Small-amplitude head casting occurs continuously during locomotor runs, is thought to bias the direction of larval crawling during runs as a form of klinotaxis (Gomez-Marin and Louis, 2014), and has been modeled as a continuous oscillatory process that is independent of peristaltic waves (Wystrach et al., 2016). It is unclear how many anterior segments are involved in the generation of these small-amplitude movements, although a recent study showed very regular, oscillatory small-amplitude activity in thoracic and anterior abdominal segments after oxotremorine was applied to nerve cords with posterior abdominal segments ablated (Jonaitis et al., 2022).

Large-amplitude head casts appear to be a distinct behavior: larvae pause locomotor runs to perform large-amplitude head casts, sweeping the entire head end (including anterior abdominal segments) to one or both sides of the body, sometimes multiple times in a row (Wang et al., 1997). They often follow up these larger head casts with turns, which use an anterior set of segments to bend the front of the body relative to the tail, before continuing locomotion in the direction the head is pointed (Holmes, 1905; Lahiri et al., 2011; Tastekin et al., 2016). While paused and head casting, larvae inhibit the activity of posterior segments, presumably to prevent

the initiation of a forward wave before the head end has finished bending (Tastekin et al., 2018). When a larva is bent, the propagation of peristaltic waves progressively either pushes or pulls tail-end segments into alignment with the head end. Which force predominates, pushing or pulling, is unclear, and may also depend on the bend angle, as a strong enough bend (>90 degrees between orientations of head and tail) can cause waves to initiate in bent, mid-body segments rather than at the tail, which would presumably rule out pushing from behind in these cases (Lahiri et al., 2011).

How do larvae control their locomotor speed? At a strategic level, this could be achieved in one of two ways: either by increasing the distance they travel on each cycle, or by increasing the cycle frequency. In practice, larvae do a little of both; but it is changes to cycle frequency that are more strongly coupled to crawling speed (Berrigan and Pepin 1995; Heckscher et al., 2012; Liu et al., 2023). Recent work found that, as larvae increase the frequency of locomotor cycles, the speed of locomotor wave propagation along the body does not change much; rather, a variable pause period between waves is shortened, such that larvae produce more waves in a given time period (Liu et al., 2023). These authors noted that, after pausing between waves has been reduced to zero, larvae can only continue to speed up by producing faster-propagating waves (which they will do, up to a point); however, it is unknown, to date, what physical and/or neural limitations constrain the maximum speed of wave propagation.

This section provided a high-level overview of larval locomotion, to establish the behavioral goals at play and the context in which they are likely to occur. We next turn to the specifics of how larvae move themselves over a surface environment, and what is known about the coordination of their body segments as they do so.

1.5.2 Soft-bodied locomotion in the environment

In this section, we first provide a broad overview of the body plan of Drosophila larvae, then describe their musculature, and lastly how body and muscles interact with a surface to enable these animals to move despite their lack of limbs or even (exo-)skeletons.

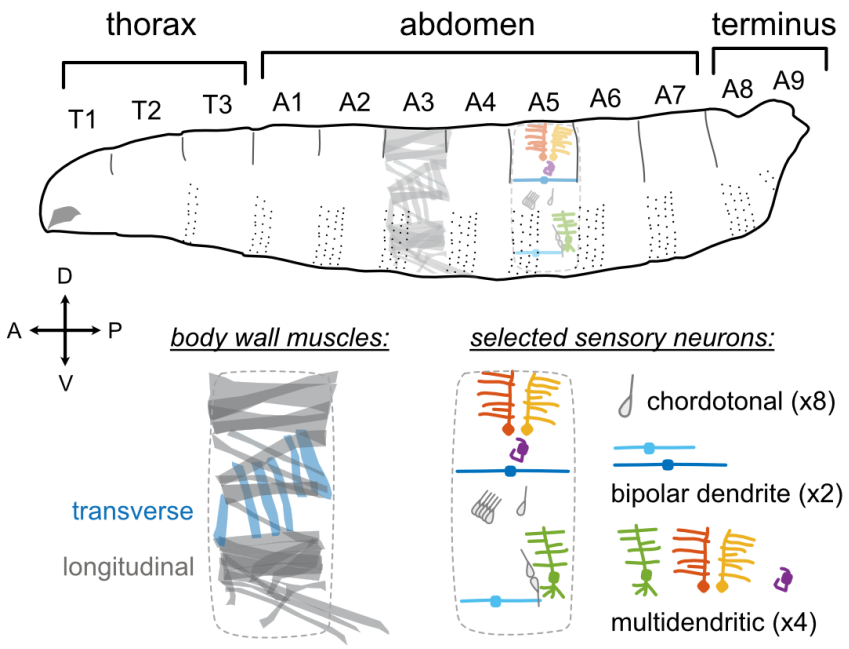

Figure 1.1: Diagram of larval body plan, musculature, and sensory neurons. Larval body regions and body segments are annotated above. Mouth hooks are shown in T1. Denticle belts are depicted as dots on the larva's ventral side, near the borders between segments. Body wall muscles and positions of sensory neurons indicated in example segments, and in cutouts below. Left, below: thirty muscles in each body segment are categorized by their orientations, transverse (blue) or longitudinal (gray). Right, below: the subset of mechanically-sensitive neurons discussed in detail in Section 1.5.4. Muscles and sensory neurons repeat across A1-A7, and are similar in segment T3. Other segments' muscles and sensory neurons not shown for clarity.

Larvae are segmented animals, with a different number of body segments in each of three regions. At the most anterior end of the body, there are three thoracic segments (abbreviated T1-3). In other animals, a true head would be anterior to the thorax; however, in larval Drosophila (and in all larvae of true flies, order Diptera), the head is developmentally inverted and remains inside the thoracic region at most times (Snodgrass, 1935). Nonetheless, we and others interchangeably refer to the anterior end of the larval body as the "head end." Posterior to

the thoracic segments are seven approximately identical abdominal segments (abbreviated A1-A7), comprising most of the length of the body. Finally, at the posterior end of the body, there is a reduced terminal segment and anal division (A8 and A9/AS) (Campos-Ortega and Hartenstein, 1997; Wipfler et al., 2013).

The anatomy of segments in each region is generally quite distinct (Campos-Ortega and Hartenstein, 1997; Rotheray, 2019). Abdominal segments are the largest in diameter and the most regular in musculature, while thoracic segments taper in height towards the head end, and terminal segments are very short compared to abdominal and thoracic segments. Further differences include the numbers and types of both muscles and sensory neurons, as well as the structures present on the body surface (Lohs-Schardin et al., 1979; Hooper, 1986; Bate, 1990; Campos-Ortega and Hartenstein, 1997). We will describe each of these features in more detail below, but will focus mainly on the muscles, sensory neurons, and surface structures present in abdominal segments, as these segments are responsible for the majority of movements underlying larval locomotion (Roberts, 1971; Dixit et al., 2008).

Larvae are soft-bodied, meaning they possess neither internal skeleton nor exoskeleton. Instead, their bodies are covered and contained by a flexible layer called the cuticle, which covers the epidermis. The 30 muscles of each abdominal body segment form a layer just beneath the epidermis, attaching mainly to tendon cells at the borders between segments or inside segments (Bate, 1990; Volk and Vijay-Raghavan, 1994; Schulman et al., 2015). Most muscles are longitudinally oriented with respect to the larval body, although certain muscles also wrap diagonally (i.e., the anterior and posterior attachment sites are at different dorsoventral locations; Figure 1.1). A small number of muscles are transversely oriented (i.e., pointing dorsoventral;

blue muscles in Figure 1.1). The directional forces that would be produced by activating combinations of these muscles have yet to be modeled; however, it is clear that the arrangement gives the larva great flexibility to move its body in three dimensions, including behaviors such as rearing and sideways rolling (Green et al., 1983; Hwang et al., 2007; Rotheray, 2019). The lack of rigid skeleton also means that larvae do not possess a fixed length: they can compress their bodies from one end, as a head or tail retraction or when beginning a locomotor wave, or from both ends, by hunching (Kernan et al., 1994; Jovanic et al., 2016, Clark et al., 2018).

The general patterns of muscle activation underlying each larval behavior are an area of active investigation; the segments whose muscles are involved for head turning behaviors have been reported (Lahiri et al., 2011), and a detailed order of muscle activations across the larval body has recently been reported for rolling (He et al., 2022; Cooney et al., 2023). For our purposes, the average order in which muscles activate in an abdominal body segment have been reported for forward and backward locomotion (Zarin et al., 2019), although data from multiple abdominal segments were treated as interchangeable in that report, so we do not know whether this order is consistent across the body. A great deal of work has also been done on transmission at the larval neuromuscular junction, a glutamatergic synapse that displays interesting properties of growth and plasticity during the larval life stage (Keshishian et al., 1996; Davis and Goodman, 1998; Kauwe and Isacoff, 2013; Newman et al., 2017), as well as measurements of excitation-contraction coupling and force production in the supercontractile muscles (Peron et al., 2009; Paterson, 2010; Ormerod et al., 2022; Sun et al., 2022). These measurements have yet to be incorporated into a model linking motor neuron activity or the activation of muscles to segmental

movements, however, perhaps because the non-rigid body and complex geometric arrangement of muscles lead to an unusal degree of challenge in estimating the effects of muscle strain.

Without a means of exploiting friction against the environment, larvae would not be able to convert their muscle contractions into locomotor movements (Lin and Trimmer, 2010). To do this, they use specialized structures on the ventral body surface called denticles, which serve as anchoring points (Rotheray, 2019; Booth et al., 2024). (They may also use attachment of the mouth hooks into the substrate to provide local anchors at the head end (Sewell et al., 1974), but this anchoring is not thought to contribute much to locomotion (Roberts, 1971; Berrigan and Pepin, 1995), and will not be discussed further here.) Denticles, which are present on all abdominal body segments and segment T3, have the appearance of small teeth; they are arranged in rows called "belts" or "bands" that span the ventral surface of the anterior half of each abdominal segment (Lohs-Schardin et al., 1972; see Figure 1.1). Denticles dig into the surface of a soft substrate and generate local ground reaction forces that anchor the animal (Booth et al., 2024). Using these contact sites as anchoring points, a larva can push itself forward or backward (Lin et al., 2010; Tanaka et al., 2011; Booth et al., 2024). As an aside, the ability to dig into the substrate is not required, as larvae can crawl vertically or even upside-down on hard surfaces as well as on soft. This ability may be due to the surface tension created by a film of water where larvae make contact with a flat surface, although the relative importance of this mechanism is unresolved (Booth et al., 2024). Regardless, it is only in very low-friction environments, such as floating in water, that larvae fail to convert segmental contractions into forward displacement (Sun et al., 2022).

Importantly, the denticle belts can be retracted away from the substrate in order to locally reduce or remove friction, which allows a larva to anchor itself transiently and in the desired locations along the body axis. In other words, when a larva needs to move one or more body segments, it can retract that segment's denticle belts away from the surface to do so. Larvae may achieve this local retraction in one of two ways, whose comparative importance for locomotion remain to be determined. First, they can contract a specialized set of ventral muscles that attach at the location of the denticle belt (Booth et al., 2024). This contraction folds the denticles up into a small indentation of the segment's ventral surface. Alternatively (or additionally), they can contract the above-mentioned transversely-oriented muscles in the same segment, which raises the segment's whole ventral surface (Heckscher et al., 2012).

Putting together the segmented body, the musculature in each segment, and the use of denticles as a means of generating adjustable tension against a surface, we can now provide a slightly more mechanistic overview of how larvae produce locomotor waves. The first step is the contraction of tail (terminal) segments. The tail end moves forward, generating a visceral piston that pushes forward the internal organs and, sometimes, the head end (Simon and Trimmer, 2010; Heckscher et al., 2012; personal observation). Next, larvae produce a wave of peristaltic contractions that pass through body segments in order from tail end to head end (Green et al., 1983). During each segment's contraction, the longitudinally-oriented muscles contract first, followed by the transverse muscles with a delay (Heckscher et al., 2012; Zwart et al., 2016; Zarin et al., 2019). This order of muscle recruitment produces tension in the direction of movement before reducing friction by lifting the ventral surface. The wave ends when it reaches an anterior segment, either T2 or T1; these segments' participation in the wave may be unnecessary (Dixit et

al., 2008; Rotheray, 2019). Thus, a combination of internal tension, orderly segmental contractions and local reductions in friction against the substrate allow an animal with no skeleton to propel itself forward against its environment (van Griethuijsen and Trimmer, 2014).

1.5.3 Locomotor circuits in the CNS

Larvae do not require central brain activity to produce locomotion or turning movements. This has been demonstrated by reversible silencing of activity in the brain lobes and sub-esophageal zone in crawling animals (Berni et al., 2012). Moreover, wave-like neuronal activity propagates unidirectionally along the isolated nerve cord, both forward and backward even in the absence of sensory inputs, including when the brain lobes and sub-esophageal zone have been removed from the preparation (Cattaert and Birman, 2001; Fox et al., 2006; Pulver et al., 2015). Fictive "turning," left-right asymmetric activity in anterior segment motor neurons, also occurs in such preparations (Berni, 2015; Pulver et al., 2015). In contrast to fictive lamprey swimming or leech crawling (Hill et al., 2003; Puhl and Mesce, 2008), no particular substance need be added to physiological saline to evoke fictive waves of locomotion in the isolated larval nerve cord (Fox et al., 2006). The site(s) and mechanisms of wave initiation remain to be demonstrated, but a posterior subset of abdominal segments are competent to produce fictive anterior-directed waves of motor activity in response to mAChR agonists (Jonaitis et al., 2022), offering one possible starting candidate. In summary, similar to most known locomotor models, there exist neural circuits in the ventral nerve cord portion of the larval CNS whose activity is sufficient to drive locomotion.

As in the leech, lamprey, and other locomotor model systems, substantial work has gone into identifying these circuits, as well as the descending or ascending inputs whose activities

contribute to locomotion. For larval Drosophila, much of this advancement has happened in the last decade, aided immensely by two resources in particular. First, a published EM dataset of the nerve cord from a first-instar larva, whose ongoing annotation by the community aims to map the complete nerve cord connectome (Ohyama et al., 2015; Schneider-Mizell et al., 2016). Second, a large number of genetic driver lines, many of whose expression patterns have been imaged and catalogued for researchers to browse (Brand and Perrimon, 1993; Pfeiffer et al., 2008; Li et al., 2014). By identifying driver lines corresponding to nerve cord neurons of interest, multiple research groups (and particularly the Nose lab) have been able to identify a set of interneurons that are likely to be important for larval locomotion, primarily via calcium imaging and optical or thermal manipulations of activity, in most cases paired with annotation of a corresponding neuron in the connectome (e.g., Jovanic et al., 2016; Zwart et al., 2016; Hiramoto et al., 2021).

Numerous reviews exist of the circuitry that has been discovered to date (Kohsaka et al., 2017; Clark et al., 2018; Gowda et al., 2021; Kohsaka, 2023). This section will not aim to reproduce this information, except to illustrate examples of the types and scales of connectivity at play, as well as methods commonly used to investigate the neurons involved and establish their roles in locomotion. Putatively locomotor-related interneurons have been found with connectivity spanning a range of spatial scales: within-segment, between neighboring segments, across multiple consecutive segments, or even ascending the entire nerve cord. (Connectivity is almost always defined using a combination of genetically-driven GFP expression, to define morphology, and annotation of a morphologically matching neuron in the connectome.) Each of these scales of connectivity is presumed to contribute to a certain scale of locomotor coordination, beginning with the intrasegmental.

Several segmentally-repeated premotor interneurons have been identified that synapse, within their own segment, onto groups of motor neurons that innervate longitudinal and/or transverse muscles, and that are rhythmically active before, during, or after motor neurons during fictive locomotor waves (see, e.g., Kohsaka et al., 2014; Itakura et al., 2015; Hasegawa et al., 2016; Zwart et al., 2016). Perturbation of these neurons, either acutely or constitutively, leads to locomotor defects, typically a decrease in locomotor speed. These interneurons have been likened to the CPGs of other locomotor models (Gjorgjieva et al., 2013; Francis et al., 2024). To support larval crawling, rather than producing an alternation of contractions across sides of the body, these interneurons must instruct an ordered contraction first of longitudinal, then of transverse muscles within the same segment, with an appropriate phase delay. Of particular interest for coordinating within-segment contraction phases, an interneuron has been identified that specifically inhibits the motor neurons that innervate transverse muscles (Zwart et al., 2016). Since it was shown using electrophysiology that (selected) motor neurons targeting longitudinal and transverse muscles do not differ in their intrinsic excitability, this inhibitory interneuron is expected to be a major source of the delay between longitudinal and transverse motor neuron firing in each segment (Zwart et al., 2016). Consistent with this hypothesis, constitutive silencing or reduction of these interneurons' activity, via expression of either tetanus toxin light chain or the hyperpolarizing Kir2.1 channel, eliminated the phase delay between contraction of a longitudinal and a transverse muscle in the same body segment (Zwart et al., 2016).

Coordination across segments is likely to be mediated, at least in part, by groups of segmentally-repeated interneurons that send projections into the adjacent segment's neuropil and there synapse onto premotor interneurons. So far, both intersegmental feedforward and feedback

motifs have been found that correspond to this description. The intersegmental feedforward motif involves a pair of interneuron classes, the excitatory "A27h" and inhibitory "GDL" interneurons (Fushiki et al., 2016). Both are present in all abdominal body segments and show rhythmic calcium activity that propagates along the nerve cord during fictive forward crawling; inhibiting either class slows larval locomotion. GDL interneurons are active earlier than motor neurons in their own segment and synapse onto premotor interneurons, including A27h. A27h interneurons synapse onto motor neurons in their own segment, and their spiking was shown to directly excite a longitudinal motor neuron via paired whole-cell recordings. They also synapse onto GDL interneurons in the next anterior segment, setting up a feedforward inhibitory chain: A27h activity in one segment is thought to excite GDL in the next segment, presumably preventing premature activation of premotor and motor neurons in that segment (Fushiki et al., 2016).

The intersegmental feedback motif involves the "Ifb-Fwd" interneurons. These are rhythmically active during fictive locomotion, cholinergic and likely excitatory; they project into the next posterior segment, i.e., opposite to the direction of forward wave propagation (Kohsaka et al., 2019). In the next posterior segment, they target both inhibitory interneurons that are premotor to longitudinal muscle motor neurons and excitatory interneurons that are premotor to transverse muscle motor neurons. Their constitutive hyperpolarization impairs transverse muscle contraction during locomotor waves and slows locomotion. Of note, the same premotor neurons that are targeted by the Ifb-Fwd interneurons are also targeted by a second cholinergic class, called Ifb-Bwd interneurons, that project in the opposite direction (into the next anterior segment), that only show calcium activity during backwards crawling, and whose silencing has similar effects on transverse muscle contractions. This suggests that these two intersegmental

interneurons share a common downstream "module" of premotor interneurons, and that their feedback during forward or backward crawling is involved in timing the transition from longitudinal to transverse muscle contractions (Kohsaka et al., 2019).

At a larger scale of connectivity, interneurons have been identified that project among multiple consecutive segments. The "Canon" interneurons are segmentally-repeated and are active during backward, but not forward, locomotion; they project both directly and indirectly to inhibitory premotor interneurons within their own segment, as well as in up to three segments more anterior (Hiramoto et al., 2021). Because their calcium activity is later than that of motor neurons in the same segment and because their optogenetic activation causes muscle relaxation, they are thought to be involved in ending segments' contractions in a timely manner (Hiramoto et al., 2021). It remains unclear whether a direct counterpart to these interneurons exists for forward crawling.

Finally, recent work has identified a class of interneurons, called "19f," that sends ascending projections along the entire nerve cord as far as the subesophageal ganglion (Jonaitis et al., 2024). As a population, these segmentally-repeated interneurons receive the majority of inputs from premotor interneurons in posterior segments, and form the majority of outputs in anterior segments. They are connected to each other axo-axonically, suggesting they may share information as a population; however, their population activity still shows a wave-like progression during fictive locomotion, and they are active later than motor neurons in their own segment during fictive forward locomotion. Their global optogenetic activation during crawling suppressed head sweeping movements and their optogenetic inhibition promoted head sweeping, in both cases slowing forward locomotion. Based on the above characteristics, they were

proposed to integrate information about an ongoing forward wave and relay this information to anterior segments, preventing conflicting head movements (Jonaitis et al., 2024).

In summary, elements of central circuits have been identified that are likely to play an important role in coordinating locomotor wave propagation and the movements produced by each body segment. First, nerve cord circuits exist that are sufficient to drive locomotor behavior, including waves and turns, without requiring either sensory feedback or descending input from the brain. Second, substantial progress has been made on mapping these circuits, primarily but not wholly relying on connectomics and genetic driver lines that permit functional imaging and acute or chronic perturbation experiments. Third, neuronal coordination across segments appears to involve a range of scales, from within-segment circuit motifs to neurons with projections that span the full nerve cord. Finally, although not discussed above, many of these premotor and other interneurons receive direct synapses from proprioceptive and other mechanosensory neurons, which may be an essential part of how these interneurons coordinate the timing of activity within and across segments. We turn to this topic next.

1.5.4 Sensory feedback in larval locomotion

Larvae rely on a multitude of sensory systems to inform their behavior, most of which are thought to support decision-making and navigation, such as identifying suitable pupation sites or performing the aforementioned chemotaxis, thermotaxis, or phototaxis. These sensory systems can also affect locomotion, broadly speaking, by stimulating a larva to crawl or stop crawling, by affecting its likelihood of performing straight locomotor runs versus re-orienting, or by prompting larvae to crawl faster away from an aversive stimulus. Here, we will focus only on

those neurons that have been shown to be required for locomotor coordination, which are all mechanically-sensitive.

Larvae have an array of mechanically-sensitive neurons tiling their bodies, which they use to sense stimuli like gentle or painful touch, heat and cold, vibrations such as sound waves, and their own movements (Grueber et al., 2002; Yan et al., 2012; Boivin et al., 2023). This latter category of sensors is particularly relevant to the coordination of body segments during locomotion (Hughes and Thomas, 2007; Song et al., 2007). Mechanically-sensitive neurons in larvae are broadly classified into "type I," those with single dendrites, and "type II," those with multiple dendrites (Bodmer and Jan, 1987). Type I neurons are further divided into external sense neurons and chordotonal neurons, based on their associated sensory organs; type II neurons are divided into bipolar dendritic, multidendritic, and tracheal dendritic neurons. External sense and tracheal dendritic neurons have not been associated with a role in locomotor coordination; we will skip these and describe only the remaining three subtypes.

Chordotonal neurons, in larval stages, are associated with one or more cilia-like sensory structures called scolopidia that attach at one end in the epidermis, the cell layer just beneath the cuticle (Singhania and Grueber, 2014). These neurons respond to vibrational movements, including sound stimuli (Zhang et al., 2013; Scholz et al., 2015). They have been alternately characterized as proprioceptors and mechanosensors, and their activity during embryonic development is necessary for larvae to later crawl at normal speeds (Merritt and Whitington, 1995; Suster and Bate, 2002; Caldwell et al., 2003; Warren and Göpfert, 2024). However, acutely silencing these neurons does not seem to impair locomotor speed (Hughes and Thomas, 2007; Song et al., 2007). Moreover, although chordotonal neurons express the mechanosensitive

transduction channel NompC, which is required for normal locomotion, genetic rescue experiments in a global NompC loss-of-function background did not need to reintroduce functional NompC expression into chordotonal neurons to rescue locomotor defects (Cheng et al., 2010); instead, reintroduction of functional NompC only into bipolar dendrite and multidendritic sensory neurons (below) was sufficient to rescue the global loss-of-function defects (Cheng et al., 2010). These negative results suggest that, if chordotonal neurons act as proprioceptors, the feedback they provide may be used for other behaviors than crawling (Warren and Göpfert, 2024).

The type II bipolar dendrite and multidendritic sensory neurons are not associated with additional sensory organs. Instead, they extend dendrites beneath the cuticular surface. Bipolar dendrite neurons have a simple morphology: they extend one dendritic process anteriorly and one process posteriorly, spanning most of the length of a body segment (Bodmer and Jan, 1987). The dorsal bipolar dendrite neuron, as well as its counterpart in *Manduca sexta* larvae, has been shown to respond to body wall stretch (Tamarkin and Levine, 1996; Suslak et al., 2015). The multidendritic neurons are classified, in order of increasingly complex dendritic morphologies, into classes I through IV (Singhania and Grueber, 2014). Each class responds to a distinct (combination of) sensory stimuli: class I multidendritic neurons are proprioceptors, and will be discussed further below. Class II and III neurons respond to different forms of gentle touch and thermal stimuli, and class IV neurons respond to several modalities of noxious stimuli, including noxious light and chemicals (Takagi et al., 2017; Boivin et al., 2023). The locations and numbers of sensory neurons varies by body region, but is consistent across abdominal segments 1-7 (Ghysen et al., 1986; Dambly-Chaudière & Ghysen, 1986; Bodmer and Jan, 1987).

In 2007, two groups independently confirmed that larval locomotor coordination requires the activity of multidendritic sensory neurons, both using reversible thermogenetic silencing of sensory neurons expressing the temperature-sensitive Shibire protein (Kitamoto, 2001). Song and colleagues, as part of a broad screen of genetic drivers, silenced all multidendritic neurons and found defects in larval locomotor coordination: while stride distance was unaffected, cycle periods became longer, segments contracted for longer than usual, and wave propagation became irregular (Song et al., 2007). Similarly, Hughes and Thomas performed a series of sensory silencing experiments, using combinations of genetic driver lines to express temperature-sensitive Shibire in different combinations of sensory neuron classes. They found minor locomotor speed defects when silencing either bipolar dendrite or class I multidendritic neurons separately. When both classes were thermally silenced simultaneously, they found strong speed defects and described a "toothpasting" locomotor phenotype similar to that described by Song and colleagues: larvae contracted body segments more tightly and for longer than usual, and the wave propagated slowly along the body axis. Larvae crawled normally again after the end of thermal silencing (Hughes and Thomas, 2007). Finally, as mentioned above, Cheng and colleagues found greatly slowed crawling in larvae with a loss-of-function mutation in the NompC mechanosensitive transduction channel, which they were able to rescue via functional NompC expression in the bipolar dendrite and class I multidendritic sensory neurons (Cheng et al., 2010). Thus, proprioceptive feedback, specifically from this subset of mechanosensitive neurons, is acutely necessary for timing segments' contractions, as well as determining contraction amplitudes.

Recently, in vivo calcium imaging experiments targeted the bipolar dendrite and class I multidendritic neurons to establish when they are activated during larval locomotion, and how. First, these experiments confirmed that the stretch sensing neuron was most active between segmental contractions, and showed a sequence of activation for the remaining proprioceptors during a segment's contraction (Vaadia et al., 2019). Further, in two of the dorsal multidendritic neurons, He and colleagues showed direction-sensitivity (greater calcium activity in forward crawling, for one, or backward crawling, for the other). They also showed that calcium activity correlated with curvature of the dendrites during movement of the body wall, and that this activity depended on expression of *Tmc*; they proposed that folding of the dendrites as the body wall moves forward or backward leads to Tmc channel activation, enabling proprioception in this pair of neurons (He et al., 2019). Lastly, Vaadia and colleagues proposed an algorithm by which central circuits could compare the activity of this same pair of neurons from either side of the body in multiple segments and generate an internal estimate of a segment's retraction and/or bend angle (Vaadia et al., 2019).

How is proprioceptive feedback used by central circuits to coordinate wave propagation during locomotion? This question remains largely unanswered, as the circuits or neurons that are required to integrate proprioceptive feedback during locomotion have not yet been identified and tested. However, a functional hypothesis was proposed by Hughes and Thomas in 2007, in which feedback that a segment has successfully contracted is sent both within-segment, to promote the end of contraction, and to the following segment, to promote that segment's contraction.

Two recent models of larval locomotion formalized this predicted role for proprioceptive feedback in two different ways (Gjorgjieva et al., 2013; Pehlevan et al., 2016). Both models

featured coupled Wilson-Cowan oscillatory units as the backbone of segmental activity (Wilson and Cowan, 1972) and initially demonstrated arrangements of these units that could propagate directional waves without any sensory feedback. The first model incorporated stretch feedback as a sensory unit in each segment activated by greater excitatory activity in neighboring segments; by incorporating this feedback, the modeled wave propagation was made more robust to different intersegmental connectivity strengths and levels of inhibitory activity (Gjorgjieva et al., 2013). The second model incorporated contraction feedback by activating a sensory unit in each segment when its segment shortened below a threshold length; the sensory unit then excited both the within-segment inhibitory population and the next-segment excitatory population (Pehlevan et al., 2016). This model likewise found a broader range of connectivity parameters that could produce forward waves with the inclusion of sensory feedback, and that sensory feedback tended to reduce variance in wave propagation between different starting parameters. Thanks to the inclusion of muscle and friction components in the second model, it was able to make additional predictions, including that larval stride distance and segmental contraction amplitudes would increase on substrates of decreasing friction. These predictions remain to be experimentally tested.

In summary: proprioceptive neurons are not necessary for locomotion, nor for the propagation of waves of fictive locomotion in the isolated nerve cord, but as a group they are necessary for normal wave propagation and segmental contraction amplitudes in the behaving animal. How they sense self-movement is beginning to be understood, but has not been characterized for all proprioceptors. Existing models for incorporating proprioceptive feedback

into locomotion can use either stretch or contraction length feedback to match experimental data on wave propagation, but no model yet incorporates both.

1.5.5 Outstanding questions and goals of this thesis

In summary, a large body of work has already been produced in the larval Drosophila model to advance our understanding of locomotor control and segmental coordination in these animals. The field has made important strides in mapping neuronal circuits and identifying neurons whose activities are likely essential for coordinating locomotion; in assessing the contributions of various sensory neurons to locomotor control, both in terms of high-level decision-making and the coordination of segmental movements; and in characterizing the larva's motor apparatus, including motor neurons and their control of muscles, muscle properties, and the interactions with the larval environment that enable these limbless, soft-bodied animals to move. Therefore, the larva is well-poised as a modern neuromechanical model for investigating both neural and physical sources of locomotor coordination. However, important gaps remain that must be filled to understand how larvae coordinate the movements of their body segments for this fundamental behavior, and to be able to compare the strategies larvae use to those used by other model systems.

One such major gap is how sensory feedback, particularly proprioceptive feedback, is incorporated into locomotor control. Both the anatomical pathways that route proprioceptive feedback into locomotor circuits, and the effects that this feedback has on ongoing circuit activity, remain to be elucidated. In Chapter Two, we make progress on the anatomical routing of proprioceptive feedback to locomotor circuits, as well as characterizing anatomical properties of

proprioceptive projections and synapses that are likely to affect downstream proprioceptive processing.

Another major gap is in the ability to link what is known about central neuronal activity to the movements ultimately produced by the body. As mentioned earlier, a wealth of measurement exists on the properties of motor neuron transmission at the neuromuscular junction, and on excitation-contraction coupling in muscles. Nonetheless, because the production of movements depends intimately on the body's own properties and its interactions with environment, it is quite complicated to predict movements from neural--or even muscular--activity. Therefore, data are needed in intact, moving animals that link muscle activity to movements. However, in crawling larvae, the relationship between muscle activity and the segmental movements that result remains all but uncharacterized (Zarin et al., 2019). Without a clearer picture of how muscle recruitment relates to the movements produced by a larval body moving through its environment, models of central circuit activity, and even of motor neuron activity, will remain only abstractly linked to behavior.

It has been challenging to acquire data about the relationship between muscle activation and movement in the Drosophila larva. This is because the animals' small size, and the fact that breaching the cuticle can lead to loss of internal hydrostatic pressure, damaging animals' abilities to move (Holmes, 1905), conspire to make electrode recording from muscles difficult to impossible in the intact, moving larva. Therefore, in the third chapter, we introduce a method designed to provide such data. The method involves constraining larvae to crawl inside channels not much wider than their bodies and relies on calcium imaging to provide muscle recruitment data; its particular advantages and drawbacks will be discussed in detail in that section. In the

fourth chapter, we use this method to produce the first segment-level comparison of muscle recruitment and contraction kinematics.

Another gap in the study of larval locomotor coordination is largely conceptual. While substantial work has gone into characterizing how larvae produce an average locomotor wave, no work has been done attempting to characterize or leverage the diversity of locomotor waves produced: in other words, to analyze patterns of segmental coordination across many cycles of locomotion, whether in terms of neural activity, muscle recruitment, or segmental kinematics. In larval crawling, statistical analyses of large numbers of locomotor cycles have been restricted to studies of whole-animal behavior, such as the analyses of runs and re-orientation events that led to elucidating the sensory decision-making algorithm larvae use for chemotaxis and thermotaxis (Luo and Gershow et al., 2010; Gomez-Marin et al., 2011). Meanwhile, in other locomotor models, comparisons of large numbers of locomotor cycles have been used to reveal kinematic features that animals co-modulate across cycles to control locomotor speed and gait (Mendes et al., 2013; Severi et al., 2014), as well as to identify changes to locomotor coordination that arise from genotypic variation (Ahamed et al., 2021; Harel et al., 2024), from presentation of particular sensory stimuli (Schwarz et al., 2015; DeAngelis et al., 2019) or from targeted perturbations, such as to proprioceptor subtypes (Mendes et al., 2013). Thus, by not similarly scaling up the analysis of segmental coordination to ask what patterns emerge across a large number of cycles (or across individuals, larval stages, etc.), the larval locomotor field is missing an opportunity to, in a manner of speaking, ask behaving larvae to tell us what aspects of their locomotion they care or do not care to coordinate.

In Chapter Four, we advance this approach to investigating locomotor coordination in the context of larvae crawling inside agarose channels. We collect over 2500 locomotor cycles across animals, and use these to investigate features of segmental contractions that are more and less strongly coordinated across the body on a cycle-to-cycle basis. Among other results, this approach reveals unanticipated differences in the coordination of anterior and posterior segments, arguing against the commonly-modeled assumption of identical abdominal units and arguing for a scaled-up statistical approach to studying locomotor behaviors, even in their most constrained forms.

CHAPTER 2

THE CENTRAL SYNAPTIC ORGANIZATION OF DROSOPHILA LARVAL PROPRIOCEPTORS

This chapter originally appeared, in modified form, as the following publication:

Greaney, M.R., Wreden, C.C., Heckscher, E.S., 2023. Distinctive features of the central synaptic organization of *Drosophila* larval proprioceptors. Front. Neural Circuits. doi: 10.3389/fncir.2023.1223334

Author Contributions: The author of this dissertation developed and performed the analyses and wrote the manuscript.

2.1. Introduction

Locomotion critically requires feedback from multiple morphological types of proprioceptors that sense different features of the body's posture and movement (Rossignol et al., 2005; Mendes et al., 2013; Akay et al., 2014; Bidaye et al., 2017). While loss of one type or another separately has minimal effect, the loss of multiple types produces severe locomotor deficits (Hughes and Thomas, 2007; Akay et al., 2014; Santuz et al., 2019), demonstrating that information from multiple proprioceptive neuron types is combined centrally for locomotor control. Despite their importance for locomotion, relative to other sensory neurons, little is understood about how proprioceptive neurons are anatomically organized once they project into the central nervous system (CNS). The question of sensory mapping has long been fundamental to our understanding of sensory processing (Hildebrandt, 2014; Giessel and Datta, 2014;

Knudsen et al., 1987; Hubel and Wiesel, 1962); but we know little about whether, or what form of, topographical maps exist for this essential sense.

Decades of work on proprioceptive circuits has built up a general picture of how proprioceptive afferents project into the CNS. These studies have largely relied on single-neuron tracing and electrophysiological approaches (Scheibel and Scheibel, 1969; Burrows, 1975; Brown and Fyffe, 1978; Hustert, 1978; Brown and Fyffe, 1979, Conradi et al., 1983; Watson and Bazzazz, 2001) and recently have been complemented by genetic techniques, especially in mice and flies (Smith and Shepherd, 1996, Niu et al., 2013, Agrawal et al., 2020, Surmeli et al., 2011). Certain anatomical principles regarding afferent projections hold across animal systems: first, like afferents of other sensory systems, proprioceptors receive synapses from inhibitory neurons (Pearson and Goodman, 1981; Burrows and Matheson, 1994; Clarac and Cattaert, 1996; Eggers et al., 2007; Wilson, 2013; Fink and Azim, 2014; Chen et al., 2021). Second, proprioceptive afferents are largely segregated from exteroceptive afferents (Brown, 1981; Pflüger et al., 1988; Murphey et al., 1985). Third, afferent projections diverge based on proprioceptor type (Brown, 1981; Murphey et al., 1985). Fourth, individual proprioceptor afferents often project to multiple locations (Burrows and Pflüger, 1988; Jankowska, 2008). Lastly, in addition to diverging, proprioceptors can converge in their connectivity, providing common input to downstream neurons that receive synapses from multiple proprioceptor types (Lundberg 1979, Jankowska 1992, Gebehart et al., 2021).

Beyond these principles, however, prior mapping efforts have revealed a complicated spatial organization of proprioceptor afferents (Scheibel and Scheibel, 1969, Edgely and Jankowska, 1984; Pflüger et al., 1988; Prasad and Wiener, 2011; Wu et al., 2021) that does not

resemble the structured, feature-based mapping seen in other sensory systems. In part because of this complexity, we have only a partial understanding of afferent anatomy, even in what is arguably the best characterized of any proprioceptive CNS region, the locust thoracic ganglia (Tyrer and Gregory, 1982, Pflüger et al., 1988, Bidaye et al., 2017). Two limitations have impeded the anatomical mapping of proprioceptors into the CNS. First, only a single cell or cell type is typically mapped at a time, providing a piecemeal rather than integrative representation of how proprioceptive central axonal projections are anatomically organized (Fyffe and Light, 1984, Smith and Shepherd, 1996, Bidaye et al., 2017). This is particularly problematic for understanding the extent and form of divergence and convergence. Second, most mapping studies do not characterize the anatomical synapses, which are the actual sites of chemical information transfer; this gap may obscure organizational principles that would emerge at the synaptic level of anatomy. We could therefore gain substantially from mapping all proprioceptors simultaneously at synaptic resolution.

This study aims to map the input and output synapses of all types of Drosophila larval proprioceptors. Comprehensive mapping at the synaptic level of detail is possible in this system thanks to the availability of an electron micrographic dataset and connectome (Saalfeld et al., 2009, Ohyama et al., 2015, Schneider-Mizell et al., 2016). Moreover, because larvae are a relatively transparent genetic model, they are amenable to non-invasive, light-based techniques for probing circuit function, such as calcium imaging and optogenetic manipulation (Jovanic et al., 2016, He et al., 2019, Vaadia et al., 2019, Tadres and Louis, 2020). Non-invasive techniques are especially important for studying how the sensing of self-movement by proprioceptors tunes locomotive behavior. Therefore, a better understanding of proprioceptors in Drosophila larvae

will ultimately complement and enable developmental and functional studies of proprioception, locomotion, and the underlying circuit-level mechanisms. Like other animals, Drosophila larvae have multiple types of proprioceptors which sense various features of movement (Grueber et al., 2002, Suslak and Jarmon, 2015, He et al., 2019, Vaadia et al., 2019); these proprioceptors are critically needed for larval locomotion (Song et al., 2007, Hughes and Thomas, 2007). Also as in other systems, functional (Hughes and Thomas, 2007) and anatomical (Schrader and Merritt, 2000; Grueber et al., 2002; Grueber et al., 2007) evidence suggests we will likely observe convergence among proprioceptor output synapses. However, we do not know to what extent output synapses will intermingle in space, nor what other features may organize their inputs. Therefore, we asked how proprioceptor synapses are organized, using the larval connectome to answer this question.

In this study, we reviewed and added to the available connectomic data for larval proprioceptors (Ohyama et al., 2015). We focus on six proprioceptive neurons: dorsal bipolar dendrite (dbd), ventral bipolar dendrite (vbd), dorsal dendritic arbor D (ddaD), dorsal dendritic arbor E (ddaE), ventral posterior dendritic arbor (vpda), and dmd1 (Ghysen et al., 1986, Grueber et al., 2003). First, we describe output synapse locations; we find that, as a rule, Drosophila larval proprioceptors have synapses distributed along the incoming afferent, at both proximal and distal locations of the axon (Figure 2.1). We then map the distribution of proprioceptors in three consecutive body segments. Generally, the output synapses for each type of proprioceptor are organized according to a principle of left-right segmental somatotopy (Figure 2.2). Next, we map the overlap among output synapses from all proprioceptors within a single segment. Drosophila larval proprioceptor output synapses intermingle extensively in space; different combinations of

output synapses contribute to six different spatial domains. Every proprioceptor type contributes synapses to at least two domains, and all but two domains have synapses from two or more proprioceptor types. This details the specific topography of convergence and divergence in the larval proprioceptive system (Figure 2.3). We also map proprioceptors' input synapses, finding little evidence of presynaptic inhibition onto Drosophila larval proprioceptors (Figure 2.4). Finally, we compare the inputs and outputs of the proprioceptive neurons to other larval somatosensory neurons: those of chordotonal and class IV multidendritic neurons (Figures 2.5-2.6). The principles of proximal axonal output, segmental somatotopy, and minimal presynaptic input do not apply broadly to larval somatosensory neurons. Thus, we have identified a suite of anatomical features that distinguish Drosophila larval proprioceptors from other larval somatosensors.

Taken together, our results reveal anatomical features that are potentially unique to larval proprioceptive processing. They open avenues to study the development and functional organization of proprioceptive circuits and offer an example of the utility of the larval connectome for uncovering fundamental cell biological observations.

2.2. Results

2.2.1. Output synapses of Drosophila larval proprioceptors show a complex spatial organization

Proprioceptors provide essential feedback about the body's movements, but how this information is incorporated into central proprioceptive processing circuits remains poorly understood. Here, we ask what principles underlie the spatial organization of proprioceptor input

and output synapses in Drosophila larvae. To begin, we review specifics of the Drosophila larval body and how it moves: Drosophila larvae are left-right symmetrical and segmented, with much of the muscular and sensory anatomy repeated across body segments (Figure 2.1A) (Bodmer and Jan, 1987; Ghysen et al., 1986; Campos-Ortega and Hartenstein, 1997). All three major modes of locomotion in Drosophila larvae—forward crawling, reverse crawling, and lateral rolling—involve sequential contraction of adjacent segments (Heckscher et al., 2012; He et al., 2022, Cooney et al., 2023). Segments are grouped into regions, including the anterior thorax with segments T1-T3 and the midbody abdomen with segments A1-A7. The nerve cord mirrors this organization: neuronal somata and axons and dendrite-rich central neuropil are grouped into regions corresponding to each body segment.

To monitor the movement of the larval body, in the periphery, each body segment contains left-right pairs of somata and dendrites belonging to six proprioceptors: ddaD, ddaE, vpda, dbd, vbd, and dmd1. The neurons from each segment initially project into that segment's region of the neuropil (Figure 2.1A). Within the neuropil, proprioceptive neurons terminate in a region more dorsal compared to other somatosensory neurons' projections, herein the **"central domain"** (Figure 2.1B) (Merritt and Whitington, 1995; Schrader and Merritt, 2000; Landgraf et al., 2003). The available Drosophila larval connectome (Ohyama et al., 2015) allows the discovery of proprioceptor synapse locations with nanometer resolution. In the connectome, proprioceptor axons and synapses in A1 were already reconstructed (Heckscher et al., 2015; Schneider-Mizell et al., 2016; Zarin et al., 2019). Due to the intersegmental nature of Drosophila locomotion (Heckscher et al., 2012), however, we need a map of proprioceptor synapses from multiple adjacent segments. Here, we reviewed the existing A1 annotations and added T3, A2,

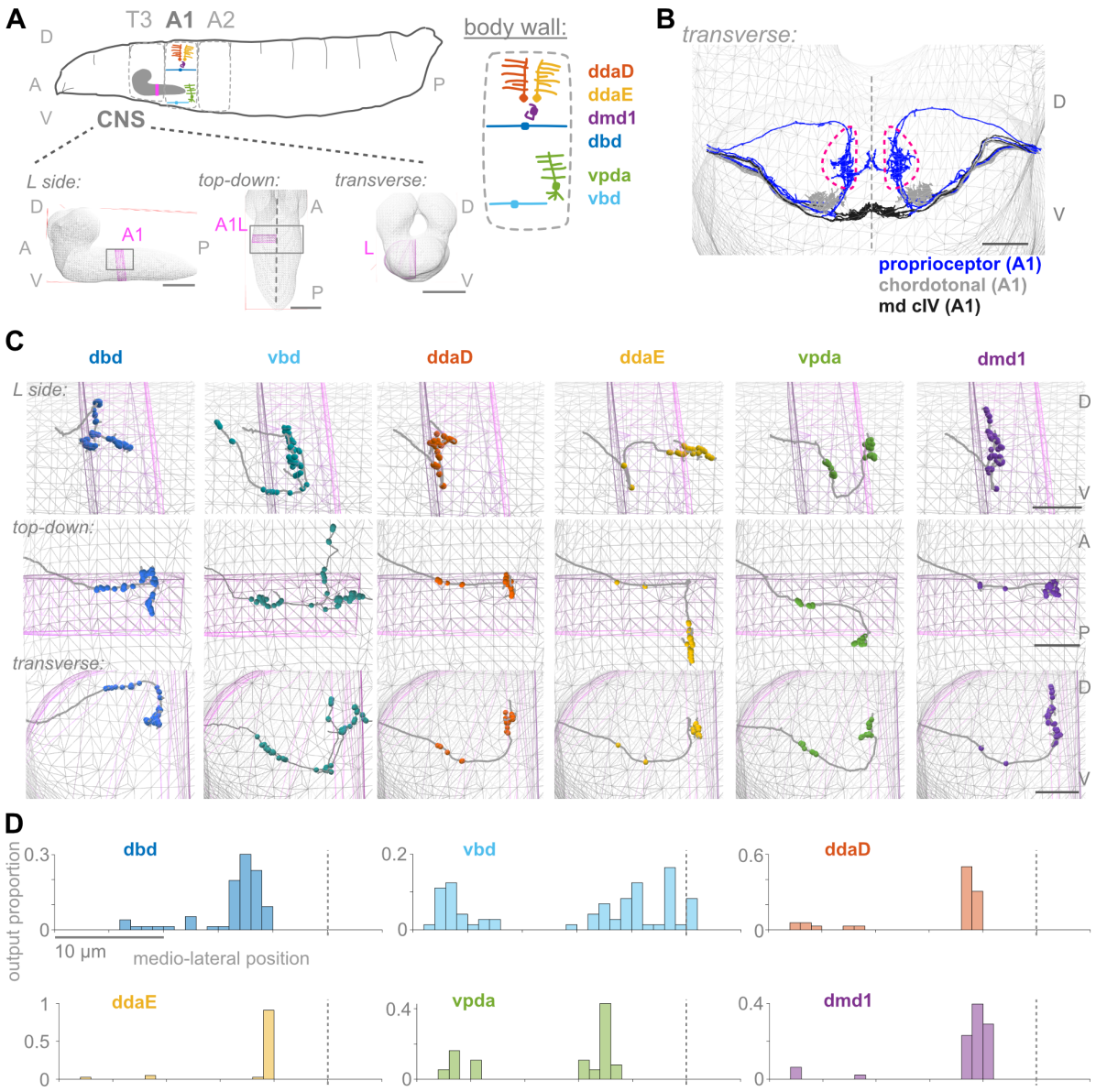

Figure 2.1: First abdominal segment proprioceptor output synapses are distributed along the proximal and distal axon. **A)** Diagrams of larval body plan, of proprioceptive neuron somata and dendrites at the larval body wall (adapted from Cheng et al. 2010, Vaadia et al. 2019), and of views of the larval CNS. The same six proprioceptive neurons are present in each abdominal hemisegment (here, A1 left). They project to neuropil segment A1 in the CNS, highlighted in pink. **B)** Transverse view of reconstructed skeletons (axonal projections) in A1 of the larval connectome: proprioceptive neurons (blue), chordotonal neurons (grey), and class IV multidendritic neurons (black). Dashed pink lines demarcate the "central domain" of proprioceptive outputs. Dashed grey line: midline. **C)** Three views of output synapses in the CNS made by each left side proprioceptor. Grey lines: neuron skeletons. Spheres: output synapse locations. Top subpanels: left side views; middle subpanels: top-down views; bottom-subpanels: transverse views, looking from the tail towards the head. Grey mesh: outline of larval CNS. Pink mesh: outline of A1 left side region of neuropil. **D)** Distribution of output synapses along the mediolateral axis for left side A1 neurons shown in (C). Proportion of that neuron's outputs made in 1 µm bins along the X axis of the connectome. Views in B, C generated using CATMAID (Saalfeld et al.,

Figure 2.1, continued. First abdominal segment proprioceptor output synapses are distributed along the proximal and distal axon.
2009). In A: scale bars = 50 µm; B and C: scale bars = 10 µm; scale bars equal for all axes. Throughout, dashed vertical lines: midline. D = dorsal, V = ventral, A = anterior, P = posterior, L = left side; T3, A1, A2 = body segment abbreviations.

and in some cases, A3 proprioceptive neurons (see Figure 2.2). We sought to understand the spatial organization of proprioceptor output synapses through these main lenses: individual proprioceptors within a segment (Figure 2.1); comparing individual proprioceptor types across segments (Figure 2.2); what information converges in spatial domains of the neuropil (Figure 2.3); inputs onto proprioceptors (Figure 2.4); and which features are common to Drosophila larval somatosensory neurons and which are unique to proprioceptors (Figure 2.5-2.6).

2.2.2. Proprioceptor output synapses are distributed along the length of the axon

To begin our characterization, we describe the positions of output synapses made by each A1 proprioceptor (Figure 2.1C-D). We looked for the distribution of outputs along the axon and whether synapses respect approximate midline and segment boundaries. The six proprioceptors under study belong to three morphological classes, which we use to organize the following description of their outputs. We give counts for the left side neuron of each left-right pair, although right side counts are similar (Appendix B, Table 1).

Two proprioceptor types belong to the bipolar dendrite class, dbd and vbd; these have dorsal and ventral dendrites, respectively. dbd is the only proprioceptor to project into the neuropil along a dorsal route (Figure 2.1) (Schrader and Merritt, 2000), and is also the only stretch receptor of the six (Tamarkin and Levine, 1996; Simon and Trimmer, 2009; Suslak and Jarmon, 2015; Vaadia et al., 2019; He et al., 2019). dbd projects medially along the dorsal route until it reaches the proprioceptor domain. It then descends ventrally and bifurcates, sending

branches both anterior (into neuropil segment T3) and posterior (Schrader and Merritt, 2007). dbd A1L makes 12 of its synapses (16%) along the proximal axonal entry route, with the remaining synapses in the dorsal portion of the A1 central domain. vbd projects into the neuropil along the more posterior of two ventral entry routes. While still ventral to the central domain, vbd bifurcates, sending one branch anterior (into neuropil segment T3), and the other dorsal towards the midline of A1, which it crosses. vbd is the only proprioceptor to cross the midline. vbd A1L makes 27 of its synapses (37%) along the proximal axonal entry route, 8 of its synapses ventrally at a medial location on the way to T3, 8 anteriorly in segment T3, 10 in the A1 proprioceptor domain, and the remaining 20 near the A1 midline. We conclude that neurons of the bipolar dendrite class distribute their synapses along both the proximal and distal axons upon entering the neuropil.

Three proprioceptor types belong to the class I multidendritic neurons (herein md cI), ddaD, ddaE, and vpda; these have dorsal-posterior, dorsal-anterior, and ventral dendrites, respectively (Figure 2.1A) (Grueber et al., 2007). ddaD and ddaE project into the neuropil along the anterior of the two ventral entry routes. Both project medially until the central domain, then turn and project dorsally. At this point, ddaD makes synapses in the A1 central domain, while ddaE turns again and projects posteriorly, making synapses in the A2 central domain (Supplementary Figure 2.1). ddaD and ddaE A1L both make synapses along their proximal entry route (19% and 7% of their total output synapses, respectively), but tend to make fewer relative to the other proprioceptors (Figure 2.1C, 2.2A; see also Figure 2.5B). vpda projects into the neuropil along the posterior of the two ventral entry routes and projects medially until the A1 central domain. Then, it turns dorsally and again posteriorly, making synapses in the A2 central

domain. vpda A1L makes 12 of its synapses (32%) along the proximal entry route and the remaining synapses posterior to the A1 central domain. We conclude that, like the bipolar dendrite class of neurons, md cI proprioceptors also have synapses along both proximal and distal axons.

One proprioceptor type, called dmd1, is not grouped into morphological classes with the other neurons (Grueber et al., 2003). dmd1 projects into the neuropil along the anterior of the two ventral entry routes, then medially until the A1 central domain, and again dorsally. dmd1 A1L makes most of its synapses in a narrow dorsoventral column that stays within the A1 central domain, with the remaining 4 synapses (10%) along the proximal entry route. We conclude that dmd1 proprioceptors also have synapses along both proximal and distal axons.

2.2.2.1. Do output synapse locations differ in other segments?

In Drosophila larvae, anterior-posterior differences exist among body segment muscles and sensory neurons (Bodmer and Jan 1987; Ghysen et al., 1986; Campos-Ortega and Hartenstein, 1997). Moreover, different body segments can participate differently in larval behaviors (Lahiri et al., 2011; Heckscher et al., 2012). Therefore, there are likely to be differences in proprioceptor output synapse number or organization between segments. First, segment T3 lacks a vbd neuron. Second, dmd1 neurons from T3 make more synapses along the proximal axon entry route than abdominal dmd1 neurons. Third, vpda neurons from T3 make extra lateral synapses relative to abdominal vpda neurons. Lastly, ddaD neurons from A2 follow a different pattern than those from A1 or T3, projecting anteriorly and making synapses extending into the central domain of A1. ddaD from A3 shows a pattern similar to ddaD from A2. In contrast, three proprioceptors—dbd, ddaE, and dmd1—did not display segment-specific

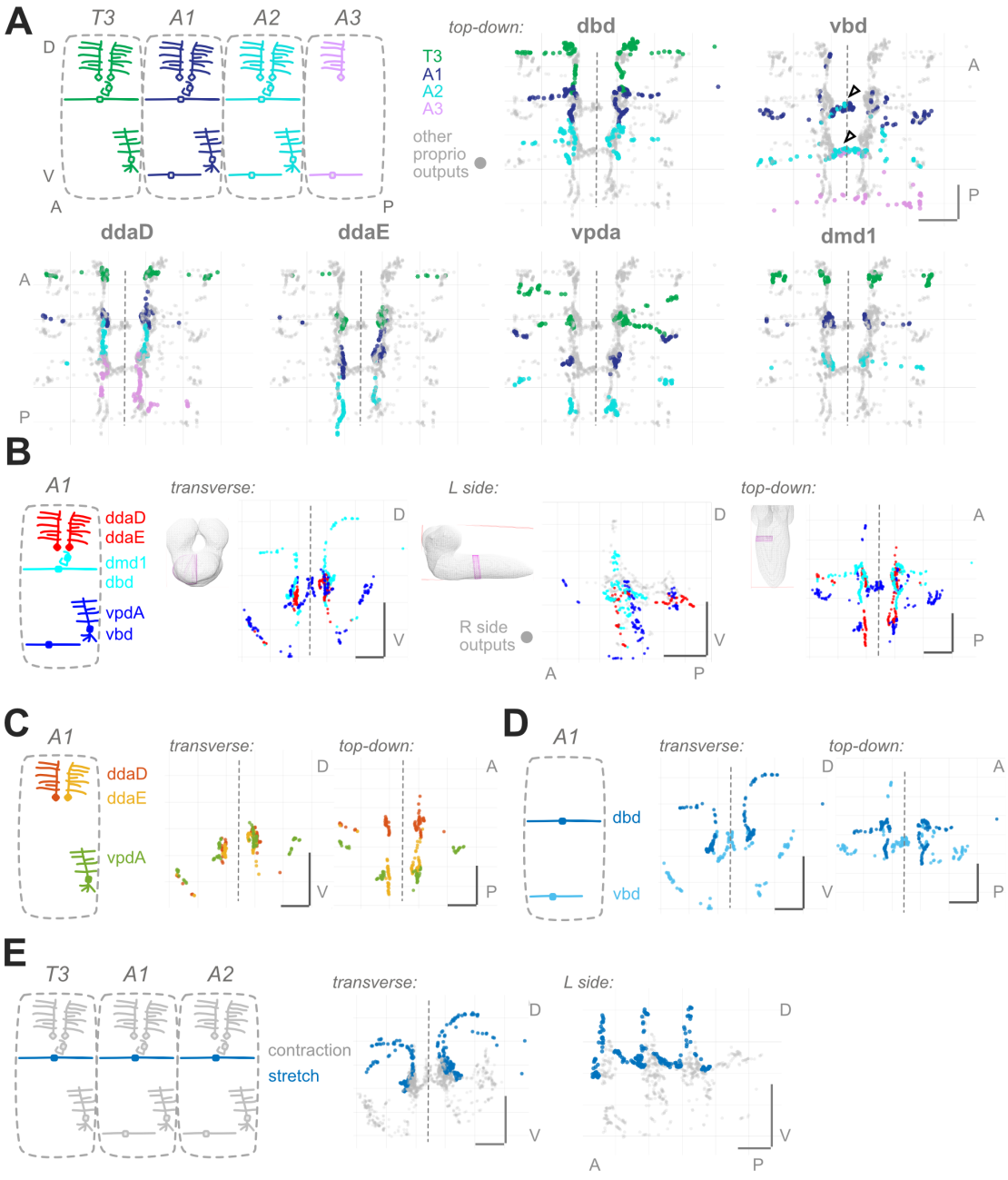

Figure 2.2: Proprioceptors show hemisegmental, but not dorsoventral or within-class, somatotopy. **A)** Each proprioceptive neuron's output synapses from segments T3-A2 or T3-A3 (for ddaD and vbd). Diagram: color scheme for neurons' outputs from each segment; all other proprioceptor outputs plotted in grey. Note that vbd does not exist in T3. Top-down views are shown for each neuron type individually. Both left and right side neurons' outputs are plotted. Black (unfilled) arrowheads show locations of segmental overlap for vbd neurons. Scale bars are same for all views. **B)** Three views of output synapses from A1 proprioceptive neurons colored by approximate dorsoventral dendrite position at the body wall (diagram). For left side view only, right side neurons are plotted in grey. **C)** Two views of output synapses from A1 class I multidendritic neurons, colored according to diagram. **D)** Two views of output synapses from A1 bipolar dendrite class neurons, colored according to diagram. **E)** Two views of output

Figure 2.2, continued. Proprioceptors show hemisegmental, but not dorsoventral or within-class, somatotopy.
synapses from stretch-sensing T3-A2 dbd neurons (blue), compared to contraction-sensing proprioceptor output synapses (grey). Throughout: scale bars = 10 μm. Dashed vertical lines: midline.

characteristics. We conclude that a subset of proprioceptors has segmentally specific output synapses, and this segmental specificity is distinctive for each neuron.

In summary, proprioceptor output synapses are distributed along the length of the axon. This distribution is most often into two groups: typically, a smaller set of output synapses along the proximal axon and a higher concentration of output synapses at the distal tips. Two of the six (ddaD and dmd1) respect A1 hemisegmental bounds, while the other four extend beyond the anterior or posterior boundary of A1, and vbd alone crosses the midline (Figure 2.1C). Additionally, the output synapse distributions seen in A1 are generally representative, but certain proprioceptors display segment-specific features (Figure 2.2A).

2.2.3. Proprioceptor output synapses, regardless of type, morphological class, or function, show hemisegmental somatotopy.

Having characterized output synapse locations for individual proprioceptors from a single segment and compared these across segments, we next compared within-segment output synapse locations across proprioceptor types. We looked for spatial organization in any of the following forms: (1) Many sensory systems display a form of somatotopy in which relative sensor positions are maintained centrally. Since different larval proprioceptors monitor different dorsal-ventral positions within a segment's body wall, we might see a corresponding map of output synapses in the neuropil. (2) Beyond somatotopy within a segment, we might see somatotopic organization across segments, since segments can be considered anterior-posterior "units" of the larval body.

We might additionally see organization that keeps the information from each side of the body (left and right) spatially separated, potentially to be used in left-right symmetrical circuits. (3) Outputs may be organized within a morphological class (e.g., bipolar dendrite neurons). In the peripheral body wall, somatosensory dendrites from the same morphological class send dendrites to different regions of space by a mechanism of active avoidance (Grueber and Sagasti, 2010). Analogous mechanisms may separate within-class outputs in the CNS. (4) Outputs may be organized by function. In the case of larval proprioceptive neurons, function and morphological class are not synonymous (He et al., 2019; Vaadia et al., 2019). Here, we ask which of the above principles, if any, govern where individual proprioceptors form their output synapses.

2.2.3.1. No evidence for dorsal-ventral somatotopy within segments

Because the larval body wall is roughly two-dimensional, we consider somatosensory dendrites as having a Dorsal-Ventral (D-V) or Anterior-Posterior (A-P) mapping. Two of the proprioceptors cover the full A-P extent of the segment with their dendrites; these could not readily be classified as "anterior" or “posterior”. Therefore, we compare all proprioceptors within a segment, focusing on D-V mapping. We grouped the six proprioceptors into three groups based on their relative dendrite positions. All groups intermingle extensively in the A1 central domain (Figure 2.2B, Supplemental Figure 2). We did not observe any axis along which there was a conservation of order from the periphery. We conclude that there is no evidence of a dorsoventral somatotopy among proprioceptors.

2.2.3.2. Proprioceptor synapses display hemisegmental somatotopy

Here, we looked for somatotopy at the level of hemisegments, where a hemisegment refers to the right or left half of a single segment. Comparing the output synapse locations of T3,

A1, and A2 segment proprioceptors, all individual dorsal proprioceptor types (dbd, ddaD, ddaE, and dmd1) display little overlap (Figure 2.2A, Supplementary Figure 3). Ventral proprioceptors are an exception: (1) vbd synapses from A1 and A2 overlap in the A1 midline (Figure 2.2A, arrowheads), and this pattern continues for vbd synapses from A2 and A3. (2) vpda synapses from T3 and A1 overlap in a ventral-lateral region (Figure 2.2A), but the pattern does not continue further posterior. We conclude that, in general, individual proprioceptors of the same type have little overlap in their output synapse positions and thus observe hemisegmental somatotopy.

2.2.3.3. Bipolar dendrite but not multi-dendritic class I output synapses are separated within their morphological class

Proprioceptors comprise multiple morphological classes. At the body wall, dendrites from neurons within a morphological class are well separated. Here, we ask whether a similar separation applies to the outputs within the CNS. Among the morphological class of md cI neurons (ddaE, ddaD, vpda), output synapses intermingle extensively (Figure 2.2C). ddaD and ddaE synapses overlap in the ventral region of their shared axonal entry route. Within the central domain, ddaD synapses also overlap extensively with ddaE and vpda synapses from the next anterior segment (Supplementary Figure 2.1). By contrast, among bipolar dendrite neurons, outputs are largely separated: dbd outputs remain at the dorsal margins of the central domain, while most vbd outputs are either more ventral or medial than dbd outputs (Figure 2.2D). Overall, we conclude that within-class separation of output synapse locations is seen for bipolar dendrite, but not for md cI proprioceptors, and thus does not represent a general principle in organizing proprioceptor outputs.

2.2.3.4. Stretch receptors partially separate their outputs from those of contraction receptors

Proprioceptive synapses might be organized centrally following their function, rather than by morphological class per se. In many systems, morphological class and function are linked (Tuthill and Azim, 2018), but in larval Drosophila, they are not. For instance, dbd and vbd are in the same morphological class, but dbd is the only known stretch receptor among all proprioceptors, including vbd (Vaadia et al., 2019). We compared dbd's output synapse locations to those of the remaining five, contraction-sensing proprioceptors. dbd's outputs along the dorsal axon entry route are well separated from those of other proprioceptors (Figure 2.2E). By contrast, the remainder of dbd's outputs are in the A1 central domain, in close proximity to outputs of ddaD, dmd1, and occasionally vbd. Therefore, we see a partial separation of stretch and contraction neuron outputs.

Overall, the main organizing principle that applies to all proprioceptors, regardless of type, morphological class, or function, is hemisegmental somatotopy.

2.2.4. Proprioceptor output synapses display a convergent and divergent spatial organization.

Information from a single proprioceptive sensor is rarely used in isolation; rather, combinations of proprioceptors are thought to convey information about the state of a body region (Boscoe and Poppele, 2001; Jankowska 2008). There is functional evidence in Drosophila that proprioceptive information is used in combination (Hughes and Thomas, 2007). Further, given our observations (Figure 2.1) that proprioceptors distribute their synapses widely along their axons, including areas beyond the previously-described “central domain” (Figure 2.1;

Merritt and Whitington, 1995; Zlatic et al., 2009), we expect proprioceptive information is likely distributed and combined in space. We first examined adjacent segments to determine where synapse outputs overlap in space (Figure 2.3A). There is extensive interdigitation across segments, much of which seems to occur in the central domain region of each segment; e.g., outputs from both adjacent segments contribute to the A1 central domain. We next looked within a single hemisegment (A1 L or R) at the outputs of the six proprioceptors from that hemisegment to identify where these outputs converge (Figure 2.3B). We noticed convergence in the A1 central domain and in multiple locations more ventrolateral and more posterior. Finally, we combined these approaches to determine which neurons contribute to the cross-segment overlap and in which spatial domains (Figure 2.3C), described below.

A1 proprioceptors contribute to six spatial domains (some of which also contain outputs from T3 and/or A2 proprioceptors). For each domain, based on the neurons that contribute output synapses, we reconstructed the domain's expected "receptive field" at the body wall (Figure 2.3D). The domains, their contributing proprioceptors, and predicted receptive fields are as follows: (1) The **dorsal domain** in A1 receives information from only one A1 proprioceptor (dbd), and forms along dbd's dorsal axonal entry route; this domain is predicted to contain information about segment stretch. (2) The **midline domain** in A1 also receives information from only one A1 proprioceptor (vbd), but forms at the distal tips of vbd axons rather than along the proximal entry route. A2 vbd also contributes to this domain. The midline domain is predicted to contain bilateral information about ventral contraction. In contrast to the dorsal and midline domains, (3) the **ventral-anterior** and (4) **ventral-posterior** domains in A1 receive information from multiple proprioceptors. These domains, which are along the ventral axonal

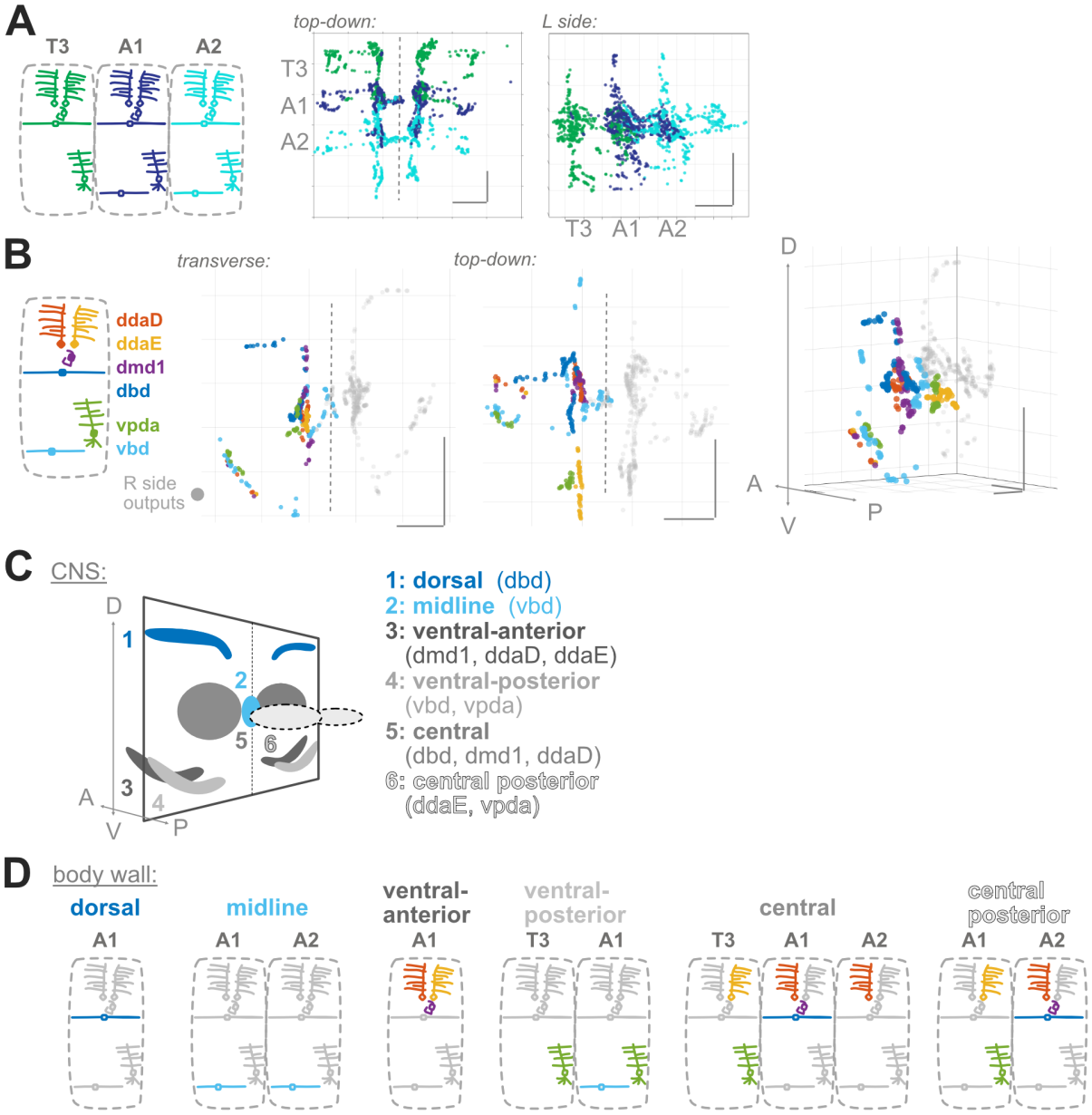

Figure 2.3: Proprioceptor outputs converge in unique combinations in multiple spatial regions. A) Two views of overlap in output synapses from segments T3-A2, colored according to diagram. **B)** Three views of overlap in output synapses from all six left side proprioceptors in A1, colored according to diagram. Right side outputs plotted in grey. **C)** Summary diagram of six spatial domains where unique combinations of A1 proprioceptor outputs converge, names and contributing A1 proprioceptors given beneath image. Note that some of these domains will also contain outputs from T3 or A2 proprioceptors. **D)** Corresponding dendritic "receptive fields" of the six spatial domains in (C). Depicted for each spatial domain are the segment and cell type identity of the neurons that typically contribute output synapses in that area. Throughout: scale bars = 10 µm.

entry routes, are predicted to contain information about dorsal contraction and ventral contraction, respectively. (5) The **central domain** receives information from multiple A1 proprioceptors and proprioceptors originating in adjacent body segments. This combination of outputs is predicted to contain a complex mixture of information about the contraction of multiple segment boundaries; because two of the contributing neurons are direction-selective (He et al., 2019; Vaadia et al., 2019), the activity of outputs in this domain likely depends on the direction of movement. (6) The **central posterior domain** is the final domain to contain synapses from A1 proprioceptors; it is the equivalent of the A1 central domain but in the next posterior segment (A2). The same predictions hold for this domain's receptive field and the information it contains.

In general, we find complex patterns of proprioceptive information converging in space, often along the axonal entry routes. Each proprioceptor contributes outputs to multiple spatial domains, and most spatial domains contain only proprioceptive information from within the segment, but the central domain contains information from multiple adjacent segments.

2.2.5. Few presynaptic inputs onto Drosophila larval proprioceptors

Presynaptic inhibition onto proprioceptive afferents is widespread across species (Clarac and Cattaert, 1996; Rudomín and Schmidt, 1999; Azim and Seki, 2019). In many cases, proprioceptive circuits use inhibition to scale the magnitude of incoming sensory signals, which may be needed to encode a wide dynamic range and/or avoid fatiguing the sensors (Straka et al., 2004; Skandalis et al., 2021; Tuthill and Azim, 2018; Gebehart et al., 2022). In addition, inhibition of proprioceptive feedback may be needed to modify motor reflexes such that they do not occur at inappropriate times (Eccles et al., 1962; Burrows, 1996; Rossignol et al., 2006; Fink

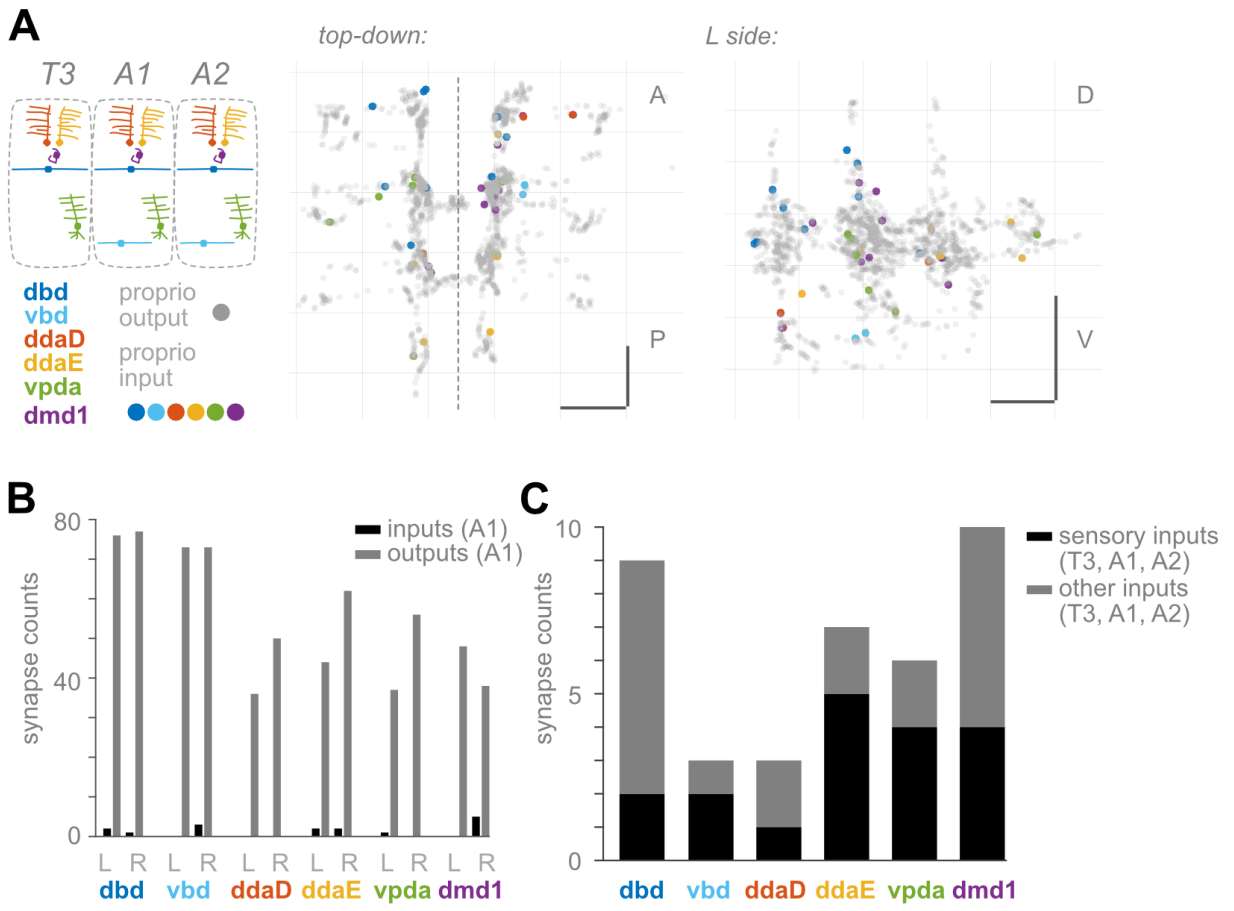

Figure 2.4: Proprioceptors receive few input synapses. **A)** Two views of input synapses onto proprioceptive neurons in T3, A1, and A2, colored by cell type according to diagram. Output synapses from same neurons shown in grey. Scale bars = 10 µm. Dashed vertical line: midline. **B)** Paired bar plots of input and output synapse counts for each proprioceptive neuron in A1. Dark bars: input synapse counts; light bars: output synapse counts. Counts are shown independently for left and right side A1 neuron of each type. **C)** Stacked bar plot of input synapses onto each proprioceptive neuron, summed across T3, A1, and A2. Bottom bars (dark): total input synapses in T3-A2 from sensory neurons. Top bars (light): total input synapses in T3-A2 from other (non-sensory or unidentified) neurons.

et al., 2014). Therefore, presynaptic inhibition is widely thought to be necessary for proprioception, and it is reasonable to expect presynaptic inhibition of Drosophila proprioceptors. However, remarkably, proprioceptors in A1 reportedly receive few presynaptic inputs (Schneider-Mizell et al., 2016). To confirm and extend these findings, we looked for presynaptic inputs onto Drosophila larval proprioceptors in other segments. Where possible, we asked if inputs were likely to be excitatory or inhibitory. Compared to inputs, we confirm A1

proprioceptors receive few inputs (Figure 2.4A-B) In A1, the most input synapses received by any single proprioceptor is five (onto R side dmd1; Figure 2.4B). This pattern holds true across segments (Appendix B, Table 1). Moreover, multiple proprioceptors do not appear to receive any input synapses. On average, a proprioceptor's number of inputs is only 2% of the number of its outputs. Indeed, the 34 proprioceptive neurons in segments T3, A1, and A2 receive only 38 synaptic inputs between them (Figure 2.4A). We find that the 38 synaptic inputs come from 32 presynaptic neurons, at least 15 of which are other sensory neurons (Figure 2.4C). Drosophila somatosensory neurons are expected to be excitatory (Ohyama et al., 2015). In summary, we confirm there are few input synapses onto proprioceptive neurons. Additionally, we find that many presynaptic partners are most likely excitatory. Overall, there is little evidence for pre-synaptic inhibition of larval proprioceptors.

2.2.6. Comparisons among somatosensory modalities

So far, we have uncovered three features that describe the anatomy of Drosophila larval proprioceptors: (1) they form output synapses along axon routes into the nerve cord; (2) they receive few presynaptic inputs; (3) individual proprioceptor types follow the principle of hemisegmental somatotopy. Given that features 1 and 2 are both surprising and potentially functionally significant (Clarac and Cattaert, 1996; Cover and Mathur, 2020), we next wanted to see whether these features were common to other Drosophila larval somatosensors. Therefore, we looked for the above three features in two additional classes of Drosophila larval somatosensory neurons (Figure 2.1B): chordotonal neurons (“chordotonals") and class IV multidendritic neurons ("md cIVs”) (Ghysen et al., 1986; Bodmer and Jan, 1987; Grueber et al., 2002), which have been annotated in the connectome by other groups (Ohyama et al., 2015;

Jovanic et al., 2016). The chordotonals in abdominal body segments comprise seven neurons: five lateral chordotonal (lch) neurons, found in a cluster together at the body wall (Figure 2.5A); one additional lateral chordotonal (v'ch); and two ventral chordotonals (vch) (Ghysen et al., 1986). The md cIV neurons in abdominal body segments comprise three neurons; their highly elaborate dendritic arbors tile most of the body surface (Figure 2.6A). Previous work has characterized their axonal projections into the neuropil (Merritt and Whitington, 1995; Schrader and Merritt, 2000; Grueber et al., 2007; Zlatic et al., 2009). Here, we evaluate the spatial organization of their output synapses, focusing on comparing patterns to those found in proprioceptors.

2.2.6.1. Compared to proprioceptors, other somatosensory neurons make fewer output synapses along the proximal-distal axis of their central axon.

Having observed that proprioceptors form a substantial fraction of their output synapses along axonal entry routes, we looked for the presence of chordotonal and md cIV output synapses along these neurons' axonal entry routes. From the chordotonal neurons in A1, we counted 11 output synapses along the incoming axon, compared to 846 total outputs (1.3%) (Figure 2.5A-B). This percentage remains at 1.0% when including chordotonals in segments T3-A2. Meanwhile, from the md cIV neurons in A1, we counted 4 output synapses along the incoming axon, compared to 294 total outputs (1.3%) (Figure 2.6A-B), and this percentage remains at 1.4% when including md cIV neurons in T3-A2. We conclude that, compared to proprioceptors, both chordotonals and md IV neurons make few output synapses along their axon routes into the central neuropil. The synapses along the axons thus appear to be a feature specific to proprioceptors.

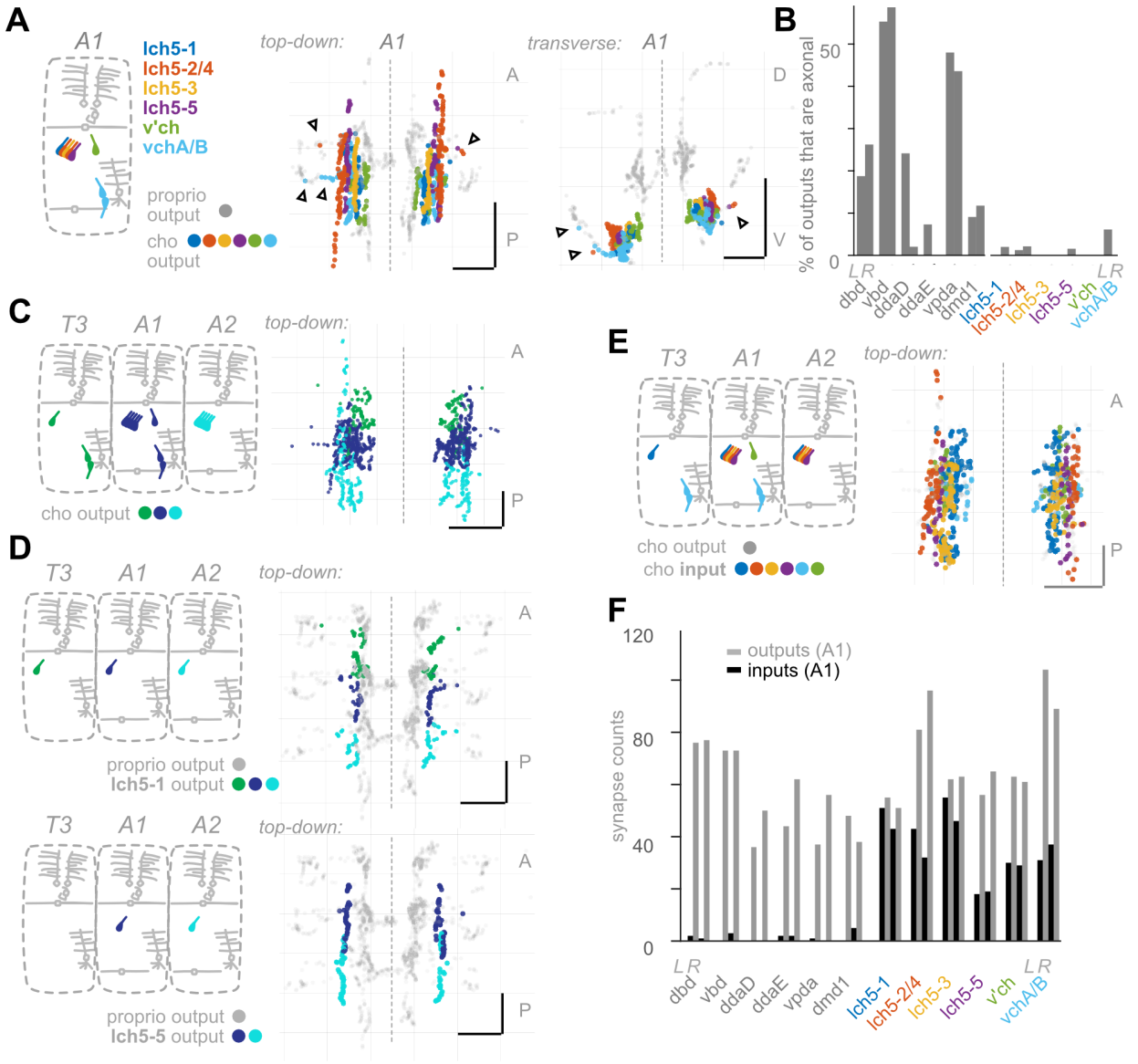

Figure 2.5: Chordotonal (cho) neurons make fewer axonal outputs than proprioceptors, show partial hemisegmental somatotopy, and receive more inputs than proprioceptors. A) Diagram of cho dendrites at the body wall in segment A1, and two views of output synapses made by A1 cho neurons in the CNS, colored according to diagram. Black (unfilled) arrowheads indicate locations of axonal output synapses. **B)** Percentage of all output synapses that are made along the proximal axon (see Methods) by each proprioceptive and cho neuron in A1. Left bars in each pair: left-side A1 neuron; right bars in each pair: right-side A1 neuron. **C)** Top-down view of output synapses made by all cho neurons that have been reconstructed in segments T3, A1, and A2, colored according to diagram. **D)** Top-down views of output synapse locations for two example cho neurons in segments T3, A1, and A2. Proprioceptor output synapses plotted in grey for comparison. **E)** Top-down view of input synapses onto all cho neurons in segment A1, colored according to diagram. Output synapses made by the same neurons plotted in grey. **F)** Paired, grouped bar plot of input and output synapse counts for each proprioceptive and chordotonal neuron in A1. Left bars in each pair (dark): input synapse counts; right bars in each pair (light): output synapse counts. Left pair of bars in each group: left-side A1 neuron; right pair of bars in each group: right-side A1 neuron. Throughout: scale bars = 10 µm. Dashed vertical lines: midline.

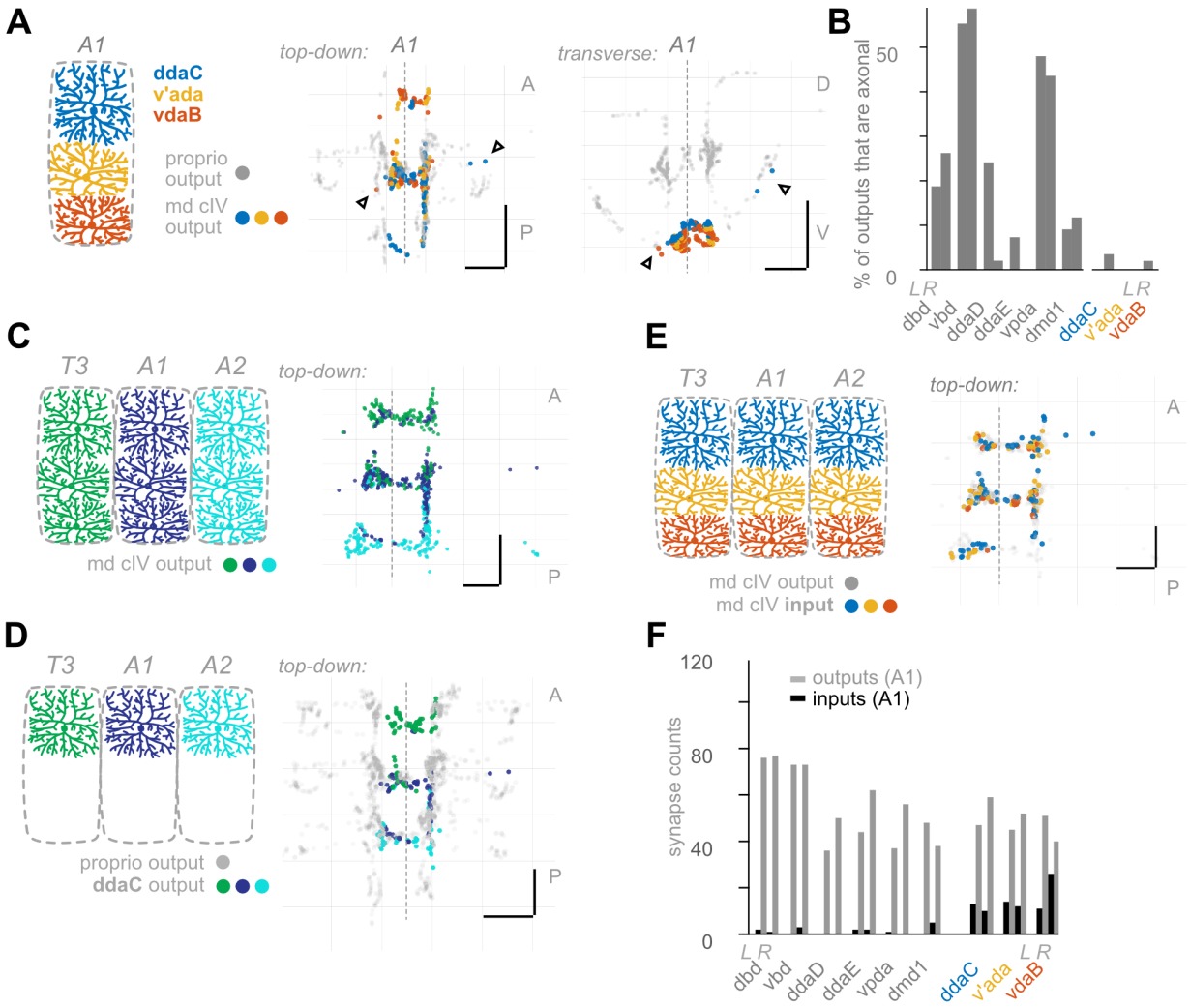

Figure 2.6: Class IV multidendritic (md cIV) neurons make fewer axonal outputs than proprioceptors, show no hemisegmental somatotopy, and receive more inputs than proprioceptors. **A)** Diagram of md cIV dendrites at the body wall in segment A1, and two views of output synapses made by A1 md cIV neurons in the CNS, colored according to diagram. Black (unfilled) arrowheads indicate locations of axonal output synapses. **B)** Percentage of all output synapses that are made along the proximal axon by each proprioceptive and md cIV neuron in A1. Left bars in each pair: left-side A1 neuron; right bars in each pair: right-side A1 neuron. **C)** Top-down view of output synapses made by all md cIV neurons in segments T3, A1, and A2, colored according to diagram. **D)** Top-down views of output synapse locations for the example md cIV neuron ddaC in segments T3, A1, and A2. Proprioceptor output synapses plotted in grey for comparison. **E)** Top-down view of input synapses onto all md cIV neurons in segment A1, colored according to diagram. Output synapses made by the same neurons plotted in grey. **F)** Paired bar plot of input and output synapse counts for each proprioceptive and md cIV neuron in A1. Left bars in each pair (dark): input synapse counts; right bars in each pair (light): output synapse counts. Left pair of bars in each group: left-side A1 neuron; right pair of bars in each group: right-side A1 neuron. Throughout: scale bars = 10 µm. Dashed vertical lines: midline.

2.2.6.2. Comparison of somatotopic organization of neurons from one class

We next asked whether hemisegmental somatotopy applies to chordotonal neurons. First, we characterized the outputs of left-right chordotonals originating in segment A1. Chordotonal synapses are organized into columns that run anteroposterior, closely resembling their previously characterized axonal trajectories (Merritt and Whitington, 1995). The outputs from A1 chordotonal neurons largely remain within the A1 neuropil segment and never cross the midline (Figure 2.5A). This columnar form of spatial organization is unlike any form of organization displayed by the Drosophila larval proprioceptors. Next, we mapped output synapses from chordotonal neurons in three adjacent segments, T3-A2. Some, but not all, chordotonal neurons in these segments restrict their outputs to their own segment of neuropil (Figure 2.5C-D, Supplementary Figure 2.4); We also found extensive overlap across segments for many chordotonals originating in segments posterior to A2 (not shown). However, hemisegmental somatotopy is present for a subset of chordotonal neurons (lch5-1 and lch5-3: Supplementary Figure 2.4). We conclude that hemisegmental somatotopy is less common among chordotonals compared to proprioceptors.

We performed the same set of analyses for md cIV neurons. First, outputs from all three md cIV neurons originating in segment A1 intermingle extensively (Figure 2.6A). This is reminiscent of the spatial organization of proprioceptors belonging to md cI (ddaD, ddaE, and vpda), but not other types of proprioceptors. Further, md cIV neurons rarely restrict their outputs to a single segment of neuropil (Figure 2.6C-D, Supplementary Figure 2.5); instead, outputs from adjacent segments overlap both lateral to and at/across the midline (Supplementary Figure 2.5). We checked this pattern for md cIV neurons annotated in other segments thus far and

confirmed that the general rule is for a neuron to form synapses across its own segment of neuropil, plus at least one adjacent segment (not shown). We therefore see no evidence of hemisegmental somatotopy among md cIVs, in contrast to proprioceptors.

We conclude that hemisegmental somatotopy is present for outputs from a subset of chordotonal neurons and absent for outputs from md cIV neurons. This feature, which was common among proprioceptors (except for vbd), is therefore not a general feature of somatosensory neurons.

2.2.6.3. Most Drosophila larval somatosensory neurons have abundant presynaptic input.

As noted earlier, presynaptic input onto sensory neurons is a common feature of many sensory systems. However, there are a small number of presynaptic inputs onto larval proprioceptors (Fig. 2.4B). To test whether this small number of input synapses is a general feature of larval somatosensory processing, we investigated the inputs onto chordotonal and md cIV neurons. These analyses confirm and extend those of Jovanic et al. (2016) and Gerhard et al. (2017). First, we visualized the input synapses onto chordotonal and md cIV neurons in segments T3, A1, and A2. Compared to proprioceptors (Figure 2.4A), chordotonal and md cIV neurons receive input synapses broadly throughout their arbors (Figure 2.5E, 2.6E). Next, we quantified the total input and output synapses for chordotonal and md cIV neurons in segment A1, as this segment has a complete set of reconstructed sensory neurons (Figure 2.5F, 2.6F; Appendix B, Table 2.) While overall numbers of output synapses are comparable in magnitude across each of the three classes— proprioceptors, chordotonals and md cVIs—the numbers of input synapses are much smaller among proprioceptors than among the other two classes. As a result, the ratio of input to output synapses is also noticeably smaller for proprioceptors. While the mean input-

to-output ratio for A1 proprioceptors (expressed as a percentage) is only 2.6%, for A1 chordotonals it is 54.4%, and for A1 md cIVs it is 30.9%. The relative lack of presynaptic input appears to be a unique feature of larval proprioceptors.

In summary, we identify unique anatomical features of larval proprioceptive neurons that set them apart from other somatosensors: (1) they form output synapses along axon routes into the nerve cord; (2) they receive very few presynaptic inputs; (3) individual proprioceptor types follow the principle of hemisegmental somatotopy.

2.2.7. A subset of dorsal proximal output synapses belong to monosynaptic reflex arcs from proprioceptors to motor neurons.

Among the best-characterized circuits in neuroscience are monosynaptic reflex arcs between proprioceptors and motor neurons, which are important in many systems for the fast retraction or stabilization of limbs (Azim and Tuthill, 2018). However, in non-limbed animals, few direct connections between proprioceptors and motor neurons have been described. A notable exception is a caterpillar, *Manduca sexta*, in which proprioceptor-to-motor neuron direct connections have been reported (Tamarkin and Levine, 1996). Because the proximal output synapses are an unusual feature of proprioceptors (compared to chordotonals and md cIVs), we asked whether their presence might be accounted for by direct connections to motor neurons. In other words, are the three proximal domains (dorsal, ventral-anterior, and ventral-posterior domains) the locations of monosynaptic connections between sensory and motor neurons?

We looked for synapses from proprioceptors onto motor neurons from A1, the only segment in which motor neurons have been comprehensively reconstructed and annotated (Zarin et al., 2019). Other authors have reported a small number of direct connections from dbd neurons

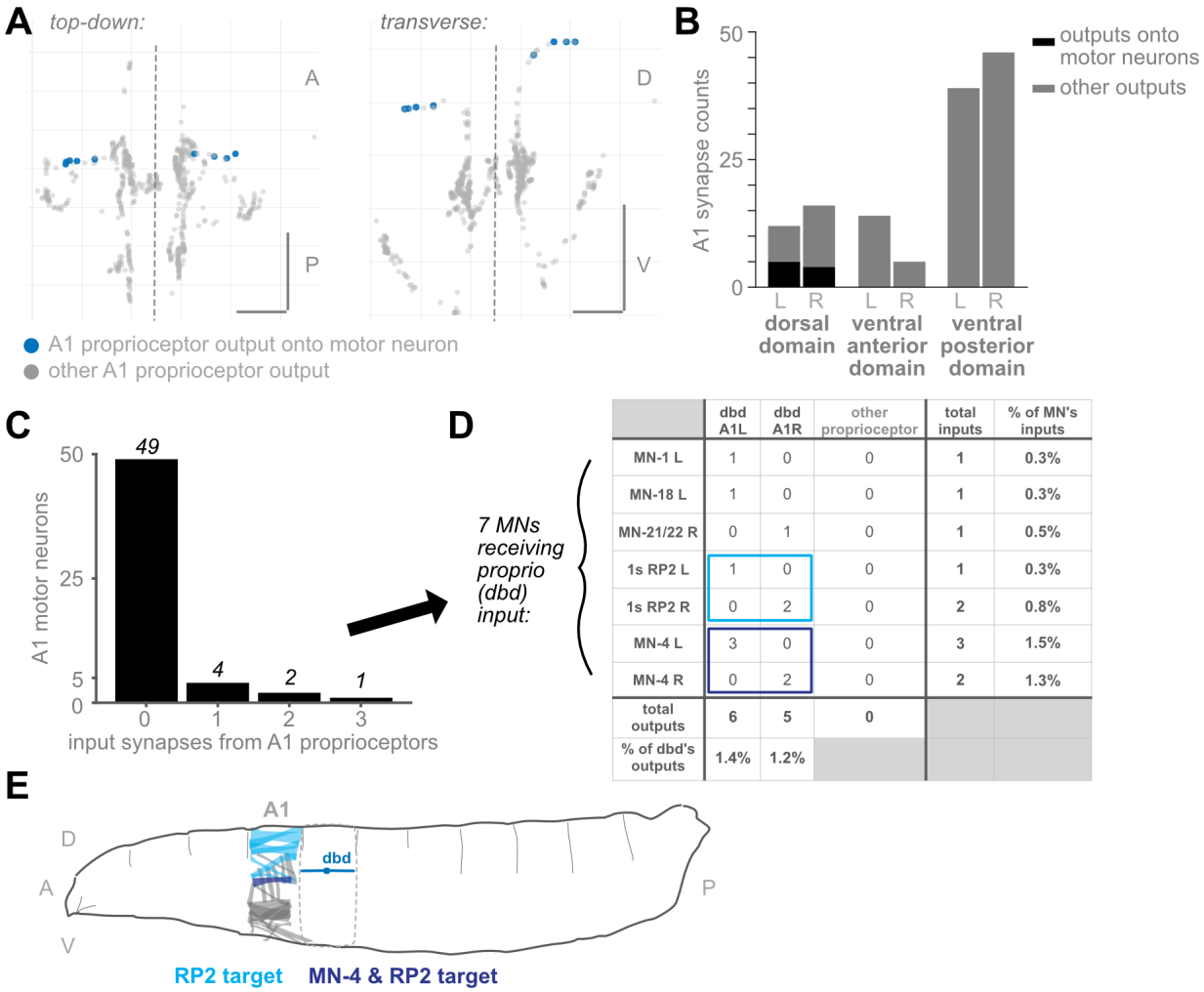

	dbd A1L	dbd A1R	other proprioceptor	total inputs	% of MN's inputs
MN-1 L	1	0	0	1	0.3%
MN-18 L	1	0	0	1	0.3%
MN-21/22 R	0	1	0	1	0.5%
1s RP2 L	1	0	0	1	0.3%
1s RP2 R	0	2	0	2	0.8%
MN-4 L	3	0	0	3	1.5%
MN-4 R	0	2	0	2	1.3%
total outputs	6	5	0		
% of dbd's outputs	1.4%	1.2%			

Figure 2.7: Subset of dorsal domain output synapses form monosynaptic reflex arcs onto motor neurons. **A)** Two views of all output synapses made by A1 proprioceptive neurons. Synapses onto motor neurons colored in blue. **B)** Stacked bar plot of output synapses in the three proximal axonal domains. Darker bars: synapses that contact motor neurons. Lighter bars: synapses that do not contact motor neurons. Counts for left- and right-side domains given separately. **C)** Counts of A1 motor neurons receiving 0, 1, 2, or 3 input synapses from proprioceptors. No motor neuron received more than 3 such input synapses. **D)** Table of proprioceptor synapse counts onto the seven motor neurons receiving direct proprioceptor input. Note that dbd accounts for all proprioceptor input. Rightmost column: percentage of all input synapses onto the motor neurons that come from dbdL/R. Bottom row: percentage of all output synapses made by dbd L and dbd R that are onto motor neurons. **E)** Diagram of muscle targets of the two A1 motor neurons receiving bilateral proprioceptor input. Lighter blue: RP2 targets, dorsal muscles 1, 2, 3, 4, 9, 10, 19, 20 (Hoang and Chiba, 2001). Darker blue: MN-4 target, dorsal muscle 4. Although dbd is shown for reference in the adjacent segment, dbd's motor neuron targets (and their muscle targets) are all located in the same segment. Throughout: scale bars = 10 µm. Dashed vertical lines: midline.

to motor neurons (Schneider-Mizell et al., 2016; Zarin and colleagues in a 2019 preprint); we reviewed these annotations to double-check for any missing proprioceptor to motor neuron

synapses. We could find only one additional synapse from proprioceptors in A1 onto motor neurons, bringing the reported total from 10 to 11 (Figure 2.7). We confirmed that, in this EM dataset, no connections are reported between chordotonal or md IV neurons and motor neurons (data not shown).

We found that, of the three proximal domains, only synapses in the dorsal domain innervated A1 motor neurons (Figure 2.7A-B). As this domain exclusively contains output synapses from dbd, we confirmed that only dbd proprioceptive neurons directly synapse onto motor neurons in A1. Of the 12 proximal synapses in the left-side dorsal domain, 5 contact motor neurons, or 42%. (These 5 output synapses innervate 6 motor neurons; in Drosophila larvae, one pre-synapse typically contacts multiple post-synaptic neurons.) Of the 16 proximal synapses in the right-side dorsal domain, 4 contact motor neurons, or 25%.

We conclude that synapses onto motor neurons can only account for a small fraction of the proprioceptors' proximal axonal synapses, and only from dbd neurons.

2.2.7.1. Direct connections from proprioceptors to motor neurons show the expected connectivity for a monosynaptic reflex arc.

We next asked whether the synapses from proprioceptors onto motor neurons show the expected connectivity for monosynaptic reflex arcs. Monosynaptic reflex arcs typically enable "corrective" reflexes: for instance, when proprioceptive feedback signaling an increase in muscle stretch (e.g., from muscle spindles) causes increased activation of motor neurons that innervate the muscle in question, counteracting the stretch (Rossignol et al., 2005). Similarly, since the only monosynaptic sensory-to-motor connections observed so far in larvae are from dbd neurons, which are dorsally-positioned longitudinal stretch sensors (Schrader and Merritt, 2000; Suslak

and Jarmon, 2015), we might expect the motor neuron targets to be those that innervate dorsal longitudinal muscles, whose elongation would promote dbd activity and whose contraction would inhibit dbd activity.

We therefore evaluated which motor neurons received input from dbd in A1 R and L. Of all 56 motor neurons with complete annotations in A1, 49 received no dbd input (Figure 2.7C). 4 motor neurons received a single input synapse, and only 3 received more than one input synapse. These synapse counts are low: dbd input accounted for no more than 1.5% of any motor neuron's inputs, and conversely, synapses onto motor neurons (combined) accounted for less than 1.5% of all dbd output synapses.

The identities of the motor neurons receiving any dbd inputs are shown in Figure 2.7D. Only two motor neurons received dbd inputs on both sides of the midline: both left- and right-side RP2 and MN-4 motor neurons received synapses from the ipsilateral dbd neuron. Because they are consistent on both sides, we consider these synaptic partnerships more likely to be genetically prespecified and to recur in other body segments (Ohyama et al., 2015). In support of this conjecture, we looked for the (incompletely reconstructed) RP2 motor neuron in two additional hemisegments, T3L and A2R, and confirmed the existence of a small number of synapses from dbd onto RP2 in these hemisegments (data not shown). Both MN-4 and RP2 show the expected connectivity for a stretch-countering reflex arc: MN-4 innervates a lateral longitudinal muscle close to dbd's dendritic field. RP2, also known as the dorsal type Is motor neuron, innervates several dorsal muscles (Figure 2.7E). Activity of either motor neuron could, presumably, cause the body segment to shorten along the longitudinal axis and counter the stretch sensed by dbd.

Finally, we note that the three A1 motor neurons receiving dbd inputs on just one side of the midline, MN-1, MN-18, and MN-21/22, all innervate dorsal muscles (Hoang and Chiba, 2001); however, MN-18 and MN-21/22 innervate muscles with a transverse orientation, whose contraction would not directly counter longitudinal stretch.

We conclude that the synapses from dbds onto motor neurons in A1, while few in number, generally show the expected connectivity for a monosynaptic reflex arc.

2.3. Discussion

Circuits that process proprioceptive information are essential to locomotor control. In this study, we describe the anatomical organization of the first stage of proprioceptive processing circuits: the input and output synapses of proprioceptors. We identified four anatomical features that differentiate Drosophila larval proprioceptors (Figures 2.1-2.4) from other somatosensory neurons (Figures 2.5 and 2.6). (1) All Drosophila larval proprioceptors project to a region of the CNS that is dorsal to other somatosensory projections, in agreement with previous reports (Merritt & Whitington, 1995; Schrader and Merritt 2000; Zlatic et al., 2009). All but vbd project to a common region, the "central domain" (Figures 2.1, 2.3). (2) Nearly all proprioceptor types display hemisegmental somatotopy, meaning their own outputs do not cross the midline and tend to repeat, but do not overlap, across adjacent segments (Figure 2.2). (3) Drosophila larval proprioceptors make proximal and distal output synapses along the axon, leading to the complex mapping of proprioceptive outputs into multiple spatial domains (Figures 2.1, 2.3). The presence of proximal output synapses in proprioceptors cannot be explained by these neurons' connections to motor neurons. (4) Drosophila larval proprioceptors receive few presynaptic inputs, in

agreement with previous reports (Schneider-Mizell et al., 2016), and we newly conclude that few inputs are inhibitory (Figure 2.4). In summary, we have described the spatial logic and distinctive features that characterize the organization of Drosophila larval proprioceptive synapses.

2.3.1. Potential limitations of our mapping efforts

Here, we focus on six proprioceptive neurons: dbd, vbd, ddaD, ddaE, vpda, and dmd1 (Ghysen et al., 1986; Orgogozo and Grueber, 2005). We do not wish to argue that these are the only neurons that sense proprioceptive information in the Drosophila larva. We focus on this set because they are widely agreed to be proprioceptive in nature (Tamarkin and Levine, 1996; Simon and Trimmer 2009; He et al., 2019; Vaadia et al., 2019). However, in adult insects, chordotonal neurons are proprioceptive (Burrows, 1996; Field and Matheson, 1998; Mamiya et al., 2018), and in larvae, chordotonal and md cIV neurons may respond to self-movement (Ainsley et al., 2003; Caldwell et al., 2003; Song et al., 2007). Significant anatomical differences exist between the six "proprioceptive neurons," chordotonal neurons, and md cIV neurons. These differences do not rule out that chordotonal or md cIV neurons encode proprioceptive information, but they do raise questions about how different anatomies arise during development and how they contribute to different circuit-level properties.

This study takes advantage of an EM dataset of the larval CNS to gain nanometer-resolution insight into the cell biological, morphological, and spatial features of proprioceptive neurons. We use EM data to generate a detailed map of larval proprioceptor inputs and outputs across three body segments, the most complete map of its kind. However, EM datasets come with their own set of limitations (Morgan and Lichtman, 2013): first, we cannot assume synapses are functional or determine their strengths, which might lead us to overlook patterns related to

functional connectivity. Second, reconstructions are subject to occasional annotation errors. Lastly, the EM dataset is from one animal at one developmental stage and may reflect idiosyncrasies in this animal's development or transient patterns (e.g., synapses that will be pruned over time; although see Gerhard et al., 2017).

Finally, we have not described proprioceptors' postsynaptic partners in this study, leaving open many important lines of follow-up inquiry (see below). The number of postsynaptic partners is likely to be in the hundreds, as in Drosophila, each presynaptic site can contact multiple postsynaptic sites, each potentially belonging to a unique neuron.

2.3.2. Novel insights into proprioceptor output synaptic divergence and convergence

Proprioceptive processing circuits have long been thought to be characterized by the properties of divergence and convergence (Bosco and Poppele, 2001; Jankowska, 2008; Tuthill and Azim, 2018). At the anatomical level, divergence and convergence have largely been understood by examining the projection patterns of individual proprioceptor afferents, leading to identification of regions of the CNS innervated by different sensory types (Eccles et al., 1957; Murphey et al., 1985; Merritt and Whitington, 1995; Smith and Shepherd, 1996; Niu et al., 2013; Lai et al., 2016). In this study, thanks to the larval EM dataset, we can demonstrate the existence of both convergence and divergence at the level of proprioceptive outputs in space and describe patterns in how specific proprioceptor types converge and diverge at this level. These descriptions are a first step in unraveling the spatial complexity of the larval proprioceptive system and extracting organizational principles, discussed below.

Divergence: Anatomical divergence of larval proprioceptive output synapses is underpinned by two main strategies.

First, hemisegmental somatotopy segregates the outputs of (most) proprioceptive types across adjacent segments. Hemisegmental somatotopy may be important from the point of view of downstream partners. A limited number of downstream partners have been identified in other studies, including both local interneurons (e.g., Jaam neurons) and intersegmental interneurons (e.g., late-born Even-skipped Lateral (EL) interneurons; Heckscher et al., 2015). The presence of both local and intersegmental downstream partners implies that proprioceptive information is likely both to be used within a segment and to be simultaneously distributed to other segments. In the case of local downstream neurons, whose dendrites are largely restricted to one segment of neuropil, a matching restriction of partner proprioceptor synapses could help establish segmentally-repeated circuits that are responsible for the local implementation of a proprioceptive processing computation (Thomas et al., 1984; Clark et al., 2018). Such local computations have been suggested for, e.g., computing a local bending angle or correcting left-right asymmetries (Heckscher et al., 2015; Vaadia et al., 2019). Other somatosensory neurons (e.g., nociceptors) do not respect the principle of hemisegmental somatotopy, implying that such local output restrictions may be more important for proprioceptive processing than for other somatosensory processing circuits.

Second, individual proprioceptors distribute output synapses along their axons at both proximal and distal locations. In the case of dbd, only the proximal synapses contact motor neurons (Figure 2.7), suggesting a potential separation of downstream partners by synapse location. However, we cannot currently determine whether this finding is the exception or the rule. Furthermore, most proprioceptor types distribute synapses into multiple domains, one of which is typically the central domain (Figure 2.3 for domain definitions). The exception is vbd,

whose outputs are not distributed to the central domain but instead contribute to the midline domain. This raises the additional question of why vbd alone locates its outputs in this region: does it participate in distinct proprioceptive processing circuits from other proprioceptors? Future analysis of downstream partners should help resolve these questions.

Convergence: Anatomical convergence of output synapses reveals interesting patterns regarding what proprioceptive information could be combined in space. There are six proprioceptor types in Drosophila larvae, whose outputs could be spatially combined in many patterns. However, given the total number of possibilities, we find evidence for a rather limited number of combinations. Five domains consist of interdigitated outputs from multiple proprioceptor types (Figure 2.3). Only in the central and midline domains are outputs combined from multiple segments. Furthermore, in these domains, we do not see indiscriminate mixing of all proprioceptors; rather, some proprioceptors appear to "skip" the domains in their own segment of neuropil and form outputs only in adjacent segments. The limited number of output combinations and specificity in how neurons converge across segments may indicate combinations of feedback signals that are important to integrate into downstream circuits (Levinsson et al., 2002; Willis Jr. and Coggeshall, 2012). For instance, in the case of the central domain, convergence may create an area where locomotor-related proprioceptive feedback is integrated. Outputs in this domain likely encode information related to contraction of the current segment (dmd1), as well as information about the movement of either of the adjacent boundaries: movement forward of the anterior boundary (ddaE, and plausibly vpda, from the anterior segment), or movement backward of the posterior boundary (ddaD from the posterior segment)

(He et al., 2019; Vaadia et al., 2019). This information could signal that a locomotor wave is progressing from the segment in question into the next.

Using our current dataset, in which a large fraction of proprioceptors' downstream targets have yet to be identified and reconstructed, we cannot currently confirm whether spatial convergence corresponds to shared downstream target neurons or, conversely, whether spatial divergence leads to unique downstream neurons. This lacuna leaves many interesting questions to be answered. For instance, how unique are the downstream target neurons that receive input from each distinct spatial domain? Is spatially divergent proprioceptive information kept separated at the level of these second-order interneurons, or instead combined by these neurons across spatial domains and/or hemisegments? A few examples have already been described of downstream interneurons that make their own outputs on both sides of the midline and/or across segment boundaries, including some of the Even-skipped Lateral neurons (Heckscher et al., 2015) and the A27h neuron (Fushiki et al., 2016), both of which contribute to coordinating (hemi-)segmental contractions during locomotion. Examples are also known of downstream interneurons, such as Jaam interneurons, that receive proprioceptive inputs from both the left and right side of a segment (Heckscher et al., 2015). Either type of second-order interneuron connectivity could quickly combine proprioceptive information that was spatially segregated at the level of sensory outputs. We note that, even in cases where downstream target neurons combine information across multiple spatial domains (such as the Jaam neurons), the local divergence/convergence of proprioceptive subtypes we describe may still be important for local dendritic computations (Clarac and Cattaert, 1996, Hao et al., 2009; Pouille et al., 2013; Wilson, 2013).

Thus, from the functional perspective, an important next step will be to identify and reconstruct all downstream targets of proprioceptive neurons. This will help elucidate the extent to which spatial convergence and divergence of proprioceptive synapses actually represent integration or distribution of proprioceptive signals, respectively. From the developmental perspective, an important next step will be to understand the genetic control of synapse placement, in cases both of convergence and divergence.

2.3.3. Little pre-synaptic inhibition onto larval proprioceptors

Presynaptic inhibition has been repeatedly described across proprioceptive systems and is considered a near-universal feature of proprioceptive sensory processing (Rudomin and Schmidt, 1999; Tuthill and Azim, 2018). Presynaptic inhibition of proprioceptive feedback is thought to play many roles in motor control, including reducing the gain of proprioceptive signals, stabilizing reflexes, and preventing oscillations that could otherwise be caused by delayed feedback (Rudomin and Schmidt, 1999; Rossignol et al., 2006; Windhorst, 2007, Fink et al., 2014). Here, we found few inputs to proprioceptors alongside evidence that many inputs are excitatory rather than inhibitory (Figure 2.4). This suggests that larval proprioceptors are distinctive, likely being subject to little to no presynaptic inhibitory control. What aspects of Drosophila larval body or behavior could explain this? In contrast to most proprioceptive systems that have been studied in depth (e.g., adult fly, larvae lack limbs; they move primarily using peristaltic contractions of consecutive body segments (Heckscher et al., 2012). This difference in body form and locomotor strategy could lead to differences in the organization of locomotor circuits that obviate the need for reflex stabilization or phase-dependent gating. Indeed, the "mission accomplished" model proposed for the role of proprioceptive feedback in

larval locomotion does not apparently depend on presynaptic inhibition (Hughes and Thomas, 2007; Pehlevan et al., 2016). Alternatively, gain control may be important for some aspects of proprioceptive processing but implemented without presynaptic inhibition: via properties of the sensory neurons themselves or of their interaction with the body that reduce synaptic transmission depending on the animal's behavioral state or the neuron's firing history (Tuthill and Azim, 2018; Dickerson et al., 2021). Future modeling and experiments are needed to determine what properties of proprioceptors, or properties of proprioceptive processing, differentiate this sensory modality in larvae from other somatosensory modalities.

2.3.4. Conclusion

Altogether, our results provide the most comprehensive and detailed map to date of a proprioceptive system's earliest stage of central organization. This map opens the door to developmental and functional studies that will ultimately elucidate the relationship between the anatomical and functional organization of proprioceptive networks, a relationship that is fundamental for understanding how proprioception contributes to larval motor control.

2.4. Materials and Methods

Dataset

The electron micrograph/connectome dataset used in this study is a CNS reconstruction from a 6-hr-old first-instar larva, first described in Ohyama et al., 2015.

Defining proprioceptive, chordotonal, class IV multidendritic, motor neurons

In general, we used the names assigned by annotators to assign reconstructed skeletons and the nodes attached to them into classes, as follows: *Proprioceptive neurons:* names

beginning with "dbd", "vbd", "ddaD", "ddaE", "vpda", or “dmd1". *Chordotonal neurons:* names beginning with "lch5", "v'ch", or "vch". *md cIV neurons:* names beginning with "ddaC", "v'ada", or "vdaB". *Motor neurons:* names beginning with "MN", which we further restricted to completely reconstructed, published motor neurons from segment A1 (see below).

We report on 138 total neurons. 104 were previously published, and 34 are new to this publication. See Supplementary Table 1 (Appendix B) for details. To confirm the identities of unpublished neurons, we compared their morphology to light level examples (Grueber et al. 2007, Grueber et al. 2002, Merritt and Whitington 1995, and Schrader and Merritt 2000). For details of matching neurons in light-level data, see both Wang et al., 2022 and Wreden et al., 2017. In addition, we compared each neuron in other segments to the A1 example of the same name and to the its left-right hemisegment sister neuron. The skeletons of identified neurons were reviewed to greater than 90% (with the exception of some published motor neurons).

Data processing and analyses

Connectomic information, including synapse ("node") locations and presynaptic and postsynaptic neuron identities, was extracted from CATMAID using the pymaid library (https://github.com/navis-org/pymaid).

Visual representations of synapse locations were made either using MATLAB or using CATMAID's 3D viewer tool. All "output" node locations plotted were presynaptic node locations (corresponding to the location annotated for the sensory neuron). All "input" node locations plotted, conversely, were postsynaptic node locations.

Other analyses were performed using MATLAB. MATLAB code for the visualizations and analyses will be made available on our Github at (github.com/HeckscherLab/proprio-synapse-org).

Defining segment and side

We restricted visualizations and analyses using information about a neuron's segment and side of origin, which we likewise obtained from the names assigned by annotators. We searched names for a tag containing segment and side, e.g., "_a1r". For all counts of input and output synapses, neurons were restricted either to those in T3, A1, and A2, or to those in A1 alone.

Defining sensory inputs

To obtain the population of sensory neurons that synapse onto proprioceptors/ chordotonals/md cIVs (Figures 4, 5, and 6), we defined sensory neurons as follows:

1. Any proprioceptor, chordotonal, or md cIV neuron, as defined above.
2. Additionally include any "es" neuron: any names beginning with "les", "v'es", or "ves".
3. Additionally include any miscellaneous (partially identified) sensory neuron: any names containing the terms "(class I)", "(class 1)", or "sensory".

Finally, we manually inspected the list of returned neuron names that met these criteria, to ensure that no obviously non-sensory neurons were accidentally returned.

Defining spatial domains

Spatial domains formed by A1 output synapses were determined by eye, using the following criteria:

Dorsal domain: all synapses proximal to where the dbd axon projects ventrally, in a more-or-less vertical line. (See below for corresponding coordinates.)

Ventral domains: all synapses proximal to where the axons turns to project dorsally (or anteriorly, in the case of the vbd axon). (See below for corresponding coordinates.) A gap of about one micron in the Z (A-P) axis separates the clusters of synapses assigned to ventral-anterior vs. ventral-posterior domains.

On the left side, A1L synapses assigned to any of the dorsal or ventral axonal domains correspond to those lateral to (greater than) X = 65000 nm, in CATMAID coordinates.
On the right side, A1R synapses assigned to the dorsal domain correspond to those dorsal to (less than) Y = 67000 nm. A1R synapses assigned to the two ventral domains lie lateral and ventral to a line drawn through (48000, 85000) and (38000, 75000) in the X,Y plane.

Midline domain: all synapses medial to the major antero-posterior tracts of the central domains. This corresponds to synapses with X positions between 53000 and 58500.

Central domain: synapses distal to the dorsal or ventral domains that group together in a cluster towards the medial part of the A1 neuropil.
This corresponds to synapses encompassed by the following ranges: X positions between 58500 and 65000 (L), or between 47000 and 53000 (R); Y positions (D-V) between 68000 and 84000; Z positions between 115000 and 125000.

Central posterior domain: all synapses posterior to the A1 segment of neuropil, with Z positions posterior to (greater than) 130000.

2.5 Acknowledgments

We would like to thank Casey Schneider-Mizell, Akira Fushiki, Javier Valdes-Aleman, and Aref Zarin for their assistance reconstructing the neurons analyzed in this paper. We would

also like to thank the members of the Heckscher lab for their insightful comments on the figures and analyses.

CHAPTER 3

STUDYING DROSOPHILA LARVAL BEHAVIOR IN AGAROSE CHANNELS

This chapter originally appeared, in modified form, as the following publication:

Greaney, M.R., Heckscher, E.S., 2024. Studying Drosophila Larval Behavior in Agarose Channels. Cold Spring Harb Protoc. doi: 10.1101/pdb.prot108420

Author Contributions: The author of this dissertation developed the methods related to channel design and channel mold manufacturing, designed the coverslip holder used in the inverted imaging setup, developed the troubleshooting steps, and wrote the manuscript.

3.1. Abstract

Larvae of the fruit fly *Drosophila melanogaster* are a popular and tractable model system for studying the development and function of sensorimotor circuits, thanks to the relative numerical simplicity of their nervous system and the wealth of genetic tools to manipulate the anatomy, activity, and function of specific cell types. Researchers studying the role of a particular gene or cell type in sensorimotor circuit activity or function may wish to observe the effects of an experimental manipulation during behavior in the intact animal. Observing these effects, which may include changes in the calcium activity or movement of small numbers of neurons, muscles, etc., typically requires high-spatial-resolution imaging, which poses several difficulties in the freely-crawling larva. Freely-crawling larvae can move quickly and with changeable heading, making manual or automatic tracking challenging; additionally, they may make three-

dimensional movements, such as rearing, that can degrade imaging focus. These challenges are potentially solvable using advanced imaging and algorithmic tracking set-ups; but cost, space, or development time may be prohibitive. This protocol describes a simple and cost-effective method for placing larvae inside agarose channels, thereby restricting larval crawling to a single dimension and enabling higher-magnification time-series imaging of fluorescently-labeled structures during many cycles of locomotion. By using larvae that express fluorescent calcium indicators in cells of interest, researchers can apply this method to study the effects of experimental manipulations on neural or muscular activity during behavior in the intact animal.

3.2. Materials

Reagents

Agarose (e.g., Genesee 20-101)
Compressed canned air (e.g., Office Depot 911245)
Drosophila adults (greater than 15 adult females and approximately half that number of males)
Select genotypes to generate larval offspring with the fluorescent protein of interest expressed in the cells of interest. For example, to visualize muscle cells, cross one set of parents from a driver line that expresses in muscles, such as Mef2-GAL4 *(BDSC_41258), to the other set of parents from a responder line encoding a fluorophore, such as* UAS-EGFP *(BDSC_5428); alternatively, use a fly line encoding a fluorophore-tagged protein that already expresses in muscles, such as* MHC-GFP *(myosin heavy chain, which is enriched in muscles, tagged with GFP; BDSC_38462). To visualize calcium dynamics, use a responder line or other transgenic line encoding a calcium indicator, such as* UAS-jGCaMP7c *(BDSC_79030) or* UAS-Gerry *(GCaMP tethered to mCherry, BDSC_8024). To correct for motion artifacts that occur while the larva crawls, we recommend choosing Gerry or a ratiometric calcium indicator rather than a single-channel indicator like a GCaMP (see Discussion section "Cellular Activity Data").*
Drosophila apple juice-agar plates (see Appendix D)
Fly food in vials (see Appendix D)
Isopropyl alcohol
Live yeast paste (see Appendix D)
Sylgard 184 (Electron Microscopy Sciences 24236-10)
Water (double-distilled or milli-Q purified)

Equipment

Channel molds

These can be generated via photolithography, laser cutting/etching, or 3D printing. Templates of channel molds are available upon request from the Heckscher Lab. Instructions for 3D printing channel molds are provided in Steps 4-6. For additional details, see Discussion.

Collection chamber

Prepare by using a syringe needle (16-21 gauge) to punch holes in a square-bottomed polyethylene Drosophila bottle (Genesee Scientific 32-130 or 32-131), to allow for air exchange.

Coverslip (e.g., Fisherbrand 112-541-020)

The size and thickness of the coverslip depend on the specific microscope used for imaging.

Humidified chamber (a plastic bin large enough to hold a collection chamber, containing a wet paper towel as a source of humidity)

Microscope capable of recording time-lapse images of fluorescent samples

Microscope slide (standard glass variety), if using upright imaging.

Microscope slide with coverslip-thick region (e.g., Ibidi 80177) OR with slot to hold coverslip (e.g., EMS 72268-01), if using inverted imaging.

Template .stl files to 3D print a microscope slide with an open slot to hold a coverslip can be obtained upon request from the Heckscher Lab.

Microwave oven

Paint brush (e.g., Ted Pella red sable #3)

Paper towels

Petri dishes (35- x 10-mm, 60- x 10-mm round)

Razor blade

Ruler (micrometer resolution; e.g., View Solutions RT20221102)

Spatula (small, metal with flat blade)

Tape (general-purpose lab tape)

Wide or blunt forceps

3.3. Method

In this protocol, users will image fluorescent larvae crawling in a restrictive agarose channel to study movement patterns. First, mating flies will be placed in a collection chamber to collect fluorescent larvae. Collected larvae will be placed in agarose channels. Their movement

in the channel will be imaged over time on a microscope. The resulting movies are analyzed for movement parameters.

3.3.1. Production of negative channel molds

See Discussion (sections on "Channel Design" and "Channel Mold Manufacturing") for information about producing molds. If the molds for agarose channels were produced using photolithography or laser etching, they will be "positive" molds with the grooves going into the mold rather than sticking out: the same configuration as the agarose channels. In this case, to cast agarose channels (Step 12), an intermediate "negative" mold with the grooves sticking out must be created in PDMS (e.g., Sylgard 184). Alternatively, negative molds can be created directly using 3D printing. Steps 1-3 below provide instructions for creating an intermediate Sylgard mold against an etched positive template; Steps 4-6 below provide instructions for 3D printing a negative mold.

Creating the Intermediate Negative Mold Using Sylgard

The user should already have a positive mold generated using photolithography or laser etching. (See Discussion section "Channel Mold Manufacturing.")

1. Mix Sylgard 184 according to the manufacturer's instructions to create a negative cast of the positive mold.

2. Pour a thin layer (~2-5 mm) of Sylgard over a positive mold placed in a wide, disposable container (e.g., 60-mm plastic Petri dish). Keep the original mold in the center of the container to minimize curvature caused by a meniscus.

3. Allow mold to fully cure before using it to cast agarose channels (Step 12). Curing of Sylgard takes multiple days at room temperature or may be sped up using heat sources.

Creating Negative Molds Using 3D Printing

These steps assume access to and materials for a 3D printer; both are commonly available from academic and commercial fabrication labs.

4. Generate/obtain a three-dimensional template for use in 3D printing. 3D models can be created using software such as Blender (open source software, blender.org), Sketchup (Trimble, Inc.) or Tinkercad (Autodesk, Inc.). Specifications of the template will depend on the 3D printing hardware available: most 3D printers accept a variety of file types, including "standard tesselated geometry" (.stl) fomats, and can print objects with a range of resolutions.

Example template .stl files can be obtained upon request from the Heckscher lab.

5. Print the molds according to the instructions for using the 3D printer. Instructions and additional materials required will vary by hardware model.

6. Estimate the true dimensions of the printed channels, which may deviate somewhat from the original template dimensions. Size estimates can be performed using a micrometer ruler. Depth estimates are likely to be less precise than length and width estimates, but can be made by (e.g.) holding a piece of paper vertically next to the channels with the bottom edge flush against the printed base of the mold, marking a line to indicate how high the channels rise above the printed base, and measuring the distance between that line and the bottom edge of the paper. We recommend averaging several measurements to estimate each dimension.

3.3.2. Collection of larvae

7. Approximately one wk before recording larval behavior, set up a cross in a standard fly food vial. Cross adult flies with the desired genotypes in a 1:2 to 1:3 ratio of males to females.

Ideally, use a minimum of 15 virgin females; add more animals if the desired larval genotype will be rare in the population. See Reagents section for notes on selection of adult genotypes.

8. Approximately 5 d before recording, knock the flies into a collection chamber (2-3 d after the initial mating). First, prepare an apple juice agar cap by placing a dab (0.5-1 mL) of yeast paste in the center of the juice agar cap using a small spatula. After the cap is prepared, add the adult flies into the chamber, then use the yeasted cap to close the chamber, with the juice agar/yeast side facing the interior of the chamber. Tape the cap to the top of the collection chamber to secure it. Maintain collection chambers, apple juice cap down (upside down), in a humidified container within a 25°C incubator. From this time on, change apple juice cap once daily.

The agar/juice cap and yeast paste provide food for the adult flies and a substrate for females to lay eggs.

9. At least 2 d before recording, remove the cap and place a new, yeasted cap on the chamber. We recommend changing caps every 24 h, or after a shorter period (e.g., 1 h) if it is important that larval age is precisely known during imaging. After releasing a lid, label it with the date, collection time, temperature, and genotype. Examine it to confirm eggs have been laid.

Expect >200 eggs for a 24 h collection. It may take a few days in the collection chamber before the flies lay at a maximum rate.

Immediately after removing a cap from a 24 h collection, one should see a few newly hatched larvae, which will be found away from the yeast paste.

10. Individually store each removed cap inside a covered 60-mm Petri dish. Keep dishes with caps in a closed plastic bin, stored at 25°C and humidified to 60-100% relative humidity. This is typically the same bin that contains the collection chamber. Incubate each cap for the desired amount of time; we typically incubate caps for 24 h to image first instar larvae.

At 25°C, for wildtype flies, it takes approximately 1 d to reach the 1st instar, 2 d to reach the 2nd instar, and 3-4 d to reach the 3rd instar.

The GAL4-UAS expression system expresses more strongly when larvae are raised at 29°C. The temperature of culture conditions can be altered, but keep in mind that changing larval temperature also impacts developmental speed (Ashburner 2005).

Caution: under proper levels of humidity, caps stored in the same container have the possibility of cross-contamination of larval genotypes, even when Petri dish lids are covered, since larvae are mobile enough to crawl out from under a Petri dish lid. If larvae are imaged at 2nd or 3rd instars, we recommend physically separating any dishes containing different genotypes (e.g., inside separate humidified plastic bins) or closing the dishes with parafilm.

If larvae are unhealthy or fail to hatch, see Troubleshooting.

3.3.3. Imaging larval behavior in channels

11. Clean the surface of the mold with isopropyl alcohol and then rinse with water. Use compressed air (e.g., canned air or building air valves), if any particulates remain. Place the mold channel-side up inside a 60-mm Petri dish (or similar heat-resistant container).

12. Prepare the agarose channels: make a solution of 2-3% (w/v) agarose in water and heat it in a microwave oven until fully dissolved. Cool briefly, allowing bubbles to rise to the

surface. Pour agarose over the mold (channel side up), covering the mold by at least 3 mm, and allow it to solidify fully at room temperature. While the agarose is still setting, use a spatula to knock loose any visible air bubbles stuck to the channels' sides. Unmold the set agarose and use a clean razor to trim down channels to the desired size, typically small enough to fit on the slides that will be imaged but still long enough that a coverslip cannot completely cover the channels lengthwise (this makes it easier to lift coverslips from the channels to make adjustments, such as freeing air bubbles, during imaging). Store channels immersed in water at 4 °C for up to 2 wk.

Agarose channels should typically have even, smooth surfaces; see Troubleshooting if they do not.

13. Prior to behavior recording, bring the container with the channels up to room temperature. At this time, if needed, screen larvae for expression of the desired fluorescent structures using a stereomicroscope with fluorescent capabililties. For example, if the goal is to image calcium dynamics in a population of neurons, make sure fluorescence is visible in cells in the expected locations (e.g., inside the larval nerve cord or at the body wall). Larvae can be screened directly from the apple juice cap.

14. Set up imaging:

i. If imaging using an upright microscope: Use a pair of wide or blunt forceps to remove channel from the water and place the channel grooved-side-up on an imaging slide. Have ready a glass coverslip to put on top.

ii. If imaging using an inverted microscope, place the channel grooved side up on a clean surface, ready to transfer. Have ready either a slide with a thinned glass bottom or a coverslip placed in a coverslip holder slide.

15. Use a paintbrush to select a larva from an agar/juice cap, handling it gently. Wash off any food by briefly submerging the larva in water, then place the larva into one of the channel grooves and adjust its position (Figure 3.1A). It can be oriented in any direction depending on what structure is to be imaged.

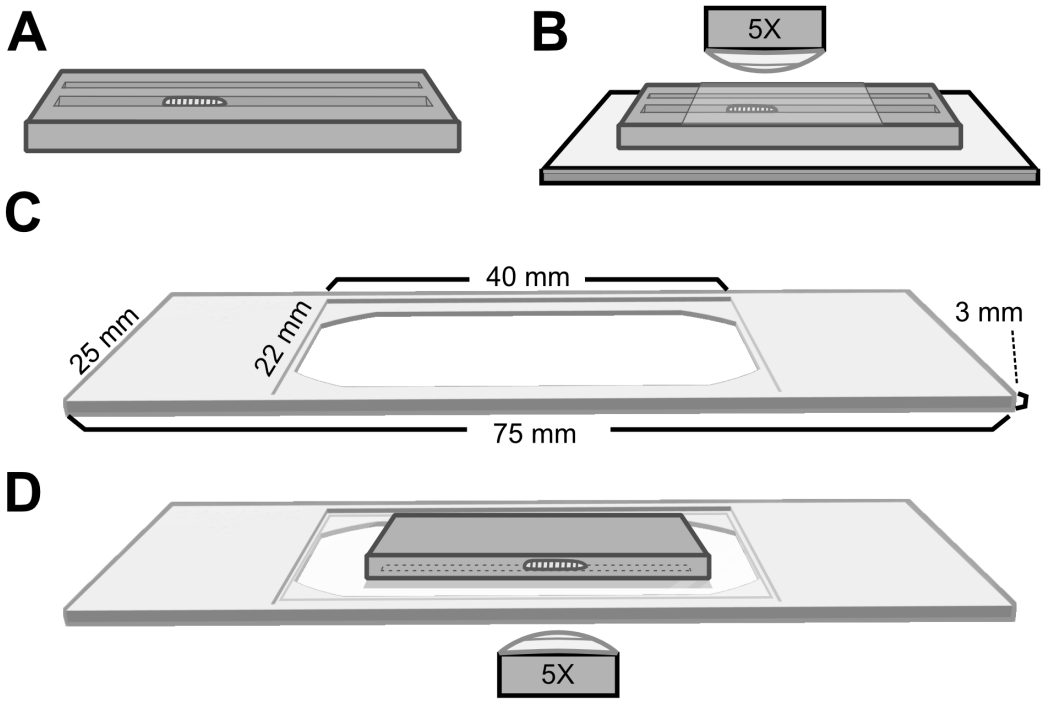

Figure 3.1. Example setups for upright and inverted imaging of larvae inside agarose channels. **A)** Schematic of agarose channels with larva inside. In the example, two channels are cast next to each other with different diameters. Using molds that have channels of different dimensions allows the experimenter to fit the larva to the appropriately-sized channel, one with a diameter that contains the larva snugly without squishing it too tightly for it to crawl. **B)** Schematic of upright imaging setup (dimensions not to scale). Larva is placed inside the agarose channels as in **(A)**, and agarose channels are placed on top of a standard glass 75 x 25 mm slide. The channels are filled with water and larva is held in place inside the channels with a coverslip. Coverslip can be of various sizes (e.g., 22 x 22 or 22 x 40 mm). Imaging can be performed with 5X objective magnification (sufficient to visualize the full body length of a first-instar larva) or with higher or lower magnification, depending on the age of the larva and scale of the structures to be imaged. **C)** To-scale model of 3D printable coverslip holder slide, which is used for inverted imaging of larvae crawling inside agarose channels. "Outer" dimensions: 75 x 25 x 3 mm; cutaway "inner" dimensions (ledge supporting coverslip): 40 x 22 mm. Hole cut through most of the inner ledge allows imaging from beneath the slide. **D)** Schematic of inverted imaging setup (dimensions not to scale). Coverslip (40 x 22 mm) is placed on the ledge of the coverslip holder slide, and the agarose channels (with larva already positioned inside) are inverted to sandwich the larva between coverslip and channels. The channels are filled with water as in upright imaging. N.B.: If the dorsal surface of the larva is to be imaged, the larva will be flipped upside-down in this configuration.

16. If imaging using an upright microscope, place the coverslip on top (Figure 3.1B). This should constrain the larva inside the channel. If needed, adjust the orientation of the larva by gently nudging the channel while holding the coverslip in place. If this does not change the orientation of the larvae, remove the coverslip and readjust the larva using the paintbrush.

If imaging using an inverted microscope, flip the entire preparation (channel and pre-positioned larva) upside-down onto the thinned-bottom glass slide or coverslip holder slide (Figure 3.1C). The larva should be at the bottom, accessible for inverted imaging (Figure 3.1D). If needed, adjust the orientation of the larva by gently nudging the channel to roll the larva.

Keep distilled water on hand during imaging to rehydrate the agarose channels as needed. The larva should be fully surrounded by water during imaging, and the channel should be free of air bubbles. If there are air bubbles, lift up the coverslip (or the edge of the channels, if these are upside down for inverted imaging) to let the bubbles escape. If there is insufficient water in the channels, add a small amount of distilled water using a clean paintbrush.

If larvae will not crawl inside channels, they may be mismatched with channel size; see Troubleshooting for tips on matching larvae with appropriately sized channels.

If larvae will not crawl inside the channel despite a good size match, see Troubleshooting for tips on agarose concentration and channel hydration.

17. Image the larva and obtain time-series data of interest (e.g., calcium activity in neurons or muscles during crawling). Fast imaging is important to maximize the ability to follow larval movements; we recommend imaging at least 20 frames per second using a stereomicroscope and camera or a spinning disk confocal microscope. To image first-instar

larvae, with the entire animal in the field of view, use a 5X objective; use a lower magnification to image larger animals.

Imaging and analysis steps are not described here due to this method's wide range of possible applications; however, example applications may be found in Heckscher et al., 2012 and Zarin et al., 2019.

We note that both manual and machine-learning-based approaches (e.g., LEAP, DeepLabCut, or others -- Pereira et al. 2019; Mathis et al. 2018) may be used to track the position of structures over time, producing kinematic data. See Heckscher et al. 2012 or Sun and Heckscher 2015 for example data.

See Troubleshooting if the structure of interest moves out of focus during imaging.

3.4. Troubleshooting

Problem (Step 10): Poor larval health is observed. Signs of poor health include many unhatched eggs, dead larval bodies away from the yeast paste, and larvae with significant dark patches in the abdomen, indicating an immune reaction.

Solution: If larvae are unhealthy, the juice caps/yeast paste may be too old or contaminated, or the adult flies may no longer be healthy/producing viable gametes. Obtain a clean chamber in case of contamination, make fresh apple juice agar caps and yeast paste, and set a fresh parental cross as in Step 1. A large size disparity between male and female adult flies (in particular, males much smaller than females) can also prevent successful mating and result in many unhatched eggs.

Problem (Step 12): Irregularities in channel surfaces are observed.

Solution: The channel molds themselves may have uneven surfaces: 3-D printing and laser etching into a substrate will typically produce irregular channel surfaces, which will translate into irregularities in the agarose channels. Consider additional steps, such as sanding, to smooth channel surfaces to even out irregularities. Note that sanding surfaces will decrease the overall size of channels cast from a negative mold or increase the overall size of channels cast from a positive mold (see Discussion); one may wish to adjust the initial dimensions accordingly when generating laser-etched or 3D-printed molds.

Problem (Step 12): After the agarose sets, the agarose channels have pockets left by dissolved air bubbles.

Solution: When casting channels, while the agarose is still hot, use a paintbrush or spatula to manually dislodge all visible bubbles. Alternatively, use a vacuum to extract bubbles while the agarose is setting, and/or slow the cooling rate by keeping the channels above room temperature (e.g., inside a warm incubator), which will give bubbles more time to detach from the channels and rise to the surface.

Problem (Step 16): The larva is too large for the channel.

Solution: If the animal is placed in too shallow of a channel, part of the animal's body will visibly overflow the sides of the top of the channel. In this case, the larva may be too squeezed to crawl. Alternatively, the larva's body may prevent the coverslip from making good contact with the agarose channels, and the larva will not be well constrained inside the channel. In any of these cases, generate a deeper channel, or replace the larva with a smaller animal.

Problem (Step 16): Larvae do not crawl in the channel, despite fitting entirely inside the channel.

Solution: In this case, it may be either that the agarose surface is too slippery for larvae to crawl on, or that the animal has dried out too much. In most circumstances, larvae will only crawl when well-moistened; we typically image larvae that are fully surrounded by water in the channels. Agarose concentration can be varied to obtain surfaces with different properties (e.g., higher % agarose: lower friction and more difficult for animals to burrow into). Lower the agarose concentration if the surface is too slippery. If a larva at first crawls in the channel but later stops, it may be too dry: add distilled water to the insides of the channels and retry. To keep channels hydrated for longer during imaging, we recommend adding a small buffer of water on the slide or coverslip, around the outside of the channels.

Problem (Step 17): Sample moves out of focus during imaging (motion in the Z-direction).

Solution: Place the larva in a smaller channel, so that more of the animal is pressed against the coverslip: for parts of the larva that are more exterior, such as muscles or other features on or beneath the cuticle, being pressed against the coverslip will reduce overall Z-axis motion (motion in depth/distance from the objective). However, for more interior parts of the larva, Z-axis motion may still be substantial. Researchers should take potential Z-axis motion into account when interpreting time series data. See Discussion (section "Cellular Activity Data") for further information.

Problem (Step 17): Larval orientation changes during the imaging session.

Solution: It is easier to maintain a dorsal or ventral up view than a lateral view. Larvae tend to roll towards having either their dorsal or ventral surface in contact with the coverslip. To

image the lateral surface, constrain larvae more tightly inside a shallower channel. Note that this will also slow larval movements.

3.5. Discussion

Thanks to the numerous and sophisticated genetic tools available, *Drosophila melanogaster* has long been a leading model system for the study of development, including neuromuscular system development (Keshishian et al. 1996). The larval stage of Drosophila has more recently emerged as a promising system for the study of motor control and the neural basis of behavior (Clark et al. 2018; Eschbach and Zlatic 2020; Kohsaka 2023; Vogelstein et al. 2014). The utility of larval Drosophila derives from the combination of readily available genetic tools (Clark et al. 2016, Li et al. 2014), connectomic datasets (Eschbach and Zlatic 2020; Ohyama et al. 2015; Schneider-Mizell et al. 2016), and the larva's optical transparency (relative to adult flies or to most other organisms), which together result in a wide range of targeted circuit perturbations that can be paired with imaging neural activity and/or behavior in the intact animal (Berni 2015; He et al. 2019; Karagyozov et al. 2018; Kohsaka 2023; Vaadia et al. 2019). To understand the effects of these perturbations on neural circuits and behavior, obtaining high-resolution behavioral data is key. Here, we describe a method for obtaining high-resolution behavioral data from larval Drosophila inside agarose channels. In this method, larvae are placed in channels and imaged under a microscope. After imaging, visible features of interest are tracked over time. (For example features of interest, see the Kinematic Data and Cellular Activity Data sections.) Imaging in agarose channels provides a convenient way to record a subset of

larval behaviors in the intact animal, as an alternative to imaging freely-crawling larvae or semi-intact preparations (Heckscher et al. 2012; Sun and Heckscher 2016; Zarin et al. 2019).

Imaging in linear channels constrains larvae to crawl forward or backward within a well-controlled depth range, which offers several advantages over freely-crawling preparations. (1) Agarose channels are optically clear, as is much of the larval body, making it possible to study the dynamic movements or changes in fluorescence intensity of larval structures that are labeled by fluorescent markers. Using channels allows the researcher to rotate larvae within the channels to place a structure of interest nearer to the objective, allowing prolonged imaging of structures that would be difficult to keep in focus over many cycles in a freely-crawling preparation (Liu et al. 2023). (2) On point-scanning microscopes, imaging can be greatly sped up by aligning the long axis of the channel with the faster scanning plane (typically the horizontal or X axis), which allows frame dimensions to be decreased from a full square to a much smaller number of rows and thereby reduces the overall time required per frame. (3) Compared to freely-crawling preparations, manual larval tracking is easier in linear channels because it is reduced to a one-dimensional problem (tracking microscopes provide an alternative solution, e.g., (Cermak et al. 2020; Yamaguchi et al. 2023), but may need to be designed around the specific use case). (4) Compared to freely-crawling preparations, larval movements are simplified, as the animals can no longer turn. This allows researchers to select for linear forward and backward locomotion or other behaviors (e.g., mouth/head movements) that the larvae can still perform inside the channels. It is important to note that although larvae will be constrained to crawl forwards or backward, these constraints should not be interpreted as eliminating other behaviors (for instance, larvae may still attempt to turn despite being unable to complete the turn). (5) In

principle, channel design could enable the study of additional behaviors while retaining the above benefits. For instance, channels could angle, curve, or branch, allowing larvae to turn, bend, or choose one of the multiple pathways within experimenter-defined limits. (6) An animal's crawling speed can be influenced by adjusting the width of the channel relative to the larval size. (7) Channels are amenable to various microscopes and objectives, from low-resolution imaging on stereoscopes to high-resolution imaging on confocal microscopes.

Caution is needed when comparing behavioral data from experiments conducted inside agarose channels to data from surface crawling experiments, as the different environments will likely lead to substantial behavioral differences. For instance, overall crawling speed is known to be slower inside channels (Heckscher et al. 2012). Additionally, larvae crawling inside agarose channels will almost certainly receive different sensory stimuli than larvae crawling along a flat surface. We therefore advise against directly comparing behavioral statistics obtained from channel crawling to those reported from freely-crawling experiments, except where other experimental conditions were identical.

3.5.1. Kinematic data

By imaging larvae inside agarose channels, researchers can obtain high-resolution video data on the movement of larval features (fluorescent markers, body parts, etc.) as animals crawl. To make use of these video data, the features of interest must be converted into kinematic data by tracking them over time. ("Kinematic" data are data that quantify the trajectories of objects, such as larval body parts, over time.) Several tracking algorithms have been developed to automate this process (e.g., DeepLabCut (Mathis et al. 2018) and LEAP (Pereira et al. 2019)), greatly

scaling up the quantity of data that can be analyzed (for an example application of automated tracking, see Liu et al. 2023).

As an example of a kinematic study, suppose a researcher wishes to test the effects of a manipulation that they expect to alter how neural activity propagates along the nerve cord during larval locomotion (for example manipulations, see Itakura et al. 2015 or Fushiki et al. 2016). The researcher develops a hypothesis as to how this manipulation will affect the recruitment of larval body segments during crawling (e.g., by increasing the amount of time individual segments spend contracted relative to the period of each locomotor cycle). To test their hypothesis, the researcher needs kinematic data on the movement of body segments during crawling in both manipulated and control locomotor cycles (or animals). In this case, the researcher would process videos of larvae crawling inside channels by tracking the features of interest: the boundaries between body segments. They could perform this tracking manually, by annotating one or more points along each segment boundary for a set of video frames (Heckscher et al. 2012, Zarin et al. 2019, Sun et al. 2022), or semi-automatically, by training a DeepLabCut/LEAP network to recognize and predict the location of such points across frames (Liu et al. 2023). By calculating the distance between equivalent points in each segment boundary over time, the researcher can test whether their manipulation has, indeed, affected the amplitude or duration of segment contractions.

We note here that many anatomical structures cannot be visualized without fluorescent labeling. In the above example where segment boundaries must be tracked, we would recommend using larvae that express a fluorophore either marking segment boundaries [e.g., at muscle attachment sites in the body wall (tubP-GAL4 combined with UAS-fondue::GFP, which

accumulates at muscle attachment sites, as in Sun et al. 2022) or inside their body wall muscles (e.g., MHC-GFP, as in Heckscher et al. 2012)] and imaging using fluorescence microscopy. As for any imaging experiment, when designing channel-based experiments and determining the genotypes of animals to use, it is essential to consider how the effects of an experimental manipulation can be visualized in the same animal. We therefore recommend confirming, as early as possible during experimental design, that the feature of interest can be imaged stably over time while larvae crawl inside channels.

3.5.2. Cellular activity data

When cellular activity is in question, it is especially important to be able to obtain high-resolution (spatial and temporal resolution) video data while keeping the cells of interest in focus at all times. Agarose channels can be especially helpful in these cases, for two reasons. First, as mentioned above, channels facilitate tracking the larva's motion under high magnification, which can help to spatially resolve the cells of interest in cases where these cells are nearby other fluorescing cells. Second, the physical constraints of the channel and cover slip reduce a larva's overall motion in the depth (Z) axis and can help keep cells in focus over time, particularly cells at or near the body surface (such as muscles or peripheral sensory neurons) that are proximal to the cover slip and are somewhat flattened against the glass (Vaadia et al. 2019, Zarin et al. 2019).

Even with the physical constraints imposed by agarose channels, however, cells or other features of interest may move in the Z axis over time. This potential motion can change the apparent brightness of the fluorescent feature, by moving it in or out of focus, and therefore should be accounted for when analyzing activity signals from calcium or voltage indicators. Correcting for motion can be done using one of two main strategies: either by pairing dynamic

activity indicators with static fluorophores and normalizing the signal from the dynamic indicator to the signal from the static indicator (e.g., expressing Ca2+-sensitive green fluorescent protein coupled with a Ca2+-insensitive red fluorescent protein, as in UAS-Gerry flies (BDSC_8024); see Creamer et al. 2022 for an example of correcting for motion using this strategy), or by using ratiometric sensors, which report dynamic activity as the ratio of two fluorophore colors (such as the Cameleon family of sensors, e.g., UAS-YC3.6 flies (BDSC_93057), which report calcium concentration as a yellow-to-cyan ratio; Nagai et al., 2004).

3.5.3. Generating linear channels

Essential to the methodology described in this protocol is the design and production of channels relevant to the question under study. Channel production occurs in three stages and is usually an iterative process. The first stage is designing the channel template to be produced, including determining the dimensions of linear channels and their layout on a mold. The second stage is manufacturing the channel molds; we describe below possible methods to do this, involving photolithography, laser cutting/etching, or 3D printing. The final step is testing the channels by creating agarose casts (see Steps 5-6) and ensuring that larvae of the correct size can fit and move inside them (Step 9-10). Existing templates for laser/photolithographic etching or for 3D printing of channel molds can be obtained upon request from the Heckscher Lab.

3.5.4. Channel design

When designing channel templates, consider first the size of the larvae and the distance a larva is expected to crawl in a given imaging setup; these will determine the diameters and lengths of the channels. For experimental convenience, we recommend designing a set of adjacent channels in multiple widths (e.g., as depicted in Figure 3.1A). Channels will typically

be shallower than larval body diameter, which tends to slow larval crawling and flatten the cuticle against the coverslip. Having several adjacent channels in different widths will make it easy for an experimenter to match larvae of slightly different sizes to the appropriate channel width. Tailor the range of widths to the instar of interest. Approximate larval widths for first instar are 100-300 μm, for second instar are 300-500 μm, and for third instar are 500-700 μm. (Graf and Sokolowski, 1989). It is also helpful to test channels with a range of depths, since a single depth may not constrain both large and small larvae from the same instar. As starting points, we have found that around 150 μm, 200 μm, and 300 μm are good depths for first, second, and third instar larvae, respectively.

Channels do not have to be straight lines: you may wish to introduce choice points or curvature to force larvae to turn or bend. When manufacturing channels, it may also be possible to produce smooth or uneven surfaces that provide larvae with different frictive and sensory elements.

3.5.5. Channel mold manufacturing

When manufacturing channel molds, the original channel molds can be either negative or positive: *negative* if channels are raised grooves (3D printed on a flat base); *positive* if channels are depressed tracks (for instance, etched or laser cut into an acrylic surface). If the original mold is negative, agarose channels can be cast directly against it. If the original mold is positive, an intermediate negative mold must first be cast in polymethylsiloxane (PDMS), such as Sylgard 184; see Steps 1–3. When laser etching or 3D printing molds, the channel dimensions of the final printed mold may not exactly match those of the original template and must be estimated after printing; see Step 6. We have found both laser-etched and 3D-printed channel diameters tend to

run larger than the original template by 100 μm. The following sections provide a more detailed guide.

Creating positive molds using photolithography

Briefly, a photoactive substrate is spun into a sheet of the desired depth ("photoresist"); the maximum depth of the photoresist layer will determine the maximum depth of the channels to be etched. The provided two-dimensional template (i.e., the shapes of the desired channels) creates a mask that prevents photocuring, and the masked photoresist is exposed to UV light; when removed, masked areas can be dissolved away, leaving grooves (a positive mold). Photolithography is typically performed by a commercial provider or other dedicated micro/nanofabrication facility; for further details about the process, we recommend consulting manufacturer-provided information (e.g., MSE Supplies: https://www.msesupplies.com/products/photolithography-services). This technique can be used to create channel depths appropriate for first-instar larvae (approx. 150 μm). Advantages include (1) smooth surfaces (compared to laser-cut channels) and precise channel dimensions. Disadvantages include (1) limited maximum depth achievable, depending on the manufacturer and (2) fabrication cost.

Creating positive molds using laser etching/cutting

CO_2 lasers, available in many academic and commercial fabrication laboratories, can etch channels into acrylic (or other laser-safe materials). Laser etching procedures use the provided 2D template (i.e., shapes of the desired channels) to determine where to apply laser power to a substrate. The depth of channels etched can be modulated by changing the amount of laser power and by performing multiple rounds of etching. Further details about the process can be obtained from manufacturers (e.g., Xometry: https://www.xometry.com/capabilities/sheet-cutting/laser-

cutting/). One drawback of laser etching is that channel depths are not directly controlled and can be challenging to measure. Depth estimates can be obtained by fitting small-diameter dowel rods into a channel and using a height gauge to measure the difference between the full rod length and the rod height above the channel surface. Either laser etching or laser cutting may result in channels slightly wider than the original template, and the minimum width obtainable will depend on the machine's resolution.

CHAPTER 4

MULTIPLE SCALES OF COORDINATION FOR LARVAL DROSOPHILA LOCOMOTION

4.1. Introduction

To produce locomotion, movement must be coordinated across the entire body. In segmented, limbless animals, this means segments must coordinate contraction and relaxation in terms of timing, amplitude, rate, duration, etc. Depending on the constraints of body form, environment, and behavioral goals, this coordination could look different between different regions of the body axis (Webb, 1973; Rotheray, 2019; Di Santo et al., 2021). In particular, the anterior and posterior ends of the body axis may have different requirements for segmental independence. In limbless locomotor behaviors, posterior regions are typically the source of locomotor power (swimming) or anchoring and stability (crawling) (Rome et al., 1993; Chen et al., 2011), while the head end directs this power to straight locomotion or performs turning, searching, and other behaviors (Stern-Tomlinson et al., 1986; Kristan Jr et al., 2005; Tytell and Cohen, 2008). Thus, flexible coordination of movements and their timings between these regions could allow animals to juggle multiple behavioral goals, such as navigating while making progress or maintaining a stable posture (Tytell and Cohen, 2008; Cacciatore et al., 2010; van Griethuijsen & Trimmer, 2010; Gomez-Marin and Louis, 2014). Alternatively, consistent coordination of movements and their timings across the body could maximize speed or energy-efficiency of waves (Lighthill, 1969), or contribute to other behavioral goals (Akanyeti et al.,

2016). Therefore, understanding how particular animals coordinate segments across the body is critical to understanding the locomotor strategies used to meet distinct behavioral goals.

How animals coordinate segments across the body has often been investigated and modeled as a problem of neuronal coupling, i.e., the strength and anatomical identity of neuronal connections between segments and their pattern-generating circuits (Grillner et al., 1991; Kristan Jr et al., 2005; Grillner and El Manira, 2019). However, a substantial portion of kinematic coupling among segments, i.e., the strength of relationships between segments' movements, may instead be due to properties of the body itself and of the body's interaction with the environment (Wardle et al., 1995; McMillen et al., 2008; Pulver et al., 2015; Schiebel et al., 2019). Therefore, to understand neural control of locomotion in the context of a particular body and environment, it is equally necessary to understand the relationship between neuronal and kinematic coupling (Tytell et al., 2011). However, determining this relationship is exceptionally challenging within the context of behaving bodies. Among the reasons for this is that it is technically challenging to record neural or muscular activity while animals move freely, and particularly from distant segments simultaneously (Ekeberg and Grillner, 1999; Mullins et al., 2011). Therefore, to parse the relative contributions of neuronal coupling and biomechanics to locomotor behavior, a model is needed in which intersegmental kinematic and neuromuscular coordination can be simultaneously characterized in the behaving animal.

The limbless, segmented larval stage of *Drosophila melanogaster* is a particularly promising model in which to link kinematic and neuromuscular coordination of locomotion, for several reasons. First, in Drosophila larvae, large portions of premotor circuits have been mapped in the ventral nerve cord connectome (Schneider-Mizell et al., 2016; Zarin et al., 2019) and many

key neurons functionally characterized (reviewed in Clark et al., 2018; Gowda et al., 2021; Hunter et al., 2021; Kohsaka, 2023), providing a strong circuit foundation for interpreting behavioral coordination. Next, recent work has characterized forces produced by larval muscles and by interactions with the substrate, which will enable modeling how muscle activation translates into body-environment interactions (Ormerod et al., 2022; Sun et al., 2022; Kohsaka, 2023; Booth et al., 2024). Crucially, diverse genetic tools provide the ability to target and manipulate a wide range of cell types (Pfeiffer et al., 2008); coupled with the larva's relative transparency, this allows acute optogenetic (among other) manipulations and optical recordings of calcium activity while observing locomotor behavior in otherwise intact animals (Inada et al., 2011; He et al., 2019; Vaadia et al., 2019; Murawski et al., 2020; McNulty et al., 2024).

Finally, in aggregate, larval locomotor behaviors have been well characterized. They are regionally specialized: locomotor waves begin with contraction of the tail end, followed by an anterior-propagating wave of segmental contractions (Green et al., 1983; Berrigan and Pepin, 1995; Heckscher et al., 2012). Between waves, anterior segments produce a range of movements for active sensing and reorientation, while posterior segments are inhibited from moving during these actions (Lahiri et al., 2011; Gomez-Marin et al., 2011; Tastekin et al., 2018). In general, therefore, neuromuscular and kinematic activity are differently coordinated across the body axis. However, it is an open question whether flexible coordination across the body axis is a feature of locomotor waves themselves. Further, the relationship between segments' muscle recruitment and the movements they produce during locomotion is unknown, leaving it unclear how much of locomotor coordination is due to coordinated neuromuscular activity, as opposed to

biomechanical or other physical coupling across segments (Chiel et al., 2009; Loveless et al., 2019).

To answer both questions, we first constrained larvae inside linear channels, to enable simultaneous recording of segmental kinematics and muscle recruitment while larvae produced locomotor waves. We then characterized how segments were coordinated across the body. First, we investigated three aspects of kinematic coordination: consistency of movements made by different body segments; timing relationships between segments' movements; and how tightly coupled were segments' movements to each other (i.e., which segments were more or less flexibly coordinated with others). We found axial heterogeneity in all three aspects of kinematic coordination. Segments contracted with axially-varying kinematics and phase intervals, and segments' contraction durations were more strongly coupled at the posterior end, suggesting that kinematic coordination depends on axial position and may reflect or support regionalized roles in behavior. Then, we compared these results to the consistency of muscle recruitment across the body. We found correspondence between kinematic and muscle recruitment coordination, with two exceptions: first, a positional offset in the closest correspondence between recruitment and kinematic features; second, strong anterior variability in segments' recruitment phases as compared to contraction phases. Both of these differences in the coordination of recruitment versus kinematics may reflect outcomes of biomechanical coupling and/or sensory feedback for the behavior. In all, for larvae crawling inside channels, we find a large degree of axial variation in the coordination and coupling of body segments, consistent with flexible central architectures that allow for anterior- and posterior-specific behavioral roles.

4.2. Results

Our primary goal was to ask how larval segments are coordinated across the body axis during locomotion. We investigated coordination in three questions: First, how consistent are the movements made by individual body segments? Second, how consistent are the timing relationships between segments? Third, how tightly coupled are segments' movements to each other on a cycle-to-cycle basis (i.e., which segments are more or less flexibly coordinated with others)?

To answer all three questions requires collection of many cycles of locomotion from intact animals, both so that a range of possible coordination patterns can be collected and so that relationships among segments can be reliably established. However, Drosophila larvae crawling on flat surfaces perform a rich repertoire of behaviors (Green et al., 1983; Kohsaka et al., 2017; Clark et al., 2018), making it difficult to obtain a large number of locomotor cycles (waves). Therefore, to limit the behavioral repertoire to forward and reverse waves, we placed larvae inside linear agarose channels while imaging them (Heckscher et al., 2012; Greaney and Heckscher, 2024) (Figure 4.1A). This had the added benefit of keeping fluorescent segmental musculature in focus while animals moved. Below, we briefly describe the experimental setup and the procedure for extracting segmental kinematic data for each locomotor cycle.

4.2.1. Many cycles of segment-level kinematic and muscle recruitment data are obtained per larva using automated segment boundary tracking

To record locomotor behavior, fluorescent larvae were placed inside linear agarose channels and imaged while they crawled using confocal fluorescence microscopy (Figure 4.1A, Methods). An initial set of 18 first-instar larvae expressed jGCaMP7f in all body wall muscle

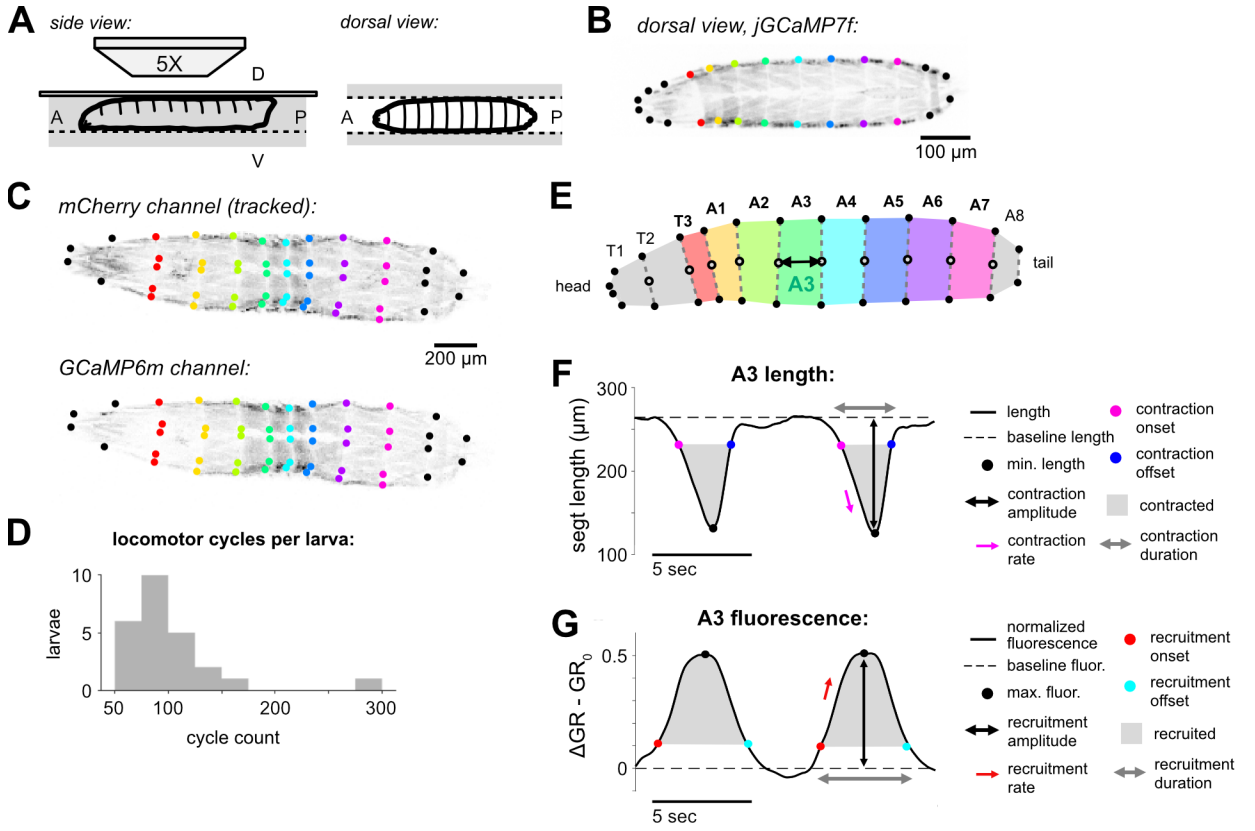

Figure 4.1: Segment-level kinematic and muscle recruitment data were obtained for many cycles of larval locomotion. A: Imaging setup. Transgenic larvae crawled inside linear agarose channels with diameters similar to their body. Larvae expressed either jGCaMP7f (n=18) or Gerry (mCherry-GCaMP6m; n=7) in all body wall muscles. Fluorescence images were acquired by confocal microscopy. **B:** Example frame for a crawling jGCaMP7f larva. Greyscale values = jGCaMP7f fluorescence intensity. A DeepLabCut (DLC) network (Mathis et al., 2018) was trained to recognize and predict segment boundaries (2x markers per segment boundary). Keypoints (colored dots) were placed on left and right edge of each segment boundary. **C:** Example frame for a crawling Gerry larva. Red (top) and green (bottom) emitted fluorescence were collected in separate channels. A DLC network was trained to recognize and predict segment boundaries (5x keypoints for most segment boundaries) using the red mCherry fluorescence (top). For each frame, the markers surrounding each segment defined a corresponding region of interest, from which fluorescence values were extracted. **D:** Number of locomotor cycles obtained per larva imaged, n=25 larvae. **E:** Example single-frame representation of larval position. Markers corresponding to each segment boundary were converted into boundary centroids (white dots). A segment's length on a given frame = the Cartesian distance between the centroids of its two boundaries (e.g., double-headed arrow shown for A3). **F:** Defining contraction features from example segment length trace (A3) during 15 seconds of recording. Baseline length (dashed line) was defined as the 95th percentile of the segment's overall length distribution. Trough lengths (black dots) were found as peaks in the inverted length trace. Contraction amplitude for a cycle (black double-headed arrow) was defined as the difference between baseline length and trough length on that cycle, normalized to baseline length. Contraction onsets around each trough (pink dots) were defined as the interpolated times at which a segment shortened to 75% of the length difference between the preceding peak and the trough; contraction offsets (blue dots) were times at which the segment lengthened to 75% of the length difference between the trough and the following peak. The total contraction duration (time spent in grey shaded area, grey double-headed arrow) was defined as the time between contraction onset and offset.

Figure 4.1, continued. Segment-level kinematic and muscle recruitment data were obtained for many cycles of larval locomotion.
G: Defining recruitment features from example normalized segment fluorescence trace (same segment, larva, and time period as in F). Normalized fluorescence on each frame was defined as $\Delta G{:}R - G{:}R_0$, where $G{:}R_0$ was the "baseline" green-to-red fluorescence ratio and $\Delta G{:}R$ was the current frame's difference from baseline. Recruitment peaks (black dots) were defined as peaks in the normalized fluorescence trace, and recruitment amplitudes (black double-headed arrow) were defined as these peak values with respect to baseline. Recruitment onsets (red dots) and offsets (cyan dots) were defined as the interpolated times at which normalized fluorescence rose to 25% of the difference between baseline and peak, then decreased to 25% of the difference between baseline and peak, respectively. The total recruitment duration (time spent in grey shaded area, grey double-headed arrow) was defined as the time between recruitment onset and offset.

cells (Figure 4.1B; Supplementary Video 1); this fluorescence enabled visualization of segment boundaries over time. A later set of 7 second-instar larvae instead expressed "Gerry," GCaMP6m tethered to mCherry, inside all body wall muscle cells (Figure 4.1C; Supplementary Video 2). In this second set of animals, the presence of a stable red signal (mCherry) alongside the calcium-dependent green signal (GCaMP6m) allowed us to account for movement artifacts in the GCaMP channel, such as increases in apparent brightness due to muscles shortening during locomotion. This enabled analysis of muscle calcium activity as a proxy for recruitment of muscles by motor neurons.

From the full set of 25 animals, we obtained an average of 101 forward locomotor cycles (see Methods), between 52 minimum and 280 maximum (Figure 4.1D). We used the full dataset to investigate the kinematic coordination of larval locomotor behavior (Figures 4.1-4.4) and the subset of 7 Gerry-expressing animals to investigate the relationship between segment kinematics and neuromuscular activity (Figures 4.5-4.6). Distributions of estimated larval sizes and cycle statistics (speeds, periods, distances) are provided in Supplementary Figure 4.1.

To obtain segmental kinematic information, we employed the DeepLabCut machine vision package (Mathis et al., 2018). Using DeepLabCut tracking, we converted the fluorescence

microscopy videos of larvae crawling into segment boundary positions over time (see Methods; Supplementary Videos 3 and 4). From these segment boundary positions, we calculated the lengths of each segment from T3 to A7 over time (Figure 4.1E). To compare contraction kinematics across segments, we used each segment's lengths over time to define three kinematic features for each locomotor cycle (Figure 4.1F). First, segments' contraction amplitudes were defined as the maximum decrease from the segment's baseline length on each cycle, normalized to baseline length. Second, segments' contraction rates were defined as the maximum rate of shortening on a given cycle. Third, segments' contraction durations were defined as the period of time between contraction onset and offset (see Methods).

Together, these kinematic features allowed us to characterize segmental contractions in depth, using measurements comparable to other recent work (Sun et al., 2022). Further, we reasoned that any of these three kinematic features might need to be coordinated across segments for successful crawling behavior. For instance, contraction amplitudes might need to be coordinated to ensure that segments returned to the correct baseline length after a wave; contraction rates, as an indicator of the strength of motor drive to each segment (Mason and Kristan, 1982; Woods et al., 2008); or contraction durations, to ensure an efficient duty cycle with an appropriate number of segments contacting the surface at once, providing stability or traction. In particular, coordinated contraction durations are likely essential for efficient crawling, as their dysregulation frequently co-occurs with slowed crawling when (e.g.) sensory inputs are perturbed (Hughes and Thomas, 2007). Alternatively, coordinating any of these features across segments might not be essential for the reasons above, but could still reveal underlying neural or biomechanical coupling mechanisms that constrain the behavior. Therefore,

we analyzed both the distributions and the coupling (co-modulation) of each of these features across the body axis (Figures 4.2-4.4).

Similarly, in the Gerry-expressing larvae, we used the boundaries of segments to extract bulk estimates of segmental fluorescence over time. To estimate each segment's change in muscle recruitment over time, we normalized green GCaMP to red mCherry fluorescence and subtracted away each segment's baseline green:red ratio (see Methods). We used this normalized fluorescence estimate to determine the times when segments were recruited, the relative amplitude of recruitment on each cycle, and the peak rates of recruitment (Figure 4.1G). By comparing these analogous features of segments' contraction kinematics and recruitment, we evaluated how the neuromuscular coordination related to the kinematic coordination of locomotor waves (Figures 4.5-4.6).

4.2.2. Segmental contraction kinematics differ along the body axis

We began characterizing the kinematic coordination of locomotor waves by addressing how consistent or varying were the movements made by individual larval body segments. In other locomotor systems, it is common to find monotonically-varying segmental kinematics (e.g., undulation/contraction amplitudes increasing from anterior to posterior in anguilliform swimming; slower elongation and faster contraction rates moving from anterior to posterior in leech crawling (Williams et al., 1989; Cacciatore et al., 2000; Di Santo et al., 2021). Such axial changes in kinematics may be critical for behavior, as in the case of anguilliform swimming, where they are part of speed control (Ellerby et al., 2001; Tytell, 2004; Anastasiadis et al., 2023). By contrast, previous investigations of larvae crawling on surfaces found consistent contractions across the body; however, segment-level contraction kinematics remained to be compared for

larvae crawling in channel environments. Therefore, we compared the kinematic features of each segment's contractions.

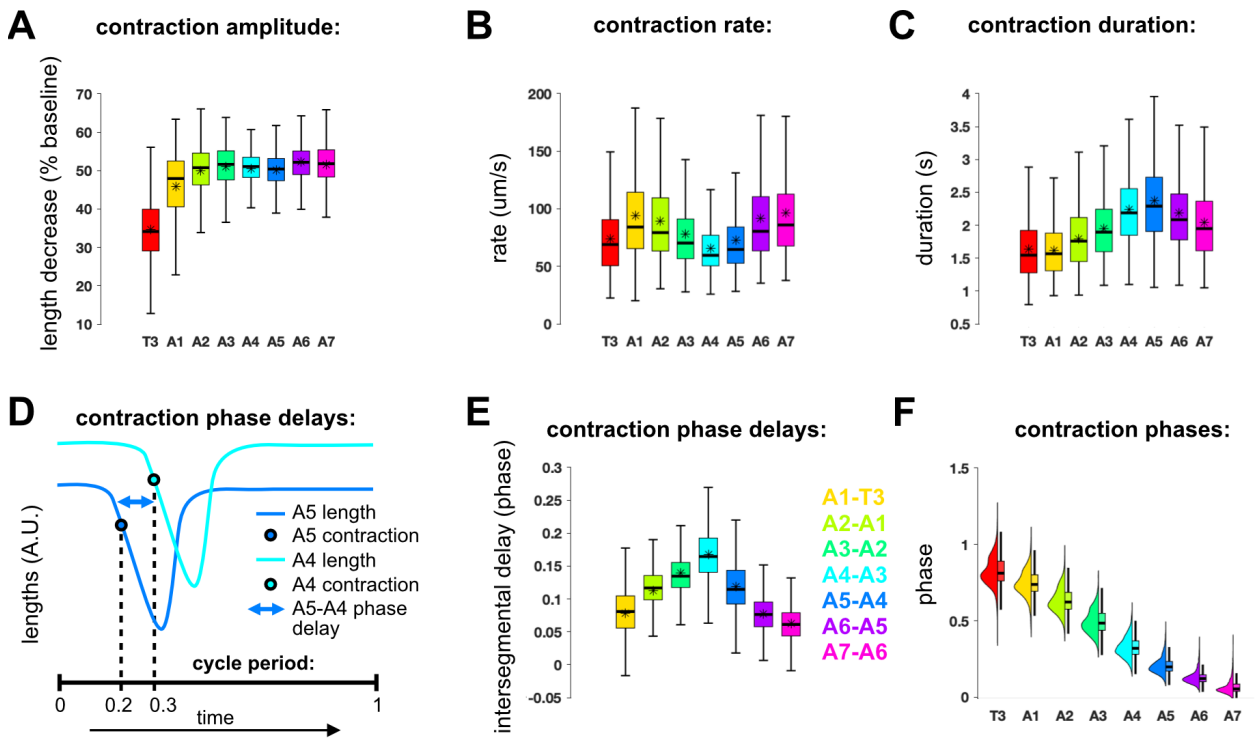

Figure 4.2: Contraction kinematics and phase relationships of individual body segments vary along the A-P axis. **A:** Distributions of per-cycle contraction amplitudes for segments T3 through A7 (from left to right), given as percentage of segment's baseline length. Box plot (without outliers) is given for each segment. Asterisk over box plot shows mean value. All pairs of distributions were significantly different ($p<0.05$) except for A2 vs. A4, A3 vs. A7, and A6 vs. A7. **B:** Segmental distributions of per-cycle maximum shortening rates. All pairs of distributions were significantly different ($p<0.05$) except for T3 vs. A5 and A1 vs. A6. **C:** Segmental distributions of per-cycle total contraction durations. All pairs of distributions were significantly different ($p<0.05$) except for A3 vs. A7. **D:** Schematic of calculating intersegmental contraction phase delays. Example simulated segment length traces for A5 (blue) and A4 (cyan) during a single cycle, vertically offset for clarity. Each segment's contraction onset labeled with dots; phase of contraction marked with respect to full cycle period (0=start of cycle; 1=end of cycle), beneath length traces. A5-A4 phase delay for the simulated cycle shown (black double-headed arrow) would be 0.1. **E:** Distributions of intersegmental contraction phase delays; each box plot represents per-cycle delay distribution between a pair of segments (e.g., delays from A1's contraction phases to T3's contraction phases, furthest left plot). All pairs of delay distributions were significantly different ($p<0.05$) except for A2-A1 vs. A5-A4. **F:** Distributions of per-cycle contraction phases for segments T3 through A7 (from left to right). Histogram and box plot (without outliers) are given for each segment. **All panels:** n=2529 cycles, 25 larvae. Significant differences between distributions in A-C and E were determined using nonparametric Friedman's test with post-hoc Dunn-Sidak corrected multiple comparisons.

We found axial variation in the segment-level distributions of all three kinematic features. First, we found differences in contraction amplitudes across segments: specifically, thoracic segment T3 contracted significantly less than abdominal segments (Figure 4.2A). Next, we found non-monotonically changing contraction rates across the body axis: contraction rates were highest for A1 and A7 and decreased in a U shape between them, with the slowest shortening in the mid-body segments A4 and A5 (Figure 4.2B). Finally, we also found non-monotonic changes in contraction durations per segment: in general, posterior segments contracted for longer than anterior segments. Segment A5 had the longest contraction durations, followed by segments A4, A6, and A7 (Figure 4.2C). Thus, segments differ in their contraction kinematics; in other words, during linear crawling in channels, a locomotor wave is not a series of uniform contractions propagating along the body.

4.2.3. Propagation of segmental contraction slows around mid-body

In addition to coordinating the amplitude and duration of movements, coordinating the relative timings of specific movements is generally critical for behavior. In the case of larval locomotion, the peristaltic wave depends on an ordered sequence of segmental contractions. The relative time at which each segment contracts can be expressed as a fraction of the total cycle period (i.e., its phase of contraction, Figure 4.2D). In swimming locomotion, timing coordination takes the form of uniform phase delays between consecutive segments, resulting in linear phase distributions along the body (Hill et al., 2003; Di Santo et al., 2021). However, soft-bodied crawling locomotion may call for, or at least tolerate, more flexible phase delays (Stern-Tomlinson et al., 1986; Cacciatore et al. 2000, Trimmer & Issberner 2007). Therefore, to ask whether timing coordination in the present behavior was consistent or flexible along the body

axis, we asked how segments' contraction timings are coordinated. We did so by evaluating the phase relationships between consecutively contracting segments.

We first quantified the intersegmental phase delays between segments' contractions (Figure 4.2D). A linearly-propagating wave would manifest as similar phase delays between all pairs of segments along the body axis. This was not what we found; instead, phase delays between consecutive pairs of segments' contractions varied along the body axis (Figure 4.2E). Propagation of contractions from one segment to the next took the longest around mid-body: in general, the longest delays were between A4's and A3's contractions. These uneven intersegmental delays resulted in non-linear phase distributions for segmental contractions (Figure 4.2F). Overall, a sigmoidal model was a better fit than a linear model for segmental contraction phase distributions (both for the combined data and for 23/25 individual larvae).

Given the differences between our findings and those previously obtained for larvae crawling on flat surfaces (Sun et al., 2022), it seemed possible that the axial differences in segmental coordination might directly result from physical constraints larvae faced when crawling inside channels. For instance, inside the channels, segment boundaries appeared widest in the mid-body (Supplementary Figure 4.2A). If larvae became more 'stuck' at particular segments, either because of these width differences or because of a 'bunching up' of tail-end segments at the beginning of the wave, we might see longer contraction durations and slower contraction rates simply because of increased difficulty in moving those segments. To test this possibility, we performed two analyses. First, we compared cycles during which individual larvae moved their tail ends forward by greater or lesser distances. We reasoned that, if a larva pushed its tail end and internal organs further forward during the initial "visceral piston" stage of

crawling (Simon et al., 2010; Heckscher et al., 2012), this would increase the compressive forces on segments during the wave, likely increasing their lateral expansion and the resistance against their forward movement when contracted. Therefore, we might expect might expect the existence, or location, of an axial peak in contraction durations to depend on how far the tail moved forward. To test this idea, we split each larva's cycles at the median into cycles with longer and shorter tail movement distances, then asked whether the trends in longest contraction durations and slowest contraction rates differed for each half of the data. However, splitting the data by tail forward movement distance did not result in different axial trends for either contraction rate or duration distributions (Supplementary Figure 4.2B).

As a second means of testing whether animals 'getting stuck' in the channels could explain our findings, we compared the segmental coordination of our two subpopulations: the smaller jGC7f larvae and the larger Gerry larvae. We noticed that, for the jGC7f larvae, cycle periods did not depend on an animal's estimated size (average segment length), suggesting that larger jGC7f larvae were not more impeded than smaller jGC7f larvae when crawling (Supplementary Figure 4.3A-B). By contrast, for the Gerry larvae, cycles took much longer to complete for larger animals, suggesting that these larvae were increasingly impeded by the channels at larger body sizes. Thus, by comparing results across our two larval subpopulations, we looked for an effect of 'getting stuck' in the channels. We observed similar axial trends in the distributions of contraction amplitudes, rates, durations, and intersegmental phase delays across the jGC7f and Gerry subpopulations (Supplementary Figure 4.3C), suggesting that the particular axial shapes of these distributions were unlikely to be a consequence of certain segments becoming more 'stuck' than others during contractions.

Therefore, both aspects of segmental coordination investigated thus far, the consistency of segmental kinematics and of segmental timing relationships, have featured a non-monotonic axial diversity.

4.2.4. Spatial structure of segmental coupling

Up to this point, we have described the coordination of locomotion inside channels on an aggregate level, considering overall distributions of segments' contraction kinematics and timings. However, another, less-studied form of coordination is also likely to have important outcomes for locomotion: the "coupling" of segments, or how tightly correlated are segments' movements on a cycle-by-cycle basis. We reasoned that kinematic features might need to be coupled tightly or flexibly depending on their roles in behavior. For instance, as larvae change crawling speed, segments' contraction durations might need to be tightly co-modulated to ensure an efficient duty cycle and/or adequate stability (number of segments not actively contracting at once). However, kinematic coupling could also need to differ between body regions. For instance, to increase swimming speed, eels increase anterior, but not posterior, contraction amplitudes (Ellerby et al., 2001; Anastasiadis et al., 2023). Here, we ask whether larval Drosophila similarly have different coordination patterns across the body during locomotion, and in particular more flexibly-coupled anterior than posterior regions. We asked how tightly coupled were segments' contractions to each other on a cycle-to-cycle basis, whether coupling emerged from changes to crawling speed, and how coupling was spatially structured across the larval body.

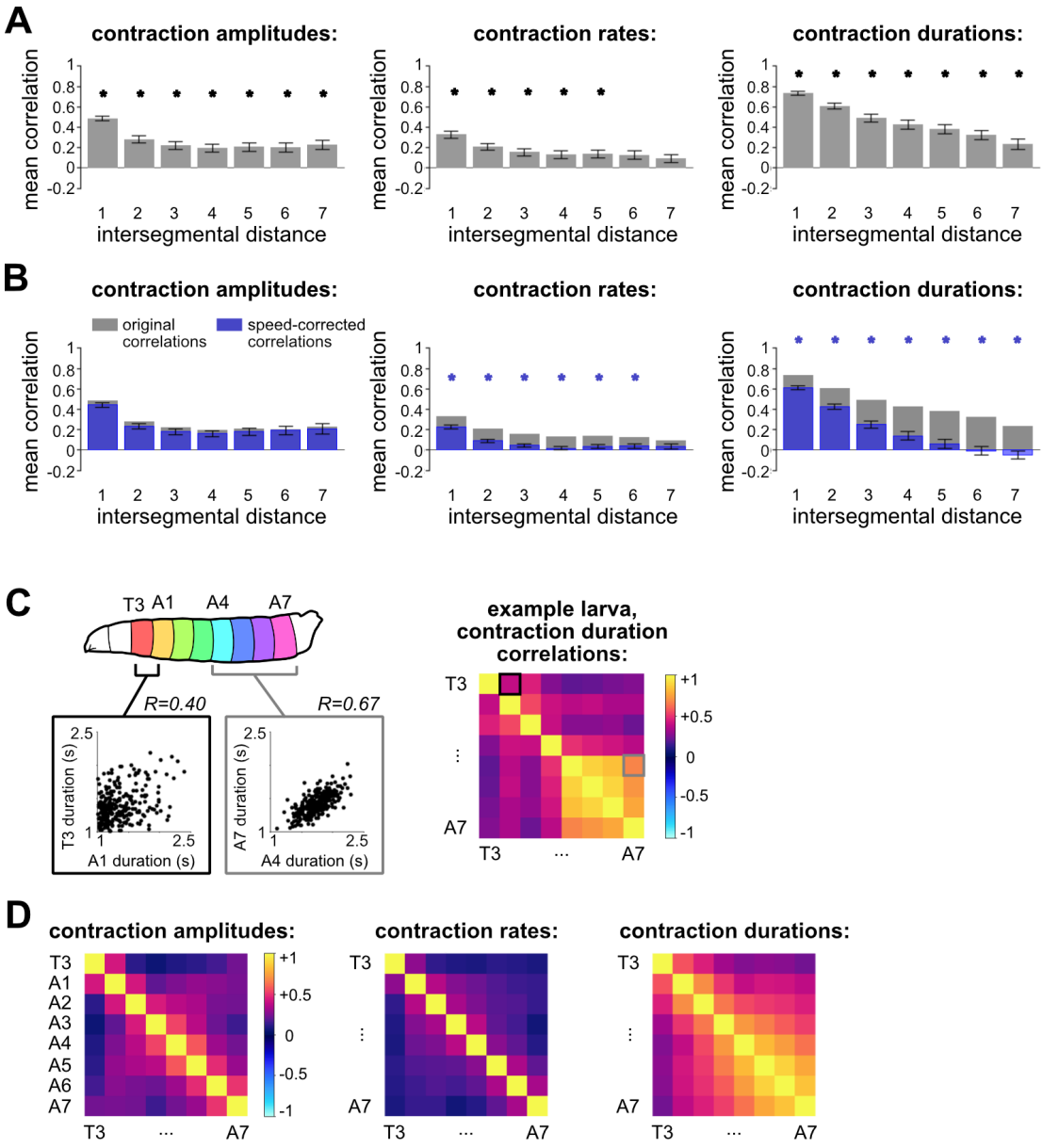

Figure 4.3: Spatial structure of segmental coupling. **A:** Pairwise intersegmental correlations (Pearson's R) of the indicated kinematic feature, averaged over all segment pairs at each intersegmental distance. (Distance=1 indicates neighboring segments, etc.) Black asterisks: correlations significantly > zero, one-tailed T-test, Bonferroni-corrected alpha ($p<0.002$). Error bars: S.E.M, n=25 larvae. **B:** Pairwise intersegmental correlations of speed-corrected residuals for each kinematic feature (Methods: Section 4.4.7), plotted over the original correlation strengths (grey bars, same as in A). Blue asterisks: correlations significantly < original values, one-tailed T-test, Bonferroni-corrected alpha ($p<0.002$). Error bars: S.E.M, n=25 larvae. **C:** Schematic of calculating pairwise intersegmental correlation matrices. Example contraction duration relationships are shown as scatter plots for two pairs of segments (left): T3 and A1 have a lower correlation (R=0.40) than do A4 and A7 (R=0.67). Example plots correspond to two pairwise comparisons in the full correlation matrix (right), marked as black and grey boxes, respectively. **D:** Mean pairwise intersegmental correlations for the indicated feature of segmental contraction (averaged over n=25 larvae). All values along the diagonal = +1.

As an initial approach to quantify how strongly pairs of segments were coupled as a function of their distance apart, we averaged the pairwise coupling strengths of segments' contraction amplitudes, rates, and durations at each intersegmental distance and compared these strengths (Figure 4.3A). This approach allowed us to evaluate the overall strength of each feature's coupling across the body, but ignored any systemic axial variations. As expected, we found the strongest average coupling between adjacent segments. Of the three kinematic features, we found contraction durations were most strongly coupled across segments (Figure 4.3A). Contraction amplitudes, rates, and durations were all significantly coupled (Pearson's $R > 0$; one-tailed T-test; $p < (0.05/21)$) at almost all intersegmental distances. Both contraction amplitudes and rates were weakly coupled at most intersegmental distances (average $R < 0.2$ at distances of 3 or more segments apart), making it unlikely that long-range coupling of either feature holds much behavioral significance. However, contraction durations were strongly coupled (average $R > 0.5$) between both adjacent segments and two-apart segment pairs, suggesting that this kinematic feature is regularly co-modulated across segments on a cycle-by-cycle basis, out of behavioral necessity or as a byproduct of neural/biomechanical properties.

We next asked to what extent the coupling described above was a function of segments co-modulating their contractions in the same way as larvae changed locomotor speed. To do so, we repeated the above analysis after accounting for the relationship between speed and segmental contraction kinematics: we regressed away the best-fit linear relationship between cycle speed and segments' cycle-by-cycle contraction kinematics, then re-calculated correlations between segments using the residual kinematic information (Figure 4.3B). We found that contraction amplitude coupling was not significantly reduced after accounting for cycle speed,

and thus appears independent of speed. By contrast, for both contraction rates and durations, the average coupling strength decreased significantly for all pairs of segments after accounting for cycle speed, suggesting speed-related co-modulations play a substantial role in coupling these features across the body.

Next, since the above analysis ignored potential axial differences in coupling, we investigated this possibility directly. To do so, we generated intersegmental correlation matrices for the three kinematic features and averaged these across larvae (Figure 4.3C; individuals given in Supplementary Figure 4.4A-C). Qualitatively, we found the structure of coupling across the body differed for the three kinematic features. On average, the spatial structure of contraction amplitude coupling across segments appeared slightly stronger in mid-body and between pairs at opposite ends of the body; the spatial structure of contraction rate coupling was weak across the body; and the spatial structure of contraction duration coupling appeared stronger among tail-end than among head-end segments (Figure 4.3D). As above, we repeated this analysis after regressing away cycle speed from segments' kinematic features (Supplementary Figures 4.4D-F, 4.5). We observed similar spatial structures, which suggests the strength, but not the spatial structure, of coupling segments' contraction rates and durations is a function of crawling speed in this behavior.

Additionally, we tested for an effect of larvae 'getting stuck,' first, by comparing the spatial structures of coupling across the smaller jGC7f and larger Gerry subpopulations (Supplementary Figure 4.6A). Overall, spatial structures in both separate subpopulations resembled those of the combined dataset: contraction amplitude coupling was slightly stronger in mid-body and contraction duration coupling was substantially stronger among tail-end segments

than head-end segments. Contraction rate coupling was stronger overall among Gerry than jGC7f larvae, and particularly among anterior abdominal segments (Supplementary Figure 4.6A); however, this difference in spatial structure did not appear to depend on larval size (Supplementary Figure 4.4B), making it unlikely to be related to a larva's degree of physical constraint. Further, we compared the spatial structure of coupling when splitting cycles into the halves with greater or lesser tail movement distances (Supplementary Figure 4.6B). We did not observe substantial differences in coupling structure between the halves of the data. Together, these analyses suggest that the spatial structure of coupling is unlikely to be a consequence of how tightly larvae (or specific body segments) were constrained inside channels.

Thus, so far, there appear to be very different coupling regimes for distinct features of segments' contractions. Contraction durations are generally strongly coupled, at least in part due to how they are co-modulated with cycle speed, and may be particularly strongly coupled among posterior segments. By contrast, there is minimal coupling of segments' contraction rates and only slightly higher coupling of segments' contraction amplitudes.

4.2.5. A posterior block of segments strongly coordinates contraction durations

To evaluate this spatial structure statistically, we first tested how often (for how many larvae) coupling strengths between segments were significantly higher than expected under the null model of consistent coupling at each intersegmental distance. Contraction amplitude and contraction rate correlations were sporadically higher than expected based on intersegmental distance (warm colors, Figure 4.4A left and center), but these effects were weak. On the other hand, contraction duration correlations were consistently higher than expected toward the tail

end of the animal (Figure 4.4A right). We found similar results when evaluating speed-corrected data, as above (Supplementary Figure 4.5B).

Figure 4.4: Intersegmental contraction duration coupling is frequently higher among a group of posterior segments. A: For each pair of segments, fraction of larvae with significantly ($p < 0.05$) higher-than-expected pairwise correlations. Expected correlations were determined for each intersegmental distance by bootstrapping distributions of pairwise correlations (n = 10,000 iterations). Significance was determined using a one-tailed test, comparing each pair of segments to the expected distribution for its intersegmental distance. **B:** Illustration of an example model tested by the model-fitting procedure. Within each block, "coupling strength" is defined as the average correlation strength between nearest-neighbor segments (correlations "A" and "B"); where two blocks overlap, coupling strength within the overlapping region is the arithmetic mean of both blocks' coupling strengths. Predicted correlation strengths for non-neighboring pairs are extrapolated by distance (e.g., correlations "B2" and "B3"). All segment pairs not included inside blocks are modeled as having the out-of-block group mean correlation ("C"). **C:** 1094 total models are fit to each larva's empirical correlation matrix, including the null model: all segments are included in the same block; correlation strength between segments is entirely a function of intersegmental distance. D: Two example best-performing block models (right) fit to empirical contraction duration correlation matrices for two individual larvae (left). After all possible block models are fit to a larva's empirical correlation matrix, they are compared using Bayesian Information Criterion (BIC) and the best-

Figure 4.4, continued. Intersegmental contraction duration coupling is frequently higher among a group of posterior segments.

scoring model is selected for further analysis. Color display scales and axes (segment order) identical to panel C. E: Number of high-correlation (coupling strength > 0.5) blocks found by the best-performing contraction duration coupling model for each of 25 larvae. **F:** Location of the edges of high-correlation blocks, indicating how often best-performing models included blocks that split up an adjacent pair of segments (where one was included, one excluded). **G:** Frequency with which best-performing models included each pair of segments inside the same high-correlation block. N.B.: Along the diagonal is equivalent to frequency with which each individual segment was included in a high-correlation block, while the 'exterior corner' (T3 and A7 included in the same block) is equivalent to how many larvae's correlations were best modeled as a single large block: the "null 2" model (as in B).

Our second statistical method drew on the observation that many individual larvae seemed to have a group of segments at the posterior end whose contraction durations were strongly coupled (Figure 4.3C, Supplementary Figures 4.2, 4.3). If true, this might suggest a pattern wherein tail-end segments' contraction durations were constrained to match each other cycle-to-cycle, while head-end segments' contraction durations could remain flexibly coupled and vary cycle-to-cycle. To test for this pattern more explicitly, we developed a statistical method to look for "block" structure in segmental coupling and identify places along the body axis where coupling strengths among segments tended to change (see Methods).

Briefly, the method compares many possible models of coupling strength and identifies the model that best explains a larva's observed correlation matrix. The central assumption of the

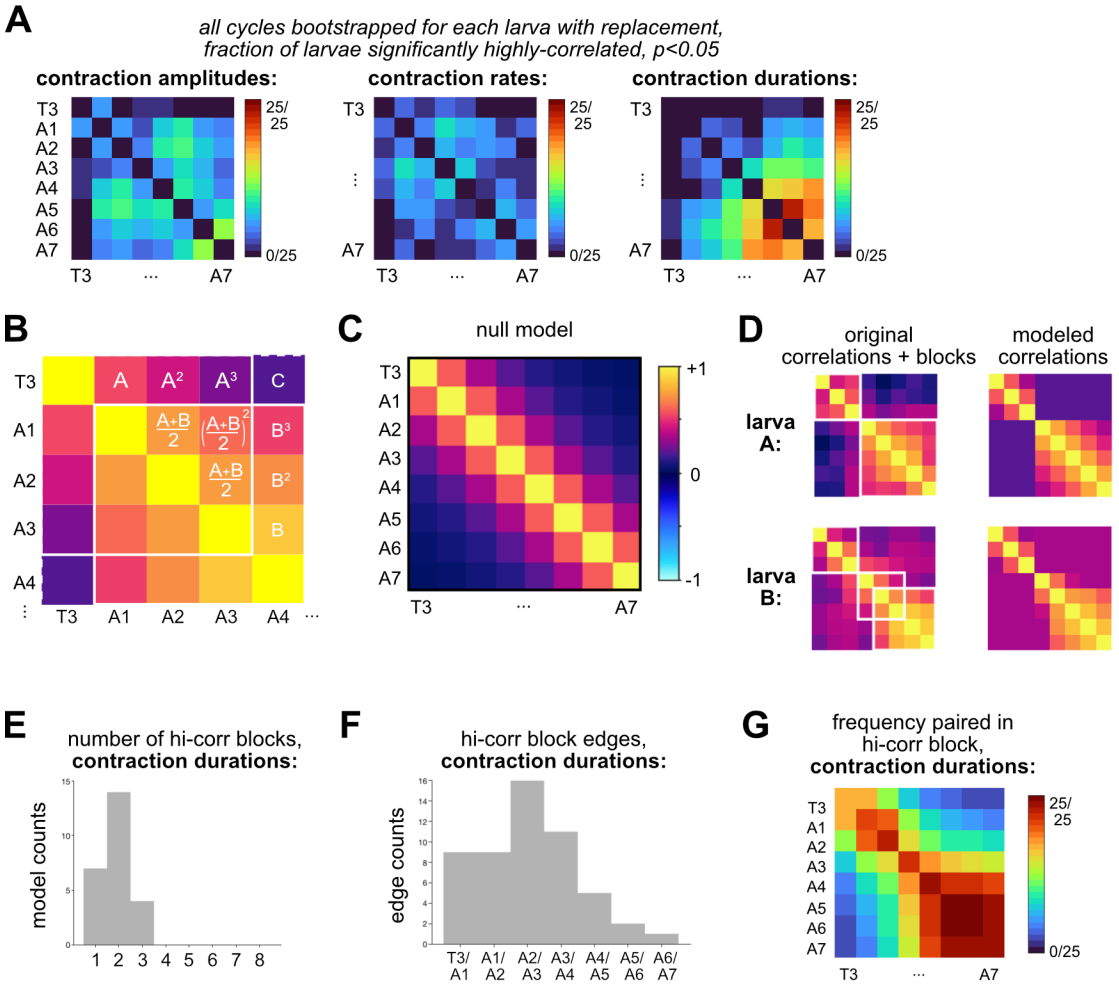

model is that segments within a contiguous group, or "block," share a coupling strength between adjacent segment pairs, and all coupling results from these adjacent-pair correlations. An example of how expected coupling strengths are modeled is given in Figure 4.4B. The null model for this method is that coupling strength depends only on distance between segments, and does not tend to change along the body axis (i.e., all segments are in a single large block, Figure 4.4C). If, instead, the best model includes multiple blocks, it indicates one or more locations

where local coupling strengths change across groups of adjacent segments. Example best-fitting models for two larvae are given in Figure 4.4D.

We evaluated the block structures of the best-fitting models, which indicate groups of segments that were consistently coupled with a similar strength. In particular, we looked for blocks with strong coupling ($R > 0.5$; conclusions were similar when evaluating all blocks (Supplementary Figures 4.7, 4.8). The best models for contraction duration correlations often found two strongly-coupled blocks of segments (Figure 4.4E), indicating two groups of segments.

To evaluate block locations, we first asked where along the body axis blocks most often ended (Figure 4.4F). Common edge locations indicated points where coupling strength tended to change across segments. For contraction duration coupling models, block edges were most common between segments A3 and A2, and fairly common between other pairs of anterior segments (Figure 4.4F). However, they rarely occurred between posterior segments A4-A7.

To quantify these groupings a second way, we asked how commonly (for how many larvae) the best model grouped each pair of segments into the same block (Figure 4.4G). We found a strong tendency for contraction duration coupling models to group posterior segments: segments A4 through A7 grouped together with the other posterior segments inside strongly-coupled blocks for most larvae (Figure 4.4G). In general, the same observations held true for block models calculated after accounting for cycle speed, and when evaluating locations of all blocks rather than just strongly-coupled blocks (Supplementary Figure 4.7). Altogether, the location of blocks is consistent with the conclusion that contraction durations are more strongly coupled in posterior segments than in anterior segments.

To check whether this statistical structure was only true for contraction duration couplings or could also be found for other kinematic features, we also tested block models for coupling of segments' contraction amplitudes and rates (Supplementary Figure 4.8). Compared to contraction duration coupling models, the best models for contraction rate and amplitude coupling had fewer strongly-coupled blocks overall; the axial locations of these block edges were more homogeneously distributed; and the segments that tended to get grouped together into strongly-coupled blocks were likewise more homogeneously distributed. Thus, contraction durations, but not contraction rates or amplitudes, appear to be strongly coupled specifically among a group of posterior segments.

In all, so far, we have observed kinematic coordination of locomotion that varies along the body axis in three respects. First, contraction kinematics are inconsistent across segments; second, phase relationships are likewise inconsistent across segments; and third, kinematic coupling of contraction durations is stronger among posterior segments than elsewhere along the body axis.

4.2.6. Segmental muscle recruitment differs along the body axis

The axial variation in locomotor coordination described thus far could arise from a number of factors: differences in segmental neural circuit activity, in neuronal activation of muscles, and/or in conversion of muscle activation into forces via body-environment interactions (see, e.g., Peron et al., 2009; Srinivasan et al., 2011; Jonaitis et al., 2022; Kohsaka, 2023). Parsing the contribution of each is central to understanding how coordination arises, but requires more information than just segmental kinematics. For instance, properties of the body or environment could introduce coupling or consistencies across segments (or, indeed, the opposite)

(McMillen et al., 2008; Tytell et al., 2011; Tytell et al., 2014). It is therefore essential to learn how muscle activation compares to the movements actually produced. However, in larval Drosophila locomotion, little is known about the relationship between segmental muscle recruitment and kinematics.

Therefore, our next goal was to determine the relationship between segments' muscle recruitment and contraction kinematics. To do so, we analyzed the Gerry-expressing subset of larvae (n=7) in which muscle recruitment could be reliably quantified. First, as for contraction kinematics (Figure 4.2A-C), we described the coordination of a set of amplitude- and timing-related features of muscle recruitment. If coordination of these recruitment features closely resembled coordination of kinematic features, this would be consistent with a largely neural source for kinematic coordination (but could also reflect incorporation of local sensory feedback); if instead there were clear differences between recruitment and kinematic coordination, this would most likely reflect a biomechanical/environmental contribution to coordination.

We began by quantifying the distribution of three features of muscle recruitment across segments (Figure 4.1G). First, we measured recruitment amplitude, which we defined as peak increase in fluorescence over baseline for each cycle. Recruitment amplitude is analogous to contraction amplitude in the sense that both reflect a maximum degree of activity or movement, respectively, on a given locomotor cycle. Next, we measured the recruitment rate, which we defined as the peak rate of increase in fluorescence. Recruitment rate is roughly analogous to contraction rate, in that it suggests how strongly a segment's muscles were "driven" on a cycle by approximating how quickly motor neuron activity increased on that cycle. Finally, we measured

the recruitment duration, which we defined as the total duration of segments' above-threshold fluorescence. Recruitment duration approximates the length of time motor neurons were firing and is analogous to contraction duration.

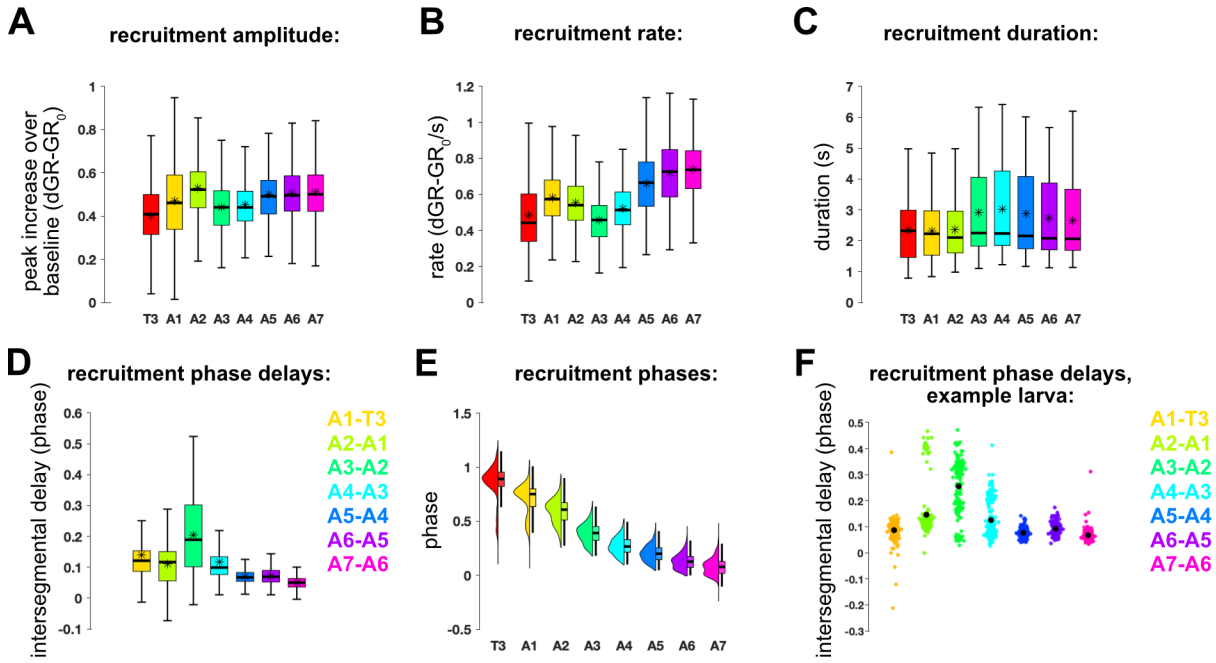

Figure 4.5: Recruitment and recruitment phase relationships of individual body segments vary along the A-P axis. **A:** Distributions of per-cycle total recruitment durations for segments T3 through A7 (from left to right). Histogram and box plot (without outliers) are given for each segment. Asterisk over box plot shows mean value. All pairs of distributions were significantly different ($p<0.05$) except the following: T3 vs. A3; T3 vs. A4; A2 vs. A5; A2 vs. A6; A3 vs. A4; A5 vs. A6. **B:** Segmental distributions of per-cycle maximum recruitment rates (maximum rate of increase in $\Delta G:R\text{-}G:R_0$). All pairs of distributions were significantly different ($p<0.05$) except for T3 vs. A3 and A1 vs. A5. **C:** Segmental distributions of per-cycle recruitment durations. All pairs of distributions were significantly different ($p<0.05$) except for T3 vs. A1 and A2 vs. A3. **D:** Distributions of intersegmental recruitment phase delays; each box plot represents per-cycle delay distribution between a pair of segments (e.g., delays from A1's recruitment phases to T3's recruitment phases, furthest left plot). All pairs of distributions were significantly different ($p<0.05$) except for T3 vs. A1, T3 vs. A4, and A5 vs. A6. **E:** Distributions of per-cycle recruitment phases for segments T3 through A7 (from left to right). Histogram and box plot (without outliers) are given for each segment. N.B.: recruitment phases can be negative if (e.g.) segment A7 began increasing in fluorescence before the tail movement marking the start of a cycle.
F: Distributions of per-cycle intersegmental recruitment phase delays (colored dots) for a single example larva. Mean phase delay values given as black dots. **A-E:** n=978 cycles, 7 larvae. Significant differences between distributions in A-D were determined using nonparametric Friedman's test with post-hoc Dunn-Sidak corrected multiple comparisons.

Similar to contraction kinematics, we found variation in segmental recruitment across the body axis. First, recruitment amplitudes were lowest in T3, followed by A1, A3 and A4 (Figure 4.5A). This largely resembled the trend for contraction amplitudes, which were lowest in anterior segments T3 and A1 (compare Figure 4.2A). Like contraction rates, the slowest recruitment rates were around mid-body, in segments A3 and A4 (Figure 4.5B). Like contraction durations, the longest segmental recruitment durations were in posterior segments, and tended to be longest in segments A3 through A5 (Figure 4.5C). Overall axial trends for recruitment and contraction features were therefore similar, although one discrepancy emerged: the slowest recruitment rates and durations both occurred one segment anterior relative to the slowest contraction rates and durations, respectively (compare Figure 4.2B-C). This spatial offset is consistent with a potential role for sensory feedback about one segment's contraction rate/duration in adjusting the recruitment rate/duration of the next anterior segment.

4.2.7. Greater anterior variability in recruitment timings than in contraction timings

Earlier, we observed nonlinear phase relationships between segments' contractions (Figure 4.2E-F), which could indicate similarly nonlinear propagation of neural and/or muscular activity between segments during locomotor waves, or could be a feature introduced by biomechanical coupling or the channel environment. For instance, propagation of neural and muscular activity might proceed at a different rate than propagation of movement due to physical interactions with the environment, as seen in undulatory swimming (Williams et al., 1989; Chen et al., 2011). To narrow down potential sources of the kinematic nonlinearity, we determined the relative phases at which segments were recruited during locomotor cycles and compared these phases to those of segments' contractions.

Like contraction delays, delays between consecutive segments' recruitments were distributed non-uniformly across the A-P axis (Figure 4.5D). Recruitment delays were relatively consistent through posterior segments (A7 through A4), but they lengthened significantly starting at the delay between A4 and A3. The longest delays between recruitments were between segments A3 and A2. As with segmental contraction phases, the non-uniform recruitment phase delays resulted in a nonlinear distribution of segmental recruitment phases (Figure 4.5E). A sigmoidal model was a better fit than a linear model for segmental recruitment phase distributions both for the combined data and for 6/7 individual larvae.

Thus, the overall trend in coordination of recruitment timings appeared largely similar to the overall trend in coordination of contraction timings. However, two differences emerged. First, as when comparing trends in segments' recruitment versus contraction rates, the longest recruitment phase delays were shifted one segment anterior to the longest contraction phase delays. Second, the recruitment delay between A3 and A2, specifically, appeared extremely variable in the overall distribution. This variability did not merely reflect differences in timing coordination across individuals, as recruitment phase delays between A3 and A2 (among other segment pairs) could be strikingly variable within individual larvae (example in Figure 4.5F).

Together, these differences between the recruitment and contraction waves suggest that the relationship between neuromuscular activity and movement differs along the body axis, but not in the monotonic manner characteristic of undulatory swimming (Williams et al., 1989; Chen et al., 2011). To better understand the relationship between coordination of recruitment and coordination of movement, we directly compared the phases of each segment's recruitment and contraction.

In most individual larvae, in at least one segment, we observed a 'misalignment' of recruitment and contraction phases, wherein the difference between recruitment and contraction phases became not only larger but also much more variable than typical for other segments (example in Figure 4.6A-B). To quantify this across larvae, we calculated the phase delays between individual segments' recruitments and contractions. Delays were longest within segment A3, meaning that A3 was where propagation of the recruitment wave was most in advance of the contraction wave (Figure 4.6C). Moreover, segments A4 and A3 showed particularly large variability in the recruitment-to-contraction phase delay. This variability was bimodally distributed and included within-larva variability (Figure 4.6B), suggesting that these segments were the most likely to have long delays between their recruitment and subsequent contraction, but that a long delay was by no means guaranteed on any given cycle.

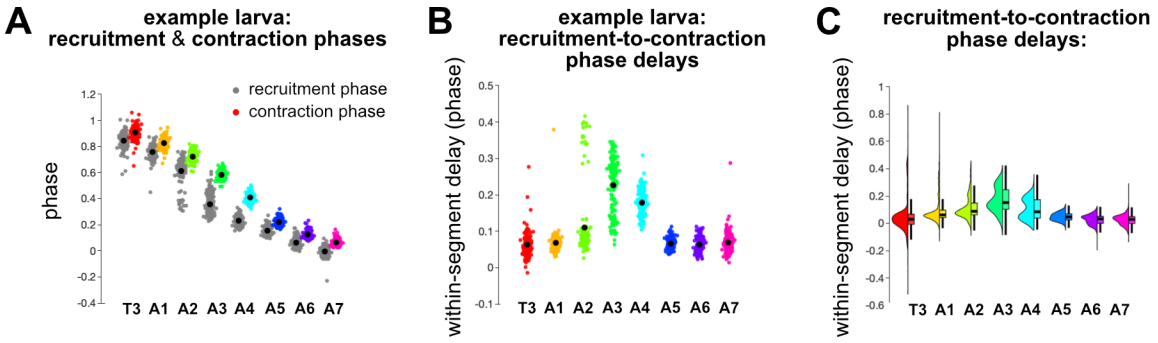

Figure 4.6: Phase relationships between recruitment and contraction vary along the A-P axis. **A:** Segmental distributions of recruitment phases (grey dots) and contraction phases (colored dots) for all cycles from a single example larva. Mean recruitment and contraction phases for each segment given as black dots. **B:** Segmental distributions of phase delays between a segment's recruitment and its contraction (colored dots) for all cycles from a single example larva. Mean phase delay values given as black dots. **C:** Segmental distributions of phase delays between a segment's recruitment and contraction, for all larvae. Histogram and box plot (without outliers) are shown for each segment. N.B.: recruitment-to-contraction phase delays can be negative if a segment began shortening before substantially increasing in fluorescence. n=978 cycles, 7 larvae. Significant differences between distributions were determined using nonparametric Friedman's test with post-hoc Dunn-Sidak corrected multiple comparisons (alpha 0.05). All pairs of distributions were significantly different ($p<0.05$) except the following: T3 vs. A6; T3 vs. A7; A1 vs. A5; A6 vs. A7.

Altogether, we find an inconsistent phase relationship between segmental muscle recruitment and contraction along the body axis. On the whole, contraction phase relationships among segments show greater within- and across-larva regularity than recruitment phase relationships. This suggests that either biomechanical properties or the interaction of the larval body with the environment have a net coordinating effect, converting less-consistent recruitment timings into more-consistent contraction timings across segments.

4.3. Discussion

In this report, we investigated how segments' contraction kinematics and muscle recruitment were coordinated across the body during larval Drosophila locomotion inside a linear channel environment. We discovered multiple axially-varying aspects of locomotor coordination, including segmental differences in contraction kinematics and differences in the propagation speeds of recruitment and contraction waves along the body axis. Further, we found anterior and posterior groups of segments were differentially coupled, with contraction durations strongly coordinated specifically among a group of posterior segments. Lastly, we discovered high anterior variability in the timing relationships between segments' muscle recruitment and subsequent contractions, pointing to a net coordinating effect of mechanical interactions during this behavior. In sum, larval locomotor coordination, both kinematic and neuromuscular, appears to depend on properties of the nervous system, body, and/or behavior that vary axially, and the structure of this coordination typically changes around the mid-abdomen.

We begin by noting that certain of our conclusions contrast with those in recent reports characterizing larval locomotion over flat agarose surfaces. These studies did not find differences

in the contraction durations or amplitudes of body segments, and described a linear propagation of contraction phases (Gjorgjieva et al., 2013; Pulver et al., 2015; Sun et al., 2022; Liu et al., 2023). This apparent discrepancy could be due to differences between locomotion on a flat substrate and in a constrained environment, for at least two reasons. First, larvae may be required to generate additional force to move in an environment where they are surrounded on all sides. This will be the case whenever, e.g., larvae are burrowing into food or other soft media. Encountering extra resistance in some part of the body might change overall coordination: for instance, changes to locomotor wave propagation and segmental kinematics have been described for lamprey swimming when a small mid-body section is constricted (Islam and Zelenin, 2008), changes that at least superficially resemble the differences in crawling we observe here. However, we did not find evidence that cycles with further tail movement or larger individual larvae, either of which would presumably face greater resistance inside the channels, were related to axial differences in kinematics, in kinematic coupling, or in wave propagation (Supplementary Figures 4.2-4.4). Second, it has been reported that proprioceptive sensory feedback may be altered or weakened in a constrained environment (He et al., 2019). Proprioceptive feedback is known to affect segments' contraction durations and the rate of recruitment wave propagation (Hughes and Thomas, 2007), although potential differences in effect along the body axis has not yet been quantified. Thus, if proprioceptive feedback were altered inside channels (as compared to surface crawling), it could play into the axial differences in recruitment we observed.

4.3.1. Sources of axial kinematic, coupling, and recruitment differences

The sources of axial variation in coupling strength, wave propagation, and contraction kinematics are presently unclear. However, several strong possibilities are well-documented.

First, differences in segmental muscle recruitment could emerge from intrinsic differences in the activity of neurons or circuits across axial positions, in differential inputs to segments, or in differing responses to inputs (see, e.g., Srinivasan et al., 2011; Takagi et al., 2017; Tastekin et al., 2018; Murawski et al., 2020; Jonaitis et al., 2022; Jonaitis et al., 2024). For instance, the location of pan-sensory optogenetic stimulation has diverse effects on ongoing larval locomotion, depending on the segment stimulated (Murawski et al., 2020); while such pan-sensor stimulation is highly artificial, endogenous sensory input during channel crawling might likewise feed into segmentally-varying circuits and thereby evoke diverging responses at the level of recruitment and kinematics. Segmental differences in intrinsic circuit activities and input-responsiveness are common across locomotor systems, including limbless systems (Pearce & Friesen, 1985; Zhang and Grillner, 1995; Hill et al., 2003; Tytell and Cohen, 2008), suggesting they are fundamentally important for locomotor behaviors.

Neuromodulatory inputs are particularly strong candidates for modifying the activities of segmental circuits (Harris-Warrick, 2011; El Manira, 2014). The differences in segmental coupling we observed are reminiscent of recently-reported differences in segmental responsiveness to an mAChR agonist in the isolated nerve cord (Jonaitis et al., 2022): in that work, a posterior group of segments (A8-A5) was observed to respond to the agonist with synchronous rhythmic bursting, while an anterior group of segments responded with asymmetric head-sweep-like activity. However, based on the failure of isolated mid-body segments (A1-A5)

to produce rhythmic activity in response to the agonist, those researchers concluded only thoracic segments and posterior segments A6-A8 are endowed with rhythmogenic response to mAChR activation. Therefore, although neuromodulatory responsiveness is an attractive explanation for regionally-specific coupling, the predicted boundaries of "blocks" of segments that would respond to acetylcholine modulation do not align with our observation that A4-A7 were frequently included together in a strongly coupled block. It is possible that other neuromodulators could act on a broader group of posterior segments to generate the blocks we observed.

In fictive crawling preparations, it is common to observe a period of elevated neuronal activity in segments at the beginning of the wave prior to wave propagation, or as posterior or anterior "bursts" that only sometimes go on to initiate a full fictive wave (Pulver et al., 2015; Liu et al., 2023; Jonaitis et al., 2022; Francis et al., 2024); similarly, bursting may occur for longer in nerves closer to the start of wave propagation (Fox et al., 2006). Therefore, in the absence of sensory input, neuronal activity occurs with uneven durations along the A-P axis. This situation resembles the longer recruitment and contraction durations we observed in posterior segments, and may be the 'baseline state' of central activity underlying larval locomotor waves. Recent work formalized posterior "bursts" in a model of locomotor coordination by including a command neuron that innervated multiple posterior segments simultaneously (Francis et al., 2024). While an anatomical correlate for this command neuron remains to be identified, such a mechanism could also explain the higher level of coupling we observed among a group of posterior segments.

Sensory feedback differences across segments could also have contributed: since segments' contraction kinematics differed, it is highly probable that at least the proprioceptive feedback received differed between segments during the behavior (Azim and Tuthill, 2018). Axially-varying sensory inputs could potentially explain axial differences in strength of coupling. They might also explain certain axial differences in recruitment-contraction coupling: For instance, feedback about one segment's contraction rate might inform the next anterior segment's recruitment rate, leading to a one-segment offset in contraction versus recruitment rate minima. Such intersegmental feedback could potentially occur via ddaE proprioceptive neurons, which are active during forward crawling and project directly to the next anterior segment, where they form synapses (Grueber et al., 2007; He et al., 2019; Vaadia et al., 2019; Greaney et al., 2023). However, feedforward proprioceptive pathways alone would be insufficient to explain non-monotonic trends in contraction kinematics, unless the effect of proprioceptive feedback reversed at the same point along the body where kinematic trends reversed.

Lastly, biomechanical differences among segments could result in axial differences in kinematics or kinematic coupling, even if muscle recruitment were identical (Chiel et al., 2009). However, major differences in segments' biomechanical properties have not been reported thus far for Drosophila larvae. On the contrary, the decrease in variability we observe in contraction phases relative to recruitment phases (Figure 4.6) suggests an opposite effect of biomechanical properties: at least in the channel environment, irregularities in intersegmental timing coordination at the neuromuscular level are 'smoothed out' during propagation of the physical wave of contractions, in agreement with earlier studies (Pulver et al., 2015).

4.3.2. Behavioral relevance of axially-varying coupling

Do the axial differences we observed in contraction durations and their segmental coupling contribute functionally to larval locomotor behavior? Alternatively, do they represent side-effects of axial differences among segments whose importance lies elsewhere? To date, it is unclear whether the duration of a segment's contraction performs a particular function in larval locomotion, although the long-duration contractions that follow from proprioceptive silencing appear to result in slowed, inefficient crawling (Hughes and Thomas, 2007). One explanation for the stronger coupling of contraction durations at the tail end could be to scale the amount of stability this region provides for the rest of the wave, by ensuring that segments are in contact with the substrate (i.e., not contracting) for longer or shorter duty cycles, as appropriate. It has recently been shown that larvae scale the ground reaction forces produced by posterior, but not anterior, segments with cycle period (Booth et al., 2024), which may indicate a need to adjust posterior anchoring depending on crawling speed. However, we observed stronger posterior coupling of contraction durations even when accounting for cycle speed (or for cycle period, not shown), which argues against this explanation. Additionally, while larvae will produce crawling waves when floated on top of water, they do not appear to adjust their segments' contraction durations in this low-friction condition (Sun et al., 2022); therefore, the coupling of contraction durations is unlikely to result from sensory feedback related to friction. Altogether, a satisfactory behavioral explanation for stronger posterior coupling remains to be discovered.

On the other hand, we speculate that the more flexible coupling of contraction durations at the anterior end may reflect a need for less rigid relationships between these segments generally, so they can more easily participate in re-orienting movements such as the lateral head

movements that occur between and during locomotor cycles (Berni et al., 2012; Gomez-Marin and Louis, 2014; Pulver et al., 2015; Wystrach et al., 2016).

4.3.3. Limitations

We note two particular limitations of the present study. First, our analyses focused on only a subset of kinematic features that could be chosen to describe segment contractions. We attempted to select features of potential behavioral relevance, as discussed in Results. However, we found similar axial coordination differences in other features we investigated in a preliminary dataset, e.g., when comparing segment contraction onset phases to the phases of peak contractions or boundary movements, or when comparing contraction (shortening) rates to lengthening rates (not shown). Therefore, while we cannot yet conclude which kinematic or timing relationships among segments are most important for larvae to coordinate for effective locomotion inside channels, we are confident that the central conclusion of axial variation in coordination holds across a range of features.

Second, our study relied on the use of linear agarose channels. By design, linear channels restrict the set of behaviors that larvae can execute. While these constraints enabled collection and tracking of many cycles of straight forward locomotor waves per animal, they also precluded us from observing what coordination strategies are used when larvae fully express locomotor behaviors, including re-orientations (Green et al., 1983; Gomez-Marin and Louis, 2014). If the "function" of the differences we observed in locomotor coordination across the body axis is to support separate roles for navigation and stability/propulsion at the head and tail ends, we hypothesize that, when larvae are allowed to turn while crawling, coordination across segments will resemble the coordination described here in linear channels: kinematic coupling will be

flexible between head and tail ends; the contraction wave may slow near mid-body, potentially to facilitate stability while turning; and recruitment-contraction phase relationships will be consistent at the tail end, but flexible starting around mid-body, where they may be driven more strongly by turning-related sensory or descending inputs. To look explicitly for the extent to which coordination across the larval body depends on sensory context, it would be useful to apply the analyses here to larval locomotion in a variety of environments.

4.3.4. Conclusion

Already, imaging technologies are emerging that should enable the simultaneous recording of neural/muscle recruitment and segmental kinematics while larvae move in unconstrained environments (Bonnard et al., 2022; Karagyozov et al., 2018; McNulty et al., 2024). These advances will permit testing how the structure of coordination employed during straight locomotion compares to the structure of coordination employed when larvae navigate and perform more complex behaviors. In combination with recent advances in the mechanics of larval crawling (Ormerod et al., 2022; Sun et al., 2022; Booth et al., 2024) and the development of neuromechanical models (Gjorgjieva et al., 2013; Pehlevan et al., 2016; Loveless and Webb, 2018), work in the Drosophila larva is rapidly advancing towards a sophisticated neuromechanical understanding of locomotion (Kohsaka, 2023). It is our hope that the methods and findings here will open pathways to link the neuromuscular and behavioral implementations of locomotor coordination in this exciting model system.

4.4. Materials and Methods

4.4.1. Animal care and genotypes

Drosophila melanogaster strains used were the following:

w; +/+; Mef2-GAL4/TM6B-Dfd-YFP (generated for this study)

w; +/+; UAS-jGCaMP7f (Bloomington 79032)

w; +/+; Mef2-GAL4, UAS-Gerry/TM6, Tb, TubP-GAL80 (generated for this study)

Drosophila stocks were maintained at 25º C on molasses-based fly food. Fly crosses and embryo/larval collections were maintained on yeasted apple juice agar plates at 25º C, humidified to at least 75%.

Obtaining larvae for imaging

Larvae of genotype *w; +/+; Mef2-GAL4,UAS-Gerry/Mef2-GAL4,UAS-Gerry* ("Gerry") were obtained from in-crosses of same-genotype adults. Larvae were screened for presence of GCaMP in body wall muscles prior to imaging sessions.

Larvae of genotype *w; +/+; Mef2-GAL4/UAS-jGCaMP7f* ("jGC7f") were obtained from adult *w; +/+; UAS-jGCaMP7f* crossed to *w; +/+; Mef2-GAL4/TM6B-Dfd-YFP*. Larvae were screened for presence of GCaMP in body wall muscles prior to imaging sessions.

Embryos were obtained from crosses during a 24-hour collection window, aged for an additional 24 to 48 hours, and larvae to be imaged were subsequently screened and selected by size (average 1mm after 24 hours for first-instar jGC7f larvae; 2.5mm after 48 hours for second-instar Gerry larvae). Larval staging was confirmed by examining larval mouth hooks under magnification to check for characteristic second-instar size and shape. Soft-bristled paintbrushes were used to handle larvae during washing, screening and imaging steps.

4.4.2. Imaging larval crawling inside agarose channels

For in-depth explanation of steps, including recipes used, see Greaney and Heckscher, 2024.

Channel preparation

Linear agarose channels were cast with 2% (w/v, in distilled water) LE agarose (APExBIO, Houston, TX) against raised channel molds (Heckscher et al., 2012; Greaney and Heckscher, 2024). Channels used for first-instar jGC7f larvae were (either 200um (n=14 larvae) or 250um (n=4 larvae) wide by 200um deep); channels used for second-instar Gerry larvae were approximately 450um wide by 450um deep. After agarose fully set, channels were unmolded, trimmed to fit on slides, and kept at 4º C immersed in water until 15 minutes prior to use. Larvae were matched to channels of appropriate widths relative to body size: larvae were snugly enclosed by channel walls and coverslip, which slowed crawling from maximum speed and prevented larvae from turning around inside channels.

Imaging larval locomotion

After screening larvae for expression of the appropriate fluorophore, larvae were kept on unyeasted apple juice agar plates for the duration of an imaging session (average 2 hours). We observed no effect of time within session on animals' crawling speeds, periods, or stride distances, and therefore grouped all animals together for analysis. Prior to imaging, larvae were washed in distilled water, then placed into an agarose channel, immersed in distilled water, and covered with a glass coverslip. Channels were saturated with water throughout the duration of video capture.

Larvae were imaged one at a time for 5-20 minutes, with a typical imaging duration of 10 minutes (equivalent to one 12k-frame video at 20 Hz). jGC7f larvae were imaged using a Marianas spinning disk confocal microscope (3i, Denver, CO) with 488nm laser illumination, at 20 Hz, using laser intensities that prevented range saturation. Gerry larvae were imaged using a Zeiss LSM 800 point-scanning confocal microscope (Zeiss, Oberkochen, Germany) with 488nm and 561nm laser illumination, at 13.3 Hz, using laser intensities that prevented saturation in either channel. All larvae were imaged using a 5X, 0.15 NA objective (Zeiss). To keep larvae in the field of view, motorized stage movements were commanded manually throughout the imaging session.

Larvae were allowed to crawl until the end of video capture (pre-set at 12k frames, for jGC7f larvae), until they paused crawling for a period of at least 20 seconds, or until they reached the end of the linear channel, whichever happened first. To acquire additional cycles, after the end of video recording, some larva were allowed to recover for 1 minute outside of the channels, then were replaced and recorded again. As recorded videos tended to be of shorter duration for the larger Gerry larvae (which crawled faster and reached the end of the channel sooner), all but one of the Gerry larva was recorded multiple times (2-4 videos); only two of the jGC7f larvae were recorded multiple times. All videos recorded of a single larva were combined for analysis.

4.4.3. Developing DeepLabCut (DLC) segment tracking pipeline

To track larval segment boundaries, the DeepLabCut (DLC) Python package was used (Mathis et al., 2018). The following steps resulted in boundary positions over time for segments

T3 through A7. Subsequent analysis was performed in Matlab version 2021b (Mathworks, Natick, MA).

Initial training

Videos were oriented so that the larva's head pointed left. For larvae that were rolled relative to the imaging plane, videos were flipped if necessary so that more visible side was the larva's left.

We trained separate DLC networks using different tracking keypoints for spinning disk confocal videos of jGCaMP7f-expressing larvae ("GCaMP network") and point-scanned confocal videos of Gerry-expressing larvae ("Gerry network").

The GCaMP network tracked two keypoints per segment boundary (Figure 4.1B), as well as two keypoints each to estimate locations of segments T2 and T1 and two points to estimate the position of a pair of longitudinal tail muscles (dorsal external oblique 1; Campos-Ortega and Hartenstein, 1997). Keypoints were placed at the exterior-most visible point of the left and right sides of a segment boundary. In frames where an animal was rolled substantially to one side, the ventral-anterior corner of 'muscle 4'/'lateral longitudinal 1' was labeled instead.

To enable better registration for estimating muscle fluorescence, the Gerry network tracked five keypoints per segment anterior boundary (T3 through A7). Keypoints were placed at the exterior-most visible anterior edges of the left and right sides of each boundary; the central anterior corner of dorsal longitudinal muscles (dorsal oblique 1; Landgraf et al., 1997); and an "extra" point at the ventral-anterior corner of the left side's dorsal acute 3 (Fig 4.1C). This network also tracked four keypoints for the anterior boundary of segment A8, two points on the

tail segment's dorsal external obliques, and two keypoints to estimate the anterior boundary of segment T2.

Training data included 23 of 25 larvae from the analyzed dataset as well as data from 61 additional larvae that were not analyzed further due to few overall locomotor cycles, unstable roll angle with respect to the imaging plane, poor manual tracking, or too few segments in view at any given time. 3550 total training frames were used. In both networks, the boundary between segments A8 and A9 was not tracked, and the anterior boundaries of T2 and T1 could not be tracked reliably. Therefore, only segments T3 through A7 were included for subsequent analyses.

Refining DLC network performance

An iterative refinement process was used to add training frames and arrive at the final GCaMP and Gerry DLC networks. A DLC network was first trained using an initial set of training frames, then used to predict keypoint locations for all videos (either GCaMP or Gerry) in the dataset. Next, prediction quality was evaluated using a multi-step process. To do so, keypoints were converted into segment lengths (see below), then both algorithmic and manual inspection of segment lengths were used to generate a list of potential problem frames. These frames were validated manually. Keypoint locations were corrected for a representative selection of these frames, then the network was retrained with the addition of the corrected frames. This process was repeated until all videos were predicted with few problem frames. Any remaining problem frames were corrected manually.

4.4.4. Converting keypoints to kinematic parameters

Filtering, finding segment boundary positions and lengths

Keypoint positions were smoothed using a 2nd-order Savitzky-Golay filter with a window of 15 frames, then converted into segment boundary positions by taking the mean of all keypoint positions belonging to the same segment boundary as the 'midpoint' for that boundary. Segment lengths were defined as the Euclidean distance between the midpoints of a segment's anterior and posterior boundaries. A "baseline" length for each segment was defined as the 95th percentile of its length distribution over all frames (Figure 4.1F).

To estimate how far a larva traveled on each wave, segment positions were converted from frame (pixel) coordinates into real spatial coordinates.

For the Gerry videos, frame coordinate positions were converted to real spatial coordinates using recorded stage movement data. For the jGC7f videos, which were captured using software/hardware that did not allow for motorized stage logging, stage movement was estimated from a consensus of pixel velocities in segments that were not actively contracting. Results agreed well with visual inspection.

Finally, segments' boundary positions were extrapolated on frames where they temporarily left the field of view, as follows. First, the expected distance between that boundary and its nearest visible neighbor was defined as the median distance between them in the original dataset (prior to any velocity and position estimation). Then, each time a boundary (typically at the head or tail end of the body) went out of frame, its positions following the out-of-frame period were compared to the position of the adjacent, more central boundary. A single value was added or subtracted to all of the former boundary's positions after the out-of-frame period, such that the median distance between the two boundaries after the out-of-frame period was corrected

to match their expected distance. This process was repeated following any block of missing frames.

Segment and tail forward movement times

To define periods of forward movement for each boundary, first, its positions over time (in real spatial coordinates) were converted to velocities. Boundary forward movement periods were defined as times when a segment's frame-to-frame displacement exceeded 1% of its baseline length. Since no baseline length could be reliably found for the tail, an empirically-determined threshold of 2 μm/frame was used as the tail forward movement threshold. This threshold produced good agreement between manual definition of tail movement times (based on visual inspection of videos) and algorithmically-defined tail movement times.

Segment movement distances

Having established each segment's moving periods, a segment's movement distance on a given cycle was calculated using its anterior boundary. First, the forward movement period was found that overlapped with the segment's contraction during that cycle's locomotor wave (see below). Then, the boundary's median positions before and after the movement period were determined, using all 'not moving' frames since the preceding 'moving' period to determine before-moving position, and all 'not moving' frames until the following 'moving' period to determine the after-moving position. The difference between before-moving and after-moving positions was taken as the movement distance for that cycle.

Segment contraction times and lengths

Segments' lengths traces were processed to determine contraction onset, peak, and offset times as follows.

First, contraction peaks (length minima) were isolated by inverting the lengths traces and applying Matlab's findpeaks function. To avoid finding small length changes that did not correspond to the primary contraction during a wave, a minimum peak prominence was enforced of 20% of the difference between segment's 90th and 10th percentile lengths.

To find contraction onset and offset times, each contraction peak was first isolated from the rest of the lengths trace by finding the length peaks on either side. Then, during this window, the contraction onset was defined as the (interpolated) time when the length decreased to 75% of the difference between maximum length before contraction and the minimum length during contraction. Similarly, the contraction offset was similarly defined as the time when the length increased to 75% of the difference between the minimum length during contraction and the maximum length after contraction (Figure 4.1F). This method was found to be robust to variation over time in between-cycle segment length.

Forward locomotor waves

Having found the periods during which each segment was contracting and moving, forward locomotor waves could be defined as tail-to-head progressions of segmental contractions, as follows. The start of a forward wave was defined as the time at which the tail began moving forward. After this time, a "completed" forward wave occurred if each segment from A7 to T3 contracted sequentially. To allow for the scenario in which neighboring segments began shortening at around the same time, up to five 'out-of-order' frames were allowed: so long as the more posterior segment's contraction started within five frames of the more anterior segment's contraction, both segments were counted as having participated in the wave. No rule was applied that segments had to de-contract in order.

To ensure that only complete, reasonably comparable forward waves were analyzed, waves were excluded using the following criteria:

Any wave in which not all 8 segments (T3-A7) contracted was excluded.

Any wave during which one or more segments contracted more than once was excluded.

Any wave preceding or following a long pause was excluded, as was any wave during which a pause happened partway through. A long pause was defined as 1 second elapsing without any segment boundary moving forward.

Any wave for which a cycle period could not be defined was excluded. (This could happen if the tail was not visible when moving forward, so the cycle start time was missing.)

Any wave during which the head end (including at least T3 and A1) was retracted, including at the beginning or end, was excluded. Head retractions were defined as periods in which one or more contiguous anterior segments (between T3-A3) contracted and de-contracted without simultaneous co-contraction of the next posterior segment.

After applying earlier exclusions, any remaining wave whose period (z-scored) exceeded 4 standard deviations away from the mean cycle period in either direction was excluded.

Cycle stride distance, period, and speed

Typically, to estimate forward stride distance for each locomotor wave, the visual centroid of a larva is tracked over time (Risse et al., 2017; Thane et al., 2023). To obtain an estimate that depended less on body perimeter estimation, stride distance for each cycle was estimated as the mean of distances moved by segments A2 through A7 on that cycle. Segments A1 and T3 were excluded from the estimation because they occasionally moved as part of a head

movement between contractions, resulting in less reliable movement distance calculation for these two segments.

The start of each locomotor wave was defined (above) as the time at which the tail began moving forward in advance of segmental contractions. Cycle periods were defined as the duration from this tail movement until the following cycle's tail movement.

Finally, each cycle was assigned an average speed by dividing the cycle stride distance by the cycle period.

Segment contraction phases

For each cycle, each segment's contraction onset was converted into a cycle phase value. This was done by calculating the delay between the start of the wave and the segment's contraction onset, then normalizing this delay by the cycle period.

4.4.5. Extracting segment fluorescence traces

The calcium sensor GCaMP was used to obtain information about segments' muscle recruitment on each cycle. Larvae expressed the Mef2-GAL4 driver, which drove expression of either jGCaMP7f (Dana et al., 2019) or Gerry (tethered GCaMP6m-mCherry, as in Ugur et al., 2017) in all body wall muscles. Because larvae were allowed to move and segments would be actively shortening and lengthening, it was essential to be able to control for movement artifacts (including increases in fluorescence intensity caused not by Ca2+ concentration but by muscle contraction compressing more fluorophores into the focal area). Therefore, recruitment was only evaluated in Gerry-expressing larvae, in which dynamic calcium sensor (GCaMP) fluorescence could be normalized by stable fluorophore (mCherry) fluorescence.

Region of interest definition

To obtain calcium sensor activity over time (a "fluorescence trace") for each segment, segment boundaries were estimated using the DLC-tracked keypoints. The keypoints belonging to a segment's anterior and posterior boundaries were connected to define the boundary around a region of interest, after which all pixels fully contained within the region of interest were combined and their values averaged, producing a single value per frame for a segment's (GCaMP or mCherry) fluorescence intensity. The two channels (GCaMP and mCherry emission) were processed separately. If a single keypoint was missing from either boundary on a given frame, the frame was omitted.

Estimating green-to-red fluorescence ratios

To account for increases in GCaMP fluorescence due to movement or contraction rather than muscle recruitment, segment fluorescence traces were expressed as a change in green-to-red ratio over time (dGR - GR0). To obtain a baseline green-to-red ratio (GR0) during times when a segment was unlikely to be recruited, the green-to-red fluorescence ratio (GR) was averaged across all frames where a segment's length exceeded its baseline length. A segment's muscle recruitment was then defined as the difference between GR and GR0 on each frame.

Fluorescence traces were Savitzky-Golay filtered, using the same kernel applied to segment lengths traces, before analysis.

4.4.6. Matching fluorescence and kinematic data (cycles)

Segments were processed one at a time to obtain the following recruitment metrics and when matching recruitment events into locomotor cycles:

Recruitment event timings and rates

To determine the timing and rate of segment recruitment events, fluorescence traces were treated near-identically to lengths traces (the only difference = threshold for peak prominence). First, recruitment events were identified by locating peaks in the fluorescence trace with prominence of at least 30% relative to the surrounding trough values. The same algorithm was used to define recruitment onset timings, applying the same threshold of 25% of the increase between the preceding trough and upcoming peak fluorescence values, and interpolating to estimate the time of threshold crossing. Likewise, recruitment offset was defined as time of crossing the 25% threshold of decreasing values between the peak and the following trough value; and fluorescence duration was defined as the time between onset and offset. Finally, the same method was used of estimating recruitment rate as the maximum (per-frame) slope that occurred during the time between trough and peak values.

Matching recruitment events to cycles

Processing the trace in the above way led to one onset/offset time, one duration, and one rate value per detected recruitment event. However, not every recruitment event matched cleanly to every already-defined locomotor cycle. For instance, "extra" recruitment events were occasionally detected during a given cycle. Additionally, sometimes a segment's fluorescence trace had gaps not present in its lengths trace, due to the stricter requirement that all of its markers be present to process a given frame; ultimately, only events for which a recruitment onset and offset timing could both be determined were retained.

Because of the "missing" and "extra" recruitment events, a "best match" algorithm was used to pair a single recruitment event to each locomotor cycle. First, recruitment peak timings were compared to their segment's length trough timings, and each peak was provisionally

"assigned" to its closest matching trough in time. Then, if there were any duplicate assignments (multiple recruitment peaks assigned to the same length trough), only the nearest match was retained. After this matching process, the remaining recruitment events (peaks, as well as their associated onset/offset timings and rate values) were assigned to the same locomotor cycle as the matched contraction event.

After matching, a few quality control steps were used to discard any probable bad matches. First, if any recruitment events assigned to one cycle occurred prior to an earlier cycle's length trough, or later than a later cycle's length trough, the recruitment events were discarded. Applying a stronger assumption, if any recruitment onset, specifically, occurred later than the same cycle's segment length trough, that cycle's recruitment events were also discarded. Finally, if any delay between a segment's recruitment onset and its contraction onset exceeded the median period of a full locomotor cycle, that cycle's recruitment events were discarded. Thus, the remaining matched recruitment events occurred within a reasonable time frame relative to their assigned contraction events.

Recruitment phases

Having assigned recruitment events into cycles, phases were determined for these events using the same procedure as for contraction events: the delay between a cycle's start time (tail movement) and a segment's recruitment onset was normalized to the total cycle period.

4.4.7. Accounting for cycle speed information

To investigate the extent to which intersegmental coupling arose from the relationships between segments' contractions and locomotor speed, speed information was regressed away from segments' kinematic data. To do so, separately for each segment, linear regression was

performed to obtain a relationship between cycle speed and each of the segment's contraction kinematic features (contraction amplitude, contraction rate, contraction duration). The predicted value of each feature on each cycle was then subtracted, leaving residual values. Pearson's correlation coefficients were calculated between segments using these residual values in place of the original values.

4.4.8. Modeling block correlation structure

To evaluate the spatial structure of contraction coupling among segments, a method was designed to find "blocks" of contiguous segments that share a coupling (correlation) strength. This method generates and compares block-based models of segments' correlation strengths for a single feature of contraction kinematics (e.g., contraction amplitude).

Model structure and assumptions

The central assumption of the method is that, within a block, adjacent segment pairs share the same correlation strength for the kinematic feature in question. Then, all further pairwise correlations within the block are modeled as the expected correlation under "local-only" segment coupling, which decreases exponentially as a function of distance. The coupling strength is determined for each block separately. Outside of blocks, segment pairs share a single baseline correlation strength (see example in Figure 4.4B).

In this method, blocks potentially range in size from including just one segment to all eight segments. Two blocks may overlap but blocks may not nest fully inside other blocks and a segment may not be contained in more than two blocks. The 8-block model corresponds to a null model in which each segment is uncoupled to any others, except for a constant average correlation strength for all segment pairs. Conversely, the 1-block model (Figure 4.4C)

corresponds to a null model in which coupling between all eight segments is purely dependent on distance, with no other variation. For all other models, in which subsets of segments group together inside blocks, expected coupling between segments is a function of whether or not they belong to the same block and, if applicable, the coupling strength for that block.

Defining and evaluating models

To fit a model given a set of block edges, we fit the expected pairwise correlations as follows (see Figure 4.4B).

Within a block, we averaged the d'th root of all correlations, where d is the distance between the segments in the pair (e.g., for adjacent segments d=1). To permit this operation, correlations less than zero were set to zero.

When two blocks overlapped, we performed the same operation but took the d'th root of the correlation as being the average of the values in the two blocks. All within-block values could be estimated simultaneously in this way by linear regression.

Out-of-block elements, which correspond to segment pairs that were not in the same block, were averaged.

To find the most likely block structure for each larva's empirical correlations, first, every possible model was fit (n=1094 possible block combinations). Then, the log likelihood of the data under each model was calculated assuming a Gaussian distribution with a covariance matrix equal to the fitted model. Finally, standard model comparison was performed using the Bayesian Information Criterion (Schwarz, 1978), which penalizes parameters to account for models with more parameters being likely to fit better. Results were similar when the Akaike Information Criterion (Akaike, 1974) was used for model selection instead.

The model as structured has one degeneracy: nearly-uncorrelated segments can be included in the same block with a very low fitted correlation, which model comparison considers more parsimonious than using several 1-segment blocks. To analyze results of block modeling, we therefore only evaluated "strongly-coupled" blocks ($R > 0.5$ for segments with distance=1). However, the same analyses were performed when instead considering all blocks (Supplementary Figures 4.4, 4.5), producing qualitatively similar results.

Alternative model assumptions

The method as described above employs the assumption that correlations between segments within a block decrease with distance. A variant of the method was tested that assumed correlations did not fall off with distance (Supplementary Figures 4.4, 4.5). In this version of the method, each block was given a constant correlation (the mean correlation strength of all in-block pairs from the empirical data). Out-of-block pairs were treated as in the model above. Results from this model variant were similar.

4.4.9. Statistics

The number of cycles required per larva was estimated early in data collection, from the first five jGC7f larvae successfully predicted by a DLC network. For five individual larvae, a threshold of at least 50 "good" forward locomotor cycles (for cycle criteria, see "Forward locomotor waves") was determined by eye to produce reasonable error bounds around pairwise intersegmental correlations. Imaging sessions were designed to maximize the number of cycles that could be well-tracked and predicted per animal, and the minimum threshold of 50 cycles was maintained for the remaining imaged animals.

To compare distributions of kinematic (Figure 4.2) and recruitment (Figure 4.5) features across eight body segments, data were combined across larvae. Normality of distributions was rejected using the Shapiro-Wilk test ($p<<0.05$) for all distributions analyzed in Figures 4.2 and 4.5. Therefore, distributions were compared using the nonparametric Friedman's test and Dunn-Šidak post-hoc multiple comparison correction.

For significance testing of correlation strengths at multiple intersegmental distances (Figure 4.3A), one-tailed Student's T-tests were used to compare correlation strengths to a null value of zero (Figure 4.3A, right-tailed test) or to the original, pre-regression correlation strength (Figure 3B, left-tailed test) with a Bonferroni-corrected alpha of 0.002.

To distinguish observed correlations from the null model that correlation strength would depend on intersegmental distance (Figure 4.4A), a bootstrapping approach was used to generate an expected distribution of correlation strengths under the null model. A separate distribution was generated for each larva. To do so, first, the larva's cycles were sampled with replacement (up to the original number of cycles). Next, pairwise intersegmental correlations were calculated using the resampled data. Then, the expected correlation at each intersegmental distance was calculated by averaging over all pairs of segments at a given distance (7 pairs of segments were averaged with distance=1, 6 pairs with distance=2, etc.). Lastly, the process was repeated (n=10,000 iterations). After generating bootstrapped distributions of expected correlation strength, empirical correlations were compared to the bootstrapped distributions and a p-value calculated for each.

CHAPTER 5

GENERAL DISCUSSION

In the preceding chapters, I introduced the central question underlying the work in this thesis: How do limbless animals coordinate their body segments to achieve locomotion? I reported results from two projects aiming to fill critical gaps in our understanding of this question in the larval Drosophila model system, as well as a method designed to facilitate future work on this question in the larval model. To conclude, I will address the larger implications of my results for answering the central question of this work, and point to a few of the new questions these results have raised.

5.1. Proprioceptive feedback and its role in limbless locomotor coordination

I investigated the larval proprioceptive system from an anatomical standpoint, starting from the expectation that the anatomical details and organization of proprioceptive neurons' central projections could reveal important principles for how this feedback is ultimately used by the central nervous system. I showed specializations of larval Drosophila proprioceptors as compared to other larval mechanosensory neurons, and as compared to the proprioceptors of limbed model systems (including the soft-bodied, limbed caterpillar, which has the direct sensory-motor reflex arcs that are apparently absent in leech and larval Drosophila; Tamarkin and Levine, 1996).

My findings predict two properties of larval proprioceptive processing that are unusual in the broader field of proprioception: first, that proprioceptive feedback is not subject to presynaptic gain control or phase-specific inhibitory modulation, which are otherwise highly conserved properties across proprioceptive systems (Azim and Seki, 2019). Second, my findings

predict that proprioceptive sensory-motor reflex arcs do not contribute to control of larval locomotion (or other behaviors). Both of these properties may be shared by leech proprioception: To date, there is no evidence for presynaptic inhibition of leech stretch receptors (Fan and Friesen, 2006). Likewise, studies have only found connections onto central interneurons, not directly onto leech motor neurons (Cang et al., 2001; Fan and Friesen, 2006). Together, the lack of these two properties in both leech and larval Drosophila suggests quite distinct handling of proprioceptive feedback in limbless soft-bodied organisms (Pearson, 2004; Rossignol et al., 2006). On the other hand, phase-specific inhibitory inputs have been demonstrated onto leech gentle-touch-responsive mechanosensors (Alonso et al., 2020). In fact, if there are any reflexes that need to be gated during larval Drosophila locomotion, they may involve mechanosensors such as the chordotonal or multidendritic neurons.

The evolutionary component of these conjectures would need to be tested by expanding anatomical study into additional soft-bodied, limbless creatures. Testing the functional component will require access to proprioceptive processing circuits, to determine how proprioceptive information is integrated with other inputs: it may be that phase-specific gating of proprioceptive feedback is still important in larval locomotion, but is performed at the level of downstream neurons, either by inhibition or by specific membrane properties.

The other main prediction of my findings in Chapter Two, that certain combinations of larval proprioceptors co-locate their outputs because they are functionally grouped into circuits, can be tested with further connectomic analyses, discussed next.

Utility of mapping proprioceptive circuits

As discussed in Chapter Two, the positioning of sensory neuron outputs on its own cannot tell us how proprioceptive neurons wire into downstream circuits; to do so requires identifying those neurons that are the targets of the output synapses. Work on characterizing the downstream neurons remains to be completed. It is worth testing the conjecture that the degree of overlap in proprioceptive neurons' output synapses inside spatial domains will predict the overlap in which circuits they contribute to, for two reasons. The first is developmental and, while interesting, has less to do with the questions of this thesis; the second is that a complete map of the targets of proprioceptive neurons, even from one example animal, would be of clear value to the field (Dallmann et al., 2023). Such a map would enable a number of approaches to asking how proprioceptive feedback contributes to locomotor coordination. For instance, no model of segmental coordination yet incorporates both stretch feedback from the dorsal bipolar dendrite neuron and contraction feedback from multidendritic neurons. At present, it remains unclear whether these proprioceptor subtypes contribute much unique information to locomotor circuits, or whether their information is mostly redundant (Hughes and Thomas, 2007). This gap will likely need to be addressed using a combination of anatomical pathway tracing, modeling, and further functional studies.

Given a complete map of proprioceptors onto locomotor circuits, how would one decide where to begin? Recent studies illustrate some of the possibilities: One could start from an anatomically-constrained model, using the basic parameters of synapse count and sign (excitatory or inhibitory) to predict which interneurons might be most important for relaying proprioceptive feedback between segments, similar to the approach taken by Zarin et al. in 2019 to predict the wave-related activity of premotor interneurons. (Of course, synapse count does not

necessarily equate to synaptic strength, which will hamper any purely connectome-based approach to circuit modeling.) Nonetheless, some value might be gained from evaluating connectivity onto these candidate interneurons, such as by looking for potential phase-dependent gating via any known rhythmically-active inhibitory interneurons. Some such downstream interneurons might also present good targets for investigations into compartmentalized dendritic processing of proprioceptive information; larval interneurons often display complex dendritic morphologies, in which input and output synapses can be highly segregated, thoroughly intermingled, or a combination (e.g., Heckscher et al., 2015; Schneider-Mizell et al., 2016; Zwart et al., 2016). It would be highly interesting to know, as a start, what other inputs and outputs are located nearby the proprioceptive inputs onto locomotor-related interneurons, and how far these proprioceptive inputs are located from the interneurons' various downstream partners.

As an alternative modeling approach, one could reduce central circuits to a few "representative" neurons, based on CPG models in other locomotor systems; this approach was recently taken by Francis et al. in 2024. Their more minimal model could be adapted to include sensory feedback based on known connectivity, and used to predict the effect of proprioceptor manipulations on particular CPG components. Ultimately, one would aspire to a neuromechanical model at the level of detail attained for leech swimming (Iwasaki et al., 2014), but with the advantage of genetic access to the model components, allowing easier testing of specific model predictions. In the Drosophila larva, it would be challenging, but not impossible, to constrain such a model or validate its predictions using electrophysiological experiments (see, e.g., Baines and Bate, 1998; Rohrbough and Broadie, 2002; Giachello et al., 2020).

Alternatively, one could start from experiments designed to narrow down the range of effects proprioceptive feedback might have on locomotor coordination. For instance, one could replicate combinatorial sensory silencing experiments performed by Hughes and Thomas and Song et al. in 2007, this time evaluating the results in terms of segmental coordination, using the analyses introduced in Chapter Four. It is worth noting that, given the suspected redundancy between subtypes of proprioceptors, manipulations of a single sensory type might not result in any observable changes to locomotor coordination (Hughes and Thomas, 2007; Dallmann et al., 2021), which could quickly increase the complexity of these experiments and make negative results uninterpretable. Moreover, despite the apparent lack of presynaptic gating onto larval proprioceptors, the timing of their experimental activation or silencing is still likely to play a determining role in the manipulation's effect on behavior (Wolff and Ölveczky, 2018; Murawski et al., 2020). The design of acute manipulation experiments, whether in vivo or in fictive preparations, should account for this possibility and treat phase of manipulation with care.

Finally, one could jump straight into probing the functional and synaptic connections between proprioceptive neurons and their downstream interneuron partners, focusing on interneurons that are already of interest for locomotor coordination, to try to understand how these synaptic connections function. Because the larva offers access to in vivo optogenetics paired with calcium imaging, it may be possible in the larva to achieve what has been elusive in other limbless models: to determine which of the functional relationships between proprioceptors and their targets, as characterized in the isolated nerve cord, hold up in vivo. This will be especially important for understanding how information about the larva's own movement is integrated with other locomotor-related activity.

Proprioception and segmental coordination

Can proprioceptive feedback help account for the various scales and forms of segmental coordination described in Chapter Four? On the one hand, proprioceptive feedback seems unlikely to account for the axial diversity in segmental contractions we observed, if only because the trends in which segments contract for longer or at a faster rate reverse partway down the body. It is not immediately obvious how this reversal would result from stretch or contraction sensation, assuming consistent wiring of sensory feedback into central circuits (which is far from guaranteed; see Chapter Four Discussion). If anything, it seems more likely that proprioceptive feedback would serve to keep a trend going along the body axis: if one segment contracts more slowly than its predecessor, the (possibly later or weaker) proprioceptive feedback about its contraction would result in a yet slower contraction in the following segment, and so forth. This is pure speculation, however. It is similarly unclear how proprioceptive feedback could explain the anterior-posterior differences in coupling we observed among segments' contraction durations.

On the other hand, my results do not yet rule out such a role for proprioception. I did make preliminary attempts to model the effect of proprioceptive feedback in my dataset, using an early subset (n=5) of the jGC7f larvae, by constructing generalized linear models that predicted segments' contraction amplitudes or contraction durations as a function of more posterior segments' contraction kinematics. The idea was that some combination of more posterior segments' contraction rates and amplitudes would reflect the sensory feedback received from class I multidendritic neurons, feedback which is known to affect segmental contraction amplitudes and durations when silenced (see Section 1.5.4). However, the linear models I tested

returned contradictory results across individuals and segments, and I abandoned them relatively early on. Future work on the dataset collected for Chapter Four might test alternative specific hypotheses about the relationship between segmental kinematics and proprioceptive feedback on a cycle-to-cycle basis. It might be particularly interesting to try to model the cycle-to-cycle variability in recruitment versus contraction onset timings (Figure 4.6) as a function of more posterior stretch or contraction feedback.

5.2. Segmental coordination in larval Drosophila locomotion

In the General Introduction, I pointed to two critical gaps in the study of larval locomotor coordination: first, a lack of data relating neuromuscular activity to in vivo movement, and second, the tendency to evaluate only average segmental kinematics analyses of segmental kinematics, rather than relationships across many cycles of movement. The methods used in Chapter Four begin to fill both gaps, and the results obtained raise new questions about segmental coordination in this system.

In Chapter Four, I showed inconsistencies in segmental contraction kinematics and in wave propagation across the body axis, features which had not been shown in previous characterizations of larval crawling. I also showed that coupling among segments' contraction durations was greater at the posterior end than at the anterior end, and that in most larvae, this coupling manifests as a block of strongly-coupled posterior segments, suggesting relatively flexible contraction coupling among anterior segments and between anterior and posterior segments. I argued in that chapter that this difference in coupling strength between posterior and anterior body segments may reflect a common need among limbless locomotor systems to more tightly coordinate movements nearer the tail end, which is more essential for stability and force

production, but to allow segments nearer the head end to vary movements in service of exploration (Tytell and Cohen, 2008; Puhl and Mesce, 2010).

My findings are descriptive and cannot reveal whether the forms of coordination described are truly essential to larval locomotion, whether they are a byproduct of other features of larval (neuro-)anatomy and physiology, or whether they emerge in certain environmental contexts and not others. To do so will require further investigation, perhaps beginning with clarifying the contribution of the environment.

Muscle recruitment, movement, and the environment

Data relating neuromuscular activity to in vivo movement are required to understand how locomotor waves arise from the interaction of neural control, body, and environment. Using such data, I was able to compare overall trends in segmental coordination at the levels of recruitment and movement, offering an initial glimpse at the recruitment-contraction relationship within one particular environment.

First, I reported a general alignment of axial trends in segment-level muscle recruitment and contraction kinematics (Figure 4.5), suggesting that, at minimum, the axial differences I found in segments' contractions are not purely the effect of identical recruitment patterns getting passed through the 'filter' of the body-environment interaction. However, in the axial distributions, there is an 'offset' of about a segment between where recruitment rates and durations reach their lowest/highest points, and where contraction rates and durations do the same. This offset could be interpreted in multiple ways. It is consistent with sensory feedback from one segment affecting the recruitment of the next anterior segment. It is also consistent with muscle activation in one segment exerting its primary effect on kinematics not within-segment,

but across-segment, potentially through pulling on the next posterior segment. Neither interpretation can explain the inflection point along the body where rate and duration trends reverse, however. I speculate that the inflection point is more likely due to intrinsic differences among segments' circuit properties, such as connectivity strengths or levels of excitability, in CNS and/or PNS circuit members. Such a "U-shaped" distribution of intrinsic properties has been seen, for instance, in the intrinsic oscillation periods of leech ganglia in the isolated nerve cord, which are shortest in the middle of the body (Hill et al., 2003).

Second, I also reported a curious mismatch in the spatial variability of recruitment versus contraction intersegmental delays: while intersegmental recruitment delays showed relatively little variability between posterior segments, they became far more variable between anterior segments, an observation that was not seen for intersegmental contraction delays. So far, I have not been able to explain the cycle-varying location of this long delay; I have ruled out a relationship with cycle-level features such as crawling speed, period, or stride distance, but have not yet been able to test other hypotheses.

Of the major results reported in Chapter Four, this is the one that I think most likely to be due to the effects of proprioceptive feedback. One interesting possibility is that it points to temporally-consecutive roles for contraction and stretch sensory feedback in advancing the wave of muscular recruitment. In this scenario, the long delay in propagating recruitment from one segment into the next would be an indication that feedback about a more posterior segment's contraction was used to advance neural activity, but that further recruitment then was held up until that same segment successfully de-contracted. As mentioned above, this might be testable in the collected data, using a model to predict anterior segments' recruitment timings/rates from

posterior segments' contraction and de-contraction timings/rates. Another place to start would be confirming whether an unusually long phase delay in propagating recruitment from one segment into the next always coincided with a long within-segment delay between recruitment and contraction (e.g., if the recruitment delay between A3 and A2 was very long, A3's contraction also came much later than its recruitment). If true, this would fit with the model in which contraction needs to occur for neural activity to continue propagating (Hughes and Thomas, 2007).

More broadly, the differences observed between recruitment and contraction phases echo those observed in anguilliform swimming (see Section 1.2). Are the anterior-posterior differences we see in recruitment versus contraction timing, like those in the lamprey, a form of "neuromechanical phase lag"? On the one hand, the recruitment-contraction lags I reported were highly inconsistent both in location and in presence when compared to the lags observed in anguilliform swimming. Therefore, in contrast to the lamprey's neuromechanical phase lag, the larva's may not be a regular feature of the interaction between body and environment, or may be quite sensitive to cycle-varying features such as slight changes to body posture. On the other hand, the lags in both systems probably similarly reflect an influence of the substrate/ environment on transforming neuromuscular activity into the final kinematic pattern. In the lamprey's case, the interaction between body and environment is a predictable enough component of generating a locomotor wave that it is very likely 'baked in' to neural control of locomotion (Chiel et al., 2009; Liao, 2022). In the larva's case, the interaction of body and environment appears to 'smooth out' cycle-by-cycle timing inconsistencies in muscle recruitment.

All of the above conjectures as to the contribution of the agarose channel environment to our results remain to be tested, by directly comparing segments' kinematic and recruitment coordination inside and outside of channels, or in alternative environments with different physical properties (hardness, texture, etc.).

Regional coupling and cycle-by-cycle coordination of locomotion

Lastly, I reported in Chapter Four that cycle-by-cycle coordination of segments' contraction durations was stronger among posterior segments and weaker between posterior and anterior segments or among anterior segments. This result suggests different levels of flexibility in how anterior and posterior regions are coordinated during locomotor waves, something that previously had been thought to be a property of larvae's turning movements, but not of peristaltic waves per se. This inter-regional flexibility is likely to be a point of similarity between larval Drosophila locomotion and locomotion in other model systems. The strongly-coordinated segments are in the posterior half of the body, which in many animals is the region required to provide more of the stability or force generation for forward locomotion. The more weakly-coordinated segments are in the anterior half, and are those involved in producing active sensing and re-orientation movements between locomotor waves (Lahiri et al., 2011). Thus, it seems that Drosophila larvae join other model systems in varying the coordination of their segments along the body axis, perhaps according to larger behavioral goals.

However, compared to lamprey or leech, the specific form of flexibility in coordinating anterior and posterior body regions appears to differ: the swimming lamprey exhibits flexible coordination of segments' contraction amplitudes; the crawling leech exhibits flexible coordination of elongation propagation phases; and the crawling Drosophila larva exhibits

flexible coordination of contraction durations. Moreover, the neural mechanisms used to effect flexible coordination are certain to differ between larva, leech, and lamprey, given these organisms' highly diverged and differently-structured nervous systems. This makes comparison among all three systems particularly attractive for elucidating the sources and consequences of axial variations in segmental coordination.

Future directions

It remains to be determined whether the between-region or within-region forms of coupling we observed are truly useful to larval locomotion; to discover this will first require identifying what causes anterior-posterior differences in coupling. A few caveats: First, from the current dataset, we can't yet conclude how truly "regional" are the coupling differences among posterior and anterior segments. Our statistical methods point to groups of segments among which coupling is likely to be higher, but cannot rule out an axial gradient of coupling strengths. Moreover, individual larvae occasionally deviate from the most common block pattern of strong coupling (Appendix D, Figs. S2, S3). Because we see differences in coupling patterns among isogenic individuals (all 18 "Gerry" larvae were isogenic), the location of strong coupling may not be strictly genetically defined. I think it would be useful, first, to confirm whether stronger posterior coupling is introduced by the larva's channel environment. If the result holds across environments, however, it could be highly interesting to identify and test candidate sources of regional coupling strengths.

To my mind, there are not any obvious forerunners among candidate sources. For one, there are few reported segmental differences that align with the mid-body location where we found frequent breaks in intersegment coupling. Segment-level differences have been described

in the presence or the anatomical/physiological properties of certain sensory neurons, motor neurons, and interneurons. However, to date, most of these reports concern differences between thoracic or terminal and abdominal segments. Likewise, the gradients of Hox gene expression patterns established during development and in the larva do not cleanly align either with the non-monotonic trends in muscle recruitment and kinematics, or with the regions of distinct contraction duration coupling (Singh and Mishra, 2014).

Nonetheless, a small number of studies have shown intriguing differences between the mid-body abdominal segments. For instance, a report from Takagi and colleagues showed that the effect of stimulating the "Wave" class of interneurons changed at the boundary between A3 and A4: optogenetic activation of only anterior Wave neurons led to fictive backward crawling, while activating only posterior Wave neurons led to fictive forward crawling (Takagi et al., 2017). Another study from Tastekin and colleagues showed specific inhibitory inputs to posterior segments (A4 and posterior) that are active during pausing while larvae perform head casts (Tastekin et al., 2018). During embryonic development, the feedforward intersegmental excitatory interneuron A27h, and its putative sibling interneuron called "M," are gap junction coupled to each other and to other A27h/M neurons only in segments T3 through A3 (Zeng et al., 2021). Whether any of this connectivity persists into larval stages is, to my knowledge, still unknown. These and other reports (e.g., Murawski et al., 2020; Jonaitis et al., 2022) indicate potentially substantial differences among even abdominal segments, depending on their locations along the larval body axis. There is not a clear (to me) mechanism by which any one of these intrinsic differences among segments would lead to stronger posterior coupling during locomotion. Nonetheless, the source of axial diversity in segmental coupling strength may lie in

one or more of these intrinsic differences, or in yet-to-be characterized differences; for instance, neuromodulators are perennially strong candidates for introducing flexibility into locomotor circuits (Selcho et al., 2012; Grillner and El Manira, 2019).

APPENDIX A: Chapter 2 Supplementary Figures

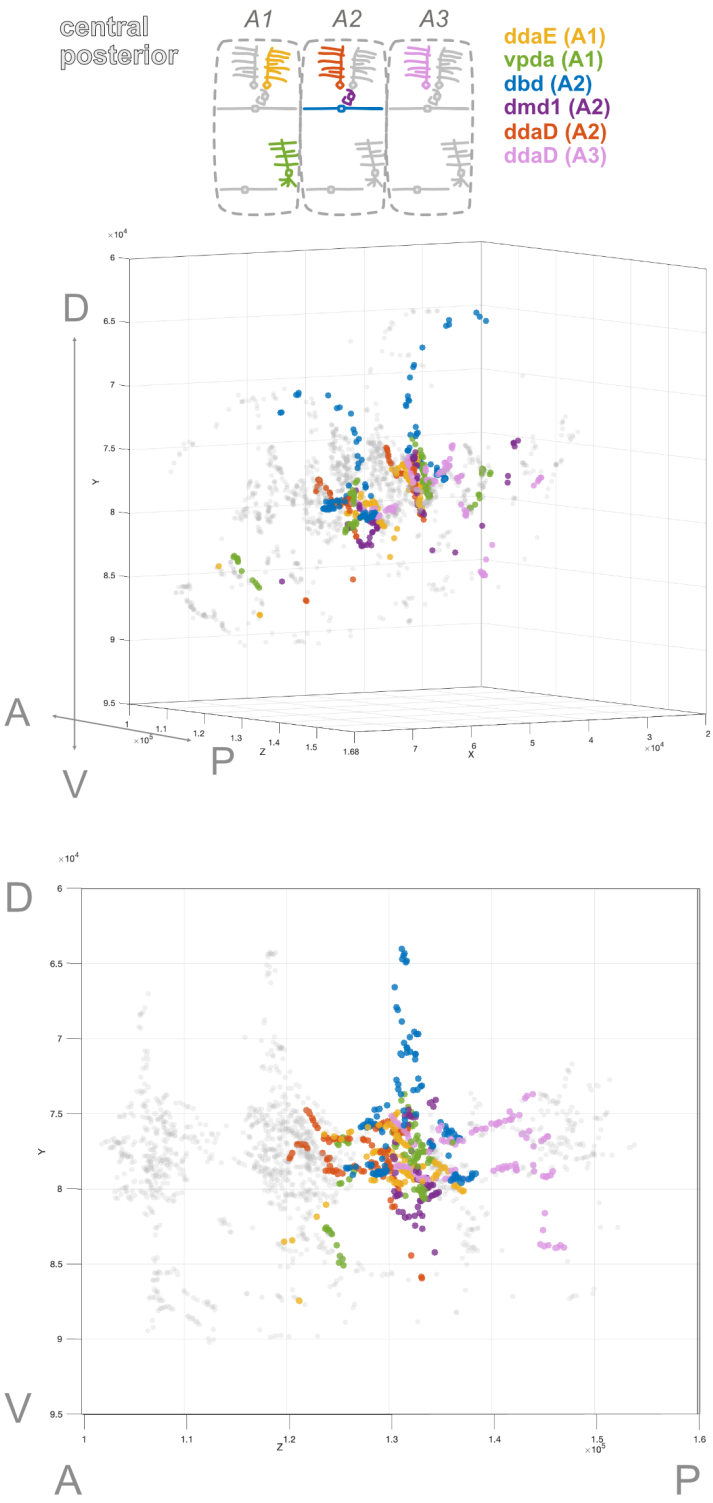

Supplementary Figure 2.1: 3-D visualization of A1 output synapses. Distributions of A1 proprioceptor output synapses along left-right (L-R/ mediolateral) axis, top panel; along dorsal-ventral (D-V) axis, middle panel; and along anterior-posterior (A-P) axis, bottom panel. (Direction of axis relative to CNS shown in insets.) Left-side proprioceptors in left set of 3 panels; right-side proprioceptors in right set of 3 panels. Each proprioceptor's output distribution plotted as the proportion of outputs in 1 µm bins, colored according to legend. Midline plotted as vertical dashed line.

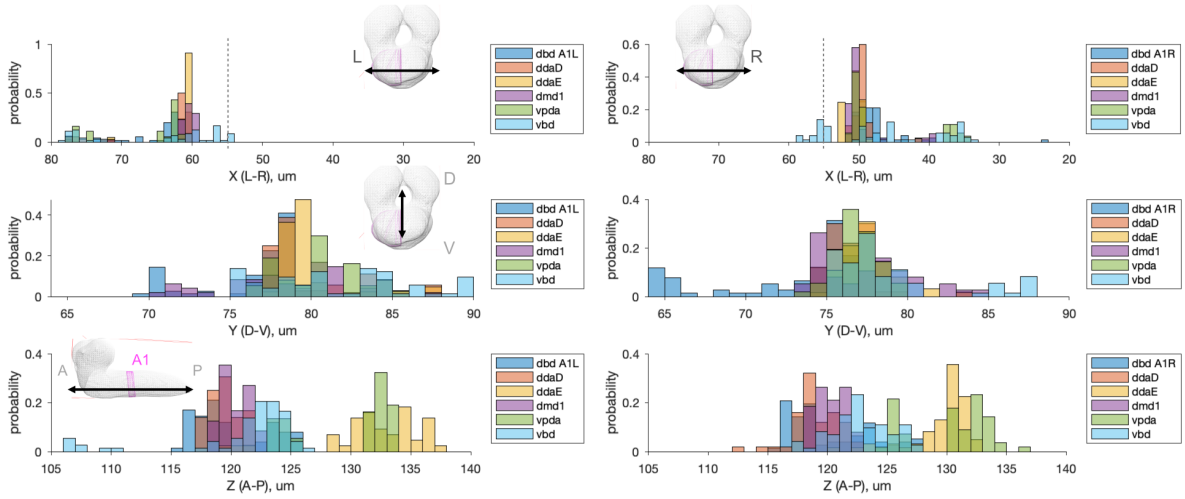

Supplementary Figure 2.2: Axial distributions of proprioceptor output synapse locations. Anterior-posterior distributions of output synapses from individual proprioceptors from segments T3, A1, and A2 (or T3-A3, ddaD and vbd only). Each segment's output distribution plotted as the proportion of outputs in 1 µm bins; segments colored according to legend. Direction of the A-P axis shown relative to CNS at bottom.

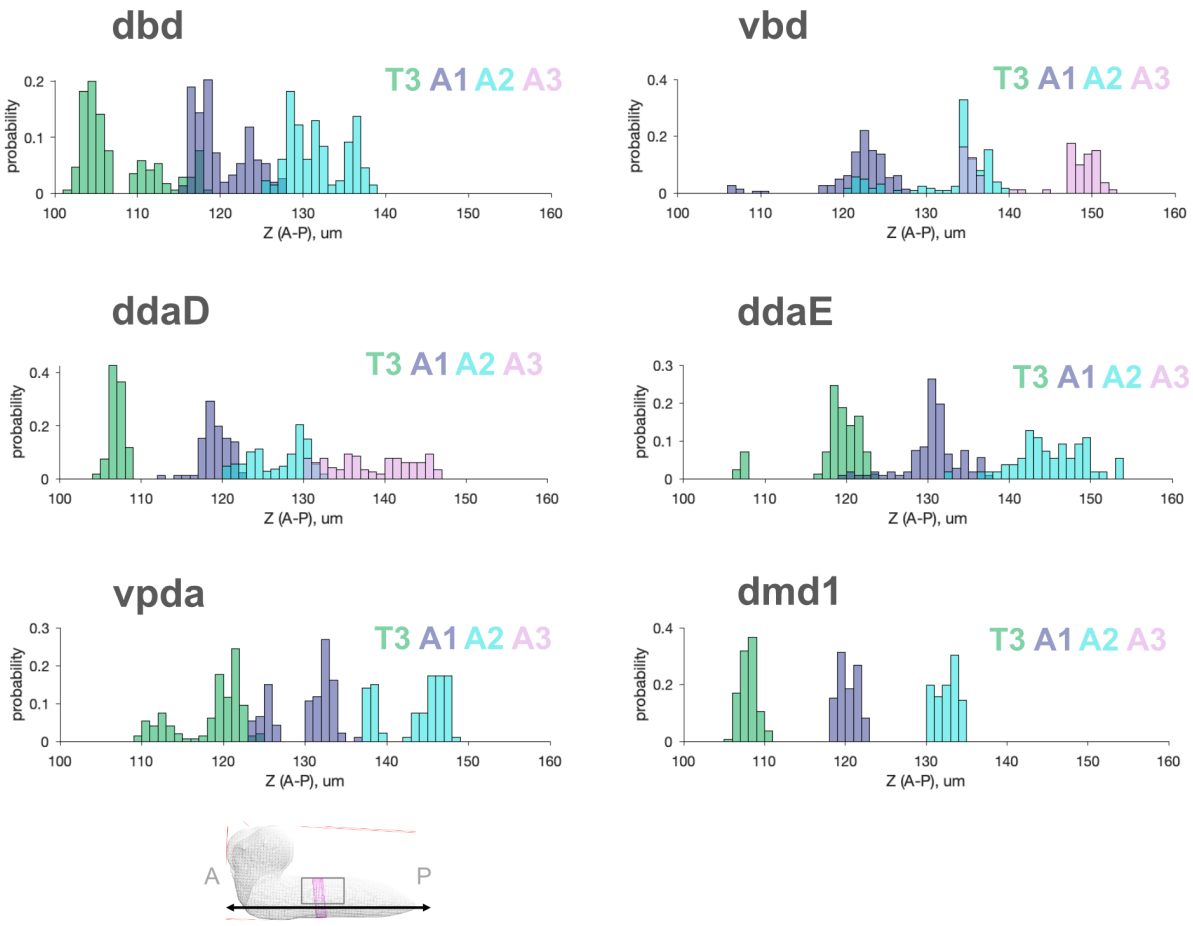

Supplementary Figure 2.3: Three-segment comparison of proprioceptor output locations. Output synapses in the "central posterior" domain (see Figure 3), corresponding to the "central domain" of segment A2. Top, body wall diagram: dendritic "receptive field" of the contributing neurons. Two views plotted below; contributing neurons colored according to body wall diagram. Note contribution of synapses from neurons in both adjacent segments. Spatial position values along axes are given in nm.

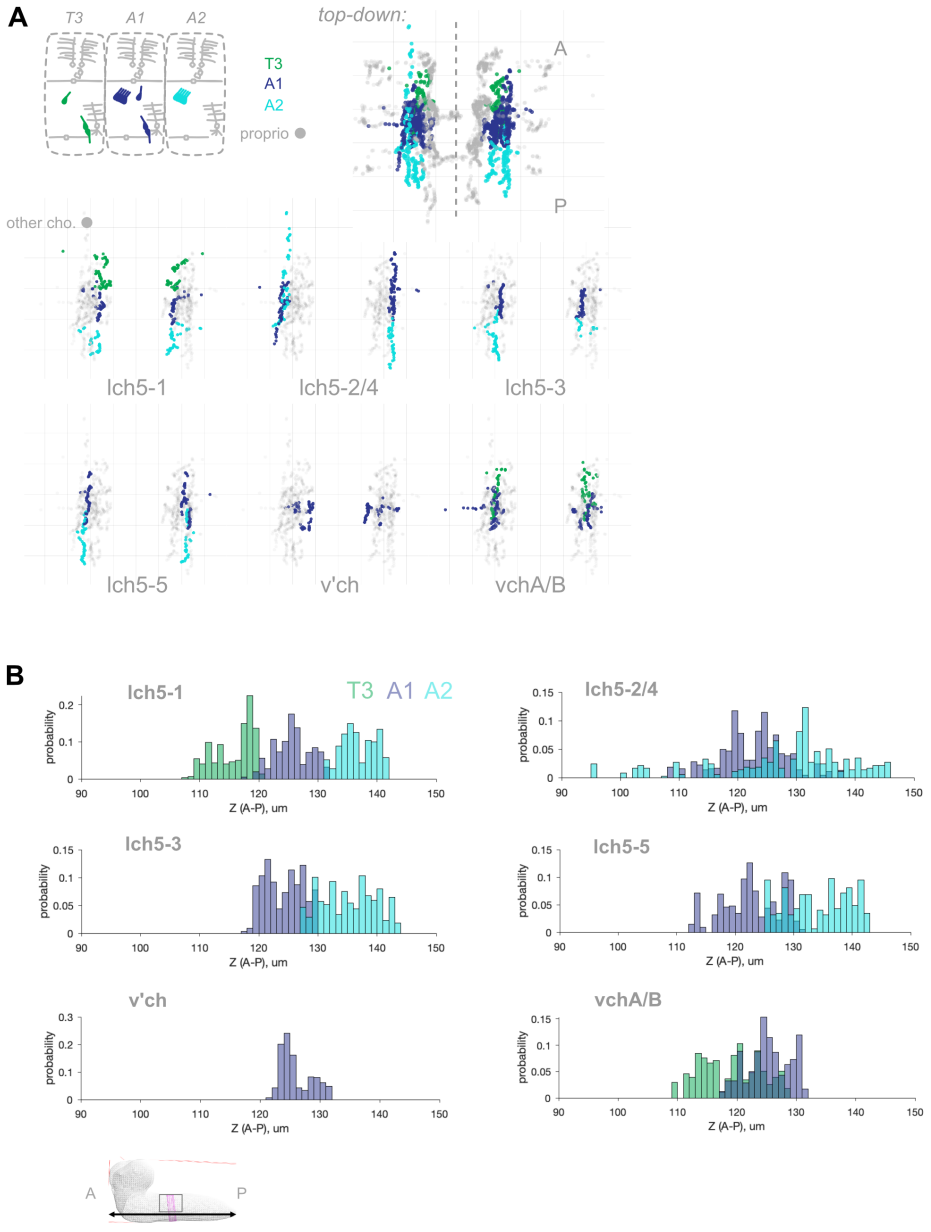

Supplementary Figure 2.4: Three-segment comparison of chos output locations. A) Top-down views of output synapses from all T3, A1, and A2 chordotonals (that have been annotated), colored according to diagram. All chordotonals combined, with proprioceptor output synapses plotted in grey for spatial context, in top panel. Individual chordotonals' T3-A2 outputs, with other chordotonals' outputs plotted in grey, in lower set of panels. **B)** Anterior-posterior (A-P) distribution of output synapses from individual chordotonals from segments T3, A1, and A2. (Direction of axis relative to CNS shown at bottom.) Each segment's output distribution plotted as the proportion of outputs in 1 µm bins; segments colored according to legend.

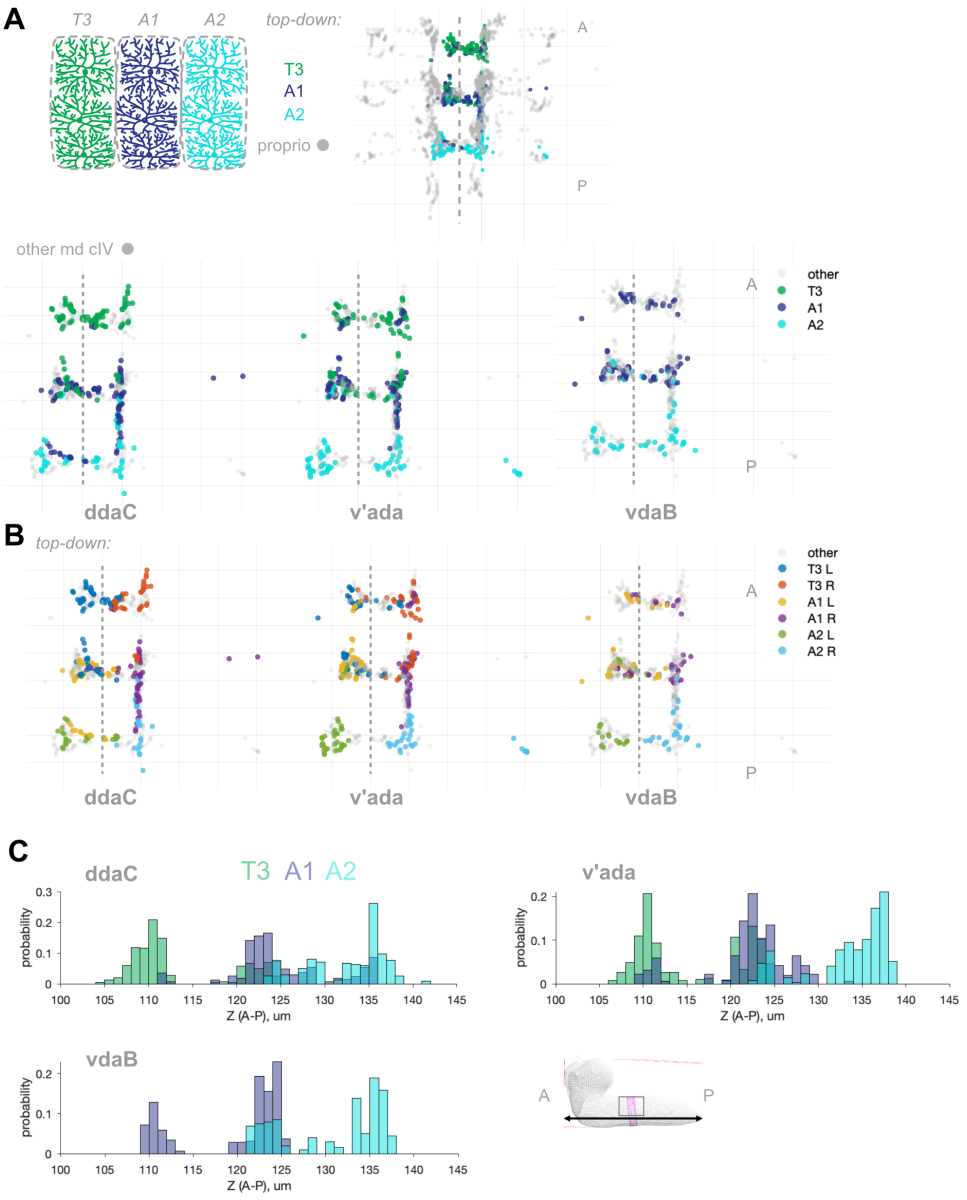

Supplementary Figure 2.5: Three-segment comparison of mds output locations. A) Top-down views of output synapses from all T3, A1, and A2 md cIV neurons (that have been annotated), colored according to diagram. All md cIVs combined, with proprioceptor output synapses plotted in grey for spatial context, in top panel. Individual md cIVs' T3-A2 outputs, with other md cIVs' outputs plotted in grey, in lower set of panels. **B)** Individual md cIV neuron's output synapses, this time colored by side and segment identity, according to legend. Other md cIVs' outputs plotted in grey. Note output synapses spanning multiple segments and sometimes crossing midline. **C)** Anterior-posterior (A-P) distribution of output synapses from individual md cIV neurons from segments T3, A1, and A2. (Direction of axis relative to CNS shown in inset.) Each segment's output distribution plotted as the proportion of outputs in 1 µm bins; segments colored according to legend.

APPENDIX B: Chapter 2 Supplementary Tables

Table 1. Input and output synapse counts for each proprioceptive neuron in segments T3, A1, and A2, on the left and right side. Where both inputs and outputs entries are 0, the neuron did not exist in the annotated dataset.

Table 1

Neuron	inputs	outputs
dbd_T3L	3	80
dbd_T3R	2	91
vbd_T3L	0	0
vbd_T3R	0	0
ddaD_T3L	0	51
ddaD_T3R	2	59
ddaE_T3L	0	36
ddaE_T3R	1	49
vpda_T3L	3	66
vpda_T3R	1	81
dmd1_T3L	0	82
dmd1_T3R	3	82
dbd_A1L	2	76
dbd_A1R	1	77
vbd_A1L	0	73
vbd_A1R	3	73
ddaD_A1L	0	36
ddaD_A1R	0	50
ddaE_A1L	2	44
ddaE_A1R	2	62
vpda_A1L	1	37
vpda_A1R	0	56
dmd1_A1L	0	48
dmd1_A1R	5	38
dbd_A2L	1	69
dbd_A2R	0	63

Table 1

Neuron	inputs	outputs
vbd_A2L	0	82
vbd_A2R	0	43
ddaD_A2L	1	51
ddaD_A2R	0	57
ddaE_A2L	1	39
ddaE_A2R	1	16
vpda_A2L	1	33
vpda_A2R	0	60
dmd1_A2L	2	40
dmd1_A2R	0	36

Table 2. Input and output synapse counts for each chordotonal and class IV multidendritic neuron in segments T3, A1, and A2. Where both inputs and outputs entries are 0, the neuron did not exist in the annotated dataset.

Table 2

Neuron	inputs	outputs
lch5-1_T3L	49	76
lch5-1_T3R	34	59
lch5-2/4_T3L	0	0
lch5-2/4_T3R	0	0
lch5-3_T3L	0	0
lch5-3_T3R	0	0
lch5-5_T3L	0	0
lch5-5_T3R	0	0
v'ch_T3L	0	0
v'ch_T3R	0	0
vchA/B_T3L	13	40
vchA/B_T3R	20	63
lch5-1_A1L	51	55

Table 2

Neuron	inputs	outputs
lch5-1_A1R	43	51
lch5-2/4_A1L	43	81
lch5-2/4_A1R	32	96
lch5-3_A1L	55	62
lch5-3_A1R	46	63
lch5-5_A1L	18	56
lch5-5_A1R	19	65
v'ch_A1L	30	63
v'ch_A1R	29	61
vchA/B_A1L	31	104
vchA/B_A1R	37	89
lch5-1_A2L	35	36
lch5-1_A2R	29	48
lch5-2/4_A2L	23	69
lch5-2/4_A2R	8	37
lch5-3_A2L	69	63
lch5-3_A2R	12	15
lch5-5_A2L	16	48
lch5-5_A2R	13	40
v'ch_A2L	0	0
v'ch_A2R	0	0
vchA/B_A2L	0	0
vchA/B_A2R	0	0
ddaC_T3L	21	62
ddaC_T3R	16	39
v'ada_T3L	15	57
v'ada_T3R	18	53
vdaB_T3L	0	0
vdaB_T3R	0	0
ddaC_A1L	13	47
ddaC_A1R	10	59

Table 2

Neuron	inputs	outputs
v'ada_A1L	14	45
v'ada_A1R	12	52
vdaB_A1L	11	51
vdaB_A1R	26	40
ddaC_A2L	10	31
ddaC_A2R	10	31
v'ada_A2L	11	46
v'ada_A2R	9	40
vdaB_A2L	8	30
vdaB_A2R	12	34
ddaC_A1L	13	47
ddaC_A1R	10	59
v_ada_A1L	14	45
v_ada_A1R	12	52
vdaB_A1L	11	51
vdaB_A1R	26	40
ddaC_A2L	10	31
ddaC_A2R	10	31
v_ada_A2L	11	46
v_ada_A2R	9	40
vdaB_A2L	8	30
vdaB_A2R	12	34

APPENDIX C: Chapter Three Recipes

Drosophila Apple Juice-Agar Plates

MATERIALS

Reagents
Agar
Apple juice
Nipagin M (20% in absolute ethanol)
Sucrose
Equipment
Flasks, conical
Jug, plastic, 2-L
Magnetic stirrer and stirring rod
Oven, microwave
Petri dishes, 50- or 90-mm
This recipe will make 65 50-mm plates or 40 90-mm plates.

METHOD

1. In a conical flask, mix 18 g of agar in 600 mL of H_2O.
2. In a separate flask, mix 20 g of sucrose in 200 mL of apple juice.
3. Place both flasks in a microwave oven on a medium setting (e.g., 7 on a scale of 0–10) for 30 min.
4. When both the agar and sucrose are dissolved, pour the apple juice into the plastic jug with a magnetic stirring rod.
5. Carefully (to avoid bubbles) add the agar solution to the jug. Place the mixture on a magnetic stirrer. Allow the mixture to cool to at least 60°C.
6. Add 20 mL of 20% Nipagin M. Stir for a few minutes.
7. Pour into plates.
8. Allow the medium to solidify. Store the plates upside down at 4°C.

Fly Food

Ingredient Amounts (for 300-bottle batch)

Water	17 L
Agar	93 g
Cornmeal	1,716 g
Brewer's yeast	310 g
Sucrose	517 g
Dextrose	1033 g

Antifungal reagents as appropriate[a]
Antibiotics as appropriate[b]

[a]Use 8.69 g/L sodium potassium tartrate and 26.1 mL of a Tegosept (methyl-p-hydroxy benzoate) Stock solution. (For the Tegosept stock solution, dissolve the Tegosept in 95% ethanol at 100 g/L.)

[b]For each batch of food, add 15 mg/L tetracycline plus one of the following two antibiotics (alternate with each batch of food): 50 mg/L ampicillin, or 17 mg/L streptomycin.

Make up the antibiotics as fresh stock solutions, with tetracycline dissolved in ethanol at 10 mg/mL and ampicillin or streptomycin dissolved in water at 100 mg/mL.

METHOD

1. Mix the agar into 13 L of water; use the other 4 L of water to wet the remaining ingredients (excluding antifungals and antibiotics).
2. Cook the medium in a steam kettle at 15 pounds per square inch (psi) for 20 min with constant stirring.
3. Switch off the steam and cover the kettle with a lid. Allow the medium to cool to exactly 55°C and then add both the antibiotics and antifungals, stirring well.
4. Dispense medium into vials and bottles, cover with cheesecloth, and allow it to solidify overnight at room temperature before capping.

This recipe is adapted from that of Lewis (1960) and from recipe 4 from the Bloomington Drosophila Stock Centre website (flystocks.bio.indiana.edu/Fly_Work/media-recipes/media-recipes.htm).

Live Yeast Paste

Fill a vial (e.g., a scintillation vial) to about one-quarter with live baker's yeast. Add water while stirring with a wooden stick until the consistency of peanut butter is attained. Keep refrigerated (otherwise the yeast will rise and spill out of the vial).

APPENDIX D: Chapter Four Supplementary Figures

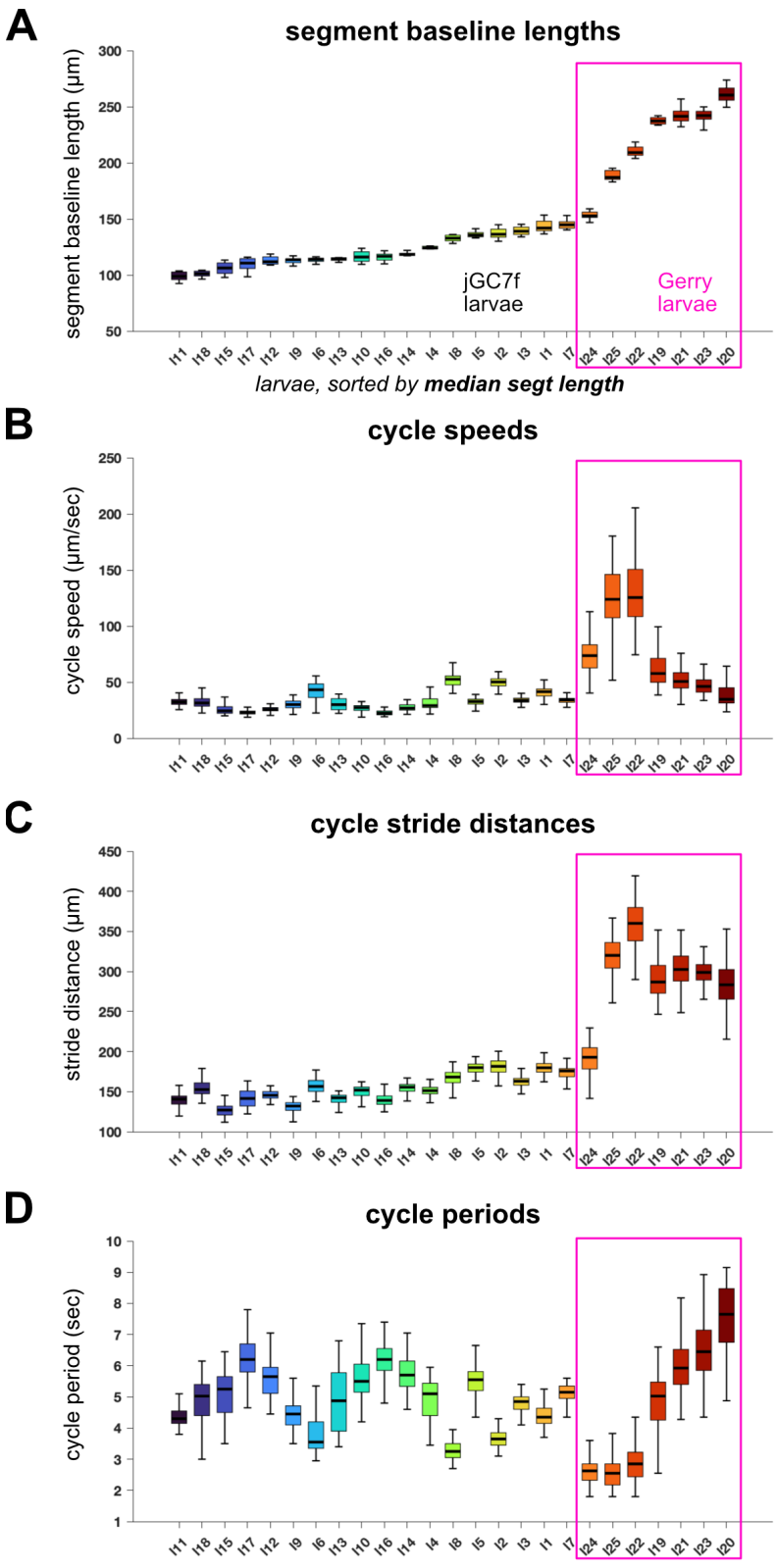

Supplementary Figure 4.1: Distribution of estimated larval sizes and locomotor cycle parameters.
A: Distribution of segment baseline lengths for each larva (proxy for animal size), sorted by increasing median length. **B:** Distribution of crawling speeds for each larva, sorted as in A. Crawl speed is calculated per cycle as cycle stride distance/cycle period (see Methods). **C:** Distribution of cycle stride distances for each larva, sorted by same order as in A. **D:** Distribution of cycle periods for each larva, sorted by same order as in A. **All panels:** n = 25 larvae. Pink box surrounds the Gerry subset of larvae.

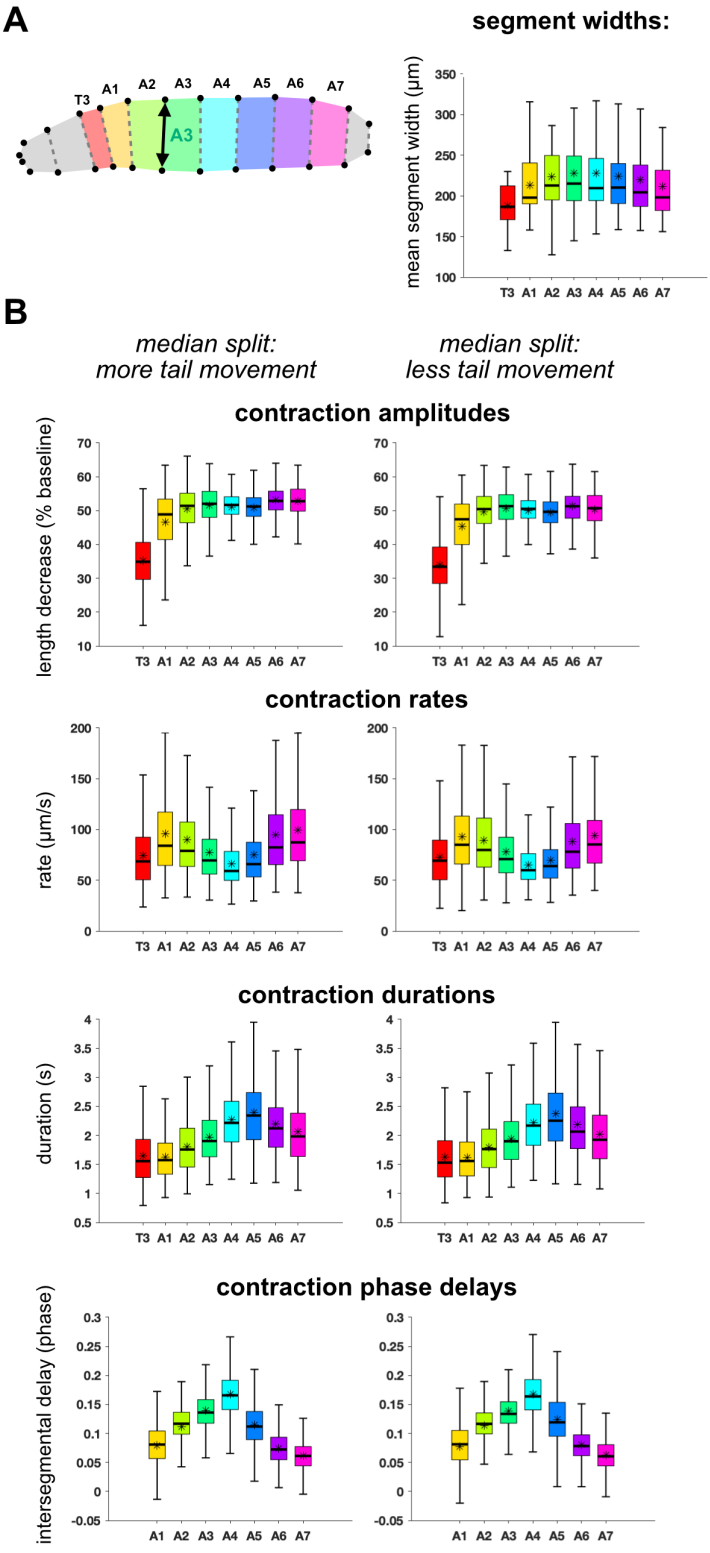

Supplementary Figure 4.2: Pushing the tail further forward does not alter axial trends in contraction kinematics.
A: (Left) illustration of segment width calculation, which used the segment's anterior boundary. (Right) Segmental distributions of mean boundary widths, n=25 larvae. **B:** Segmental distributions for the indicated feature of segmental contraction, for the 50% of cycles where larvae moved their tails forward by a greater distance (left column) or a lesser distance (right column). Median split of cycles was performed separately for each larva. n=1231 cycles for each column.

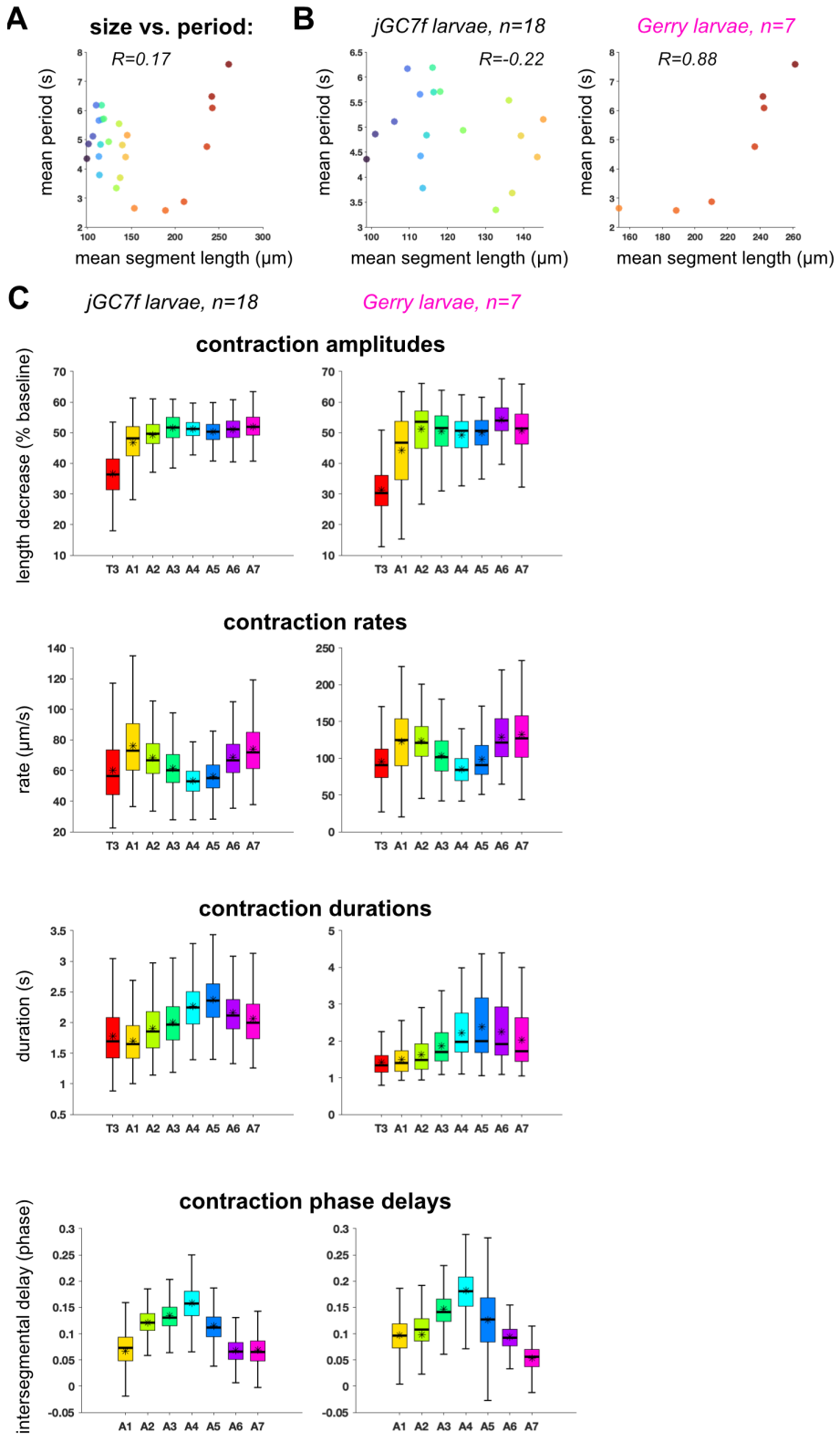

Supplementary Figure 4.3: Axial trends in contraction kinematics are conserved across populations that appear differently constrained inside channels.
A: Scatter plot of individual larvae's mean segment lengths against mean cycle periods. n=25 larvae; points colored as in Supplementary Figure 4.1. **B:** Scatter plots of same data as in (**A**), separated into jGC7f (left) and Gerry (right) subpopulations.
C: Segmental distributions for the indicated feature of segmental contraction, given separately for jGC7f (left column) and Gerry (right column) subpopulations.

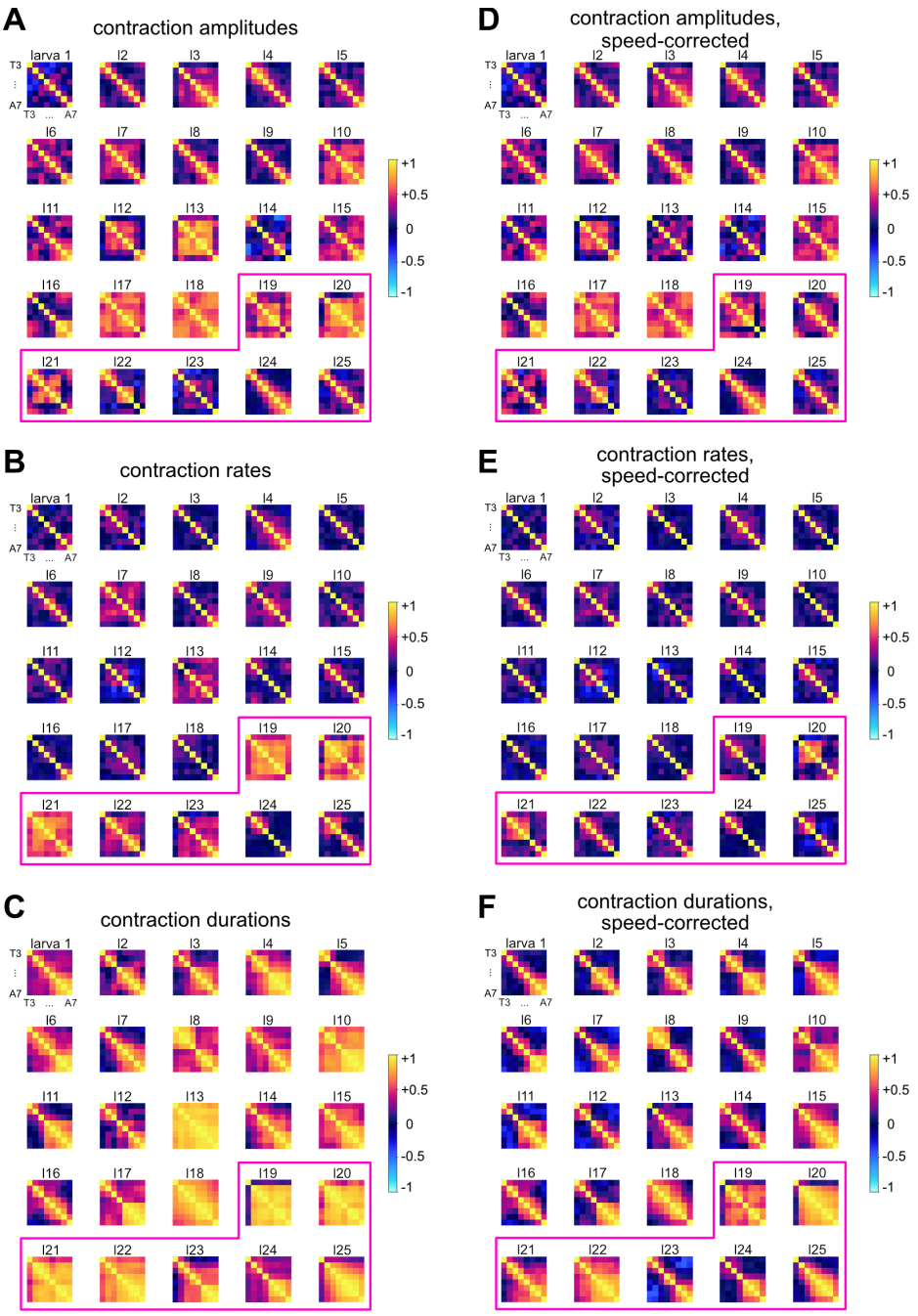

Supplementary Figure 4.4: Individual larval intersegmental coupling of contraction amplitudes, rates, and durations.
A-C: For each larva in the full dataset (n=25), mean pairwise intersegmental correlations (Pearson's R) for the indicated feature of segmental contraction.
D-F: For each larva in the full dataset, mean pairwise intersegmental correlations for the indicated feature of segmental contraction, following speed correction (residualized values after regressing away cycle speed information; Methods, section 4.4.7).
All panels: All correlation values along the diagonal = +1. Axes (segment ordering) and color scaling are identical for all panels. Pink box surrounds Gerry larvae.

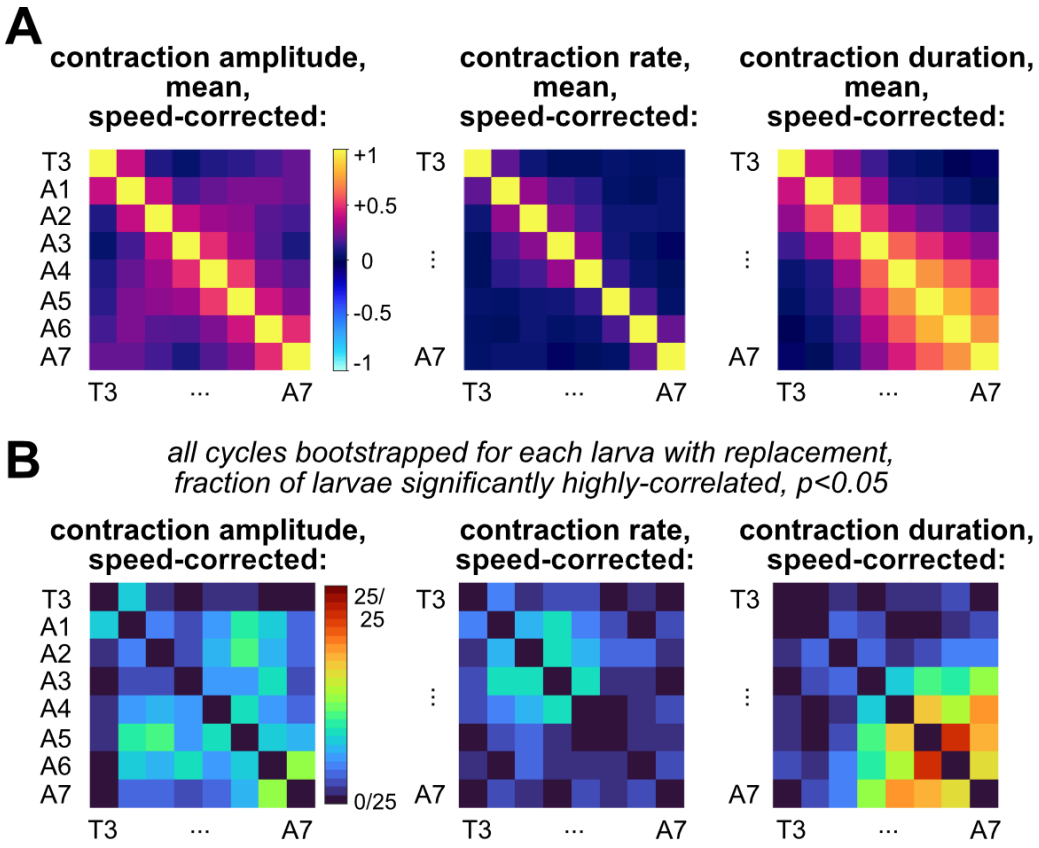

Supplementary Figure 4.5: Averaged intersegmental kinematic coupling of contraction amplitudes, rates, and durations, after accounting for cycle speed.
A: Mean pairwise intersegmental correlations for the indicated feature of segmental contraction, following speed correction (Methods, section 4.4.7). Correlation values averaged across n=25 larvae.
B: For each pair of segments, fraction of larvae with significantly ($p<0.05$) higher-than-expected pairwise correlations, following speed correction. Expected correlations were determined for each intersegmental distance by bootstrapping distributions of pairwise correlations (n=10,000 iterations). Significance was determined using a one-tailed test, comparing each pair of segments to the expected distribution for its intersegmental distance.

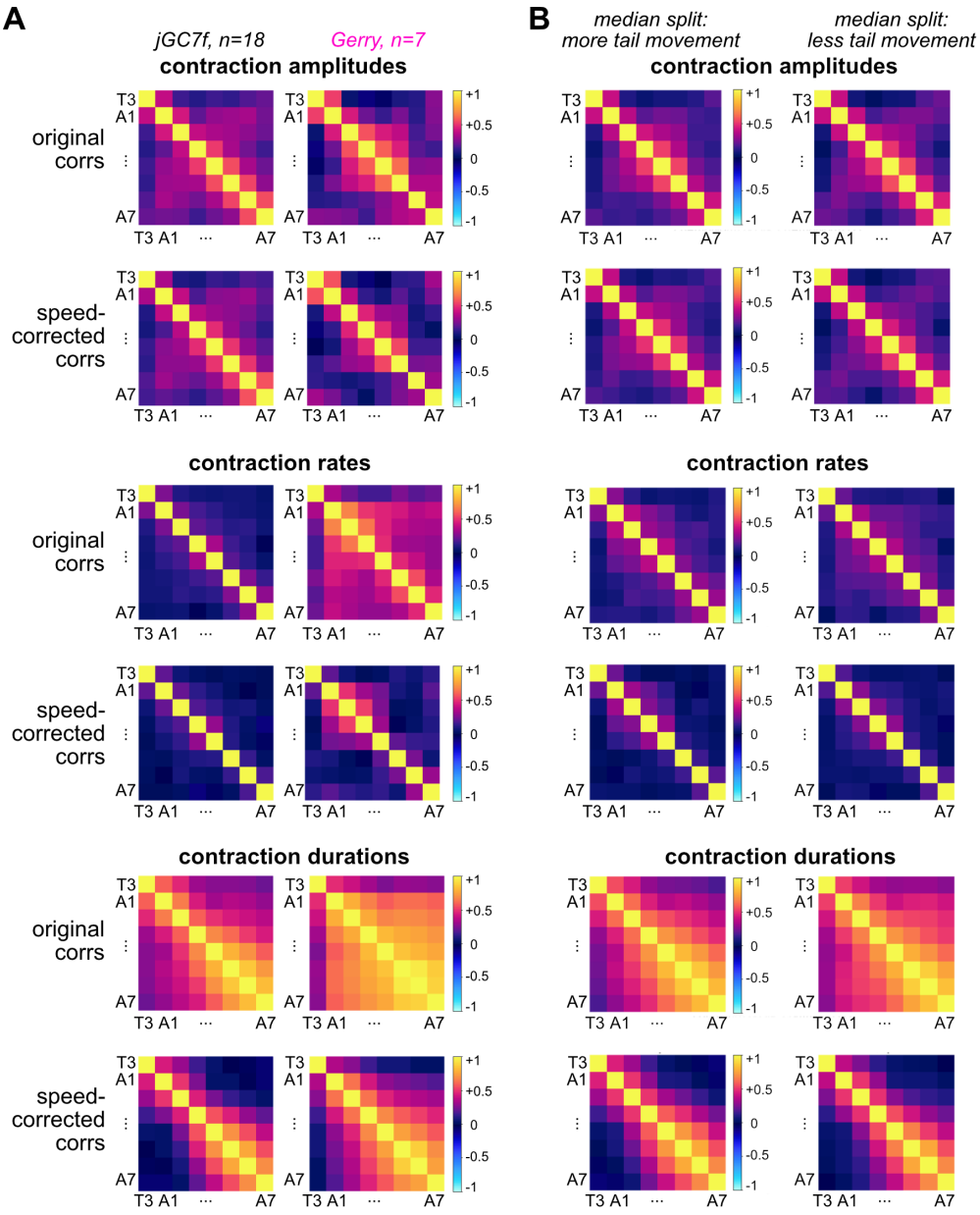

Supplementary Figure 4.6: Axial trends in kinematic coupling are generally conserved when splitting cycles by tail movement distance or by larval size/genotype.
A: Comparison of mean pairwise intersegmental correlations for the indicated feature of segmental contraction, averaged over all jGC7f larvae (left column) or all Gerry larvae (right column). Each comparison performed both for correlations among the original kinematic values and for correlations among the speed-corrected kinematic values (Methods, section 4.4.7). **B:** Comparison of mean pairwise intersegmental correlations for the indicated feature of segmental contraction, averaged over the 50% of cycles during which larvae moved their tails forward by greater (left column) or lesser distances (right column). Each comparison performed both for correlations among the original kinematic values and for correlations among the speed-corrected kinematic values.

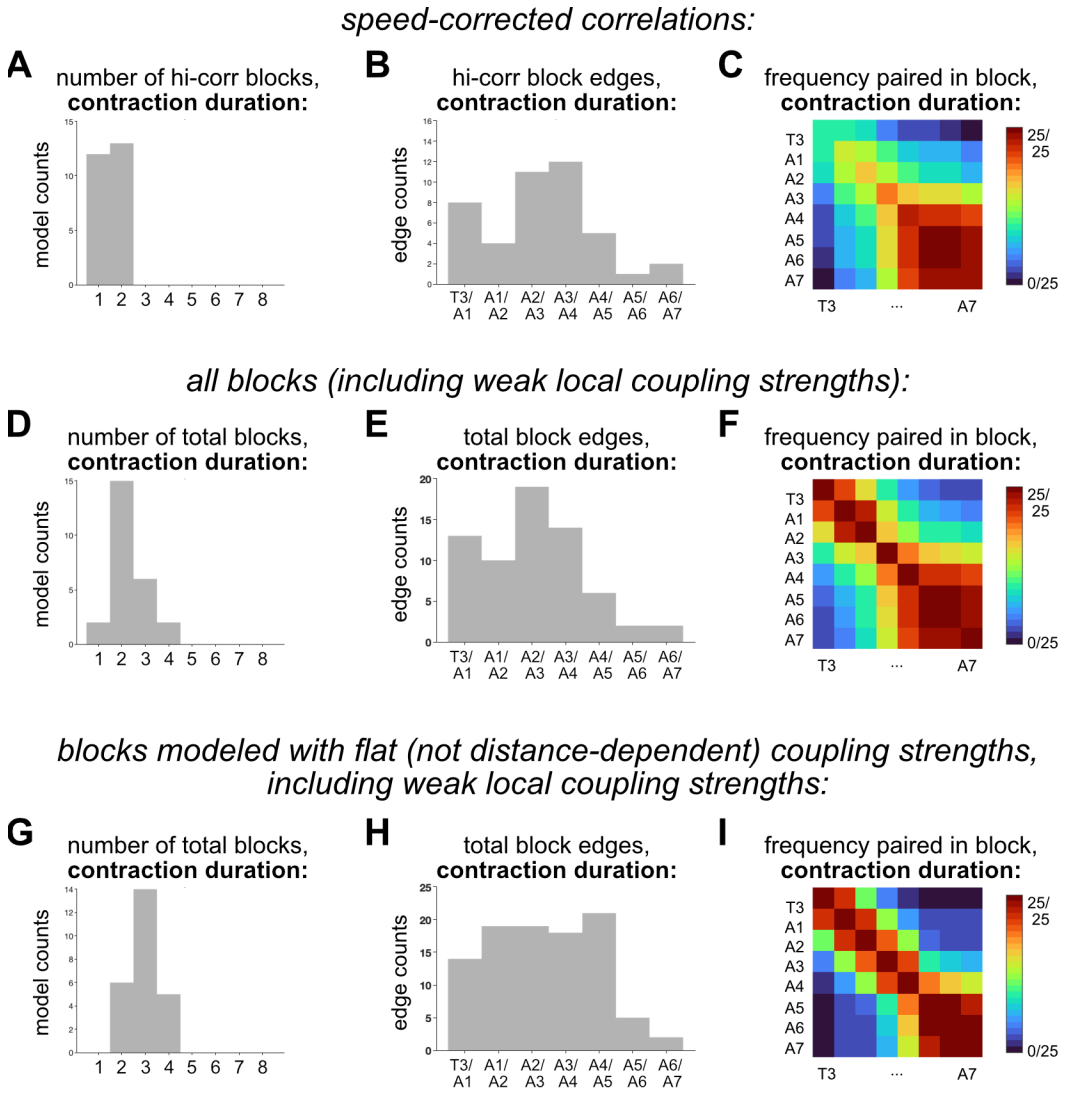

Supplementary Figure 4.7: A posterior block of segments with strongly-coupled contraction durations frequently emerges under a variety of block modeling assumptions.
A-C: Analyses comparable to Figure 4E-G, performed for speed-corrected contraction duration data. Before calculating correlations, values for each segment were regressed against cycle speed and the result subtracted; blocks were found for correlations calculated using residual values. **D-F**: Analyses comparable to Figure 4E-G, considering all blocks found by best-performing contraction duration coupling models (not thresholding by high local coupling strengths). **G-I:** Analyses comparable to Figure 4E-G, using a different internal coupling assumption when modeling blocks: Rather than assume coupling strength decreasing as a function of intersegmental distance within a block, models assumed a flat (equal) coupling strength for all pairs of segments within a block. This modeling assumption tended to find more and smaller blocks. **A:** Number of high-correlation (coupling strength > 0.5) blocks found by the best-performing model for each of 25 larvae. **B:** Location of the edges of high-correlation blocks, indicating how often best-performing models included blocks that split up an adjacent pair of segments (where one was included, one excluded). **C:** Frequency with which best-performing models included each pair of segments inside the same high-correlation block. **D, G:** Total number of blocks found by the best-performing model for each of 25 larvae. **E, H:** Location of the edges of all blocks in the best-performing models. **F, I:** Frequency with which best-performing models included each pair of segments inside the same block.

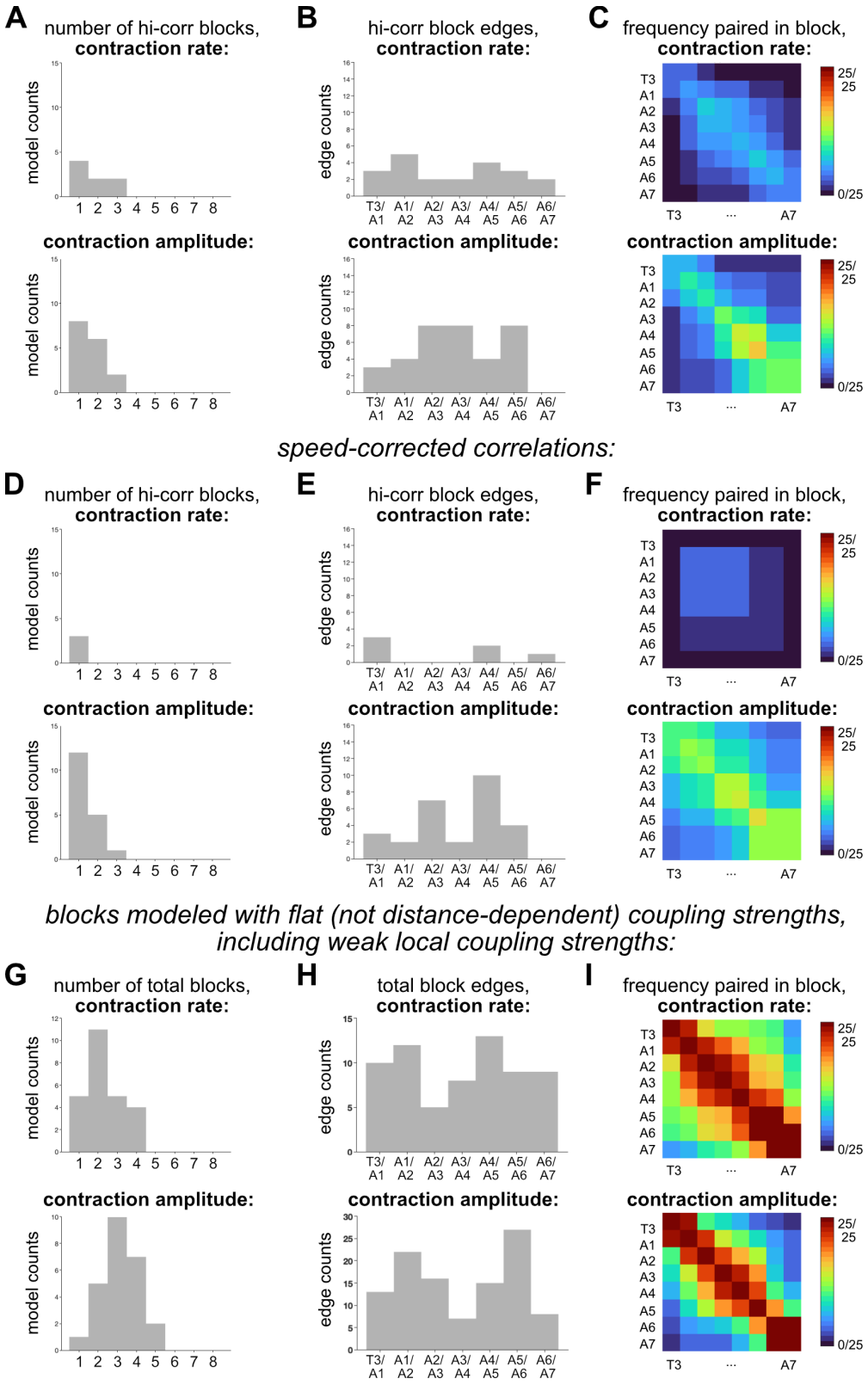

Supplementary Figure 4.8: Block structure of contraction rate and amplitude coupling.

Supplementary Figure 4.8, continued. Block structure of contraction rate and amplitude coupling. **A-C:** analyses comparable to Figure 4E-G, performed for contraction rate coupling models (top row) and contraction amplitude coupling models (bottom row). **D-F:** analyses comparable to Supplementary Figure 4A-C, performed on speed-corrected data. Before calculating correlations, values for each segment were regressed against cycle speed and the result subtracted; blocks were found for correlations calculated using residual values. **G-I:** analyses comparable to Supplementary Figure 4G-I. Rather than assume coupling strength decreasing as a function of intersegmental distance within a block, models assumed a flat (equal) coupling strength for all pairs of segments within a block. **A, D:** Number of high-correlation (coupling strength > 0.5) blocks found by the best-performing model for each of 25 larvae.
B, E: Location of the edges of high-correlation blocks, indicating how often best-performing models included blocks that split up an adjacent pair of segments (where one was included, one excluded).
C, F: Frequency with which best-performing models included each pair of segments inside the same high-correlation block. **G:** Total number of blocks found by the best-performing model for each of 25 larvae. **H:** Location of the edges of all blocks in the best-performing models. **I:** Frequency with which best-performing models included each pair of segments inside the same block.

REFERENCES

Agrawal, S., Dickinson, E.S., Sustar, A., Gurung, P., Shepherd, D., Truman, J.W., Tuthill, J.C., 2020. Central processing of leg proprioception in Drosophila. eLife. https://doi.org/10.7554/elife.60299

Ahamed, T., Costa, A. C., Stephens, G. J., 2020. Capturing the continuous complexity of behaviour in Caenorhabditis elegans. Nat. Phys. 17, 275–283. doi: 10.1038/s41567-020-01036-8

Ainsley, J.A., Pettus, J.M., Bosenko, D., Gerstein, C.E., Zinkevich, N., Anderson, M.G., Adams, C.M., Welsh, M.J., Johnson, W.A., 2003. Enhanced Locomotion Caused by Loss of the Drosophila DEG/ENaC Protein Pickpocket1. Current Biology. https://doi.org/10.1016/s0960-9822(03)00596-7

Akay, T., Tourtellotte, W.G., Arber, S., Jessell, T.M., 2014. Degradation of mouse locomotor pattern in the absence of proprioceptive sensory feedback. Proc. Natl. Acad. Sci. U.S.A. https://doi.org/10.1073/pnas.1419045111

Akaike, H., 1974. "A new look at the statistical model identification", IEEE Transactions on Automatic Control, 19 (6): 716–723, doi:10.1109/TAC.1974.1100705

Akanyeti, O., Thornycroft, P. J. M., Lauder, G. V., Yanagitsuru, Y. R., Peterson, A. N., and Liao, J. C., 2016. Fish optimize sensing and respiration during undulatory swimming. Nat Commun 7. doi: 10.1038/ncomms11044

Alonso, I., Sanchez Merlinsky, A., Szczupak, L. 2020. Phase-Specific Motor Efference during a Rhythmic Motor Pattern. J. Neurosci. 40, 1888–1896. doi: 10.1523/jneurosci.1201-19.2020

Anastasiadis, A., Paez, L., Melo, K., Tytell, E. D., Ijspeert, A. J., and Mulleners, K., 2023. Identification of the trade-off between speed and efficiency in undulatory swimming using a bio-inspired robot. Sci Rep 13. doi: 10.1038/s41598-023-41074-9

Ashburner M, Golic KG, Hawley RS. 2005. Drosophila: a laboratory handbook. 2nd ed. Cold Spring Harbor Laboratory Press, Cold Spring Harbor, NY.

Ausborn, J., Shevtsova, N. A., Danner, S. M. 2021. Computational Modeling of Spinal Locomotor Circuitry in the Age of Molecular Genetics. IJMS 22, 6835. doi: 10.3390/ijms22136835

Ayali, A., Fuchs, E., Ben-Jacob, E., Cohen, A. 2007. The function of intersegmental connections in determining temporal characteristics of the spinal cord rhythmic output. Neuroscience 147, 236–246. doi: 10.1016/j.neuroscience.2007.04.014

Azim, E., Seki, K., 2019. Gain control in the sensorimotor system. Current Opinion in Physiology. https://doi.org/10.1016/j.cophys.2019.03.005

Baader, A. P., 1997. Interneuronal and Motor Patterns During Crawling Behavior of Semi-Intact Leeches. Journal of Experimental Biology 200, 1369–1381. doi: 10.1242/jeb.200.9.1369

Baines, R. A., Bate, M., 1998. Electrophysiological Development of Central Neurons in the Drosophila Embryo. J. Neurosci. 18, 4673–4683. doi: 10.1523/jneurosci.18-12-04673.1998

Bate, M., 1990. The embryonic development of larval muscles in Drosophila. Development 110, 791–804. doi: 10.1242/dev.110.3.791

Bässler, U., 1993. The femur-tibia control system of stick insects — a model system for the study of the neural basis of joint control. Brain Research Reviews 18, 207–226. doi: 10.1016/0165-0173(93)90002-h

Berni, J., 2015. Genetic dissection of a regionally differentiated network for exploratory behavior in Drosophila larvae. Curr Biol 25: 1319–1326. doi:10.1016/j.cub.2015.03.023

Berni, J., Pulver, S. R., Griffith, L. C., and Bate, M., 2012. Autonomous Circuitry for Substrate Exploration in Freely Moving Drosophila Larvae. Current Biology 22, 1861–1870. doi: 10.1016/j.cub.2012.07.048

Berrigan, D., and Pepin, D. J., 1995. How maggots move: Allometry and kinematics of crawling in larval Diptera. Journal of Insect Physiology 41, 329–337. doi: 10.1016/0022-1910(94)00113-u

Bidaye, S.S., Bockemühl, T., Büschges, A., 2017. Six-legged walking in insects: how CPGs, peripheral feedback, and descending signals generate coordinated and adaptive motor rhythms. Journal of Neurophysiology. https://doi.org/10.1152/jn.00658.2017

Biró, Z., Hill, R. H., Grillner, S., 2006. 5-HT Modulation of Identified Segmental Premotor Interneurons in the Lamprey Spinal Cord. Journal of Neurophysiology 96, 931–935. doi: 10.1152/jn.00309.2006

Bodmer, R., Jan, Y.N., 1987. Morphological differentiation of the embryonic peripheral neurons in Drosophila. Roux's Arch. Dev. Biol. https://doi.org/10.1007/bf00402027

Boivin, J.-C., Zhu, J., Ohyama, T., 2023. Nociception in fruit fly larvae. Front. Pain Res. 4. doi: 10.3389/fpain.2023.1076017

Bonnard, E., Liu, J., Zjacic, N., Alvarez, L., and Scholz, M., 2022. Automatically tracking feeding behavior in populations of foraging C. elegans. eLife 11. doi: 10.7554/elife.77252

Booth, J. H., Meek, A. T., Kronenberg, N. M., Pulver, S. R., and Gather, M. C., 2024. Optical mapping of ground reaction force dynamics in freely behaving Drosophila melanogaster larvae. eLife 12. doi: 10.7554/elife.87746.3

Bosco, G., Poppele, R.E., 2001. Proprioception From a Spinocerebellar Perspective. Physiological Reviews. https://doi.org/10.1152/physrev.2001.81.2.539

Brand, A. H., Perrimon, N., 1993. Targeted gene expression as a means of altering cell fates and generating dominant phenotypes. Development 118, 401–415. doi: 10.1242/dev.118.2.401

Briggman, K. L., Abarbanel, H. D. I., and Kristan, W. B., Jr. (2005). Optical Imaging of Neuronal Populations During Decision-Making. Science 307, 896–901. doi: 10.1126/science.1103736

Brodfuehrer, P. D., Friesen, W. O., 1986. Control of leech swimming activity by the cephalic ganglia. J. Neurobiol. 17, 697–705. doi: 10.1002/neu.480170612

Brodin, L., Grillner, S., Rovainen, C. M. 1985. N-methyl-d-aspartate (NMDA), kainate and quisqualate receptors and the generation of fictive locomotion in the lamprey spinal cord. Brain Research 325, 302–306. doi: 10.1016/0006-8993(85)90328-2

Brown, A.G., 1981. Organization in the Spinal Cord. Springer London. https://doi.org/10.1007/978-1-4471-1305-8

Brown, A.G., Fyffe, R.E., 1978. The morphology of group Ia afferent fibre collaterals in the spinal cord of the cat. The Journal of Physiology. https://doi.org/10.1113/jphysiol.1978.sp012137

Buchanan, J. T., 1982. Identification of interneurons with contralateral, caudal axons in the lamprey spinal cord: synaptic interactions and morphology. Journal of Neurophysiology 47, 961–975. doi: 10.1152/jn.1982.47.5.961

Buchanan, J. T., 1999. Commissural Interneurons in Rhythm Generation and Intersegmental Coupling in the Lamprey Spinal Cord. Journal of Neurophysiology 81, 2037–2045. doi: 10.1152/jn.1999.81.5.2037

Buchanan, J. T., Cohen, A. H., 1982. Activities of identified interneurons, motoneurons, and muscle fibers during fictive swimming in the lamprey and effects of reticulospinal and dorsal cell stimulation. Journal of Neurophysiology 47, 948–960. doi: 10.1152/jn.1982.47.5.948

Burrows, M., 1975. Monosynaptic connexions between wing stretch receptors and flight motoneurones of the locust. Journal of Experimental Biology. https://doi.org/10.1242/jeb.62.1.189

Burrows, M., Matheson, T., 1994. A presynaptic gain control mechanism among sensory neurons of a locust leg proprioceptor. J. Neurosci. https://doi.org/10.1523/jneurosci.14-01-00272.1994

Burrows, M., 1996. The neurobiology of an Insect Brain. Oxford: Oxford University Press. https://doi.org/10.1093/acprof:oso/9780198523444.001.0001

Burrows, M., Pflüger, H.J., 1988. Positive feedback loops from proprioceptors involved in leg movements of the locust. J. Comp. Physiol. https://doi.org/10.1007/BF00604897

Cacciatore, T. W., Rozenshteyn, R., and Kristan, W. B., Jr, 2000. Kinematics and Modeling of Leech Crawling: Evidence for an Oscillatory Behavior Produced by Propagating Waves of Excitation. J. Neurosci. 20, 1643–1655. doi: 10.1523/jneurosci.20-04-01643.2000

Caldwell, J.C., Miller, M.M., Wing, S., Soll, D.R., Eberl, D.F., 2003. Dynamic analysis of larval locomotion in Drosophila chordotonal organ mutants. Proc. Natl. Acad. Sci. U.S.A. https://doi.org/10.1073/pnas.2535546100

Calviño, M. A., Szczupak, L., 2008. Spatial-specific action of serotonin within the leech midbody ganglion. J Comp Physiol A 194, 523–531. doi: 10.1007/s00359-008-0326-2

Campos-Ortega, J.A., Hartenstein, V., 1997. The Embryonic Development of Drosophila melanogaster. Springer Berlin Heidelberg. https://doi.org/10.1007/978-3-662-22489-2

Cang, J., Friesen, W. O., 2000. Sensory Modification of Leech Swimming: Rhythmic Activity of Ventral Stretch Receptors Can Change Intersegmental Phase Relationships. J. Neurosci. 20, 7822–7829. doi: 10.1523/jneurosci.20-20-07822.2000

Cang, J., Yu, X., Friesen, O. W., 2001. Sensory modification of leech swimming: interactions between ventral stretch receptors and swim-related neurons. J Comp Physiol A 187, 569–579. doi: 10.1007/s003590100229

Cangiano, L., Grillner, S., 2003. Fast and Slow Locomotor Burst Generation in the Hemispinal Cord of the Lamprey. Journal of Neurophysiology 89, 2931–2942. doi: 10.1152/jn.01100.2002

Cangiano, L., Grillner, S., 2018. Commentary: Elimination of Left-Right Reciprocal Coupling in the Adult Lamprey Spinal Cord Abolishes the Generation of Locomotor Activity. Front. Neural Circuits 12. doi: 10.3389/fncir.2018.00034

Cattaert, D., Birman, S., 2001. Blockade of the central generator of locomotor rhythm by noncompetitive NMDA receptor antagonists in Drosophila larvae. J. Neurobiol. 48, 58–73. doi: 10.1002/neu.1042

Cermak N, Yu SK, Clark R, Huang YC, Baskoylu SN, Flavell SW. 2020. Whole-organism behavioral profiling reveals a role for dopamine in state-dependent motor program coupling in C. elegans. eLife 9:e57093. doi:10.7554/eLife.57093

Chen, C., Agrawal, S., Mark, B., Mamiya, A., Sustar, A., Phelps, J.S., Lee, W.-C.A., Dickson, B.J., Card, G.M., Tuthill, J.C., 2021. Functional architecture of neural circuits for leg proprioception in Drosophila. Current Biology. https://doi.org/10.1016/j.cub.2021.09.035

Chen, J., Friesen, W. O., Iwasaki, T., 2011. Mechanisms underlying rhythmic locomotion: body–fluid interaction in undulatory swimming. Journal of Experimental Biology 214, 561–574. doi: 10.1242/jeb.048751

Chen, J., Friesen, W. O., Iwasaki, T., 2012. Mechanisms underlying rhythmic locomotion: interactions between activation, tension and body curvature waves. Journal of Experimental Biology 215, 211–219. doi: 10.1242/jeb.058669

Cheng, L. E., Song, W., Looger, L. L., Jan, L. Y., Jan, Y. N., 2010. The Role of the TRP Channel NompC in Drosophila Larval and Adult Locomotion. Neuron 67, 373–380. doi: 10.1016/j.neuron.2010.07.004

Chiel, H. J., Ting, L. H., Ekeberg, Ö., Hartmann, M. J. Z., 2009. The Brain in Its Body: Motor Control and Sensing in a Biomechanical Context. J. Neurosci. 29, 12807–12814. doi: 10.1523/jneurosci.3338-09.2009

Clarac, F., Cattaert, D., 1996. Invertebrate presynaptic inhibition and motor control. Exp Brain Res. https://doi.org/10.1007/bf00227635

Clark MQ, McCumsey SJ, Lopez-Darwin SL, Heckscher ES, Doe CQ. 2016. Functional genetic screen to identify interneurons governing behaviorally distinct aspects of Drosophila larval motor programs. Genes Genomes Genetics 6: 2023–2031. doi:10.1534/g3.116.028472

Clark, M.Q., Zarin, A.A., Carreira-Rosario, A., Doe, C.Q., 2018. Neural circuits driving larval locomotion in Drosophila. Neural Dev. https://doi.org/10.1186/s13064-018-0103-z

Cohen, A. H., 1987. Effects of oscillator frequency on phase-locking in the lamprey central pattern generator. Journal of Neuroscience Methods 21, 113–125. doi: 10.1016/0165-0270(87)90109-9

Cohen, A. H., Wallén, P., 1980. The neuronal correlate of locomotion in fish. Exp Brain Res 41. doi: 10.1007/bf00236674

Cohen, A. H., Holmes, P. J., Rand, R. H., 1982. The nature of the coupling between segmental oscillators of the lamprey spinal generator for locomotion: A mathematical model. J. Math. Biology 13, 345–369. doi: 10.1007/bf00276069

Conradi, S., Cullheim, S., Gollvik, L., Kellerth, J.-O., 1983. Electron microscopic observations on the synaptic contacts of group Ia muscle spindle afferents in the cat lumbosacral spinal cord. Brain Research. https://doi.org/10.1016/0006-8993(83)91330-6

Cooney, P.C., Li, W., Huang, Y., Hormigo, R., Tabachnik, T., Hillman, E.M.C., Grueber, W.B., Zarin, A.A., 2023. Neuromuscular Basis of Drosophila Larval Escape Behavior. bioRxiv [preprint]. Available at https://doi.org/10.1101/2023.02.01.526733 (Accessed May 15, 2023).

Cover, K. K., Mathur, B. N., 2020. Axo-axonic synapses: Diversity in neural circuit function. J Comp Neurol. https://doi.org/10.1002/cne.25087

Creamer M. S., Chen K. S., Leifer A. M., Pillow J. W., 2022. Correcting motion induced fluorescence artifacts in two-channel neural imaging. PLoS Comput Biol 18: e1010421. doi:10.1371/journal.pcbi.1010421

Crisp, K. M., Mesce, K. A., 2003. To swim or not to swim: regional effects of serotonin, octopamine and amine mixtures in the medicinal leech. Journal of Comparative Physiology A: Sensory, Neural, and Behavioral Physiology 189, 461–470. doi: 10.1007/s00359-003-0424-0

Crisp, K. M., Mesce, K. A., 2004. A cephalic projection neuron involved in locomotion is dye coupled to the dopaminergic neural network in the medicinal leech. Journal of Experimental Biology 207, 4535–4542. doi: 10.1242/jeb.01315

Dallmann, C. J., Karashchuk, P., Brunton, B. W., Tuthill, J. C., 2021. A leg to stand on: computational models of proprioception. Current Opinion in Physiology 22, 100426. doi: 10.1016/j.cophys.2021.03.001

Dallmann, C. J., Dickerson, B. H., Simpson, J. H., Wyart, C., Jayaram, K., 2023. Mechanosensory Control of Locomotion in Animals and Robots: Moving Forward. Integrative And Comparative Biology 63, 450–463. doi: 10.1093/icb/icad057

Dambly-Chaudière, C., Ghysen, A., 1986. The sense organs in the Drosophila larva and their relation to the embryonic pattern of sensory neurons. Roux's Arch Dev Biol 195, 222–228. doi: 10.1007/bf02438954

Dana, H., Sun, Y., Mohar, B., Hulse, B. K., Kerlin, A. M., Hasseman, J. P., et al., 2019. High-performance calcium sensors for imaging activity in neuronal populations and microcompartments. Nat Methods 16, 649–657. doi: 10.1038/s41592-019-0435-6

Davis, G. W., Goodman, C. S., 1998. Synapse-specific control of synaptic efficacy at the terminals of a single neuron. Nature 392, 82–86. doi: 10.1038/32176

DeAngelis, B. D., Zavatone-Veth, J. A., Clark, D. A., 2019. The manifold structure of limb coordination in walking Drosophila. eLife 8. doi: 10.7554/elife.46409

Di Prisco, G., Wallén, P., Grillner, S., 1990. Synaptic effects of intraspinal stretch receptor neurons mediating movement-related feedback during locomotion. Brain Research 530, 161–166. doi: 10.1016/0006-8993(90)90675-2

Di Santo, V., Goerig, E., Wainwright, D. K., Akanyeti, O., Liao, J. C., Castro-Santos, T., et al., 2021. Convergence of undulatory swimming kinematics across a diversity of fishes. Proc. Natl. Acad. Sci. U.S.A. 118. doi: 10.1073/pnas.2113206118

Dickerson, B.H., Fox, J.L., Sponberg, S., 2021. Functional diversity from generic encoding in insect campaniform sensilla. Current Opinion in Physiology. https://doi.org/10.1016/j.cophys.2020.11.004

Dixit, R., VijayRaghavan, K., Bate, M., 2007. Hox genes and the regulation of movement in Drosophila. Developmental Neurobiology 68, 309–316. doi: 10.1002/dneu.20589

Dorgan, K. M., 2010. Environmental Constraints on the Mechanics of Crawling and Burrowing Using Hydrostatic Skeletons. Exp Mech 50, 1373–1381. doi: 10.1007/s11340-010-9399-2

Eccles, J.C., Eccles, R.M., Lundberg, A., 1957. The convergence of monosynaptic excitatory afferents on to many different species of alpha motoneurones. The Journal of Physiology. https://doi.org/10.1113/jphysiol.1957.sp005794

Eccles, J.C., Kostyuk, P.G., Schmidt, R.F., 1962. Presynaptic inhibition of the central actions of flexor reflex afferents. The Journal of Physiology. https://doi.org/10.1113/jphysiol.1962.sp006885

Edgley, S.A., Jankowska, E., 1987. Field potentials generated by group II muscle afferents in the middle lumbar segments of the cat spinal cord. The Journal of Physiology. https://doi.org/10.1113/jphysiol.1987.sp016498

Eggers, E.D., McCall, M.A., Lukasiewicz, P.D., 2007. Presynaptic inhibition differentially shapes transmission in distinct circuits in the mouse retina. The Journal of Physiology. https://doi.org/10.1113/jphysiol.2007.131763

Ekeberg, Ö., Grillner, S., 1999. Simulations of neuromuscular control in lamprey swimming. Phil. Trans. R. Soc. Lond. B 354, 895–902. doi: 10.1098/rstb.1999.0441

El Manira, A., 2014. Dynamics and plasticity of spinal locomotor circuits. Current Opinion in Neurobiology 29, 133–141. doi: 10.1016/j.conb.2014.06.016

Ellerby, D. J., Spierts, I. L. Y., Altringham, J. D., 2001. Slow muscle power output of yellow- and silver-phase European eels (Anguilla anguilla L.): changes in muscle performance prior to migration. Journal of Experimental Biology 204, 1369–1379. doi: 10.1242/jeb.204.7.1369

Esch, T., Mesce, K. A., Kristan, W. B., 2002. Evidence for Sequential Decision Making in the Medicinal Leech. J. Neurosci. 22, 11045–11054. doi: 10.1523/jneurosci.22-24-11045.2002

Eschbach C, Zlatic M. 2020. Useful road maps: studying Drosophila larva's central nervous system with the help of connectomics. Curr Opin Neurobiol 65: 129–137. doi:10.1016/j.conb.2020.09.008

Field, L.H., Matheson, T., 1998. Chordotonal Organs of Insects. Advances in Insect Physiology. https://doi.org/10.1016/s0065-2806(08)60013-2

Fink, A.J.P., Croce, K.R., Huang, Z.J., Abbott, L.F., Jessell, T.M., Azim, E., 2014. Presynaptic inhibition of spinal sensory feedback ensures smooth movement. Nature. https://doi.org/10.1038/nature13276

Flaive, A., Fougère, M., van der Zouwen, C. I., Ryczko, D. 2020. Serotonergic Modulation of Locomotor Activity From Basal Vertebrates to Mammals. Front. Neural Circuits 14. doi: 10.3389/fncir.2020.590299

Fouad, A. D., Teng, S., Mark, J. R., Liu, A., Alvarez-Illera, P., Ji, H., et al., 2018. Distributed rhythm generators underlie Caenorhabditis elegans forward locomotion. eLife 7. doi: 10.7554/elife.29913

Fox, L.E., Soll, D.R., Wu, C.-F., 2006. Coordination and Modulation of Locomotion Pattern Generators in Drosophila Larvae: Effects of Altered Biogenic Amine Levels by the Tyramine β Hydroxlyase Mutation. J. Neurosci. 26, 1486–1498. doi: 10.1523/jneurosci.4749-05.2006

Francis, J., Gibeily, C. R., Smith, W. V., Petropoulos, I. S., Anderson, M., Heitler, W. J., Prinz, A. A., Pulver, S. R., 2024. Generation of motor program diversity and variability through inhibitory circuit motifs in the Drosophila larval locomotor system. bioRxiv [preprint]. Accessible at: https://doi.org/10.1101/2024.09.02.610491. Accessed Jan 30, 2025.

Friesen, W. O., Hocker, C. G., 2001. Functional Analyses of the Leech Swim Oscillator. J Neurophysiol 86, 824–835. doi: 10.1152/jn.2001.86.2.824

Friesen, W. O., Kristan, W. B., 2008. Leech locomotion: swimming, crawling, and decisions. Curr Opin Neurobiol 17, 704–711. doi: 10.1016/j.conb.2008.01.006

Fushiki, A., Zwart, M.F., Kohsaka, H., Fetter, R.D., Cardona, A., Nose, A., 2014. A circuit mechanism for the propagation of waves of muscle contraction in Drosophila. eLife. https://doi.org/10.7554/eLife.13253

Fushiki A, Zwart MF, Kohsaka H, Fetter RD, Cardona A, Nose A., 2016. A circuit mechanism for the propagation of waves of muscle contraction in Drosophila. eLife 5: e13253. doi:10.7554/eLife.13253

Fyffe, R.E.W., Light, A.R., 1984. The ultrastructure of group Ia afferent fiber synapses in the lumbosacral spinal cord of the cat. Brain Res. https://doi.org/10.1016/0006-8993(84)90831-x

Gans, C., 1973. Locomotion and Burrowing in Limbless Vertebrates. Nature 242, 414–415. doi: 10.1038/242414a0

Gaymer, R., 1971. New Method of Locomotion in Limbless Terrestrial Vertebrates. Nature 234, 150–151. doi: 10.1038/234150a0

Gebehart, C., Schmidt, J., Büschges, A., 2021. Distributed processing of load and movement feedback in the premotor network controlling an insect leg joint. J Neurophysiol. https://doi.org/10.1152/jn.00090.2021

Gebehart, C., Hooper, S.L., Büschges, A., 2022. Load Non-Linearly Modulates Movement Reflex Gain in an Insect Leg via a Distributed Network of Identified Nonspiking Interneurons. bioRxiv [preprint]. Accessible at: https://doi.org/10.1101/2022.02.24.481822. Accessed May 15, 2023.

Georgopoulos, A. P., Grillner, S., 1989. Visuomotor Coordination in Reaching and Locomotion. Science 245, 1209–1210. doi: 10.1126/science.2675307

Gerhard, S., Andrade, I., Fetter, R.D., Cardona, A., Schneider-Mizell, C.M., 2017. Conserved neural circuit structure across Drosophila larval development revealed by comparative connectomics. eLife. https://doi.org/10.7554/elife.29089

Ghysen, A., Dambly-Chaudière, C., Aceves, E., Jan, L.-Y., Jan, Y.-N., 1986. Sensory neurons and peripheral pathways in Drosophila embryos. Roux's Arch Dev Biol. https://doi.org/10.1007/bf00376060

Gjorgjieva, J., Berni, J., Evers, J.F., Eglen, S.J., 2013. Neural circuits for peristaltic wave propagation in crawling Drosophila larvae: analysis and modeling. Front Comput Neurosci. 7. doi: 10.3389/fncom.2013.00024

Giachello, C.N.G., Zarin, A.A., Kohsaka, H., Fan, Y.N., Nose, A., Landgraf, M., Baines, R.A., 2020. Electrophysiological validation of premotor interneurons monosynaptically connected to the aCC motoneuron in the Drosophila larval CNS. bioRxiv [preprint]. Available at https://doi.org/10.1101/2020.06.17.156430 (Accessed Feb 2, 2025).

Giessel, A.J., Datta, S.R., 2014. Olfactory maps, circuits and computations. Current Opinion in Neurobiology. https://doi.org/10.1016/j.conb.2013.09.010

Gomez-Marin, A., Louis, M., 2012. Active sensation during orientation behavior in the Drosophila larva: more sense than luck. Current Opinion in Neurobiology 22, 208–215. doi: 10.1016/j.conb.2011.11.008

Gomez-Marin, A., Louis, M., 2014. Multilevel control of run orientation in Drosophila larval chemotaxis. Front. Behav. Neurosci. 8. doi: 10.3389/fnbeh.2014.00038

Gomez-Marin, A., Stephens, G.J., Louis, M., 2011. Active sampling and decision making in Drosophila chemotaxis. Nat Commun 2. doi: 10.1038/ncomms1455

Gowda, S. B. M., Salim, S., Mohammad, F., 2021. Anatomy and Neural Pathways Modulating Distinct Locomotor Behaviors in Drosophila Larva. Biology 10, 90. doi: 10.3390/biology10020090

Gray, J., Lissmann, H. W., Pumphrey, R. J., 1938. The Mechanism of Locomotion in the Leech (Hirudo Medicinalis Ray). Journal of Experimental Biology 15, 408–430. doi: 10.1242/jeb.15.3.408

Greaney, M.R., Wreden, C.C., Heckscher, E.S., 2023. Distinctive features of the central synaptic organization of Drosophila larval proprioceptors. Front Neural Circuits. doi: 10.3389/fncir.2023.1223334

Greaney, M.R., Heckscher, E.S., 2024. Studying Drosophila Larval Behavior in Agarose Channels. Cold Spring Harb Protoc. doi: 10.1101/pdb.prot108420

Green, C.H., Burnet, B., Connolly, K.J., 1983. Organization and patterns of inter- and intraspecific variation in the behaviour of Drosophila larvae. Animal Behaviour 31, 282–291. doi: 10.1016/s0003-3472(83)80198-5

Gregg, T. G., McCrate, A., Reveal, G., Hall, S., Rypstra, A. L., 1990. Insectivory and social digestion inDrosophila. Biochem Genet 28, 197–207. doi: 10.1007/bf00561337

Grillner, S., 1985. Neurobiological Bases of Rhythmic Motor Acts in Vertebrates. Science 228, 143–149. doi: 10.1126/science.3975635

Grillner, S., 2003. The motor infrastructure: from ion channels to neuronal networks. Nat Rev Neurosci 4, 573–586. doi: 10.1038/nrn1137

Grillner, S., El Manira, A., 2019. Current Principles of Motor Control, with Special Reference to Vertebrate Locomotion. Physiological Reviews 100, 271–320. doi: 10.1152/physrev.00015.2019

Grillner, S., Kashin, S., 1976. On the Generation and Performance of Swimming in Fish. Advances in Behavioral Biology, 181–201. doi: 10.1007/978-1-4757-0964-3_8

Grillner, S., Kozlov, A., 2021. The CPGs for Limbed Locomotion–Facts and Fiction. IJMS 22, 5882. doi: 10.3390/ijms22115882

Grillner, S., Wallén, P., 2002. Cellular bases of a vertebrate locomotor system–steering, intersegmental and segmental co-ordination and sensory control. Brain Research Reviews 40, 92–106. doi: 10.1016/s0165-0173(02)00193-5

Grillner, S., McClellan, A., Sigvardt, K., 1982. Mechanosensitive neurons in the spinal cord of the lamprey. Brain Research 235, 169–173. doi: 10.1016/0006-8993(82)90208-6

Grillner, S., Williams, T., Lagerbäck, P.-Å., 1984. The Edge Cell, a Possible Intraspinal Mechanoreceptor. Science 223, 500–503. doi: 10.1126/science.6691161

Grillner, S., Wallen, P., Brodin, L., Lansner, A., 1991. Neuronal Network Generating Locomotor Behavior in Lamprey: Circuitry, Transmitters, Membrane Properties, and Simulation. Annu. Rev. Neurosci. 14, 169–199. doi: 10.1146/annurev.ne.14.030191.001125

Grueber, W.B., Jan, L.Y., Jan, Y.N., 2002. Tiling of the Drosophila epidermis by multidendritic sensory neurons. Development. https://doi.org/10.1242/dev.129.12.2867

Grueber, W.B., Jan, L.Y., Jan, Y.N., 2003. Different Levels of the Homeodomain Protein Cut Regulate Distinct Dendrite Branching Patterns of Drosophila Multidendritic Neurons. Cell. https://doi.org/10.1016/s0092-8674(03)00160-0

Grueber, W.B., Ye, B., Yang, C.-H., Younger, S., Borden, K., Jan, L.Y., Jan, Y.-N., 2007. Projections of Drosophila multidendritic neurons in the central nervous system: links with peripheral dendrite morphology. Development. https://doi.org/10.1242/dev.02666

Grueber, W.B., Sagasti, A., 2010. Self-avoidance and Tiling: Mechanisms of Dendrite and Axon Spacing. Cold Spring Harbor Perspectives in Biology. https://doi.org/10.1101/cshperspect.a001750

Guan, L., Kiemel, T., Cohen, A. H., 2001. Impact of movement and movement-related feedback on the lamprey central pattern generator for locomotion. Journal of Experimental Biology 204, 2361–2370. doi: 10.1242/jeb.204.13.2361

Hagevik, A., McClellan, A.D., 1999. Coordination of locomotor activity in the lamprey: role of descending drive to oscillators along the spinal cord. Experimental Brain Research 128, 481–490. doi: 10.1007/s002210050871

Hao, J., Wang, X., Dan, Y., Poo, M., Zhang, X., 2009. An arithmetic rule for spatial summation of excitatory and inhibitory inputs in pyramidal neurons. Proc. Natl. Acad. Sci. U.S.A. https://doi.org/10.1073/pnas.0912022106

Harel, Y., Nasser, R. A., Stern, S., 2024. Mapping the developmental structure of stereotyped and individual-unique behavioral spaces in C. elegans. Cell Reports 43, 114683. doi: 10.1016/j.celrep.2024.114683

Harley, C. M., Rossi, M., Cienfuegos, J., Wagenaar, D., 2013. Discontinuous locomotion and prey sensing in the leech. Journal of Experimental Biology 216, 1890–1897. doi: 10.1242/jeb.075911

Harris-Warrick, R.M., 2011. Neuromodulation and flexibility in Central Pattern Generator networks. Current Opinion in Neurobiology 21, 685–692. doi: 10.1016/j.conb.2011.05.011

Harris-Warrick, R. M., Cohen, A. H. 1985. Serotonin Modulates the Central Pattern Generator for Locomotion in the Isolated Lamprey Spinal Cord. Journal of Experimental Biology 116, 27–46. doi: 10.1242/jeb.116.1.27

Hasegawa, E., Truman, J. W., Nose, A., 2016. Identification of excitatory premotor interneurons which regulate local muscle contraction during Drosophila larval locomotion. Sci Rep 6. doi: 10.1038/srep30806

He, L., Gulyanon, S., Mihovilovic Skanata, M., Karagyozov, D., Heckscher, E.S., Krieg, M., Tsechpenakis, G., Gershow, M., Tracey, W.D., Jr., 2019. Direction Selectivity in Drosophila Proprioceptors Requires the Mechanosensory Channel Tmc. Current Biology. https://doi.org/10.1016/j.cub.2019.02.025

He, L., Borjon, L., Tracey, W.D., Jr., 2022. The motor pattern of rolling escape locomotion in Drosophila larvae. bioRxiv [preprint]. Available at: https://doi.org/10.1101/2022.11.03.514605. Accessed Feb 2, 2025.

Heckscher, E.S., Lockery, S.R., Doe, C.Q., 2012. Characterization of Drosophila Larval Crawling at the Level of Organism, Segment, and Somatic Body Wall Musculature. J. Neurosci. https://doi.org/10.1523/jneurosci.0222-12.2012

Heckscher, E. S., Zarin, A. A., Faumont, S., Clark, M. Q., Manning, L., Fushiki, A., et al., 2015. Even-Skipped+ Interneurons Are Core Components of a Sensorimotor Circuit that Maintains Left-Right Symmetric Muscle Contraction Amplitude. Neuron 88, 314–329. doi: 10.1016/j.neuron.2015.09.009

Hildebrandt, K.J., 2014. Neural maps in insect versus vertebrate auditory systems. Current Opinion in Neurobiology. https://doi.org/10.1016/j.conb.2013.08.020

Hill, A.A.V., Masino, M.A., Calabrese, R.L., 2003. Intersegmental Coordination of Rhythmic Motor Patterns. Journal of Neurophysiology 90, 531–538. doi: 10.1152/jn.00338.2003

Hiramoto, A., Jonaitis, J., Niki, S., Kohsaka, H., Fetter, R. D., Cardona, A., et al., 2021. Regulation of coordinated muscular relaxation in Drosophila larvae by a pattern-regulating intersegmental circuit. Nat Commun 12. doi: 10.1038/s41467-021-23273-y

Hoang, B., Chiba, A., 2001. Single-cell analysis of Drosophila larval neuromuscular synapses. Dev. Biol. https://doi.org/10.1006/dbio.2000.9983

Holmes, S. J., 1905. The selection of random movements as a factor in phototaxis. J. Comp. Neurol. Psychol. 15, 98–112. doi: 10.1002/cne.920150203

Hooper, J. E., 1986. Homeotic gene function in the muscles of Drosophila larvae. The EMBO Journal 5, 2321–2329. doi: 10.1002/j.1460-2075.1986.tb04500.x

Hu, D. L., Nirody, J., Scott, T., Shelley, M. J., 2009. The mechanics of slithering locomotion. Proc. Natl. Acad. Sci. U.S.A. 106, 10081–10085. doi: 10.1073/pnas.0812533106

Hubel, D.H., Wiesel, T.N., 1962. Receptive fields, binocular interaction and functional architecture in the cat's visual cortex. The Journal of Physiology. https://doi.org/10.1113/jphysiol.1962.sp006837

Hughes, C.L., Thomas, J.B., 2007. A sensory feedback circuit coordinates muscle activity in Drosophila. Molecular and Cellular Neuroscience. https://doi.org/10.1016/j.mcn.2007.04.001

Hustert, R., 1982. The proprioceptive function of a complex chordotonal organ associated with the mesothoracic coxa in locusts. J. Comp. Physiol. https://doi.org/10.1007/bf00609673

Hwang, R. Y., Zhong, L., Xu, Y., Johnson, T., Zhang, F., Deisseroth, K., et al., 2007. Nociceptive Neurons Protect Drosophila Larvae from Parasitoid Wasps. Current Biology 17, 2105–2116. doi: 10.1016/j.cub.2007.11.029

Inada, K., Kohsaka, H., Takasu, E., Matsunaga, T., Nose, A., 2011. Optical Dissection of Neural Circuits Responsible for Drosophila Larval Locomotion with Halorhodopsin. PLoS ONE 6, e29019. doi: 10.1371/journal.pone.0029019

Inestrosa, N.C., Sunkel, C.E., Arriagada, J., Garrido, J., Godoy-Herrera, R., 1996. Abnormal development of the locomotor activity in yellow larvae of Drosophila: a cuticular defect? Genetica 97, 205–210. doi: 10.1007/bf00054627

Itakura, Y., Kohsaka, H., Ohyama, T., Zlatic, M., Pulver, S. R., Nose, A., 2015. Identification of Inhibitory Premotor Interneurons Activated at a Late Phase in a Motor Cycle during Drosophila Larval Locomotion. PLoS ONE 10, e0136660. doi: 10.1371/journal.pone.0136660

Islam, S.S., Zelenin, P.V., 2008. Modifications of Locomotor Pattern Underlying Escape Behavior in the Lamprey. Journal of Neurophysiology 99, 297–307. doi: 10.1152/jn.00903.2007

Itakura Y., Kohsaka H., Ohyama T., Zlatic M., Pulver S.R., Nose A., 2015. Identification of inhibitory premotor interneurons activated at a late phase in a motor cycle during Drosophila larval locomotion. PLoS ONE 10: e0136660. doi:10.1371/journal.pone.0136660

Iwasaki, T., Chen, J., Friesen, W. O., 2014. Biological clockwork underlying adaptive rhythmic movements. Proc. Natl. Acad. Sci. U.S.A. 111, 978–983. doi: 10.1073/pnas.1313933111

Jankowska, E., 1992. Interneuronal relay in spinal pathways from proprioceptors. Progress in Neurobiology. https://doi.org/10.1016/0301-0082(92)90024-9

Jankowska, E., 2008. Spinal interneuronal networks in the cat: Elementary components. Brain Research Reviews. https://doi.org/10.1016/j.brainresrev.2007.06.022

Jimenez, Y. E., Lucas, K. N., Long, J. H., Jr, Tytell, E. D., 2024. Flexibility is a hidden axis of biomechanical diversity in fishes. Journal of Experimental Biology 226. doi: 10.1242/jeb.245308

Jonaitis, J., MacLeod, J., Pulver, S.R., 2022. Localization of muscarinic acetylcholine receptor-dependent rhythm-generating modules in the Drosophila larval locomotor network. Journal of Neurophysiology 127, 1098–1116. doi: 10.1152/jn.00106.2021

Jonaitis, J., Hibbard, K.L., Layte, K.M., Hiramoto, A., Cardona, A., Truman, J.W., Nose, A., Zwart, M.F., Pulver, S.R., 2024. Steering From the Rear: Coordination of Central Pattern Generators Underlying Navigation by Ascending Interneurons. bioRxiv [preprint]. Accessible at: https://doi.org/10.1101/2024.06.17.598162. Accessed Jan 30, 2025.

Jovanic, T., Schneider-Mizell, C.M., Shao, M., Masson, J.-B., Denisov, G., Fetter, R.D., Mensh, B.D., Truman, J.W., Cardona, A., Zlatic, M., 2016. Competitive Disinhibition Mediates Behavioral Choice and Sequences in Drosophila. Cell. https://doi.org/10.1016/j.cell.2016.09.009

Karagyozov D., Skanata M.M., Lesar A., Gershow M., 2018. Recording neural activity in unrestrained animals with three-dimensional tracking twophoton microscopy. Cell 25: 1371–1383. doi:10.1016/j.celrep.2018.10.013

Kauwe, G., Isacoff, E. Y., 2013. Rapid feedback regulation of synaptic efficacy during high-frequency activity at the Drosophila larval neuromuscular junction. Proc. Natl. Acad. Sci. U.S.A. 110, 9142–9147. doi: 10.1073/pnas.1221314110

Kearney, G., Radice, M., Merlinsky, A. S., Szczupak, L., 2022. Intersegmental Interactions Give Rise to a Global Network. Front. Neural Circuits 16. doi: 10.3389/fncir.2022.843731

Kernan, M. ,1994. Genetic dissection of mechanosensory transduction: Mechanoreception-defective mutations of drosophila. Neuron 12, 1195–1206. doi: 10.1016/0896-6273(94)90437-5

Keshishian H., Broadie K., Chiba A., Bate M., 1996. The Drosophila neuromuscular junction: a model system for studying synaptic development and function. Annu Rev Neurosci 19: 545–575. doi:10.1146/annurev.ne.19.030196.002553

Kettunen, P., Kyriakatos, A., Hallén, K., El Manira, A., 2005. Neuromodulation via Conditional Release of Endocannabinoids in the Spinal Locomotor Network. Neuron 45, 95–104. doi: 10.1016/j.neuron.2004.12.022

Kiehn, O., 2006. Locomotor circuits in the mammalian spinal cord. Annu. Rev. Neurosci. 29, 279–306. doi: 10.1146/annurev.neuro.29.051605.112910

Kiehn, O., 2016. Decoding the organization of spinal circuits that control locomotion. Nat Rev Neurosci 17, 224–238. doi: 10.1038/nrn.2016.9

Kitamoto, T., 2001. Conditional modification of behavior in Drosophila by targeted expression of a temperature-sensitive shibire allele in defined neurons. J. Neurobiol. 47, 81–92. doi: 10.1002/neu.1018

Knudsen, E.I., Lac, S., Esterly, S.D., 1987. Computational Maps in the Brain. Annu. Rev. Neurosci. https://doi.org/10.1146/annurev.ne.10.030187.000353

Kohsaka H., 2023. Linking neural circuits to the mechanics of animal behavior in Drosophila larval locomotion. Front Neural Circuits 17: 1175899. doi:10.3389/fncir.2023.1175899

Kohsaka, H., Takasu, E., Morimoto, T., Nose, A., 2014. A Group of Segmental Premotor Interneurons Regulates the Speed of Axial Locomotion in Drosophila Larvae. Current Biology 24, 2632–2642. doi: 10.1016/j.cub.2014.09.026

Kohsaka, H., Guertin, P.A., Nose, A., 2017. Neural Circuits Underlying Fly Larval Locomotion. CPD 23, 1722–1733. doi: 10.2174/1381612822666161208120835

Kristan, W.B., Jr, Calabrese, R.L., Friesen, W.O., 2005. Neuronal control of leech behavior. Progress in Neurobiology 76, 279–327. doi: 10.1016/j.pneurobio.2005.09.004

Kyriakatos, A., El Manira, A., 2007. Long-Term Plasticity of the Spinal Locomotor Circuitry Mediated by Endocannabinoid and Nitric Oxide Signaling. J. Neurosci. 27, 12664–12674. doi: 10.1523/jneurosci.3174-07.2007

Landgraf, M., Bossing, T., Technau, G.M., Bate, M., 1997. The Origin, Location, and Projections of the Embryonic Abdominal Motorneurons of Drosophila. J. Neurosci. 17, 9642–9655. doi: 10.1523/jneurosci.17-24-09642.1997

Landgraf, M., Sánchez-Soriano, N., Technau, G.M., Urban, J., Prokop, A., 2003. Charting the Drosophila neuropile: a strategy for the standardised characterisation of genetically amenable neurites. Developmental Biology. https://doi.org/10.1016/s0012-1606(03)00215-x

Lahiri, S., Shen, K., Klein, M., Tang, A., Kane, E., Gershow, M., Garrity, P., Samuel, A.D.T., 2011. Two Alternating Motor Programs Drive Navigation in Drosophila Larva. PLoS ONE. https://doi.org/10.1371/journal.pone.0023180

Lai, H.C., Seal, R.P., Johnson, J.E., 2016. Making sense out of spinal cord somatosensory development. Development. https://doi.org/10.1242/dev.139592

Lavoie, S., McFadyen, B., Drew, T., 1995. A kinematic and kinetic analysis of locomotion during voluntary gait modification in the cat. Exp Brain Res 106. doi: 10.1007/bf00241355

Levinsson, A., Holmberg, H., Broman, J., Zhang, M., Schouenborg, J., 2002. Spinal Sensorimotor Transformation: Relation between Cutaneous Somatotopy and a Reflex Network. J. Neurosci. https://doi.org/10.1523/jneurosci.22-18-08170.2002

Li H.H., Kroll J.R., Lennox S.M., Ogundeyi O., Jeter J., Depasquale G., Truman J.W., 2014. A GAL4 driver resource for developmental and behavioral studies on the larval CNS of Drosophila. Cell Rep 8: 897–908. doi:10.1016/j.celrep.2014.06.065

Liao, J. C., 2022. Fish swimming efficiency. Current Biology 32, R666–R671. doi: 10.1016/j.cub.2022.04.073

Lighthill, M. J., 1969. Hydromechanics of Aquatic Animal Propulsion. Annu. Rev. Fluid Mech. 1, 413–446. doi: 10.1146/annurev.fl.01.010169.002213

Lin, H.-T., Trimmer, B., 2010. Caterpillars use the substrate as their external skeleton. Communicative & Integrative Biology 3, 471–474. doi: 10.4161/cib.3.5.12560

Liu Y., Hasegawa E., Nose A., Zwart M.F., Kohsaka H., 2023. Synchronous multi-segmental activity between metachronal waves controls locomotion speed in Drosophila larvae. eLifee 12: e83328. doi:10.7554/eLife.83328

Lohs-Schardin, M., Cremer, C., Nüsslein-Volhard, C., 1979. A fate map for the larval epidermis of Drosophila melanogaster: localized cuticle defects following irradiation of the blastoderm with an ultraviolet laser microbeam. Developmental Biology 73, 239–255. doi: 10.1016/0012-1606(79)90065-4

Loveless, J., Webb, B., 2018. A Neuromechanical Model of Larval Chemotaxis. Integrative and Comparative Biology. doi: 10.1093/icb/icy094

Loveless, J., Lagogiannis, K., Webb, B., 2019. Modelling the mechanics of exploration in larval Drosophila. PLoS Comput Biol 15, e1006635. doi: 10.1371/journal.pcbi.1006635

Lucas, K. N., Lauder, G. V., Tytell, E. D., 2020. Airfoil-like mechanics generate thrust on the anterior body of swimming fishes. Proc. Natl. Acad. Sci. U.S.A. 117, 10585–10592. doi: 10.1073/pnas.1919055117

Lundberg, A., 1979. Multisensory Control of Spinal Reflex Pathways. Progress in Brain Research. https://doi.org/10.1016/s0079-6123(08)60803-1

Luo, L., Gershow, M., Rosenzweig, M., Kang, K., Fang-Yen, C., Garrity, P. A., et al., 2010. Navigational Decision Making in Drosophila Thermotaxis. J. Neurosci. 30, 4261–4272. doi: 10.1523/jneurosci.4090-09.2010

Mamiya, A., Gurung, P., Tuthill, J.C., 2018. Neural Coding of Leg Proprioception in Drosophila. Neuron. https://doi.org/10.1016/j.neuron.2018.09.009

Marder, E., 2012. Neuromodulation of Neuronal Circuits: Back to the Future. Neuron 76, 1–11. doi: 10.1016/j.neuron.2012.09.010

Marder, E., Bucher, D., 2001. Central pattern generators and the control of rhythmic movements. Current Biology 11, R986–R996. doi: 10.1016/s0960-9822(01)00581-4

Marken, R. S., Powers, W. T., 1989. Random-walk chemotaxis: Trial and error as a control process. Behavioral Neuroscience 103, 1348–1355. doi: 10.1037/0735-7044.103.6.1348

Markow, T. A., 1979. A survey of intra -and interspecific variation for pupation height in Drosophila. Behav Genet 9, 209–217. doi: 10.1007/bf01071301

Mason, A., Kristan, W.B., Jr., 1982. Neuronal excitation, inhibition and modulation of leech longitudinal muscle. J. Comp. Physiol. 146, 527–536. doi: 10.1007/bf00609449

Mathis A., Mamidanna P., Cury K.M., Abe T., Murthy V.N., Mathis M.W., Bethge M., 2018. DeepLabCut: markerless pose estimation of user-defined body parts with deep learning. Nat Neurosci 9: 1281–1289. doi:10.1038/s41593-018-0209-y

Matsushima, T., Grillner, S., 1992. Neural mechanisms of intersegmental coordination in lamprey: local excitability changes modify the phase coupling along the spinal cord. Journal of Neurophysiology 67, 373–388. doi: 10.1152/jn.1992.67.2.373

McClellan, A. D., 2018. Response: Commentary: Elimination of Left-Right Reciprocal Coupling in the Adult Lamprey Spinal Cord Abolishes the Generation of Locomotor Activity. Front. Neural Circuits 12. doi: 10.3389/fncir.2018.00062

McClellan, A., Sigvardt, K., 1988. Features of entrainment of spinal pattern generators for locomotor activity in the lamprey spinal cord. J. Neurosci. 8, 133–145. doi: 10.1523/jneurosci.08-01-00133.1988

McMillen, T., Williams, T., Holmes, P., 2008. Nonlinear Muscles, Passive Viscoelasticity and Body Taper Conspire To Create Neuromechanical Phase Lags in Anguilliform Swimmers. PLoS Comput Biol 4, e1000157. doi: 10.1371/journal.pcbi.1000157

McNulty, P., Wu, R., Yamaguchi, A., Heckscher, E. S., Haas, A., Nwankpa, A., Skanata, M. M., Gershow, M., 2024. CRASH2p: Closed-loop Two Photon Imaging in a Freely Moving Animal. bioRxiv [preprint]. Accessible at: https://doi.org/10.1101/2024.05.22.595209. Accessed Jan 30, 2025.

Mendes, C.S., Bartos, I., Akay, T., Márka, S., Mann, R.S., 2013. Quantification of gait parameters in freely walking wild type and sensory deprived Drosophila melanogaster. eLife. https://doi.org/10.7554/elife.00231

Mentel, T., Krause, A., Pabst, M., El Manira, A., Büschges, A., 2006. Activity of fin muscles and fin motoneurons during swimming motor pattern in the lamprey. Eur J of Neuroscience 23, 2012–2026. doi: 10.1111/j.1460-9568.2006.04738.x

Merritt, D., Whitington, P., 1995. Central projections of sensory neurons in the Drosophila embryo correlate with sensory modality, soma position, and proneural gene function. J. Neurosci. https://doi.org/10.1523/jneurosci.15-03-01755.1995

Messina, J. A., St. Paul, A., Hargis, S., Thompson, W. E., McClellan, A. D., 2017. Elimination of Left-Right Reciprocal Coupling in the Adult Lamprey Spinal Cord Abolishes the Generation of Locomotor Activity. Front. Neural Circuits 11. doi: 10.3389/fncir.2017.00089

Miller, W. L., Sigvardt, K. A., 2000. Extent and Role of Multisegmental Coupling in the Lamprey Spinal Locomotor Pattern Generator. Journal of Neurophysiology 83, 465–476. doi: 10.1152/jn.2000.83.1.465

Morgan, J.L., Lichtman, J.W., 2013. Why not connectomics? Nat Methods. https://doi.org/10.1038/nmeth.2480

Mullins, O. J., Friesen, W. O., 2012. The brain matters: effects of descending signals on motor control. Journal of Neurophysiology 107, 2730–2741. doi: 10.1152/jn.00107.2012

Mullins, O. J., Hackett, J. T., Buchanan, J. T., Friesen, W. O., 2011. Neuronal control of swimming behavior: Comparison of vertebrate and invertebrate model systems. Progress in Neurobiology 93, 244–269. doi: 10.1016/j.pneurobio.2010.11.001

Murawski, C., Pulver, S.R., Gather, M.C., 2020. Segment-specific optogenetic stimulation in Drosophila melanogaster with linear arrays of organic light-emitting diodes. Nat Commun 11. doi: 10.1038/s41467-020-20013-6

Murphey, R.K., Bacon, J.P., Johnson, S.E., 1985. Ectopic neurons and the organization of insect sensory systems. J. Comp. Physiol. https://doi.org/10.1007/bf00610730

Nagai T., Yamada S., Tominaga T., Ichikawa M., Miyawaki A,. 2004. Expanded dynamic range of fluorescent indicators for Ca2+ by circularly permuted yellow fluorescent proteins. Proc Natl Acad Sci 101: 10554–10559. doi:10.1073/pnas.0400417101

Newman, Z. L., Hoagland, A., Aghi, K., Worden, K., Levy, S. L., Son, J. H., et al., 2017. Input-Specific Plasticity and Homeostasis at the Drosophila Larval Neuromuscular Junction. Neuron 93, 1388-1404.e10. doi: 10.1016/j.neuron.2017.02.028

Niu, J., Ding, L., Li, J.J., Kim, H., Liu, J., Li, H., Moberly, A., Badea, T.C., Duncan, I.D., Son, Y.-J., Scherer, S.S., Luo, W., 2013. Modality-Based Organization of Ascending Somatosensory Axons in the Direct Dorsal Column Pathway. J. Neurosci. https://doi.org/10.1523/jneurosci.3429-13.2013

Nusbaum, M. P., 1986. Synaptic Basis of Swim Initiation in the Leech: III. Synaptic Effects of Serotonin-Containing Interneurones (Cells 21 and 61) on Swim Cpg Neurones (Cells 18 and 208). Journal of Experimental Biology 122, 303–321. doi: 10.1242/jeb.122.1.303

Nusbaum, M. P., Kristan, W. B., Jr., 1986. Swim Initiation in the Leech by Serotonin-Containing Interneurones, Cells 21 and 61. Journal of Experimental Biology 122, 277–302. doi: 10.1242/jeb.122.1.277

Ohyama, T., Schneider-Mizell, C.M., Fetter, R.D., Aleman, J.V., Franconville, R., Rivera-Alba, M., Mensh, B.D., Branson, K.M., Simpson, J.H., Truman, J.W., Cardona, A., Zlatic, M., 2015. A multilevel multimodal circuit enhances action selection in Drosophila. Nature. https://doi.org/10.1038/nature14297

Orgogozo, V., Grueber, W.B., 2005. FlyPNS, a database of the Drosophila embryonic and larval peripheral nervous system. BMC Dev Biol. https://doi.org/10.1186/1471-213x-5-4

Ormerod, K.G., Scibelli, A.E., Littleton, J.T., 2022. Regulation of excitation-contraction coupling at the Drosophila neuromuscular junction. The Journal of Physiology 600, 349–372. doi: 10.1113/jp282092

Pandey, M.B., Singh, B.N., 1993. Effect of biotic and abiotic factors on pupation height in four species of Drosophila. Indian journal of experimental biology, 31 11, 912-7.

Parker, D., Bevan, S., 2007. Modulation of Cellular and Synaptic Variability in the Lamprey Spinal Cord. Journal of Neurophysiology 97, 44–56. doi: 10.1152/jn.00717.2006

Paterson, B. A., Anikin, I. M., Krans, J. L., 2010. Hysteresis in the production of force by larval Dipteran muscle. Journal of Experimental Biology 213, 2483–2493. doi: 10.1242/jeb.043026

Pearce, R.A., Friesen, W.O., 1985. Intersegmental coordination of the leech swimming rhythm. II. Comparison of long and short chains of ganglia. Journal of Neurophysiology 54, 1460–1472. doi: 10.1152/jn.1985.54.6.1460

Pearson, K.G., Goodman, C.S., 1981. Presynaptic inhibition of transmission from identified interneurons in locust central nervous system. Journal of Neurophysiology. https://doi.org/10.1152/jn.1981.45.3.501

Pehlevan, C., Paoletti, P., Mahadevan, L., 2016. Integrative neuromechanics of crawling in D. melanogaster larvae. eLife. https://doi.org/10.7554/elife.11031

Pereira T.D., Aldarondo D.E., Willmore L., Kislin M., Wang S.S., Murthy M., Shaevitz J.W., 2019. Fast animal pose estimation using deep neural networks. Nat Methods 16: 117–125. doi:10.1038/s41592-018-0234-5

Peron, S., Zordan, M.A., Magnabosco, A., Reggiani, C., Megighian, A., 2009. From action potential to contraction: Neural control and excitation–contraction coupling in larval muscles of Drosophila. Comparative Biochemistry and Physiology Part A: Molecular & Integrative Physiology 154, 173–183. doi: 10.1016/j.cbpa.2009.04.626

Pfeiffer, B.D., Jenett, A., Hammonds, A.S., Ngo, T.-T.B., Misra, S., Murphy, C., et al., 2008. Tools for neuroanatomy and neurogenetics in Drosophila. Proc. Natl. Acad. Sci. U.S.A. 105, 9715–9720. doi: 10.1073/pnas.0803697105

Pflüger, H.J., Bräunig, P., Hustert, R., 1988. The organization of mechanosensory neuropiles in locust thoracic ganglia, Phil. Trans. R. Soc. Lond. B. https://doi.org/10.1098/rstb.1988.0090

Poon, M., Friesen, W. O., Stent, G. S., 1978. Neuronal Control of Swimming in the Medicinal Leech. Journal of Experimental Biology 75, 45–63. doi: 10.1242/jeb.75.1.45

Pouille, F., Watkinson, O., Scanziani, M., Trevelyan, A.J., 2013. The contribution of synaptic location to inhibitory gain control in pyramidal cells. Physiol Rep. https://doi.org/10.1002/phy2.67

Prasad, T., Weiner, J.A., 2011. Direct and Indirect Regulation of Spinal Cord Ia Afferent Terminal Formation by the γ-Protocadherins. Front. Mol. Neurosci. https://doi.org/10.3389/fnmol.2011.00054

Puhl, J. G., Mesce, K. A., 2008. Dopamine Activates the Motor Pattern for Crawling in the Medicinal Leech. J. Neurosci. 28, 4192–4200. doi: 10.1523/jneurosci.0136-08.2008

Puhl, J. G., Mesce, K. A., 2010. Keeping It Together: Mechanisms of Intersegmental Coordination for a Flexible Locomotor Behavior. J. Neurosci. 30, 2373–2383. doi: 10.1523/jneurosci.5765-09.2010

Puhl, J. G., Masino, M. A., Mesce, K. A., 2012. Necessary, Sufficient and Permissive: A Single Locomotor Command Neuron Important for Intersegmental Coordination. J. Neurosci. 32, 17646–17657. doi: 10.1523/jneurosci.2249-12.2012

Pulver, S.R., Bayley, T.G., Taylor, A.L., Berni, J., Bate, M., Hedwig, B., 2015. Imaging fictive locomotor patterns in larval Drosophila. Journal of Neurophysiology 114, 2564–2577. doi: 10.1152/jn.00731.2015

Quillin, K. J., 1999. Kinematic scaling of locomotion by hydrostatic animals: ontogeny of peristaltic crawling by the earthworm Lumbricus terrestris. Journal of Experimental Biology 202, 661–674. doi: 10.1242/jeb.202.6.661

Risse, B., Berh, D., Otto, N., Klämbt, C., Jiang, X., 2017. FIMTrack: An open source tracking and locomotion analysis software for small animals. PLoS Comput Biol 13, e1005530. doi: 10.1371/journal.pcbi.1005530

Roberts, M. J., 1971. On the locomotion of cyclorrhaphan maggots (Diptera). Journal of Natural History 5, 583–590. doi: 10.1080/00222937100770421

Rohrbough, J., Broadie, K., 2002. Electrophysiological Analysis of Synaptic Transmission in Central Neurons of Drosophila Larvae. Journal of Neurophysiology 88, 847–860. doi: 10.1152/jn.2002.88.2.847

Rome, L.C., Swank, D., Corda, D., 1993. How Fish Power Swimming. Science 261, 340–343. doi: 10.1126/science.8332898

Rossignol, S., Dubuc, R., Gossard, J.-P., 2006. Dynamic Sensorimotor Interactions in Locomotion. Physiological Reviews. https://doi.org/10.1152/physrev.00028.2005

Rotheray, G. E., 2019. Forms, Functions and Names. Zoological Monographs, 53–86. doi: 10.1007/978-3-319-92546-2_3

Rotstein, H. G., Schneider, E., Szczupak, L., 2017. Feedback Signal from Motoneurons Influences a Rhythmic Pattern Generator. J. Neurosci. 37, 9149–9159. doi: 10.1523/jneurosci.0756-17.2017

Rovainen, C. M., 1985. Effects of groups of propriospinal interneurons on fictive swimming in the isolated spinal cord of the lamprey. Journal of Neurophysiology 54, 959–977. doi: 10.1152/jn.1985.54.4.959

Rudomin, P., Schmidt, R.F., 1999. Presynaptic inhibition in the vertebrate spinal cord revisited. Experimental Brain Research. https://doi.org/10.1007/s002210050933

Ruiz-Dubreuil, G., Burnet, B., Connolly, K., Furness, P., 1996. Larval foraging behaviour and competition in Drosophila melanogaster. Heredity 76, 55–64. doi: 10.1038/hdy.1996.7

Ryczko, D., Dubuc, R., Cabelguen, J.-M., 2010. Rhythmogenesis in axial locomotor networks: an interspecies comparison. Progress in Brain Research, 189–211. doi: 10.1016/b978-0-444-53613-6.00013-7

Saalfeld, S., Cardona, A., Hartenstein, V., Tomančák, P., 2009. CATMAID: collaborative annotation toolkit for massive amounts of image data. Bioinformatics. https://doi.org/10.1093/bioinformatics/btp266

Santuz, A., Akay, T., Mayer, W.P., Wells, T.L., Schroll, A., Arampatzis, A., 2019. Modular organization of murine locomotor pattern in the presence and absence of sensory feedback from muscle spindles. J Physiol. https://doi.org/10.1113/jp277515

Scheibel, M.E., Schiebel, A.B., 1969. Terminal patterns in cat spinal cord III. Primary afferent collaterals. Brain Research. https://doi.org/10.1016/0006-8993(69)90258-3

Schmidt, B. J., Jordan, L. M., 2000. The role of serotonin in reflex modulation and locomotor rhythm production in the mammalian spinal cord. Brain Research Bulletin 53, 689–710. doi: 10.1016/s0361-9230(00)00402-0

Schneider-Mizell, C.M., Gerhard, S., Longair, M., Kazimiers, T., Li, F., Zwart, M.F., Champion, A., Midgley, F.M., Fetter, R.D., Saalfeld, S., Cardona, A., 2016. Quantitative neuroanatomy for connectomics in Drosophila. eLife. https://doi.org/10.7554/elife.12059

Scholz, N., Gehring, J., Guan, C., Ljaschenko, D., Fischer, R., Lakshmanan, V., et al., 2015. The Adhesion GPCR Latrophilin/CIRL Shapes Mechanosensation. Cell Reports 11, 866–874. doi: 10.1016/j.celrep.2015.04.008

Schrader, Š., Merritt, D.J., 2000. Central projections ofDrosophila sensory neurons in the transition from embryo to larva. J. Comp. Neurol. https://doi.org/10.1002/1096-9861(20000911)425:1<34::aid-cne4>3.0.co;2-g

Schrader, Š., Merritt, D.J., 2007. Dorsal longitudinal stretch receptor of Drosophila melanogaster larva – Fine structure and maturation. Arthropod Structure & Development. https://doi.org/10.1016/j.asd.2006.08.014

Schulman, V. K., Dobi, K. C., Baylies, M. K., 2015. Morphogenesis of the somatic musculature in Drosophila melanogaster. WIREs Developmental Biology 4, 313–334. doi: 10.1002/wdev.180

Schwarz, G., 1978. Estimating the Dimension of a Model. Ann. Statist. 6. doi: 10.1214/aos/1176344136

Schwarz, R. F., Branicky, R., Grundy, L. J., Schafer, W. R., Brown, A. E. X., 2015. Changes in Postural Syntax Characterize Sensory Modulation and Natural Variation of C. elegans Locomotion. PLoS Comput Biol 11, e1004322. doi: 10.1371/journal.pcbi.1004322

Selcho, M., Pauls, D., el Jundi, B., Stocker, R. F., Thum, A. S., 2012. The Role of octopamine and tyramine in Drosophila larval locomotion. J of Comparative Neurology 520, 3764–3785. doi: 10.1002/cne.23152

Severi, K. E., Portugues, R., Marques, J. C., O'Malley, D. M., Orger, M. B., Engert, F., 2014. Neural Control and Modulation of Swimming Speed in the Larval Zebrafish. Neuron 83, 692–707. doi: 10.1016/j.neuron.2014.06.032

Sewell, D., Burnet, B., Connolly, K., 1974. Genetic analysis of larval feeding behaviour in Drosophila melanogaster. Genet. Res. 24, 163–173. doi: 10.1017/s0016672300015196

Sigvardt, K. A., 1989. Spinal Mechanisms in the Control of Lamprey Swimming. Am Zool 29, 19–35. doi: 10.1093/icb/29.1.19

Skinner, F. K., Mulloney, B., 1998. Intersegmental coordination in invertebrates and vertebrates. Current Opinion in Neurobiology 8, 725–732. doi: 10.1016/s0959-4388(98)80114-1

Simon, M.A., Trimmer, B.A., 2010. Movement encoding by a stretch receptor in the soft-bodied caterpillar, Manduca sexta. Journal of Experimental Biology. https://doi.org/10.1242/jeb.023507

Simon, M.A., Woods Jr., W.A., Serebrenik, Y.V., Simon, S.M., van Griethuijsen, L.I., Socha, J.J., Lee, W-K., Trimmer, B.A., 2010. Visceral-Locomotory Pistoning in Crawling Caterpillars. Current Biology. doi: 10.1016/j.cub.2010.06.059

Singh, N. P., Mishra, R. K., 2014. Role of abd-A and Abd-B in Development of Abdominal Epithelia Breaks Posterior Prevalence Rule. PLoS Genet 10, e1004717. doi: 10.1371/journal.pgen.1004717

Singhania, A., Grueber, W. B., 2014. Development of the embryonic and larval peripheral nervous system of Drosophila. WIREs Developmental Biology 3, 193–210. doi: 10.1002/wdev.135

Skandalis, D.A., Lunsford, E.T., Liao, J.C., 2021. Corollary discharge enables proprioception from lateral line sensory feedback. PLoS Biol. https://doi.org/10.1371/journal.pbio.3001420

Smith, S.A., Shepherd, D., 1996. Central afferent projections of proprioceptive sensory neurons inDrosophila revealed with the enhancer-trap technique. J. Comp. Neurol. https://doi.org/10.1002/(sici)1096-9861(19960108)364:2<311::aid-cne9>3.0.co;2-8

Snodgrass, R., 1935. Principles of Insect Morphology. New York: McGraw-Hill.

Sokolowski, M. B., 1980. Foraging strategies of Drosophila melanogaster: A chromosomal analysis. Behav Genet 10, 291–302. doi: 10.1007/bf01067774

Sokolowski, M. B., 1985. Genetics and ecology of Drosophila melanogaster larval foraging and pupation behaviour. Journal of Insect Physiology 31, 857–864. doi: 10.1016/0022-1910(85)90103-9

Song, W., Onishi, M., Jan, L.Y., Jan, Y.N., 2007. Peripheral multidendritic sensory neurons are necessary for rhythmic locomotion behavior in Drosophila larvae. Proc. Natl. Acad. Sci. U.S.A. https://doi.org/10.1073/pnas.0700895104

Srinivasan, S., Lance, K., Levine, R.B., 2012. Segmental differences in firing properties and potassium currents in Drosophila larval motoneurons. Journal of Neurophysiology 107, 1356–1365. doi: 10.1152/jn.00200.2011

Stern-Tomlinson, W., Nusbaum, M.P., Perez, L.E., Kristan, W.B., Jr., 1986. A kinematic study of crawling behavior in the leech, Hirudo medicinalis. J. Comp. Physiol. 158, 593–603. doi: 10.1007/bf00603803

Straka, H., Simmers, J., Chagnaud, B.P., 2018. A New Perspective on Predictive Motor Signaling. Current Biology. https://doi.org/10.1016/j.cub.2018.01.033

Summers, A. P., Long, J. H., Jr., 2005. Skin and Bones, Sinew and Gristle: the Mechanical Behavior of Fish Skeletal Tissues. Fish Physiology, 141–177. doi: 10.1016/s1546-5098(05)23005-4

Sun X., Heckscher E.S., 2016. Using linear agarose channels to study Drosophila larval crawling behavior. J Vis Exp 117: 54892. doi:10.3791/54892

Sun X., Liu Y., Liu C., Mayumi K., Ito K., Nose A., Kohsaka H., 2022. A neuromechanical model for Drosophila larval crawling based on physical measurements. BMC Biol 20: 130. doi:10.1186/s12915-022-01336-w

Suslak, T.J., Jarman, A.P., 2015. Stretching the imagination beyond muscle spindles - stretch-sensitive mechanisms in arthropods. J. Anat. https://doi.org/10.1111/joa.12329

Suster, M. L., Bate, M., 2002. Embryonic assembly of a central pattern generator without sensory input. Nature 416, 174–178. doi: 10.1038/416174a

Sürmeli, G., Akay, T., Ippolito, G.C., Tucker, P.W., Jessell, T.M., 2011. Patterns of Spinal Sensory-Motor Connectivity Prescribed by a Dorsoventral Positional Template. Cell. https://doi.org/10.1016/j.cell.2011.10.012

Tadres, D., Louis, M., 2020. PiVR: An affordable and versatile closed-loop platform to study unrestrained sensorimotor behavior. PLoS Biol. https://doi.org/10.1371/journal.pbio.3000712

Takagi, S., Cocanougher, B.T., Niki, S., Miyamoto, D., Kohsaka, H., Kazama, H., et al., 2017. Divergent Connectivity of Homologous Command-like Neurons Mediates Segment-Specific Touch Responses in Drosophila. Neuron 96, 1373-1387.e6. doi: 10.1016/j.neuron.2017.10.030

Tamarkin, D.A., Levine, R.B., 1996. Synaptic interactions between a muscle-associated proprioceptor and body wall muscle motor neurons in larval and Adult manduca sexta. Journal of Neurophysiology. https://doi.org/10.1152/jn.1996.76.3.1597

Tanaka, Y., Ito, K., Nakagaki, T., Kobayashi, R., 2011. Mechanics of peristaltic locomotion and role of anchoring. J. R. Soc. Interface. 9, 222–233. doi: 10.1098/rsif.2011.0339

Tastekin, I., Riedl, J., Schilling-Kurz, V., Gomez-Marin, A., Truman, J. W., Louis, M., 2015. Role of the Subesophageal Zone in Sensorimotor Control of Orientation in Drosophila Larva. Current Biology 25, 1448–1460. doi: 10.1016/j.cub.2015.04.016

Tastekin, I., Khandelwal, A., Tadres, D., Fessner, N.D., Truman, J.W., Zlatic, M., et al., 2018. Sensorimotor pathway controlling stopping behavior during chemotaxis in the Drosophila melanogaster larva. eLife 7. doi: 10.7554/elife.38740

Thane, M., Paisios, E., Stöter, T., Krüger, A.-R., Gläß, S., Dahse, A.-K., et al., 2023. High-resolution analysis of individual Drosophila melanogaster larvae uncovers individual variability in locomotion and its neurogenetic modulation. Open Biol. 13. doi: 10.1098/rsob.220308

Thomas, J.B., Bastiani, M.J., Bate, M., Goodman, C.S., 1984. From grasshopper to Drosophila: a common plan for neuronal development. Nature. https://doi.org/10.1038/310203a0

Thörn Pérez, C., Hill, R. H., Manira, A. El., Grillner, S., 2009. Endocannabinoids Mediate Tachykinin-Induced Effects in the Lamprey Locomotor Network. Journal of Neurophysiology 102, 1358–1365. doi: 10.1152/jn.00294.2009

Trimmer, B., Issberner, J., 2007. Kinematics of Soft-bodied, Legged Locomotion in Manduca sexta Larvae. The Biological Bulletin 212, 130–142. doi: 10.2307/25066590

Tuthill, J.C., Azim, E., 2018. Proprioception. Current Biology 28, R194–R203. doi: 10.1016/j.cub.2018.01.064

Tyrer, N.M., Gregory, G.E., 1982. A guide to the neuroanatomy of locust suboesophageal and thoracic ganglia. Phil. Trans. R. Soc. Lond. B. https://doi.org/10.1098/rstb.1982.0035

Tytell, E.D., 2004. Kinematics and hydrodynamics of linear acceleration in eels, Anguilla rostrata. Proc. R. Soc. Lond. B 271, 2535–2540. doi: 10.1098/rspb.2004.2901

Tytell, E.D., Cohen, A.H., 2008. Rostral Versus Caudal Differences in Mechanical Entrainment of the Lamprey Central Pattern Generator for Locomotion. Journal of Neurophysiology 99, 2408–2419. doi: 10.1152/jn.01085.2007

Tytell, E. D., Hsu, C.-Y., Williams, T. L., Cohen, A. H., Fauci, L. J., 2010. Interactions between internal forces, body stiffness, and fluid environment in a neuromechanical model of lamprey swimming. Proc. Natl. Acad. Sci. U.S.A. 107, 19832–19837. doi: 10.1073/pnas.1011564107

Tytell, E.D., Holmes, P., Cohen, A.H., 2011. Spikes alone do not behavior make: why neuroscience needs biomechanics. Current Opinion in Neurobiology 21, 816–822. doi: 10.1016/j.conb.2011.05.017

Tytell, E.D., Hsu, C.-Y., Fauci, L. J., 2014. The role of mechanical resonance in the neural control of swimming in fishes. Zoology 117, 48–56. doi: 10.1016/j.zool.2013.10.011

Tytell, E. D., Carr, J. A., Danos, N., Wagenbach, C., Sullivan, C. M., Kiemel, T., et al., 2018. Body stiffness and damping depend sensitively on the timing of muscle activation in lampreys. Integrative and Comparative Biology. doi: 10.1093/icb/icy042

Ugur, B., Bao, H., Stawarski, M., Duraine, L.R., Zuo, Z., Lin, Y.Q., et al., 2017. The Krebs Cycle Enzyme Isocitrate Dehydrogenase 3A Couples Mitochondrial Metabolism to Synaptic Transmission. Cell Reports 21, 3794–3806. doi: 10.1016/j.celrep.2017.12.005

Vaadia, R.D., Li, W., Voleti, V., Singhania, A., Hillman, E.M.C., Grueber, W.B., 2019. Characterization of Proprioceptive System Dynamics in Behaving Drosophila Larvae Using High-Speed Volumetric Microscopy. Current Biology. https://doi.org/10.1016/j.cub.2019.01.060

van Griethuijsen, L.I., Trimmer, B.A., 2010. Caterpillar crawling over irregular terrain: anticipation and local sensing. J Comp Physiol A 196, 397–406. doi: 10.1007/s00359-010-0525-5

van Griethuijsen, L. I., Trimmer, B. A., 2014. Locomotion in caterpillars. Biological Reviews 89, 656–670. doi: 10.1111/brv.12073

Vogelstein J.T., Park Y., Ohyama T., Kerr R.A., Truman J.W., Priebe C.E., Zlatic M., 2014. Discovery of brainwide neural–behavioral maps via multiscale unsupervised structure learning. Science 344: 386–392. doi:10.1126/science.1250298

Volk, T., VijayRaghavan, K., 1994. A central role for epidermal segment border cells in the induction of muscle patterning in the Drosophila embryo. Development 120, 59–70. doi: 10.1242/dev.120.1.59

Wallén, P., Williams, T. L., 1984. Fictive locomotion in the lamprey spinal cord in vitro compared with swimming in the intact and spinal animal. The Journal of Physiology 347, 225–239. doi: 10.1113/jphysiol.1984.sp015063

Wallén, P., Buchanan, J. T., Grillner, S., Hill, R. H., Christenson, J., Hokfelt, T., 1989. Effects of 5-hydroxytryptamine on the afterhyperpolarization, spike frequency regulation, and oscillatory membrane properties in lamprey spinal cord neurons. Journal of Neurophysiology 61, 759–768. doi: 10.1152/jn.1989.61.4.759

Wang, J. W., Sylwester, A. W., Reed, D., Wu, D.-A. J., Soll, D. R., Wu, C.-F., 1997. Morphometric Description of the Wandering Behavior in Drosophila Larvae: Aberrant Locomotion in Na+and K+Channel Mutants Revealed by Computer-Assisted Motion Analysis. Journal of Neurogenetics 11, 231–254. doi: 10.3109/01677069709115098

Wang, Y., Wreden, C.C., Levy, M., Meng, J.L., Marshall, Z.D., MacLean, J., Heckscher, E., 2022. Sequential addition of neuronal stem cell temporal cohorts generates a feed-forward circuit in the Drosophila larval nerve cord. eLife. https://doi.org/10.7554/elife.79276

Wardle, C.S., Videler, J.J., Altringham, J.D., 1995. Tuning In To Fish Swimming Waves: Body Form, Swimming Mode And Muscle Function. Journal of Experimental Biology 198, 1629–1636. doi: 10.1242/jeb.198.8.1629

Warren, B., Göpfert, M. C., 2024. Mechanically evoked spike responses of pentascolopidial chordotonal organs of Drosophila melanogaster larvae. Journal of Experimental Biology 227. doi: 10.1242/jeb.246197

Watson, A.H.D., Bazzaz, A.A., 2001. GABA and glycine-like immunoreactivity at axoaxonic synapses on 1a muscle afferent terminals in the spinal cord of the rat. J. Comp. Neurol. https://doi.org/10.1002/cne.1143

Webb, J.E., 1973. The role of the notochard in forward and reverse swimming and burrowing in the amphioxus Branchiostoma lanceolatum. Journal of Zoology 170, 325–338. doi: 10.1111/j.1469-7998.1973.tb01381.x

Weeks, J. C., 1982. Synaptic basis of swim initiation in the leech. J. Comp. Physiol. 148, 265–279. doi: 10.1007/bf00619133

Wen, Q., Gao, S., Zhen, M., 2018. Caenorhabditis elegans excitatory ventral cord motor neurons derive rhythm for body undulation. Phil. Trans. R. Soc. B 373, 20170370. doi: 10.1098/rstb.2017.0370

Williams, T.L., Grillner, S., Smoljaninov, V.V., Wallén, P., Kashin, S., Rossignol, S., 1989. Locomotion in Lamprey and Trout: the Relative Timing of Activation and Movement. Journal of Experimental Biology 143, 559–557. doi: 10.1242/jeb.143.1.559

Williams, T. L., Sigvardt, K. A., Kopell, N., Ermentrout, G. B., Remler, M. P., 1990. Forcing of coupled nonlinear oscillators: studies of intersegmental coordination in the lamprey locomotor central pattern generator. Journal of Neurophysiology 64, 862–871. doi: 10.1152/jn.1990.64.3.862

Willis, W.D., Jr., Coggeshall, R.E., 2004. Sensory Mechanisms of the Spinal Cord. Springer US. https://doi.org/10.1007/978-1-4615-0037-7

Wilson, R.I., 2013. Early Olfactory Processing in Drosophila: Mechanisms and Principles. Annu. Rev. Neurosci. https://doi.org/10.1146/annurev-neuro-062111-150533

Wilson, H. R., Cowan, J. D., 1972. Excitatory and Inhibitory Interactions in Localized Populations of Model Neurons. Biophysical Journal 12, 1–24. doi: 10.1016/s0006-3495(72)86068-5

Windhorst, U., 2007. Muscle proprioceptive feedback and spinal networks. Brain Research Bulletin. https://doi.org/10.1016/j.brainresbull.2007.03.010

Wipfler, B., Schneeberg, K., Löffler, A., Hünefeld, F., Meier, R., Beutel, R. G., 2013. The skeletomuscular system of the larva of Drosophila melanogaster (Drosophilidae, Diptera) – A contribution to the morphology of a model organism. Arthropod Structure & Development 42, 47–68. doi: 10.1016/j.asd.2012.09.005

Wolff, S. B., Ölveczky, B. P., 2018. The promise and perils of causal circuit manipulations. Current Opinion in Neurobiology 49, 84–94. doi: 10.1016/j.conb.2018.01.004

Woods, W.A., Jr, Fusillo, S.J., Trimmer, B.A., 2008. Dynamic properties of a locomotory muscle of the tobacco hornworm Manduca sexta during strain cycling and simulated natural crawling. Journal of Experimental Biology 211, 873–882. doi: 10.1242/jeb.006031

Wosniack, M. E., Festa, D., Hu, N., Gjorgjieva, J., Berni, J., 2022. Adaptation of Drosophila larva foraging in response to changes in food resources. eLife 11. doi: 10.7554/elife.75826

Wu, H., Petitpré, C., Fontanet, P., Sharma, A., Bellardita, C., Quadros, R.M., Jannig, P.R., Wang, Y., Heimel, J.A., Cheung, K.K.Y., Wanderoy, S., Xuan, Y., Meletis, K., Ruas, J., Gurumurthy, C.B., Kiehn, O., Hadjab, S., Lallemend, F., 2021. Distinct subtypes of proprioceptive dorsal root ganglion neurons regulate adaptive proprioception in mice. Nat Commun. https://doi.org/10.1038/s41467-021-21173-9

Wystrach, A., Lagogiannis, K., Webb, B., 2016. Continuous lateral oscillations as a core mechanism for taxis in Drosophila larvae. eLife 5. doi: 10.7554/elife.15504

Yamaguchi A., Wu R., McNulty P., Karagyozov D., Skanata M.M., Gershow M., 2023. Multi-neuronal recording in unrestrained animals with all acousto–optic random-access line-scanning two-photon microscopy. Front Neurosci 17: 1135457. doi:10.3389/fnins.2023.1135457

Yan, Z., Zhang, W., He, Y., Gorczyca, D., Xiang, Y., Cheng, L. E., et al., 2012. Drosophila NOMPC is a mechanotransduction channel subunit for gentle-touch sensation. Nature 493, 221–225. doi: 10.1038/nature11685

Yu, X., Friesen, W. O., 2004. Entrainment of leech swimming activity by the ventral stretch receptor. J Comp Physiol A. doi: 10.1007/s00359-004-0549-9

Yu, X., Nguyen, B., Friesen, W. O., 1999. Sensory Feedback Can Coordinate the Swimming Activity of the Leech. J. Neurosci. 19, 4634–4643. doi: 10.1523/jneurosci.19-11-04634.1999

Zarin, A.A., Mark, B., Cardona, A., Litwin-Kumar, A., Doe, C.Q., 2019. A multilayer circuit architecture for the generation of distinct locomotor behaviors in Drosophila. eLife. https://doi.org/10.7554/elife.51781

Zarin, A.A., Mark, B., Cardona, A., Litwin-Kumar, A., Doe, C.Q., 2019. A Drosophila larval premotor/motor neuron connectome generating two behaviors via distinct spatio-temporal muscle activity. bioRxiv [preprint]. Available at https://doi.org/10.1101/617977 (Accessed June 21, 2023).

Zeng, X., Komanome, Y., Kawasaki, T., Inada, K., Jonaitis, J., Pulver, S. R., et al., 2021. An electrically coupled pioneer circuit enables motor development via proprioceptive feedback in Drosophila embryos. Current Biology 31, 5327-5340.e5. doi: 10.1016/j.cub.2021.10.005

Zhang, W., Pombal, M.A., El Manira, A., Grillner, S., 1996. Rostrocaudal distribution of 5-HT innervation in the lamprey spinal cord and differential effects of 5-HT on fictive locomotion. J. Comp. Neurol. 374, 278–290. doi: 10.1002/(sici)1096-9861(19961014)374:2<278::aid-cne9>3.0.co;2-#

Zhang, W., Grillner, S., 2000. The spinal 5-HT system contributes to the generation of fictive locomotion in lamprey. Brain Research 879, 188–192. doi: 10.1016/s0006-8993(00)02747-5

Zhang, W., Yan, Z., Jan, L. Y., Jan, Y. N., 2013. Sound response mediated by the TRP channels NOMPC, NANCHUNG, and INACTIVE in chordotonal organs of Drosophila larvae. Proc. Natl. Acad. Sci. U.S.A. 110, 13612–13617. doi: 10.1073/pnas.1312477110

Zlatic, M., Li, F., Strigini, M., Grueber, W., Bate, M., 2009. Positional Cues in the Drosophila Nerve Cord: Semaphorins Pattern the Dorso-Ventral Axis. PLoS Biol. https://doi.org/10.1371/journal.pbio.1000135

Zwart, M. F., Pulver, S. R., Truman, J. W., Fushiki, A., Fetter, R. D., Cardona, A., et al., 2016. Selective Inhibition Mediates the Sequential Recruitment of Motor Pools. Neuron 91, 615–628. doi: 10.1016/j.neuron.2016.06.031